



저작자표시-비영리-변경금지 2.0 대한민국

이용자는 아래의 조건을 따르는 경우에 한하여 자유롭게

- 이 저작물을 복제, 배포, 전송, 전시, 공연 및 방송할 수 있습니다.

다음과 같은 조건을 따라야 합니다:



저작자표시. 귀하는 원저작자를 표시하여야 합니다.



비영리. 귀하는 이 저작물을 영리 목적으로 이용할 수 없습니다.



변경금지. 귀하는 이 저작물을 개작, 변형 또는 가공할 수 없습니다.

- 귀하는, 이 저작물의 재이용이나 배포의 경우, 이 저작물에 적용된 이용허락조건을 명확하게 나타내어야 합니다.
- 저작권자로부터 별도의 허가를 받으면 이러한 조건들은 적용되지 않습니다.

저작권법에 따른 이용자의 권리는 위의 내용에 의하여 영향을 받지 않습니다.

이것은 [이용허락규약\(Legal Code\)](#)을 이해하기 쉽게 요약한 것입니다.

[Disclaimer](#)

Exploring the Macromolecular Frontier:  
Determining Stereochemical Effects in Strained  
Poly(alkenamer)s and Utilizing Auger Electron  
Spectroscopy to Evaluate Synthetic Polymers

Stanfield Youngwon Lee

Department of Chemistry

Graduate School of UNIST

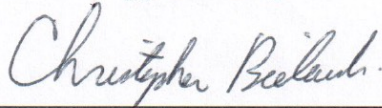
Exploring the Macromolecular Frontier:  
Determining Stereochemical Effects in Strained  
Poly(alkenamer)s and Utilizing Auger Electron  
Spectroscopy to Evaluate Synthetic Polymers

A thesis/dissertation  
submitted to the Graduate School of UNIST  
in partial fulfillment of the  
requirements for the degree of  
Doctor of Philosophy

Stanfield Youngwon Lee

December 4<sup>th</sup> 2018

Approved by



Advisor

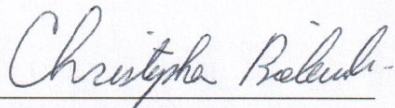
Christopher W. Bielawski

Exploring the Macromolecular Frontier:  
Determining Stereochemical Effects in Strained  
Poly(alkenamer)s and Utilizing Auger Electron  
Spectroscopy to Evaluate Synthetic Polymers

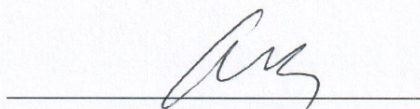
Stanfield Youngwon Lee

This certifies that the thesis/dissertation of Stanfield Youngwon Lee  
is approved.

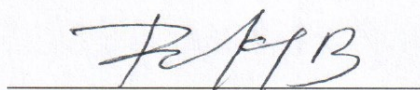
December 4<sup>th</sup> 2018



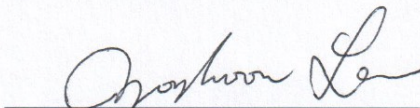
Christopher W. Bielawski: Advisor:



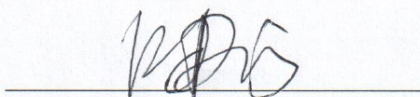
Hyeon Suk Shin: Thesis Committee Member #1



Jong-Beom Baek: Thesis Committee Member #2



Zonghoon Lee: Thesis Committee Member #3



Feng Ding: Thesis Committee Member #4;

Portions of this thesis were submitted to the *Journal of Physical Chemistry C* on March 6, 2018. The corresponding article was accepted for publication on May 23, 2018. It is my understanding that the article may be re-used as part of this thesis without permission from the publisher (ACS Publications); see <https://pubs.acs.org/pb-assets/acspubs/Migrated/dissertation.pdf/>

## Abstract

The utilization of synthetic methods to introduce specific functional groups into a monomer provides just a glimpse at the possibilities that exist with the cohesion of organic and polymer chemistry. This dissertation introduces the synthetic steps taken to synthesize small molecules containing a diester substituted cyclobutane scaffold and their usage as a monomer in ring opening metathesis polymerization (ROMP) reactions. The resulting polymers exhibited different thermal properties, which were traced back to originating from differences in the stereochemistry of the functional groups. In addition, multi-block copolymers with the block components only differing in the stereochemistry of the diester functional groups were successfully synthesized and found to undergo phase separation upon reaching a threshold molecular weight. Finally, attempts at degradation of the polymer through irradiation of the cyclobutyl groups will be shown and discussed.

Although research into the synthesis and application of new polymers continues to grow, being able to analyze the underlying causes for why certain polymers exhibit certain properties is just as important. Analytical techniques, such as nuclear magnetic resonance (NMR) spectroscopy and size exclusion chromatography (SEC) provide polymer chemists with a wealth of knowledge towards characterizing polymers. However, these techniques become much more limited with insoluble polymers. Thus, the second half of this dissertation introduces the use of X-ray induced Auger electron spectroscopy (XAES) to ascertain the hybridization states of synthetic polymers containing carbons with differing degrees of  $sp$ -,  $sp^2$ - and  $sp^3$ -hybridization states as well as heteroatoms. For comparison, a series of related small molecules was also studied. Linear correlations were observed and a universal calibration method for quantifying the average hybridization states of a wide variety of synthetic polymeric materials is offered. Being able to determine the hybridization state of synthetic polymers provides polymer and analytical chemists with another tool towards improving and synthesizing polymers with unique properties.



## Table of Contents

Abstract.....	v
List of Tables.....	ix
List of Figures.....	x
List of Schemes.....	xii
Chapter 1: Introduction.....	1
1.1. Harnessing the Synergistic Effects of Organic Synthesis and Polymer Chemistry. ....	1
1.2. Living Ring Opening Metathesis Polymerization (ROMP) Mediated Through Transition Metal Complexes.....	6
1.3. Research Objectives of this Dissertation.....	13
Chapter 2: Examining the Stereochemical Influence on the Thermal Properties of Strained Poly(alkenamer)s .....	15
2.1. Introduction .....	15
2.2. Results and Discussion.....	21
2.2.1. Synthesis of Monomers and Polymerization via ROMP .....	21
2.2.2. Stereochemical Influences on the Thermal Properties of Strained Poly(alkenamer)s.....	31
2.3. Conclusions .....	39
2.4. Experimental .....	43
2.5. Acknowledgements .....	48
Chapter 3: Determining the Stereochemical Influences on the Electronic Properties of Strained Poly(alkenamer)s .....	49
3.1. Introduction .....	49
3.2. Results and Discussion.....	53
3.3. Conclusions and Future Outlooks .....	59
3.4. Experimental .....	63
Chapter 4: Ascertaining the Hybridization State of Carbon Based Materials and Polymers by <i>D</i> - Parameter Values.....	64
4.1. Introduction .....	64



4.2. Results and Discussion.....	67
4.2.1. Correlating Orbital Hybridization to <i>D</i> -Parameter Values.....	67
4.2.2. Extension of the <i>D</i> -Parameter via a Calibration Curve based on $\pi$ -to- $\sigma$ -Bonding Ratios. ..	73
4.3. Conclusions .....	78
4.4. Experimental .....	79
4.5. Acknowledgements .....	81
Chapter 5: Conclusions and Future Outlooks .....	82
5.1. Conclusions .....	82
5.2. Future Outlooks.....	82
References.....	85
Acknowledgements.....	102
Appendix A: NMR Spectra.....	105
Appendix B: ATR-IR Spectra .....	118
Appendix C: GPC Chromatograms.....	122
Appendix D: TGA Curves.....	146
Appendix E: DSC Traces .....	152
Appendix F: Derivative and Auger Spectra .....	160

## List of Tables

<b>Table 2.1:</b> Glass transition temperatures and melting temperatures of commercial polymers.....	17
<b>Table 2.2.</b> Molecular weights for the series of homopolymers <b>8</b> and <b>9</b> .....	23
<b>Table 2.3.</b> Molecular weights for the series of diblock copolymers <b>10, 11,</b> and <b>12</b> .....	26
<b>Table 2.4.</b> Molecular weights for the series of triblock copolymers <b>13-14</b> .....	29
<b>Table 2.5.</b> Glass transition temperature ( $T_g$ ) and decomposition temperature ( $T_d$ ) values for homopolymers, diblock copolymers, and triblock copolymers .....	32
<b>Table 2.6.</b> Comparison of possible structures that monomer <b>5</b> can attach to the growing polymer chain .....	34
<b>Table 2.7.</b> Comparison of possible structures that monomer <b>7</b> can attach to the growing polymer chain .....	36
<b>Table 2.8</b> Catalyst loading and yields for the series of random copolymer <b>15</b> .....	38
<b>Table 2.9.</b> Glass transition temperature ( $T_g$ ) and decomposition temperature ( $T_d$ ) values for homopolymers, physical mixtures of homopolymers, and random copolymers.....	40
<b>Table 2.10.</b> Glass transition temperature ( $T_g$ ) and decomposition temperature ( $T_d$ ) values for diblock copolymers of different molecular weights.....	41
<b>Table 2.11.</b> Molecular weights and glass transition temperatures ( $T_g$ ) before and after hydrogenation of diblock copolymer <b>10e</b> .....	42
<b>Table 3.1.</b> Woodward-Hoffmann rules for bond rotation during electrocyclic ring opening and closing .....	50
<b>Table 4.1</b> Summary of $D$ -parameter values and standard errors calculated for diamond, graphite, various physical mixtures of those two carbon materials, and graphite fluoride.....	70
<b>Table 4.2</b> Summary of $D$ -parameter values, and standard errors measured for various polymers.....	72
<b>Table 4.3.</b> $\pi$ -to- $\sigma$ -bond ratios and $D$ -parameter values for various polymers, blends and small molecules. ....	75

## List of Figures

<b>Figure 1.1.</b> Representative example for the stepwise growth of Nylon .....	2
<b>Figure 1.2.</b> Representative example of chain growth polymerization via a radical pathway.....	3
<b>Figure 1.3.</b> Examples of backbiting leading to polymer branching (a) and chain transfer leading to early termination and subsequent polymer branching (b).....	4
<b>Figure 1.4.</b> Representative graphs showing the correlation between molecular weight and monomer conversion for chain growth (a), step growth (b), and living (c) polymerizations .....	7
<b>Figure 1.5.</b> A representative mechanism for ring opening metathesis polymerization (ROMP) and examples of intramolecular chain transfer via ring closing metathesis (RCM) and intermolecular chain transfer via cross metathesis (CM).....	10
<b>Figure 1.6.</b> Grubbs 1 <sup>st</sup> , 2 <sup>nd</sup> , and 3 <sup>rd</sup> generation catalysts.....	12
<b>Figure 2.1.</b> Representative scan showing the different phase transition that can occur to a polymer when heated .....	16
<b>Figure 2.2.</b> Representative illustration of the phase separation between poly(styrene) and poly(butadiene) in a poly(styrene)- <i>block</i> -poly(butadiene)- <i>block</i> -poly(styrene) block copolymer .....	18
<b>Figure 2.3.</b> Representative illustration of isotactic, syndiotactic, and atactic poly(propylene).....	19
<b>Figure 2.4.</b> Molecular weight control of polymers synthesized from <b>5</b> (a) and block copolymer formation upon the addition of <b>7</b> after consumption of <b>5</b> (b).....	24
<b>Figure 2.5.</b> Comparison of 2- <i>exo</i> -3- <i>exo</i> -dimethyl ester bicyclo [2.2.1] hept-5-ene and 2- <i>endo</i> -3- <i>exo</i> -dimethyl ester bicyclo [2.2.1] hept-5-ene with monomers <b>5</b> and <b>7</b> .....	28
<b>Figure 2.6.</b> Representative <sup>1</sup> H NMR spectra for the monomers, homo-, di-, and tri-block copolymers .....	30
<b>Figure 2.7.</b> <sup>1</sup> H NMR of <b>8a</b> (top) and <b>9a</b> (bottom) .....	33
<b>Figure 2.8.</b> Proposed addition of monomer <b>5</b> to the growing polymer chain.....	34
<b>Figure 2.9.</b> Proposed addition of monomer <b>7</b> to the growing polymer chain.....	36
<b>Figure 3.1.</b> Simplified Jablonski diagram outlining the possible electronic states and transitions that can occur upon photoirradiation .....	50
<b>Figure 3.2.</b> 1,3-Butadiene undergoing electrocyclic ring closing through conrotatory bond rotation when thermally driven .....	51
<b>Figure 3.3.</b> 1,3-Butadiene undergoing electrocyclic ring closing through disrotatory bond rotation when photochemically driven .....	51
<b>Figure 3.4.</b> Frontier molecular orbitals for two ethylene molecules under thermal and photochemical conditions.....	52

<b>Figure 3.5.</b> GC chromatograms for diblock polymer <b>10f</b> before and after 30 hours of irradiation with 300 nm light .....	54
<b>Figure 3.6.</b> Mass spectra for the signals seen at 6.68 and 8.00 minutes in Figure 3.5 .....	54
<b>Figure 3.7.</b> GC chromatograms for polymer <b>8a</b> before and after 30 hours of photoirradiation .....	55
<b>Figure 3.8.</b> Mass spectrum for the signal seen at 8.02 minutes in Figure 3.7 .....	55
<b>Figure 3.9.</b> GC chromatograms for polymer <b>9a</b> before and after 30 hours of photoirradiation .....	56
<b>Figure 3.10.</b> Mass spectra for the signal seen at signal seen at 6.77 minutes and at 8.10 minutes in Figure 3.9 .....	56
<b>Figure 3.11.</b> Representative image for the diabatic photoreaction of dimethyl fumarate to dimethyl maleate upon irradiation with UV light .....	57
<b>Figure 3.12.</b> UV-Vis spectra for dimethyl maleate and dimethyl fumarate .....	58
<b>Figure 3.13.</b> UV-Vis spectra for polymer <b>8a</b> and polymer <b>9a</b> .....	61
<b>Figure 3.14.</b> Representative example for how the stereochemistry of the functional groups influence the pathway in which the retro [2+2] reaction proceeds .....	61
<b>Figure 3.15</b> UV-Vis GPC chromatograms for polymer <b>8a</b> before and after photoirradiation .....	62
<b>Figure 3.16.</b> UV-Vis GPC chromatograms for polymer <b>9a</b> before and after photoirradiation .....	62
<b>Figure 4.1.</b> Electron ejection due to excitation and auger electron emission for XPS and AES .....	66
<b>Figure 4.2.</b> The correlation between an element's atomic # and auger emission or fluorescence .....	66
<b>Figure 4.3.</b> Representative carbon 1s spectra recorded by XPS for graphite, diamond and various physical mixtures of graphite (G) and diamond (D) .....	68
<b>Figure 4.4.</b> Representative C KLL Auger (a) and first-derivative C KLL Auger (b) spectra of diamond and graphite powder .....	69
<b>Figure 4.5.</b> Plot of <i>D</i> -parameter values versus the percentage of <i>sp</i> <sup>3</sup> hybridized carbons in graphite, diamond, various physical mixtures of graphite (G) and diamond (D), and graphite fluoride .....	70
<b>Figure 4.6.</b> Plot of <i>D</i> -parameter values versus the percentage of <i>sp</i> <sup>3</sup> hybridized carbons found in various polymers .....	71
<b>Figure 4.7.</b> Plot of the <i>D</i> -parameter values to the canonical $\pi$ -to- $\sigma$ bonding ratios of polymers containing carbons in different hybridization states, small molecules, polymers containing heteroatoms, and polymer blends .....	74
<b>Figure 4.8</b> First-derivative Auger spectra recorded for PE, PA and a stoichiometric, physical mixture of PE and PA .....	77
<b>Figure 4.9.</b> First-derivative Auger spectra recorded for poly(ethylene) (PE), poly(styrene) (PS), a poly(styrene)-block-poly(ethylene)-block-poly(styrene) block copolymer, and various poly(ethylene)/poly(styrene) blends (ratios are indicated). .....	77

## List of Schemes

<b>Scheme 2.1.</b> Synthetic scheme for dimethyl (1R,2S,3R,4S)-bicyclo[2.2.0]hex-5-ene-2,3-dicarboxylate (5) and dimethyl (1R,2S,3S,4S)-bicyclo[2.2.0]hex-5-ene-2,3-dicarboxylate (7) .....	22
<b>Scheme 2.2.</b> Polymerization of homopolymers 8 and 9 .....	23
<b>Scheme 2.3.</b> Polymerization of diblock copolymers 10-12 .....	26
<b>Scheme 2.4.</b> Polymerization of triblock copolymers 13 and 14 .....	29
<b>Scheme 2.5.</b> Polymerization of random copolymer 15 .....	38
<b>Scheme 2.6.</b> Synthetic scheme toward the hydrogenation of diblock copolymers .....	42
<b>Scheme 3.1.</b> Proposed mechanism for the photodegradation of homopolymers 8 and 9 .....	52

## Chapter 1: Introduction

### 1.1. Harnessing the Synergistic Effects of Organic Synthesis and Polymer Chemistry

*“Most branches of science pass through a ‘pioneering period’ where different concepts and approaches create for a while, a turbulent atmosphere until, on the basis of new experimental evidence, clear and durable principles emerge, which lead to a broad and continuous growth of basic understanding and practical application.”*

–Hermann F. Mark on his recollections of the early days of polymer chemistry<sup>1,2</sup>

Polymer chemistry has considerably grown from the days where Hermann Staudinger, often considered the father of polymer chemistry, was constantly defending the concepts and definitions outlined in his article “Uber Polymerisation” (On Polymerization) from organic chemists.<sup>1, 3</sup> Although J.J. Berzelius had already defined polymers as molecules that had the same empirical formula but a larger molecular weight, i.e. glucose (C<sub>6</sub>H<sub>12</sub>O<sub>6</sub>) being a polymer of formaldehyde (CH<sub>2</sub>O),<sup>4</sup> we now know that this definition would not include what we consider polymers today. Likewise, Thomas Graham attempted to define polymers as colloids.<sup>5</sup> However, this definition was not able to stand the tests of time as well. It was not until Staudinger proposed large molecular weight molecules consisting of repeating units linked through covalent bonds that polymers as we know today were identified and the field of polymer chemistry was born.<sup>3</sup> Originally defined as macromolecules, Staudinger’s ideas were initially met with skepticism by organic chemists, who continued to believe that polymers were a subset of colloids rather than a covalently bonded network of repeating unit chains. However, Staudinger continued to pursue his ideas and his persistence was rewarded with him receiving the Nobel Prize in Chemistry in 1953.

Representative of the early days of polymer chemistry, Heinrich Wieland, a fellow Nobel Prize winning chemist, once advised Staudinger to “drop the idea of large molecules; organic molecules with a molecular weight higher than 5,000 do not exist. Purify your products, such as rubber, then they will crystallize and prove to be low molecular weight compounds.”<sup>2, 6</sup> Over time however, this divide between organic chemistry and polymer science has steadily decreased and instead, have begun to merge. This cohesion has already led to reports of polymers not only with unique architectures, but also exhibiting new and/or improved properties. Functionalizing polymers to conform into shapes such as stars<sup>7</sup>, dendrites<sup>8</sup>, and brushes<sup>9-10</sup> have all been reported with wide spreading applications, such as in targeted drug delivery<sup>11-12</sup> and as bioimaging materials.<sup>12-13</sup>

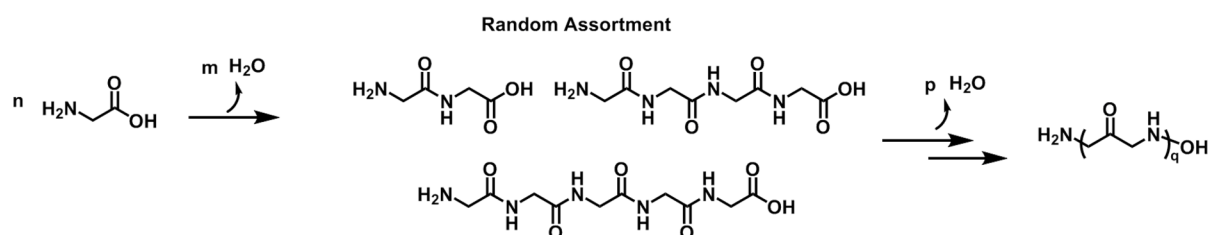
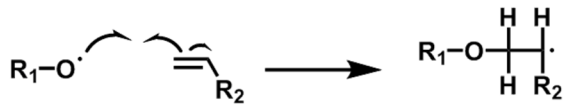
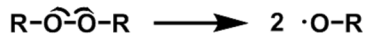


**Figure 1.1.** Representative example for the stepwise growth of Nylon. One water molecule is released per new bond formation.

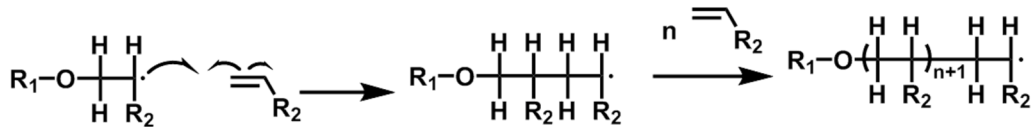
The development and advancement of polymer methods can be traced back to having roots in organic chemistry. To start, polymer chains can grow through a stepwise or chain growth pathway. As shown in Figure 1.1, step growth polymerization occurs through a series of addition or condensation reactions that leads to a random assortment of dimers, trimers, tetramers, etc. These chains of random lengths eventually combine when nearly all the monomer is consumed, leading to a large molecular weight polymer. Although stepwise grown polymers, such as Nylon, have commercial uses, it is difficult to grow high molecular weight polymers, as the chains of assorted lengths do not combine until nearly the end of polymerization. On the other hand, chain growth polymerization involves fast initiation with the active species being recreated at the end of the growing polymer chain upon addition of a monomer unit. As a result, high molecular weight polymers can be attained at even low monomer to polymer conversions.<sup>14</sup> Propagation ceases upon deactivation of the reactive center, which can occur through multiple methods such as by bonding with another growing polymer chain (combination) or hydrogen abstraction, leading to radical migration and termination (disproportionation) (see Figure 1.2). The active center for chain growth polymerizations is initially created through an initiator and can be radical, anionic, or cationic in nature. However, each of these types of polymerizations have their own sets of challenges and difficulties.

As alluded to earlier in this chapter, polymers differ from small molecules in that their molecular weights are a distribution. Since polymer properties are influenced by molecular weights,<sup>15-19</sup> mixtures of polymers with wide molecular weight distributions would be difficult to apply for applications where specific properties are required. For example, low molecular weight poly(ethylene) is often used for adhesives while high molecular weight poly(ethylene) is utilized in bullet-proof vests.<sup>20</sup> Naturally, although they are the same material, you wouldn't want a bullet proof vest consisting of segments of low molecular weight poly(ethylene)! Since radical chain growth occurs through the formation of radicals, side reactions such as backbiting, branching, early

## Initiation

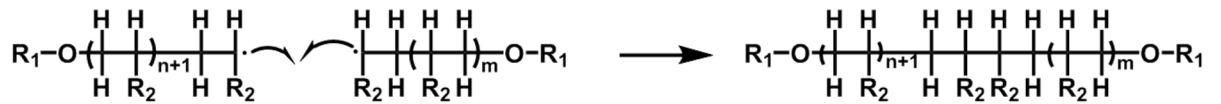


## Propagation



## Termination

## Combination



## Disproportionation

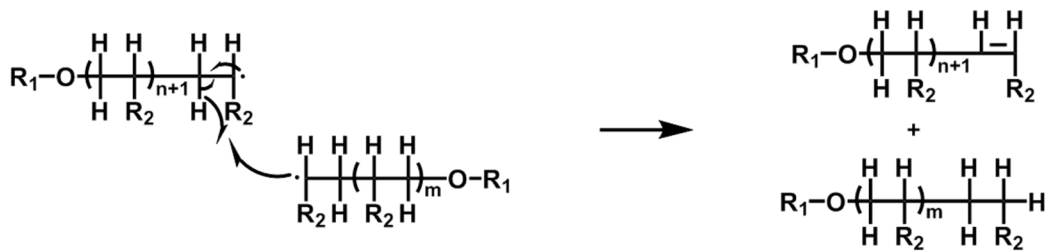


**Figure 1.2.** Representative example of chain growth polymerization via a radical pathway. Derivatives of chain growth polymerizations via anionic and cationic pathways are also possible using different initiators.



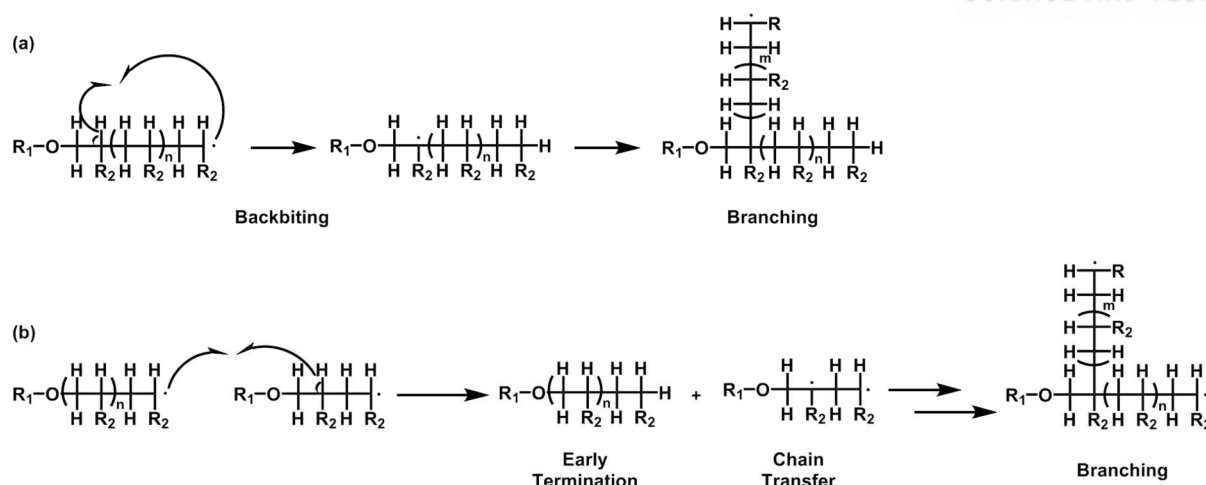


**Figure 1.3.** Examples of backbiting leading to polymer branching (a) and chain transfer leading to early termination and subsequent polymer branching (b). All of these events lead to a wider distribution in molecular weight.

combination and termination, and/or chain transfer are all possible (Figures 1.3). Any or all of these occurrences lead to polymers with different molecular weights, which, in turn, widens the molecular weight distribution. Although ionic polymerizations tend to minimize these side reactions and allow for control over the molecular weight, requirements such as high sensitivity to air and moisture and premature termination in the presence of impurities, make polymerization through these means an arduous task.

These difficulties were overcome with the development of living polymerization as coined by Michael Szwarc.<sup>21</sup> Living polymerization methods such as reversible deactivation of radicals<sup>22</sup> (i.e. nitroxide mediated radical polymerization (NMP), reversible addition fragmentation chain transfer (RAFT) polymerization) or chain growth polymerization mediated through transition metal based catalysts, offered alternative ways to control molecular weight while minimizing branching or other unwanted side reactions. Of these methods, the initial concepts of two of the more common methods utilized today, atom transfer radical polymerization (ATRP) and ring opening metathesis polymerization (ROMP), can be attributed to synthetic reactions. ATRP, which minimizes side reactions and controls polymer growth through control of the equilibrium between the dormant and active states for polymer propagation,<sup>23-24</sup> was developed from transition metal catalyzed atomic transfer radical addition (ATRA),<sup>25-26</sup> which, in turn, was derived from the Kharasch addition reaction.<sup>27</sup> Likewise, ROMP mediated by certain transition metal based catalysts, which will be discussed in detail later in this chapter, is based off of the olefin metathesis reaction;<sup>28</sup> the mechanism proposed by Yves Chauvin<sup>29</sup> paved the way for the development of well-defined catalysts such as the

Schrock's and Grubbs' catalyst for ROMP. These catalysts afforded polymers with control over the molecular weight and narrow molecular weight distributions, which further opened up the scope for polymer applications.

The influences of organic chemistry can also be found when delving into research involving pre- and or post- polymerization modifications.<sup>30</sup> Although polymers, such as poly(acetylene) have been synthesized in multiple ways using different starting monomers,<sup>31-32</sup> reaching high molecular weights have proven to be unsuccessful due to the growing polymer becoming insoluble past a certain number of chain lengths, and thus precipitating out before the propagation step is complete.<sup>32</sup> In earlier times, this limitation may have quenched any further developments into poly(acetylene). However, as a testament to how much polymer chemistry has already developed, successful methods to create soluble poly(acetylene) using organic transformations have been reported. The Grubbs group took the approach of substituting the monomer (1,3,5,7-cyclooctatetraene) with functional groups that hindered stacking forces once polymerized.<sup>33</sup> Although substitution of every acetylene unit leads to losses in conductivity<sup>34</sup>, the method outlined by the Grubbs group was especially appealing since by only monosubstituting cyclooctatetraene, the resulting poly(acetylene) only possessed a functional group once every four repeat units. Subsequent polymerization yielded a poly(acetylene) derivative that was still conductive and whose substituents caused enough steric repulsion to be soluble in common organic solvents.<sup>33</sup>

Multiple approaches involving polymerization of poly(acetylene) precursors followed by post-polymerization modifications have also been reported as methods to bypass the issues with solubility. Edwards and Feast polymerized the Durham precursor, which then could be modified to poly(acetylene) via a heat induced retro [2+2] Diels Alder reaction.<sup>35-36</sup> Likewise, Swager et al. showed the formation of poly(acetylene) via the polymerization of benzvalene, which was subsequently converted to poly(acetylene) via metal mediated isomerization.<sup>37</sup> More recently, the Xia group polymerized a ladderene derivative, which was then transformed into poly(acetylene) through sonochemistry.<sup>38</sup> This ladderene derivative didn't have the solubility issues that occur when polymerizing poly(acetylene) and thus, upon conversion, high molecular weight poly(acetylene) could be produced in a controlled manner.<sup>38</sup> As poly(acetylene) has already been utilized as a conducting polymer in a variety of different fields,<sup>39</sup> providing methods to access and control high molecular weights as well as increasing solubility is bound to lead to even further applications. Further examples using post-polymerization methods via click chemistry<sup>40-41</sup> and activated esters<sup>42</sup> have also shown the versatility and power of how simple chemical reactions can manipulate the polymer's molecular structure.

The field of polymer chemistry has advanced rapidly from the nascent stages where scientists didn't believe macromolecules, as defined by Staudinger, could exist. Assisted by concepts and methods derived from organic chemistry, we are now at the point where not only have high molecular weight macromolecules been proven to exist, but their molecular weights can also be predicted and polymerized with narrow distributions. In addition to the creation of polymers possessing new structures, modifications to the monomer before polymerization or directly to the polymer post-polymerization have not only been shown as methods to introduce different properties, but also as viable pathways to produce polymers that are normally difficult to polymerize under regular conditions. As this synergetic effect between organic chemistry and polymer chemistry continues to blossom, nobody can predict what further outcomes and discoveries may be made. However, what is certain is that the field of polymer chemistry is firmly entrenched as a rapidly advancing field; no longer are polymers considered colloids that when purified will be proven to be "small molecules".

## **1.2. Living Ring Opening Metathesis Polymerization (ROMP) Mediated Through Transition Metal Complexes**

As briefly discussed earlier in this chapter, polymerization can occur through a step-wise mechanism or through a chain growth pathway. These two pathways differ in that polymer chains of different lengths (i.e. dimers, trimers, tetramers, etc.) can all bond with each other in step-wise polymerization whereas propagation only occurs through monomers attaching to the reactive center in chain growth polymerization.<sup>14</sup> Naturally, these differences influence the correlation between molecular weight and conversion, as stepwise polymerizations require high degrees of conversion to create high molecular weight polymers while chain growth polymerization produces high molecular weight polymers even at low conversions (Figure 1.4).

As shown in Figure 1.2, chain polymerizations proceed through three main stages, initiation, propagation, and termination. The initiation step involves the creation or activation of a reactive center, while propagation involves subsequent addition of monomer units to the growing polymer chain. Unlike step growth, upon monomer addition, chain growth leads to regeneration of the reactive center at the end of the growing polymer chain. Therefore, only monomers are able to interact with the reactive center during propagation. Finally, the polymerization ceases to grow and terminates upon destruction of the reactive center through a myriad of possibilities (Figure 1.2).<sup>14</sup> Although chain growth polymerizations produce high molecular weight polymers at low conversions, the high reactivity of the radical species subjugates the growing polymer chain to various side reactions (Figure 1.3).

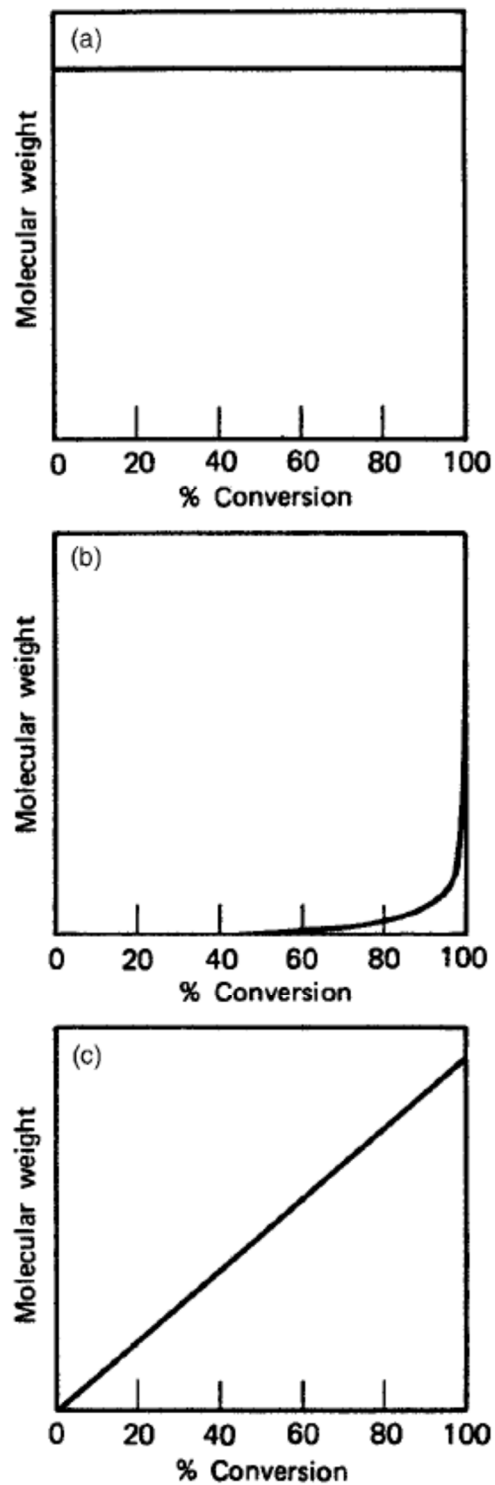


**Figure 1.4.** Representative graphs showing the correlation between molecular weight and monomer conversion for chain growth (a), step growth (b), and living (c) polymerizations. Adapted from reference 14.

Recognizing that minimizing or eliminating unwanted side reactions was the key to controlling the molecular weight of a growing polymer, Michael Szwarc proved that the prevention of a “natural death” for the growing polymer during propagation would remove many of the challenges faced by radical chain growth. Natural deaths were defined by Szwarc as any internal event that lead to termination (i.e. backbiting, chain transfer, combination, etc.).<sup>21</sup> Although designing ideal conditions for stabilization of radicals proved to be too difficult due to the extreme reactivity of radical species, Szwarc was able to show the prevention of events leading to early termination when he polymerized styrene via anionic polymerization in THF. Realizing that an anionic polymerization done in acidic solvents and non-polar solvents would lead to early termination via proton donation from the solvent and electron transfer back to the cation respectively, Szwarc showed that polymerizations done in tetrahydrofuran not only mitigated these issues, but the reactive center remained active even after complete monomer consumption.<sup>21</sup> Thus, since the reactive center did not “die” from natural causes, the polymer chain remained active and would remain active until it was “killed” by an external event such as the addition of an end group reagent. Named living polymerizations, these polymerizations opened up a new field in polymer research since not only could molecular weights of polymers be linearly correlated to the amount of monomer conversion, but the formation of block copolymers with blocks originating from different monomer units was also feasible. Unfortunately, due to the stringent requirements for ionic polymerizations, Szwarc still observed the deactivation of the active center upon exposure to impurities or oxygen.<sup>21</sup> Nevertheless, Szwarc’s discovery of the ability to predict and control the molecular weight of a polymer helped pave the way for the discovery of many of the polymerization methods utilized today.

In order for a chain growth polymerization to be classified as living, certain criteria must be met.<sup>43</sup> To start off, as outlined by Szwarc,<sup>43</sup> the number average molecular weight ( $M_n$ ) must show a linear correlation to conversion or the monomer to initiator concentration ratio, thus proving that molecular weights of the polymer can be predicted and controlled by varying the concentration of monomer and/or initiator.<sup>21</sup> Second, polymerization must proceed until monomer consumption is complete. Yet, polymerization must continue upon further addition of monomer, which proves that the reactive center remains active, and has not undergone termination.<sup>21</sup> Third, polymers with functionalized chain ends can be prepared through the addition of a terminating agent,<sup>43</sup> and finally, all the polymers must possess a narrow molecular weight distributions ( $\mathcal{D}$ ).<sup>43</sup>

Polymerization methods that fulfilled the requirements for living polymerization offered a multitude of advantages and also created further applications for polymers. As the molecular weight of a polymer has been shown to influence its properties,<sup>15-19</sup> being able to target certain molecular

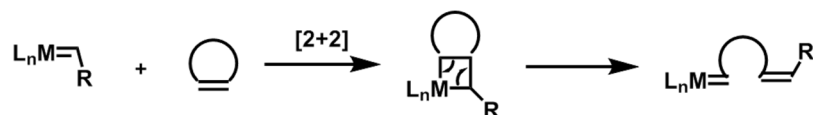
weights with the resulting polymers possessing narrow molecular weight distributions offer tailoring of polymers for specific applications. Likewise, if the reactive center remains active after complete monomer consumption, the addition of a different monomer should lead to the formation of block copolymers. As a result, block copolymers exhibiting combined properties originating from the individual components were possible. The Choi group took advantage of this concept to create block copolymers consisting of poly(acetylene) and a poly(norbornene) derivative.<sup>44</sup> Unlike poly(acetylene), the resulting block copolymer was found to be soluble in a variety of organic solvents and also to be stable in an oxygen environment. Further characterization of the block copolymer confirmed the presence of the poly(acetylene) component and exhibited properties consistent with that of poly(acetylene).<sup>44</sup> The ability to attach functional groups to the chain end via a termination agent also created opportunities for further polymerization<sup>45-46</sup> and/or post polymerization modifications.<sup>47</sup>

The benefits offered by living polymerization methods spurred research into the development of well-defined catalysts that initiate living polymerization. Of these developments, a new type of polymerization, which employed strained cyclic olefins as monomers emerged as a powerful method for creating macromolecular materials. Termed, ring opening metathesis polymerization (ROMP), ROMP differed from previously reported polymerizations since any unsaturation within the polymer was preserved, even after polymerization.<sup>48</sup> In addition, ROMP was discovered to exhibit living characteristics when the polymerization was mediated by certain transition metal based catalysts.

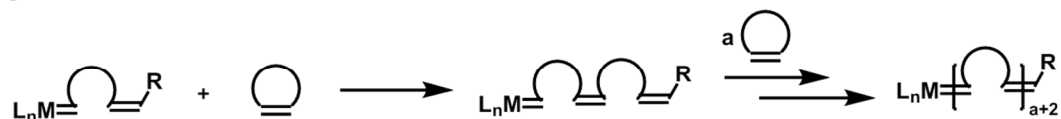
The mechanism for metathesis through which ROMP proceeds was initially proposed by Yves Chauvin<sup>29</sup> and further confirmed by Robert Grubbs and Thomas Katz.<sup>49-51</sup> As seen in Figure 1.5, ROMP initiates through the coordination of a transition metal alkylidene complex to a cyclic olefin via [2+2] cycloaddition. The resulting cyclobutane intermediate then undergoes a retro [2+2] cycloaddition reaction, which opens up the cyclic olefin and leaves the transition metal alkylidene bonded to a terminal olefin. This new alkylidene can then repeatedly undergo the same process during propagation, with each cycle adding an additional monomer unit to the growing polymer chain. Upon complete monomer consumption, the metal alkylidene remains at the end of the polymer chain until it is terminated via addition of an end group reagent.

Even though from an entropic standpoint, ROMP is disfavored, polymerization still occurs provided that the release of enthalpic energy due to ring opening of the cyclic olefin is enough to overcome the entropy cost. Thus, cyclic olefins with high ring strain, such as derivatives of cyclobutene<sup>52-54</sup> and norbornene<sup>54-60</sup> are often used as monomers for ROMP, as the high ring strains in these molecules drive the polymerization to completion. However, similar to radical chain growth,

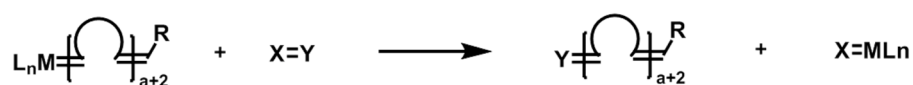
## Initiation



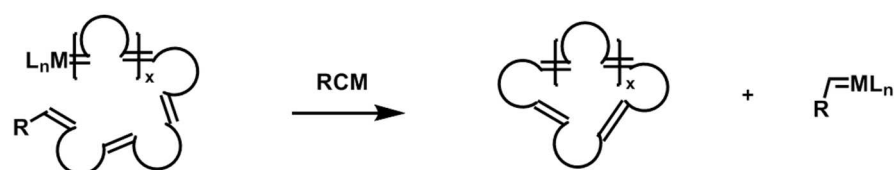
## Propagation



## Termination



## Intramolecular Chain Transfer (Backbiting)



## Intermolecular Chain Transfer



**Figure 1.5.** A representative mechanism for ring opening metathesis polymerization (ROMP) and examples of intramolecular chain transfer via ring closing metathesis (RCM) and intermolecular chain transfer via cross metathesis (CM).

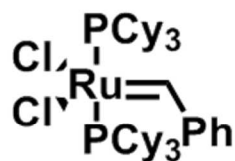
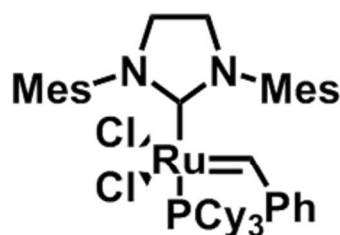
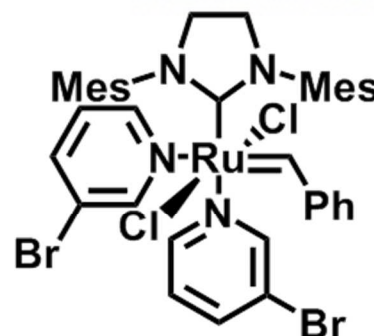
chain transfer reactions can occur through both intramolecular (ring closing metathesis) and intermolecular (cross metathesis) pathways during ROMP, with the result being a broader molecular weight distribution (Figure 1.5).<sup>61</sup>

The widespread application of ROMP can be directly tied to the development and discovery of well-defined transition metal catalysts that minimized chain transfer reactions and thus, rendered ROMP into a living polymerization method.<sup>48</sup> Initially, catalysts based off of titanium complexes were utilized to facilitate ROMP with varying degrees of success.<sup>48</sup> However, titanium's propensity to bind to oxygen limited its application, as oxygen containing functional groups would deactivate the catalyst.<sup>48, 62</sup> Advancements first using tungsten<sup>63-64</sup> and later on with molybdenum<sup>63, 65</sup> based complexes by Richard Schrock further expanded the scope of which ROMP could be utilized. When employed for ROMP, these well-defined, highly active catalysts not only catalyzed a wider range of monomers than the titanium complexes, but also allowed for stereochemical and tacticity control through manipulation of the ligands coordinated to the transition metal.<sup>66-67</sup> Although these catalysts showed a higher tolerance toward oxygen containing compounds than titanium, a still relatively high oxophilicity hindered their usage with a diverse range of monomers and also required handling under an inert atmosphere.<sup>62, 68</sup> In addition, their high reactivity towards metathesis led to higher propensities for chain transfer reactions to occur during polymerization, which in turn led to loss of molecular weight control.<sup>48</sup>

Unlike their early transition metal counterparts, late transition metals exhibit a lower oxophilicity and thus were expected to possess a higher tolerance towards oxygen containing and/or polar functional groups. Early studies reported that the polymerization of norbornene derivatives could be facilitated by hydrated trichlorides of ruthenium, osmium, and iridium in protic solvents.<sup>69</sup> Further studies with group VIII transition metal coordinated compounds showed a high stability to air and moisture and also the successful polymerization of norbornene derivatives in aqueous mediums. However, although these catalysts did initiate polymerization in anhydrous solvents, a lengthy initiation period, sometimes up to 24 hours, hindered the use of these catalysts for living ROMP.<sup>70-71</sup> Yet the ability to polymerize cyclic olefins that contained polar functional groups in an aqueous medium provided a glimpse of the potential these late transition metal based catalysts had to offer.

The efforts of countless researchers throughout the years culminated in the development of the Grubbs' 1<sup>st</sup> generation catalyst (G1) (Figure 1.6). Due to ruthenium favoring soft Lewis bases and acids, such as olefins, over hard acids and bases, i.e. oxygen based ligands,<sup>68</sup> G1 afforded high stability and exceptional catalytic activity in both organic<sup>72</sup> and aqueous<sup>73</sup> mediums. As such, living



**G1****G2****G3**

**Figure 1.6.** Grubbs 1<sup>st</sup>, 2<sup>nd</sup>, and 3<sup>rd</sup> generation catalysts (G1, G2, and G3 respectively). The replacement of a phosphine ligand with a N-heterocyclic carbene (NHC) (G2) led to increased reactivity while the replacement with 3-bromopyridine (G3) led to faster initiation.

polymerization was found to be possible for both norbornene and cyclobutene derivatives. Though G1 displayed exceptional functional group tolerance and environmental stability, a slow initiation step limited the monomers that could be polymerized in a living manner.<sup>48</sup> Therefore, in order to increase the reactivity of the catalyst, optimization of G1 via replacement of one of the phosphine ligands with an N-heterocyclic carbene (NHC) led to the development of the Grubbs 2<sup>nd</sup> generation catalyst (G2).<sup>74</sup> The increase in reactivity of G2 was attributed to the NHC's ability to stabilize the intermediate state of the catalyst after dissociation of tricyclohexylphosphine due to the increased electron density arising from NHC's being strong  $\sigma$ -donors.<sup>48, 74</sup> Additionally, the stronger bond between the NHC ligand and the ruthenium center when compared with tricyclohexylphosphine was found to impede catalyst decomposition.<sup>48</sup>

The increase in reactivity of G2 expanded the scope of monomers that undergo ROMP to even include cyclic olefins with low ring strain.<sup>75</sup> The polymerization rates of monomers with low ring strain such as cyclooctene<sup>75</sup>, *cis*-cyclooctadiene<sup>75</sup>, and 1,3,5,7-cyclooctatetraene<sup>31</sup> were found to be higher than when done with G1 and the polymerization of *cis*-cyclooctadiene using G2 exhibited even higher rates of polymerization than the Schrock's molybdenum based catalysts.<sup>48, 75</sup> Yet, even though high catalytic activity was observed, slow initiation led to the polymers polymerized by G2 having wide molecular weight distributions, which in turn, rendered them as non-living catalysts. In addition, the increased reactivity raised the vulnerability of the catalysts to undergo secondary metathesis reactions during polymerization. Attempts to increase the initiation efficiency through direct replacement of the tricyclohexylphosphine ligand<sup>76</sup> or through phosphine ligand exchange with more labile phosphines<sup>77</sup> have resulted in polymers having much narrower  $\bar{M}_w/\bar{M}_n$ . However, the best reactivity and fastest initiation to date was found when the phosphine ligand was replaced with a

pyridine derivative. This new derivative, termed the Grubbs 3<sup>rd</sup> generation catalyst (G3), not only possessed the high reactivity exhibited by G2, but also displayed initiation rates nearly six orders of magnitude faster than G1.<sup>78</sup> Therefore, G3 was found to not only polymerize a much broader scope of monomers, but polymerize them in a living manner.

The development of well-defined catalysts that possess high functional group tolerance, are stable to moisture and oxygen, and polymerize cyclic olefins in a living manner, naturally opened the door towards tuning the size and molecular weight of polymers derived from highly functionalized monomers. In addition, due to the reactive center remaining at the end of the growing polymer chain, a diverse range of copolymers exhibiting well defined molecular weights and interesting properties along with new topologies arising from the interaction of the individual polymer components have also been reported. Without the development of these catalysts that mediate living polymerization, many of the contributions that have and continue to advance the field of polymer chemistry, including the results presented in this dissertation, would have at best been hindered or at worst, not have been possible at all.

Polymer chemistry has come a long way from its nascent stages where scientists did not believe high molecular weight molecules were even a possibility. Through the immeasurable efforts of countless researchers from a diverse range of expertise, not only were macromolecules found to be real, but methods to control molecular weights and their properties have already been found. Although in no way is this a complete history of how the field of polymer chemistry became the area of research it is today, the contributions outlined in this introduction significantly paved the way for future scientists to continue to push against the macromolecular frontier and to keep advancing the field of polymer chemistry.

### 1.3. Research Objectives of this Dissertation

Part I (Chapters 2 and 3) of this dissertation involves the investigation of the influences of stereochemistry on the thermal and electronic properties of poly(alkenamer)s. Bicyclic diester functionalized monomers with the ester groups *cis* and *trans* to each other were synthesized and both homopolymers and copolymers of different molecular weights were polymerized. Further analysis on the effect of the *cis* and *trans* stereochemistry on the glass transition temperature were done using analytical techniques, such as differential scanning calorimetry (DSC). In addition, successful polymerization of high molecular weight block copolymers whose components only differed in stereochemistry were found to not only be possible, but also could be induced to phase separate.

Finally, the electronic properties of the polymers were investigated through photodegradation of the cyclobutyl group within the polymer. The stereochemical influence toward hindering or favoring the photodegradation of the polymer to small molecules were determined.

Part II (Chapter 4) of this dissertation outlines a novel method for determining the carbon hybridization state of synthetic polymers. As ROMP preserves the degree of unsaturation even after polymerization, poly(alkenamer)s with varying degrees of  $sp^2$  and  $sp^3$  hybridization were synthesized and analyzed by X-Ray Induced Auger Electron Spectroscopy (XAES). A linear correlation between the ratio of  $sp^2/sp^3$  hybridization and the  $D$ -Parameter, calculated from the maximum and minimum point of the first derivative Auger spectra, was observed. Further extension towards a universal calibration curve correlating the  $D$ -Parameter to the  $\pi$ -to- $\sigma$ -bonding ratio within a monomer unit of a polymer was also shown and found to correlate with polymers containing  $sp$ -hybridized carbon atoms as well as with small molecule analogs of graphene. As the methods for analyzing insoluble polymers is much more limited, analysis by XAES provides an additional method to analyze insoluble polymers and also to correlate the properties of a polymer to the hybridization state of the carbon atoms.

## Chapter 2: Examining the Stereochemical Influence on the Thermal Properties of Strained Poly(alkenamer)s

### 2.1. Introduction

As shown in Figure 2.1, heating a polymer exhibits phase transitions other than melting and solidification. For polymers that are able to stack into well-ordered structures, a crystallization signal is observed before the melting temperature of the polymer. However, most polymers are amorphous by nature, which in turn, means that only a few polymers, such as isotactic poly(propylene) exhibit a crystallization signal.<sup>79</sup> More common among polymers is a signal corresponding to the glass transition temperature ( $T_g$ ). The glass transition temperature is defined as the temperature at which the polymer structure becomes rubber like in nature or alternatively, the temperature at which an amorphous polymer takes on glass-like properties.<sup>14</sup> Simply put, the glass transition occurs at the temperature at which if exceeded, results in the polymer chains having increased mobility and more elastomeric properties. Consequently, the mobility of the polymer chains would be hindered below the glass transition temperature and thus, would lead to the polymer being much stiffer and brittle.

The glass transition temperature plays an influential role in determining a polymer's potential for industrial applications. Polymers possessing  $T_g$  values below ambient temperature (i.e. poly(butadiene) and poly(isoprene)) often are soft and pliable with little to no mechanical strength at room temperature. These types of polymers are unique in that they can be stretched over long distances and “bounce” back when at temperatures above their  $T_g$ , which makes them useful as synthetic rubbers.<sup>80</sup> On the other hand, polymers that possess glass transition temperatures at values higher than ambient temperature are often stiff and brittle in nature and have found applications where high mechanical strengths are required. For example, poly(paraphenylene terephthalamide), commonly known as Kevlar, exhibits a glass transition temperature in the range of 307-347 °C and as such, is often employed in bullet proof vests.<sup>15, 81</sup>

As the glass transition temperature plays an influential role in determining a polymer's properties, methods to manipulate the  $T_g$ , have been and continues to be extensively researched. Since the glass transition temperature can be considered to be the transitioning point from where freely moving polymer chains become increasingly immobile, factors that favor stacking into well-ordered structures and/or lead to immobilization of the polymer have been found to increase the  $T_g$ .<sup>15,</sup>

<sup>82</sup> Studies involving polymers polymerized from acrylates<sup>83</sup> and carbonates<sup>84-85</sup> show an increase in

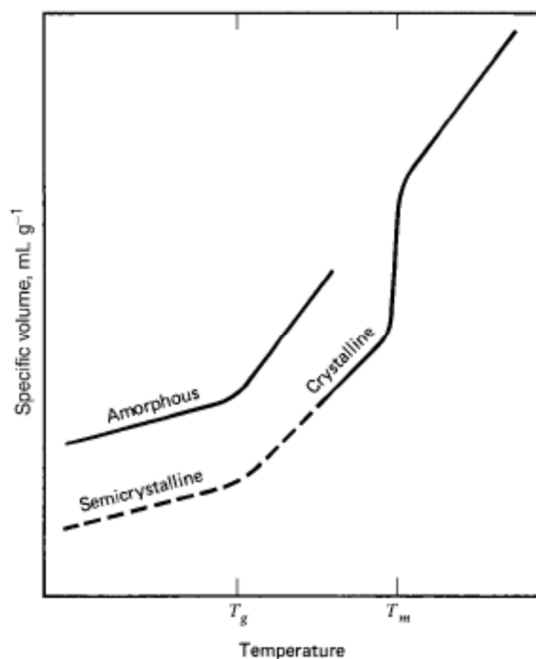


**Figure 2.1.** Representative scan showing the different phase transition that can occur to a polymer when heated. Figure adapted from reference 14.

$T_g$  when the functional groups were replaced with bulkier side chains. These increases in temperature were explained by the bulkier functional groups hindering free rotation and overall polymer movement. For example, although poly(styrene) is connected through a carbon-carbon single bond backbone, which should allow for free rotation, it still possesses a relatively high  $T_g$  since the phenyl side chain prevents facile rotation.<sup>86-87</sup>

Other efforts toward manipulating the glass transition temperature through immobilization of the polymer backbone have also been found to be successful. As can be seen in Table 2.1, *trans* isomers of polymers often show higher glass transition temperatures than their *cis* analogs, since polymers in the *trans* conformation favor stacking which ultimately leads to motion impediment, as is the case for poly(butadiene) and poly(isoprene). Previous works done by Nishihara et al. concluded that changes (ca. 40 °C) in the glass transition temperatures could also be observed in disubstituted poly(norbornene) derivatives by altering the stereochemistry of the cyano and ethyl ester functional groups to be in the *endo* or *exo* position.<sup>58</sup> Although explaining this discrepancy remained elusive, the high glass transition temperatures (ca. 120 °C) were attributed to the interaction of the functional groups with the rigid olefin backbone of poly(norbornene). Others have focused on incorporating cyclic rings into the backbone of the polymer and controlling the stereochemistry of the rings, with a positive correlation being seen between the  $T_g$  and the amount of *trans* stereochemistry.<sup>88-91</sup>

**Table 2.1.** Glass transition temperatures ( $T_g$ ) and melting temperatures ( $T_m$ ) of commercial polymers. Values were taken from reference 81.

Polymer	$T_g$ (°C)	$T_m$ (°C)
<i>cis</i> -Poly(butadiene)	-101	4
<i>cis</i> -Poly(isoprene)	-73	29
<i>trans</i> -Poly(isoprene)	-58	70
Linear Poly(ethylene)	-70 to -20	132
Poly(propylene)	-16	170
<i>trans</i> -1-4-Poly(butadiene)	-9	139
Nylon 6,6	47	235
Poly(methyl methacrylate)	49	155
Poly(vinyl chloride)	70	140
Poly(styrene)	94	227
Poly(carbonate)	152	267
Cellulose Triacetate	111	300
Poly(tetrafluoroethylene)	135	327
Poly( <i>para</i> -phenylene terephthalamide)	307-347	480

Alteration of the glass transition temperature of polymers through structural modifications can force a polymer to display traits originating from being in or out of the “glassy” state at certain temperatures. However, these techniques are still limited in that the polymer can only still exhibit the traits of either the glassy state or the freely moving state. In contrast, copolymers, defined as polymers containing monomeric units from multiple monomer species, have found many industrial applications due to the being able to display a combination of properties unique to the individual homopolymers. For example, copolymerization of acrylonitrile with monomers bearing halogen functional groups yields flame retardant properties, whereas solubility can be increased with the copolymerization of acrylonitrile and methyl or vinyl acetate.<sup>14</sup> In a similar vein, triblock copolymers of poly(styrene)-*block*-poly(butadiene)-*block*-poly(styrene) exhibit elastic traits originating from the poly(butadiene) component while also showing improved durability due to poly(styrene).<sup>92</sup> As such, these types of materials that show a two phase system have found usage as thermoplastic elastomers since the stiffness and durability of these materials allow them hold their structure, but at the same time can be molded at higher temperatures.

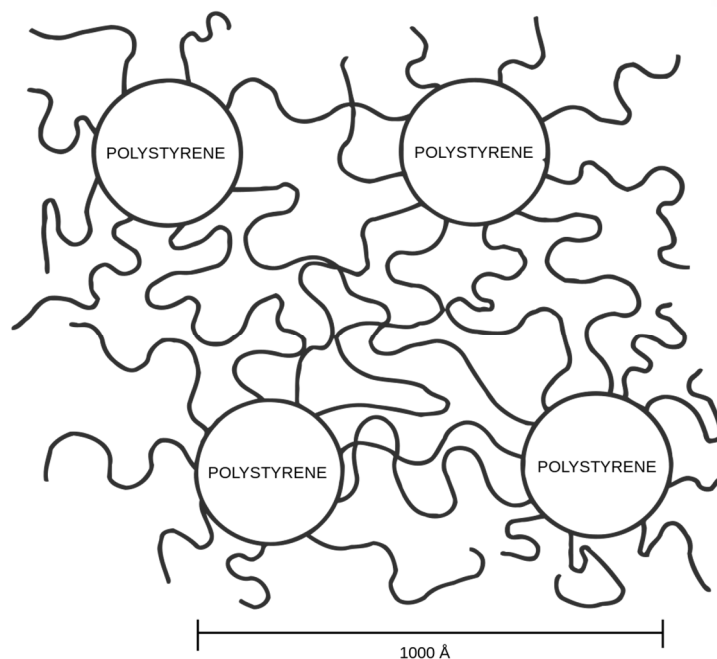


**Figure 2.2.** Representative illustration of the phase separation between poly(styrene) and poly(butadiene) in a poly(styrene)-*block*-poly(butadiene)-*block*-poly(styrene) block copolymer. Poly(styrene) is represented by the spheres while the segmental lines represent polymer chains of poly(butadiene). Adapted from reference 93.

As shown in Figure 2.2, poly(styrene)-*block*-poly(butadiene)-*block*-poly(styrene) exhibits the combined properties of both poly(styrene) and poly(butadiene) because the separate components are incompatible and thus able to phase separate.<sup>93</sup> Likewise, block copolymers that are able to phase separate have found applications in creating micellar morphologies,<sup>94-96</sup> as physical cross linkers,<sup>97</sup> and as drug delivery agents.<sup>98-99</sup> Although many factors need to be considered for determining the level of incompatibility between two polymers, a simplified explanation would be “like likes like”. From an enthalpy point of view, components of polymer chains possessing the same or similar structures will want to pack into an ordered structure while entropy favors complete miscibility. Therefore, when the enthalpic energy generated from the packing of polymer chains can overcome the entropic penalty, phase separation occurs. This explains why random copolymers, which, due to their random nature, do not have long segments consisting of a single monomeric unit, are entropically favored and often do not phase separate, while block copolymers, which can be polymerized so that each component is long enough to favor packing, can be made to phase separate. As discussed in the previous chapter, the development of well-defined catalysts has led to a multitude of living polymerization methods. Key among the characteristics of living polymerization is that the reactive center remains active at the end of the polymer chain even after complete monomer.

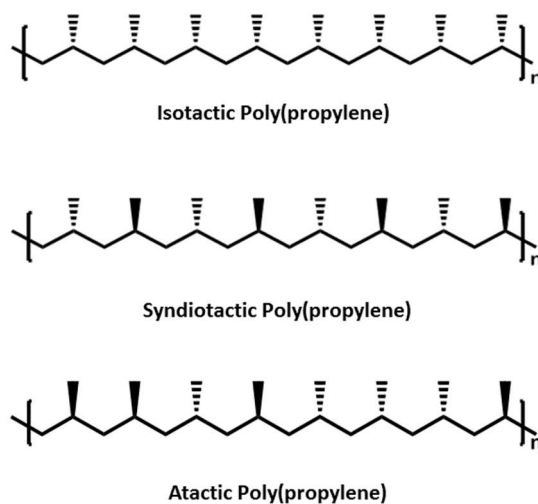
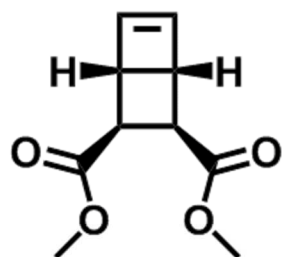


**Figure 2.3.** Representative illustration of isotactic, syndiotactic, and atactic poly(propylene).

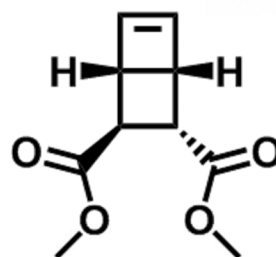
consumption. Therefore, block copolymers comprised of long segments of each individual component is possible, and thus can be favored to phase separate

Through the development of well-defined catalysts that tolerate a diverse range of functional groups,<sup>48</sup> manipulation of a polymer's morphology and properties have been found to be possible by attaching and/or replacing substituents.<sup>58, 84-85, 100</sup> However, chelation and coordination effects of certain functional groups to the active metal center have been found to decrease catalytic activity, and thus, impede polymerization.<sup>101-102</sup> Alternatively, certain polymers possessing the same elemental composition but differing in their molecular structure have also led to differences in properties, with poly(propylene) being a representative example. As shown in Figure 2.3, poly(propylene) can be found in three different conformations. Isotactic poly(propylene) is defined as having all the methyl groups stereochemically configured in the same direction, while syndiotactic poly(propylene) has the methyl groups alternating in and out of the plane. Finally, atactic poly(propylene) has the position of the methyl groups randomly assorted throughout the backbone. Due to the stereoregularity of the methyl groups in isotactic and syndiotactic poly(propylene), the polymer chains can stack to create well-ordered structures.<sup>103-104</sup> As a result, although melting temperatures for both isotactic and syndiotactic poly(propylene) exist, the random nature of atactic poly(propylene) prevents the formation of a well ordered structure, and in turn, renders a melting temperature nonexistent. Furthermore, differences in the method that the polymer chains stack to create ordered structures in isotactic and syndiotactic poly(propylene) can be directly attributed to the stereochemistry of the methyl groups. This contrast in packing leads to isotactic and syndiotactic poly(propylene) having





dimethyl (1*R*,2*S*,3*R*,4*S*)-  
 bicyclo[2.2.0]hex-5-ene-  
 2,3-dicarboxylate



dimethyl (1*R*,2*S*,3*S*,4*S*)-  
 bicyclo[2.2.0]hex-5-ene-  
 2,3-dicarboxylate

**Figure 2.4.** Monomers (dimethyl (1*R*,2*S*,3*R*,4*S*)-bicyclo[2.2.0] hex-5-ene-2,3-dicarboxylate and dimethyl (1*R*,2*S*,3*S*,4*S*)-bicyclo[2.2.0] hex-5-ene-2,3-dicarboxylate) used for the polymerization of homo-, di-, and tri-block copolymers throughout this study. As can be seen, the monomers only differ in the stereochemistry of the diester functional groups.

different melting and glass transition temperatures.<sup>79, 105-106</sup> Although poly(propylene) remains the most studied polymer when determining the influence of stereoregularity on a polymer's properties, recent results involving similar effects on vinyl polymers,<sup>83, 86</sup> and acrylates<sup>107-109</sup> have been reported.

The polymers presented in this work were polymerized from monomers designed to impede chain movement (Figure 2.4). The presence of the cyclobutane scaffold, which was expected to “lock” the polymer in place,<sup>85</sup> combined with an unsaturated backbone when polymerized via ROMP, was expected to drastically immobilize the polymer,<sup>56</sup> leading to high  $T_g$  values. In addition, as the monomers only differ in the stereochemistry of the diester functional groups, differences in properties between polymers polymerized from the two different monomers could be attributed to stereochemical influences. In addition, block copolymers with components consisting of the stereochemical analogs were synthesized and shown to phase separate. These block copolymers were different from commonly reported block copolymers known to phase separate in that different functional groups or monomers differing drastically on a structural level (i.e. poly(butadiene) and poly(styrene)) were not needed to induce phase separation.

## 2.2. Results and Discussion

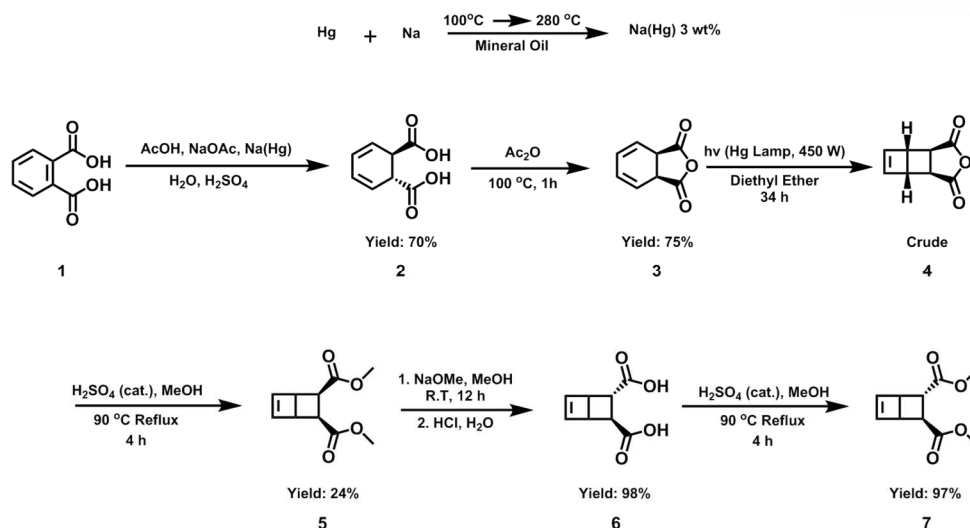
### 2.2.1. Synthesis of Monomers and Polymerization via ROMP

The route used to synthesize monomers **5** and **7** were modified from previously reported procedures<sup>110-111</sup> and is summarized in Scheme 2.1. Phthalic acid (**1**) was reduced using a 3 weight % sodium amalgam to afford **2**, which was purified by recrystallization in aqueous sulfuric acid and isolated in 70% yield. Subsequent dehydration of the 1,3-cyclohexadiene derivative using acetic anhydride afforded the corresponding anhydride **3**, which was purified by sublimation and collected in 75% yield as a white crystalline solid. With **3** in hand, photochemical isomerization was carried out in diethyl ether at room temperatures and monitored for completion by <sup>1</sup>H NMR spectroscopy, to afford **4**. Following removal of the residual solvent under reduced pressure, the crude product (**4**) was directly esterified with methyl alcohol in the presence of a catalytic amount of sulfuric acid to afford the monomer **5** as colorless liquid, which was purified via column chromatography.

The synthesis of the monomer **7** began with the epimerization of **5** using methyl alcohol and sodium methoxide. After removal of methanol under reduced pressure, acidification using a 1 N hydrochloric acid solution afforded **6** with a 98% yield after extraction. The dicarboxylic acid (**6**) was then esterified with methyl alcohol in the presence of a catalytic amount of sulfuric acid. Subsequent removal of methanol afforded **7** as a clear liquid in 97% yield after extraction. To ensure purification, both **5** and **7** were distilled prior to polymerization.

With monomers **5** and **7** in hand, initial efforts began with the polymerizations of **5** and **7** with the Grubbs 3<sup>rd</sup> generation catalyst (G3) to produced polymers **8** and **9** respectively (Scheme 2.2). Dependent on the targeted molecular weight (see Table 2.2 for monomer to catalyst ratios), G3 was added to an anhydrous dichloromethane solution of monomer **5** (0.2M) and stirred under a nitrogen atmosphere at ambient temperature. Quenching of the reaction using ethyl vinyl ether after 30 minutes followed by precipitation in cold hexane afforded polymer **8**. Polymerization of homopolymer **9** was done following the same procedure with the replacement of monomer **5** with monomer **7** (See Table 2.2. for yields).

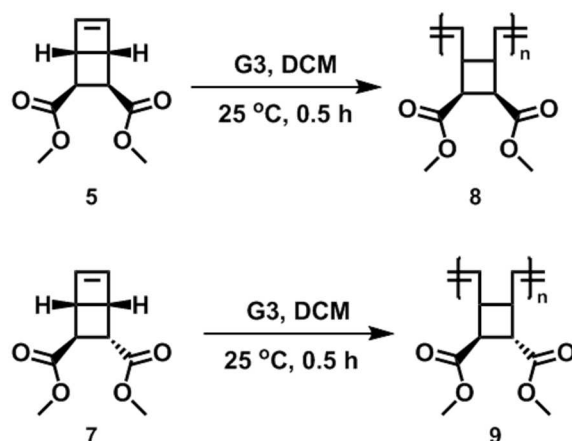
Previous reports have shown that properties of polymers, especially mechanical and thermal properties, increase with increasing degrees of polymerization and eventually reach an asymptotic value.<sup>15-19</sup> Polymers with short chain lengths offer little to no resistance as they move about in solution. Naturally, at low molecular weights, or low degrees of polymerization, polymers will often



**Scheme 2.1.** Synthetic scheme for dimethyl (1R,2S,3R,4S)-bicyclo[2.2.0]hex-5-ene-2,3-dicarboxylate (**5**) and dimethyl (1R,2S,3S,4S)-bicyclo[2.2.0]hex-5-ene-2,3-dicarboxylate (**7**).

exhibit little to no tensile strength and be soft in nature. However, as the chain lengths increase, the individual polymer chains begin to entangle and physically crosslink with each other. As a result, movement of the polymer chains becomes hindered, which increases the viscosity and the mechanical properties. Once the polymer's molecular weight reaches a certain point, the rate of disentanglement of the polymer chains becomes equal to the rate of entanglement and thus no longer influences the properties of the polymer.<sup>14</sup> Therefore, to ensure that the properties of the polymers were independent of the molecular weight, homopolymers targeted at various molecular weights (see Table 2.2. for monomer to catalyst ratios) were attempted and successfully polymerized.

As the formation of block copolymers require the reactive center to remain active at the end of the polymer chain even after complete monomer consumption,<sup>43</sup> a series of experiments designed to determine if the polymerization proceeded under a living manner were undertaken before the polymerization of copolymers were attempted. In order to be considered living, the polymerization must 1) proceed until all the monomer is consumed, upon which polymerization will continue with the addition of additional monomer, 2) the number average molecular weight ( $M_n$ ) and the monomer to catalyst ratio ( $M/C$ ) must show a linear correlation, 3) polymers with narrow molecular weight distributions are produced, and 4) upon complete consumption of the initial monomer, addition of a different monomer should produce a block copolymer.<sup>43</sup> As seen in Figure 2.4, a linear correlation between the  $M_n$  and the monomer to catalyst ratio of the polymers was confirmed. In addition, all of the polymers exhibited a narrow polydispersity index ( $\mathcal{D}$ ). Confirmation that the metal catalyst remained active at the end of the polymer was evidenced by an increase in the  $M_n$  of the polymer



**Scheme 2.2.** Polymerization of homopolymers **8** and **9**.

**Table 2.2.** Molecular weights for the series of homopolymers **8** and **9**.

Entry	M/C <sup>a</sup>	Target M <sub>n</sub> (kDa)	M <sub>n</sub> <sup>b, c</sup> (kDa)	M <sub>w</sub> <sup>b, c</sup> (kDa)	Đ	Yield (%)
<b>8a</b>	<b>76</b>	<b>15.0</b>	<b>14.6</b>	<b>17.1</b>	<b>1.2</b>	<b>95</b>
<b>8b</b>	<b>102</b>	<b>20.0</b>	<b>20.0</b>	<b>23.6</b>	<b>1.2</b>	<b>87</b>
<b>8c</b>	<b>382</b>	<b>75.0</b>	<b>66.4</b>	<b>82.8</b>	<b>1.2</b>	<b>87</b>
<b>9a</b>	<b>76</b>	<b>15.0</b>	<b>16.6</b>	<b>18.6</b>	<b>1.1</b>	<b>89</b>
<b>9b</b>	<b>102</b>	<b>20.0</b>	<b>20.3</b>	<b>22.2</b>	<b>1.1</b>	<b>87</b>
<b>9c</b>	<b>382</b>	<b>75.0</b>	<b>62.8</b>	<b>69.8</b>	<b>1.1</b>	<b>87</b>

<sup>a</sup> Monomer to catalyst ratios (M/C) were calculated using the total amount of monomer. <sup>b</sup> Values were determined relative to poly(styrene) standards in tetrahydrofuran. <sup>c</sup> See Appendix C for GPC chromatograms.

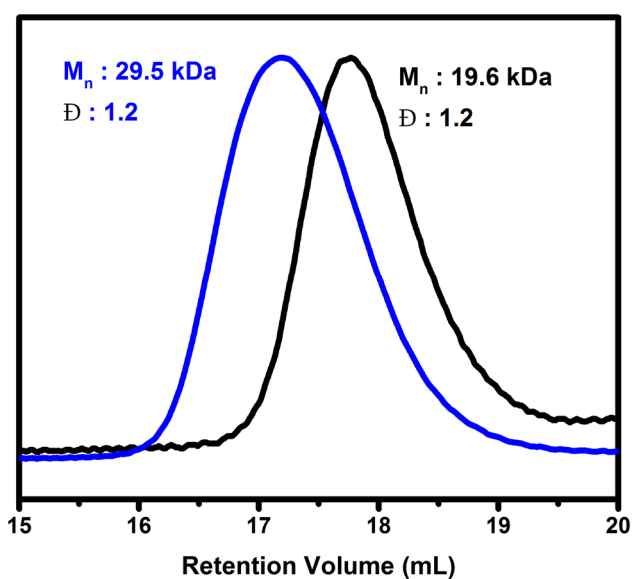
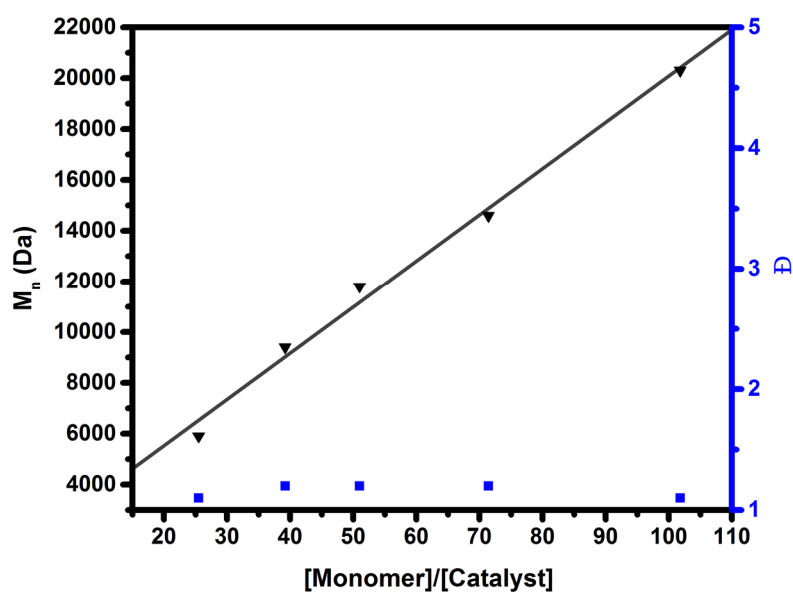


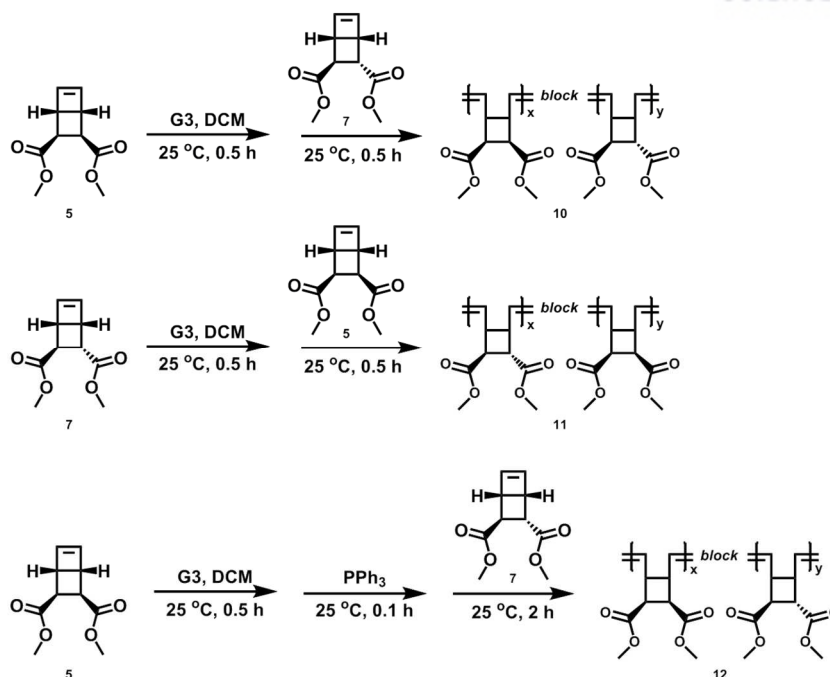
**Figure 2.4.** Molecular weight control of polymers synthesized from **5** (a) and block copolymer formation upon the addition of **7** after consumption of **5** (b). All measurements were taken using THF as the mobile phase at a flow rate of 0.8 mL/min. Molecular weights and polydispersity were determined relative to poly(styrene) standards in tetrahydrofuran.

upon addition of **7** after the complete consumption of **5** (Figure 2.4). The results of these experiments confirmed that the polymerization was proceeding through a well-controlled manner, and correspondingly that the formation of block copolymers was possible.

With confirmation that the polymerization of block copolymers was possible using G3, diblock copolymers with both **5** and **7** being the initiating block were attempted (Scheme 2.3). Similar to the polymerization of the homopolymers, G3 (see Table 2.3 for monomer to catalyst ratios), was added to an anhydrous dichloromethane solution of monomer **5** (0.2M) and stirred under a nitrogen atmosphere at an ambient temperature for 30 minutes. After confirmation of complete monomer consumption via thin layer chromatography, monomer **7** was dissolved in a minimal amount of anhydrous dichloromethane and injected. After allowing for the polymerization to proceed for 30 minutes at room temperature under a nitrogen atmosphere, the reaction was quenched with ethyl vinyl ether. Subsequent precipitation in cold hexane afforded diblock copolymer **10** (See Table 2.3. for molecular weights and yields). Polymerization of diblock copolymer **11** was done following the same procedure except G3 was added to a 0.2 M dichloromethane solution of monomer **7** and monomer **5** was added after confirmation of complete consumption of **7**.

As shown in Table 2.3, the series of diblock copolymers **10** and **11** displayed molecular weight values close to those of theoretical values with narrow polydispersity index's ( $\bar{D}$ ). However, the GPC traces of **10f** consistently exhibited a bimodal signal (see Appendix C). Methods such as lowering the temperature and varying the monomer concentration to drive the reaction toward polymer formation<sup>112-113</sup> proved unsuccessful. On the hypothesis that the issues were initiation related, triphenyl phosphine was introduced before the addition of monomer **7**. Previous studies with G1 have shown that the addition of triphenyl phosphine increased the efficiency of polymerization.<sup>77</sup> As the rate of phosphine ligand exchange between triphenyl phosphine and tricyclohexylphosphine was found to be fast, exchange of the phosphine ligands lead to a G1 derivative containing a bulkier triphenyl phosphine ligand before initiation.<sup>77</sup> The triphenyl phosphine ligand, in turn, was found to be more labile, and thus allowed for better dissociation to the active state of the catalyst, which promoted faster rates of initiation ( $k_i$ ).<sup>77</sup> In addition, competition between the monomer and the excess phosphine for the active site of the catalyst during the propagation step was found to lower the rate of propagation ( $k_p$ ).<sup>77</sup> The combination of these two effects resulted in an increase in the  $k_i/k_p$  ratio, which is required for living polymerizations.<sup>48, 77</sup>

With the hope that similar effects would occur with G3 if the issues were indeed initiation related, polymerization of a block copolymer targeted at 200 kDa in the presence of excess triphenyl



**Scheme 2.3.** Polymerization of diblock copolymers **10-12**.

**Table 2.3.** Molecular weights for the series of diblock copolymers **10, 11, and 12**.

Entry	M/C <sup>a</sup>	Target M <sub>n</sub> (kDa)	1 <sup>st</sup> Block			2 <sup>nd</sup> Block			Yield (%)
			M <sub>n</sub> <sup>b, c</sup> (kDa)	M <sub>w</sub> <sup>b, c</sup> (kDa)	Đ	M <sub>n</sub> <sup>b, c</sup> (kDa)	M <sub>w</sub> <sup>b, c</sup> (kDa)	Đ	
<b>10a</b>	<b>76</b>	<b>15.0</b>	<b>9.4</b>	<b>11.3</b>	<b>1.2</b>	<b>15.7</b>	<b>18.0</b>	<b>1.2</b>	<b>95</b>
<b>10b</b>	<b>254</b>	<b>50.0</b>	<b>25.9</b>	<b>32.5</b>	<b>1.2</b>	<b>44.9</b>	<b>53.2</b>	<b>1.1</b>	<b>93</b>
<b>10c</b>	<b>510</b>	<b>100.0</b>	<b>53.9</b>	<b>65.7</b>	<b>1.2</b>	<b>92.8</b>	<b>106.3</b>	<b>1.2</b>	<b>89</b>
<b>10d</b>	<b>612</b>	<b>120.0</b>	<b>58.4</b>	<b>72.3</b>	<b>1.2</b>	<b>111.3</b>	<b>133.2</b>	<b>1.2</b>	<b>98</b>
<b>10e</b>	<b>762</b>	<b>150.0</b>	<b>68.0</b>	<b>82.0</b>	<b>1.2</b>	<b>118.7</b>	<b>134.2</b>	<b>1.1</b>	<b>95</b>
<b>10f<sup>d</sup></b>	<b>1020</b>	<b>200.0</b>	<b>117.3</b>	<b>130.1</b>	<b>1.1</b>	<b>173.0</b>	<b>210.7</b>	<b>1.2</b>	<b>90</b>
<b>11</b>	<b>76</b>	<b>15.0</b>	<b>7.0</b>	<b>8.2</b>	<b>1.2</b>	<b>16.2</b>	<b>21.1</b>	<b>1.3</b>	<b>80</b>
<b>12<sup>e</sup></b>	<b>1020</b>	<b>200.0</b>	<b>62.4</b>	<b>77.0</b>	<b>1.2</b>	<b>94.4</b>	<b>118.0</b>	<b>1.2</b>	<b>90</b>

<sup>a</sup> Monomer to catalyst ratios (M/C) were calculated using the total amount of monomer. <sup>b</sup> Values were determined relative to poly(styrene) standards in tetrahydrofuran. <sup>c</sup> See Appendix C for GPC chromatograms. <sup>d</sup> GPC traces consistently showed bimodal signals upon addition of the second block. <sup>e</sup> Polymerized in the presence of triphenyl phosphine.

phosphine was attempted. The same procedure outlined above was followed except prior to addition of monomer **7**, triphenyl phosphine (50 equivalents relative to the initiator) was added and stirred at an ambient temperature for 10 minutes. Subsequent GPC traces of **12** showed the disappearance of the bimodal signal (see Appendix C) and exhibited a narrow Đ. Yet, the number average molecular weight ( $M_n$ ) was significantly lower than the targeted value (see Table 2.3). As mentioned earlier, competition arises between the excess phosphine derivatives and the monomer for access to the active site of the catalyst.<sup>77</sup> Therefore, although the  $k_t/k_p$  ratio improved, the increased competition may create too much hindrance for complete monomer consumption. In addition, steric factors may also be playing a role in preventing monomer consumption. At low degrees of polymerization, the growing polymer chain would be relatively short and thus provide no steric hindrance to the incoming monomer. However, as the polymer continues to grow, one can imagine that the catalyst would be attached to a very long polymer chain. Once this chain reaches a certain length, the polymer could possibly garner enough flexibility to undergo long range segmental motion. This motion, in turn, could actively coordinate the diester groups of the polymer to the active center and/or hinder the trajectory of the incoming monomer. Therefore, impediment of the monomer by triphenyl phosphine, coupled with the additional hindrance of the growing polymer chain as it reaches higher molecular weights<sup>77</sup> may prevent complete monomer consumption, and ultimately, lead to  $M_n$  values lower than the initially targeted  $M_n$ .<sup>114</sup>

Although polymers **10a** and **11** are technically the same diblock polymer with similar molecular weights, initializing polymerization with **7** rather than **5** consistently led to higher Đ values. Investigations into this discrepancy revealed that the activity of both the Schrock's<sup>67</sup> and Grubbs'<sup>52, 58, 115-118</sup> catalysts were influenced by the stereochemistry of the functional groups; a decrease in catalytic activity was seen in the order of *exo, exo* > *exo, endo* > *endo, endo* for the polymerization of disubstituted norbornene. Although a definitive reason is yet to be proven, this trend was believed to be due to a combination of steric effects and functional group chelation to the transition metal catalyst. The substituents on *exo, exo* norbornene face away from the cyclic olefin. Therefore, the catalyst can gain access to the olefin regardless of whether the monomer approaches from above or below (see Figure 2.5). However, *endo, endo* norbornene has both of its substituents facing the cyclic olefin, which may hinder the approach of the monomer to the active site, and thus deactivate catalyst activity. In addition, if the substituents are oxygen containing functional groups, the closer proximity of the substituents to the active site in the *endo, endo* configuration may cause chelation of the oxygen atoms to the transition metal center, which would also result in a decrease in catalytic activity.<sup>52, 58, 115-118</sup>



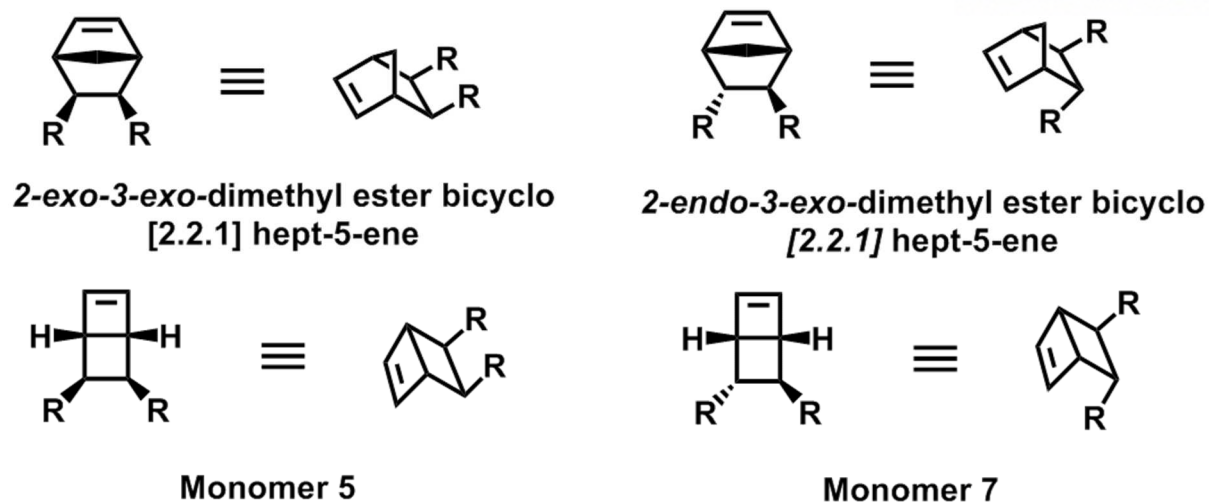
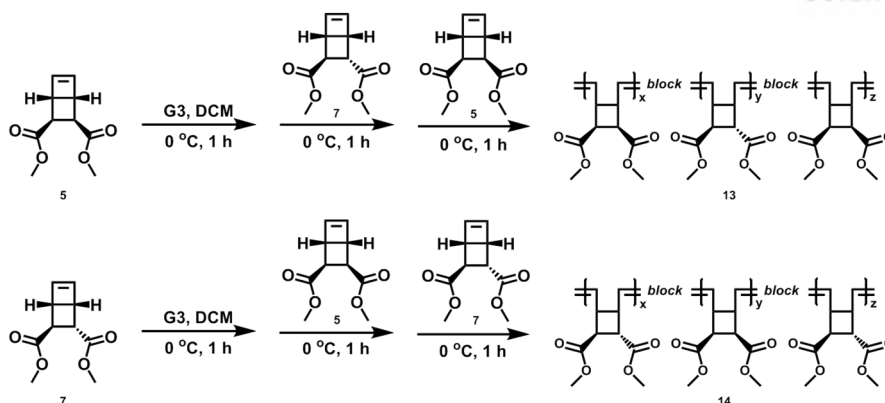


**Figure 2.5.** Comparison of 2-*exo*-3-*exo*-dimethyl ester bicyclo [2.2.1] hept-5-ene and 2-*endo*-3-*exo*-dimethyl ester bicyclo [2.2.1] hept-5-ene with monomers **5** and **7**. The methyl ester groups are represented by “R”.

As shown in Figure 2.5, monomer **5** resembles *exo, exo* norbornene and monomer **7** resembles that of *endo, exo* norbornene.<sup>119</sup> Due to the reasons outlined in the above, although the greatest decrease in catalytic activity is observed with *endo, endo* disubstituted norbornene analogs, molecules with substituents in the *endo, exo* position still exhibit a decrease in catalytic activity when compared with their *exo, exo* counterparts. Thus, a similar effect may be occurring with the polymerization of **7**, with the end result being a wider molecular weight distribution.

Triblock copolymers, such as poly(styrene)-*block*-poly(butadiene)-*block*-poly(styrene) exhibit higher durability and mechanical strength since the poly(styrene) components act as a physical cross-linker.<sup>93</sup> Hoping similar trends could be seen, the polymerization of triblock copolymers polymerized from monomers **5** and **7** were attempted (Scheme 2.4). Initial attempts at polymerizing the triblock copolymers at room temperature led to the appearance of bimodal signals in the GPC traces. Therefore, in an attempt to retard possible chain transfer reactions, the polymerizations were performed at 0 °C. Similar to the polymerization of the diblock copolymers, G3 (see Table 2.4 for monomer to catalyst ratios), was added to an anhydrous dichloromethane solution of monomer **5** (0.2M) and stirred under a nitrogen atmosphere at 0 °C temperature for 1 hour. After confirmation of complete monomer consumption via thin layer chromatography, monomer **7** was dissolved in a minimal amount of anhydrous dichloromethane and injected. After allowing for the polymerization to proceed for 1 hour at 0 °C, under a nitrogen atmosphere, complete monomer consumption was confirmed via thin layer chromatography. Monomer **5** was then again dissolved in a minimal



**Scheme 2.4.** Polymerization of triblock copolymers **13** and **14**.

**Table 2.4.** Molecular weights for the series of triblock copolymers **13-14**.

Entry	M/C <sup>a</sup>	Target M <sub>n</sub> (kDa)	1 <sup>st</sup> Block			2 <sup>nd</sup> Block			3 <sup>rd</sup> Block			Yield (%)
			M <sub>n</sub> <sup>b, c</sup> (kDa)	M <sub>w</sub> <sup>b, c</sup> (kDa)	Đ	M <sub>n</sub> <sup>b, c</sup> (kDa)	M <sub>w</sub> <sup>b, c</sup> (kDa)	Đ	M <sub>n</sub> <sup>b, c</sup> (kDa)	M <sub>w</sub> <sup>b, c</sup> (kDa)	Đ	
<b>13a</b>	76	15.0	5.9	6.7	1.1	10.5	11.7	1.1	16.4	19.2	1.2	93
<b>13b<sup>d</sup></b>	153	30.0	10.0	12.7	1.2	20.0	21.3	1.2	30.0	32.3	1.7	88
<b>14a</b>	76	15.0	5.9	6.8	1.2	12.4	15.5	1.2	18.7	21.7	1.2	80
<b>14b<sup>d</sup></b>	153	30.0	14.0	16.3	1.2	16.5	20.3	1.2	23.7	36.5	1.5	91

<sup>a</sup> Monomer to catalyst ratios (M/C) were calculated using the total amount of monomer. <sup>b</sup> Values were determined relative to poly(styrene) standards in tetrahydrofuran. <sup>c</sup> See Appendix C for GPC chromatograms. <sup>d</sup> GPC traces consistently showed bimodal signals upon addition of the third block.

amount of anhydrous dichloromethane and injected with the subsequent polymerization allowing to proceed for 1 hour at 0 °C, under a nitrogen atmosphere. After confirmation that the monomer was completely consumed, the reaction was quenched with ethyl vinyl ether. Subsequent precipitation in cold hexane afforded triblock copolymer **13** (See Table 2.4. for molecular weights and yields).

Polymerization of triblock copolymer **14** was done following the same procedure except G3 was added to a 0.2 M dichloromethane solution of monomer **7** and monomer **5** was added after confirmation of complete consumption of **7**, followed by addition of monomer **7** again after consumption of **5**. As shown in Table 2.4, although the triblock copolymers targeted at lower molecular weights (**13a** and **14a**) were successfully polymerized, attempts at higher molecular weight polymers led to broad Đ's as well as the appearance of bimodal signals in the gel permeation chromatograms (GPC) traces (see Appendix C).

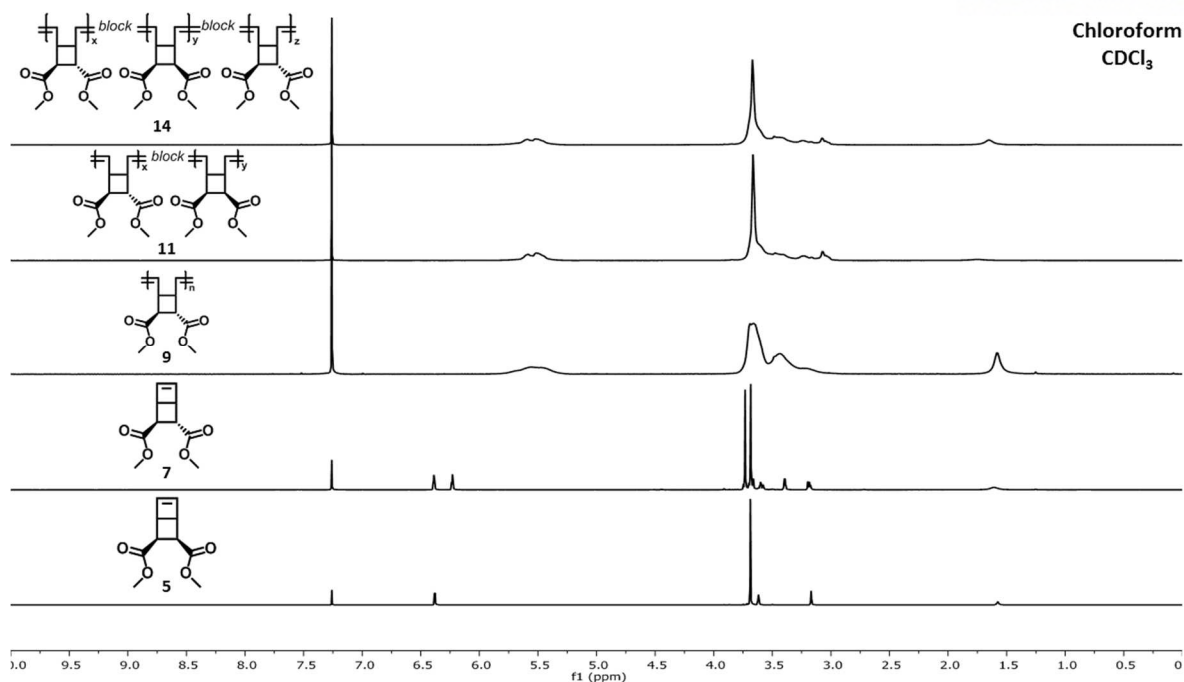


**Figure 2.6.** Representative  $^1\text{H}$  NMR spectra for the monomers, homo-, di-, and tri-block copolymers. All measurements were taken at ambient temperature in deuterated chloroform ( $\text{CDCl}_3$ ).

As shown in the tables for each of the polymerizations, gel permeation chromatography (GPC) confirmed that the polymerizations proceeded in a monodisperse manner and possessed number average molecular weights ( $M_n$ ) in the range of the theoretical values. Likewise,  $^1\text{H}$  NMR spectra of the polymers also revealed broadening of the signals as well as an upfield shift ( $\delta$  5.5-5.8 ppm;  $\text{CDCl}_3$ ) of the signals corresponding to the protons on the cyclobutene ring of the monomer ( $\delta$  6.2-6.4 ppm), which was expected if ring opening had occurred (Figure 2.6). Broadening of the  $^1\text{H}$  NMR signals upon polymerization was also expected as polymers are a distribution of molecular weights, which, in turn, leads to a wider range of different chemical environments.

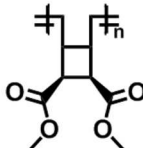
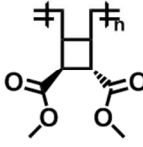
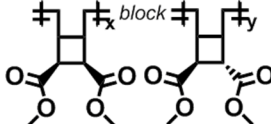
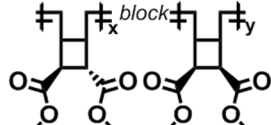
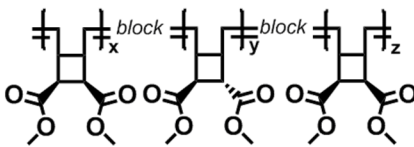
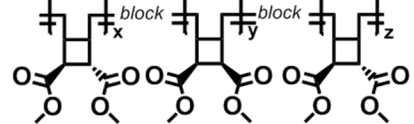
Living polymerization via utilization of the Grubbs 3<sup>rd</sup> generation catalyst to afford homo-, diblock, and triblock polymers from monomers **5** and **7** was proven to be successful. Although attempts toward polymerizing higher molecular weight ( $M_n > 15$  kDa) triblock copolymers were unsuccessful, diblock copolymers targeted up to 150 kDa were successfully polymerized with narrow molecular weight distributions ( $\mathcal{D} \leq 1.2$ ). Physical characterizations by  $^1\text{H}$  NMR and IR spectroscopy (see Appendix B) showed no significant differences between all the various types of polymers, though differences in thermal properties, as will be discussed in the following section, were expected.

## 2.2.2. Stereochemical Influences on the Thermal Properties of Strained Poly(alkenamer)s

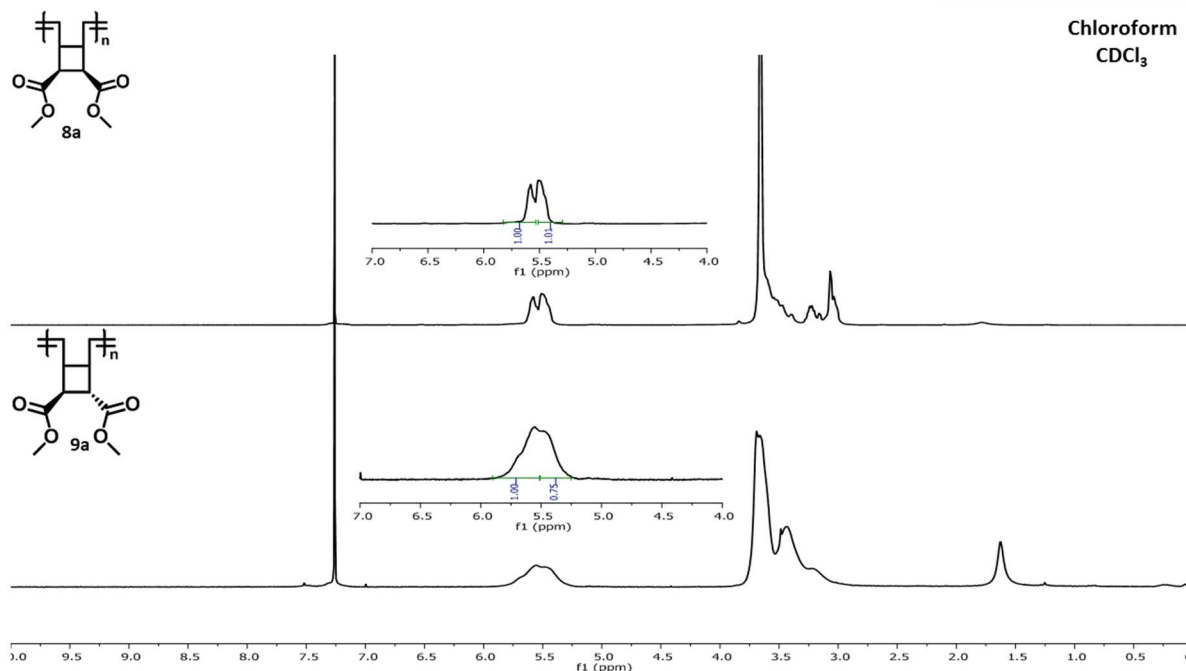
With the homopolymers, diblock copolymers, and triblock copolymers of varying molecular weights in hand, experiments to analyze the thermal properties of the polymers were undertaken. Interestingly, as shown in Table 2.5, although both **8a** and **9a** showed relatively high glass transition temperatures (see Table 2.1 for  $T_g$  values of commercial polymers), they had different thermal properties. The high glass transition temperatures could be attributed to a combination of the olefinic double bonds within the backbone of the polymers and the presence of a rigid cyclobutane scaffold. For polymers linked through a  $sp^3$ -hybridized carbon backbone, free rotation around the single bonds is possible, which favors increased movement.<sup>15, 83-85</sup> However, when a polymer is connected through  $sp^2$ -hybridized carbons, the backbone becomes locked in place, which increases the rigidity of the polymer.<sup>56</sup> This, in turn, makes it so that more energy is needed to make the polymers move, which in turn, correlates to a higher  $T_g$ . Further immobilization was attributed to the cyclobutane scaffold, as the cyclic ring would “lock” the polymer in place and prevent functional group rotation.<sup>85</sup>

Polymer **9a** (entry 2 in Table 2.5) exhibits a decomposition temperature and glass transition temperature approximately  $23\text{ }^\circ\text{C} \pm 3\text{ }^\circ\text{C}$  higher than that of its stereochemical isomer **8a** (entry 1 in Table 2.5). Although rare, similar trends, though to a lesser degree in magnitude, are observed in compact polymers, such as poly(propylene).<sup>79, 105-106, 120</sup> Isotactic poly(propylene), where the methyl groups are all on the same side, has a lower  $T_g$  (ca.  $5\text{ }^\circ\text{C}$ ) than that of syndiotactic poly(propylene), where the methyl groups alternate in and out of the plane with each repeat unit.<sup>106</sup> This difference in temperature was attributed to the polymer chains of syndiotactic poly(propylene) being able to get in closer proximity to each other, which ultimately hinders the free movement of the polymer chain.<sup>79, 105-106, 120</sup> Consequently, more energy is required to allow the polymers to move about freely, which directly translates to a higher  $T_g$ . Additional studies on a variety of different types of polymers have concluded that polymers exhibiting *trans* stereochemistry within the polymer backbone favored closer interactions between the polymer chains. Similar to syndiotactic poly(propylene), closer interactions lead to immobilization of the polymer backbone, and ultimately results in a decrease in the segmental motion of the polymer. Thus, more energy would be required for the polymer to have enough movement to reach a “rubbery” state, which in turn, translated to a higher  $T_g$ .<sup>88-91</sup> Although the polymers presented here do possess a rigid olefin backbone, they differ from previous works in that the functional groups of the polymers only differ in stereochemistry and also no modifications were made to the polymer backbone. As a result, the explanations for the differences in  $T_g$  values outlined above do not seem to apply to the polymers in this work.

**Table 2.5.** Glass transition temperature ( $T_g$ ) and decomposition temperature ( $T_d$ ) values for homopolymers, diblock copolymers, and triblock copolymers polymerized with a target  $M_n$  of 15 kDa. See Appendix D and E for TGA and DSC traces.

Entry	Polymer	Structure	$M_n^a$ (kDa)	$T_d^b$ (°C)	$T_g^c$ (°C)
1	8a		14.6	223.8	68.7
2	9a		16.6	241.0	92.0
3	10a		15.7	227.4	78.1
4	11		16.2	225.9	79.2
5	13a		16.4	227.3	75.3
6	14a		18.7	232.6	82.9

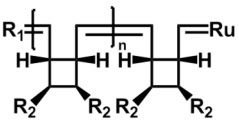
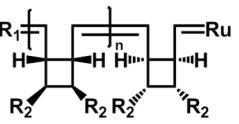
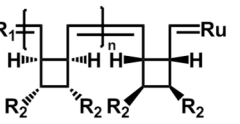
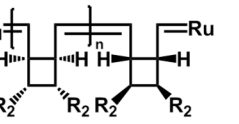
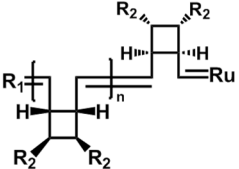
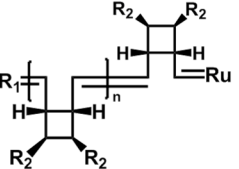
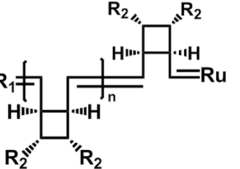
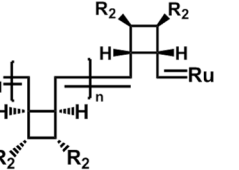
<sup>a</sup>  $M_n$  values were determined relative to poly(styrene) standards in THF. <sup>b</sup> Thermal decomposition ( $T_d$ ) measurements were done at a heating rate of 10 °C min<sup>-1</sup> under a nitrogen atmosphere. The  $T_d$  was determined to be the temperature of the inflection point between 0-50% weight loss. <sup>c</sup> Samples underwent two heating and cooling cycles at a rate of 20 °C min<sup>-1</sup> under a nitrogen atmosphere prior to determination of the glass transition temperature ( $T_g$ ). The  $T_g$  values were determined from the DSC traces of the third heating cycle.



**Figure 2.7.**  $^1\text{H}$  NMR of **8a** (top) and **9a** (bottom). Integration of the olefin region showed a 1:1 *trans* to *cis* ratio for **8a** and a 1:0.75 *trans* to *cis* ratio for **9a**. All measurements were taken at ambient temperature in deuterated chloroform ( $\text{CDCl}_3$ ).

Analysis of the olefin region in the  $^1\text{H}$  NMR spectra of polymers **8a** and **9a** revealed that polymer **9a** possessed a higher *trans* to *cis* ratio (1.0 to 0.75) than **8a** (1.00 to 1.00) (Figure 2.7). A higher *trans* concentration, as mentioned above within the polymer backbone would favor stacking of the polymer chains, and thus increase the glass transition temperature, as free movement of the polymer chains would be hindered. Efforts to rationalize the differences in stereochemistry along the polymer backbone led us to believe that the stereochemistry of the diester substituents were the underlying cause. As mentioned in the previous section, the position of the disubstituted substituents on norbornene derivatives were found to influence the catalytic reactivity of the Grubbs' catalyst.<sup>52, 58, 115-118</sup> Although slightly higher molecular weight distributions were observed when monomer **7** was used to initiate the diblock copolymers instead of monomer **5**, the large release of enthalpic energy from the ring opening of the highly strained cyclobutene negated any possible decrease in catalytic activity. However, the steric effects of the substituents may play a role in the formation of a higher *trans* containing backbone. Table 2.6 outlines the possible ways that monomer **5** could attach to the growing polymer chain of **8**. In addition to possibly attaching to the polymer backbone in a *cis* or *trans* manner, the monomer can bond head to head, head to tail, tail to head, or tail to tail. However, regardless of how monomer **5** attaches, the substituents are facing away from the olefin. Thus, as shown in Figure 2.8, the incoming monomer faces no steric hindrance regardless of the pathway it

**Table 2.6.** Comparison of possible structures that monomer **5** can attach to the growing polymer chain.

Backbone Configuration	Head to Head	Head to Tail	Tail to Head	Tail to Tail
<i>cis</i> $R_2 = \text{COOME}$				
<i>trans</i> $R_2 = \text{COOME}$				

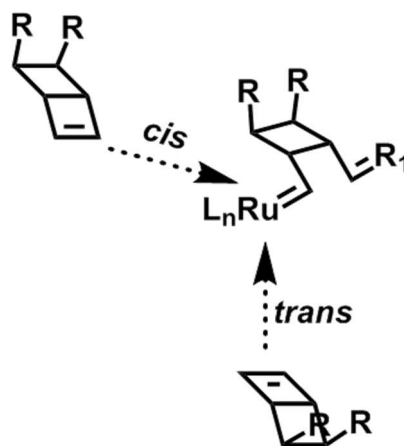


**Figure 2.8.** Proposed addition of monomer **5** to the growing polymer chain. Since the functional groups are facing away from the olefin, no steric hindrance from the functional groups would be expected regardless of whether the monomer adds *cis* or *trans* to the polymer chain. The methyl ester groups are represented by “R”.

takes to attach to the growing polymer chain, leading to an equal opportunity for the incoming monomer unit to adopt any of the structures outlined in Table 2.6. As such, a 1.00 to 1.00 *trans* to *cis* ratio would be possible, as observed.

Table 2.7 shows the possible structures that can arise with the addition of monomer **7** to a growing polymer chain of polymer **9**. Unlike **8**, outcomes involving the addition of the monomer *cis* to the growing polymer chain would be sterically hindered by the methyl ester group facing the olefin. Therefore, as monomer **8** approaches the growing polymer chain, it is more likely to add in a *trans* configuration (Figure 2.9). As expected, analysis of the olefinic region of **9a** showed a 1.00 to 0.75 *trans* to *cis* ratio, implying that the backbone of polymer **9a** possessed a higher *trans* content. This trend was found to be independent from molecular weight as all the polymers of the **8** and **9** series exhibited this trend.

As seen in Table 2.5, both the diblock (**10a**, **11**) and triblock (**13a**, **14a**) copolymers exhibited a decomposition temperature between that of the two homopolymers. Likewise, only a single  $T_g$  located between the two  $T_g$ 's of homopolymers **8a** and **9a** was found upon analysis of the differential scanning calorimetry (DSC) traces. These results implied that the components of the block copolymer were not phase separated.<sup>121-122</sup> Although unfortunate, these results were not unexpected since phase separation within block copolymers usually occurs between two distinctly different blocks,<sup>122-124</sup> such as with poly(styrene) and poly(isoprene).<sup>125</sup> As the components of the diblock and triblock copolymers only differ in the stereochemistry of the disubstituted methyl ester groups, we believed that phase separation was not arising due to the high structural similarity between the components of the block copolymer.

The interaction of polymers with solvents or other polymers can be predicted using the Flory interaction parameter ( $\chi$ ), which can further be derived to reflect its correlation to the degree of polymerization.<sup>82, 126</sup> The derived equation can be expressed as:

$$\chi_c = \frac{(N_B^{0.5} + N_A^{0.5})^2}{2N_A N_B}$$

where  $\chi_c$  symbolizes the critical value upon which phase separation occurs and  $N_a$  and  $N_b$  represent the degree of polymerization for polymers A and B respectively.<sup>126</sup> Based on the assumption that polymer chains are governed by van der Waal interactions ( $\chi \geq 0$ ), the equation predicts a critical point



**Table 2.7.** Comparison of possible structures that monomer 7 can attach to the growing polymer chain.

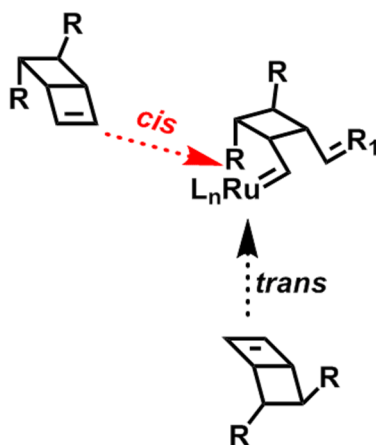
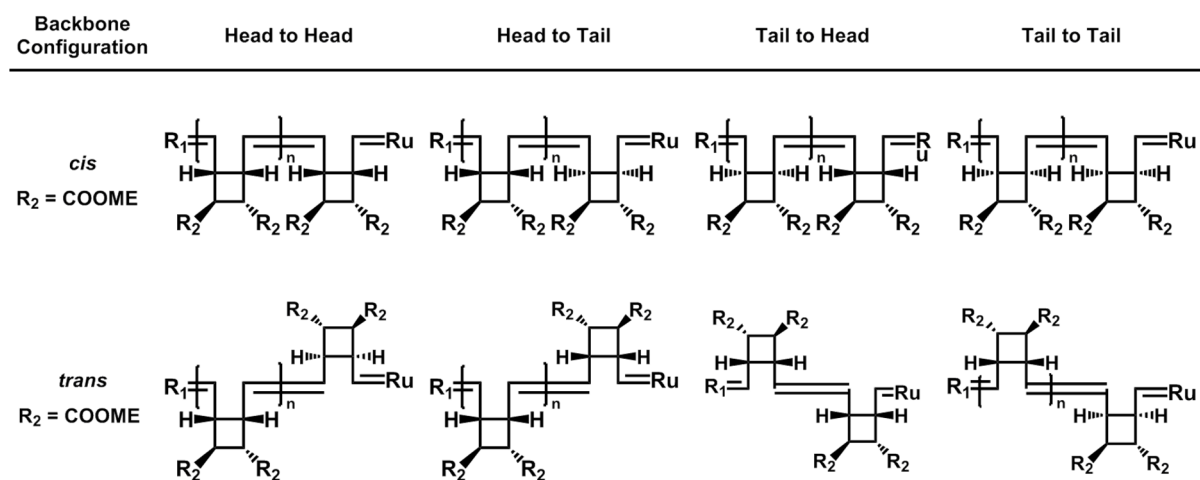
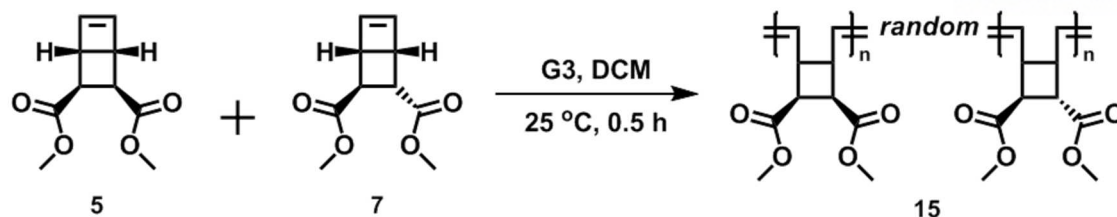


**Figure 2.9.** Proposed addition of monomer 7 to the growing polymer chain. Since one of the functional groups faces the olefin, steric hindrance from the functional groups would be expected when the monomer adds *cis* to the polymer chain (red). Thus, addition *trans* to the polymer chain would be expected to be favored. The methyl ester groups are represented by “R”.

value ( $\chi_c$ ) where the van der Waal interaction between the similar components of polymer chains overcome the loss of entropy. Once this point is reached or exceeded, the release of enthalpic energy from the stacking of polymer chains would overcome the entropic penalty and lead to phase separation.<sup>126</sup> As such, one can expect this critical point to decrease with increasing incompatibility between the components and vice versa. Thus, if  $\chi_c$  is a large number, increasing the degree of polymerization for either or both components ( $N_A$ ,  $N_B$ ) would be necessary to instigate phase separation.

In order to determine if phase separation could be possible with higher degrees of polymerization, homopolymers **8b** and **9b** as well as **8c** and **9c** were dissolved in dichloromethane and precipitated. In addition, random copolymers targeted at 20 kDa (**15a**) and 75 kDa (**15b**) were polymerized as well (Scheme 2.5, Table 2.8). As random copolymers have the monomer units randomly placed within the polymer chain, long segments originating from individual monomeric units would not be present. Thus, stacking between similar components would not be viable and phase separation would not be expected to occur. However, if the physical mixtures did not show any phase separation, phase separation of block copolymers would be unrealistic. As expected, random copolymers **15a** and **15b** showed single  $T_d$  and  $T_g$  values in between those of **8b** and **9b** and **8c** and **9c** respectively. In contrast, although a physical mixture of homopolymers **8b** and **9b** once again exhibited a single  $T_g$  at a temperature between the  $T_g$ 's of the respective homopolymers (entry 4 in Table 2.9), physical mixtures of homopolymers **8c** and **9c** exhibited two separate glass transition temperatures that were similar to the glass transition temperatures of the homopolymers (entry 8 in Table 2.9). Thus, the critical point at which phase separation occurs seemed to require a degree of polymerization value between 102 and 382, which corresponded to a molecular weight between 20 and 75 kDa per block. Although these values may appear high, degrees of polymerizations up to 7,700 were required to observe phase separation between poly(ethylene) and deuterated poly(ethylene).<sup>127</sup> Likewise, phase separation between branched poly(ethylene) and linear poly(ethylene) was not observed until  $M_w$  values exceeding 70 kDa per block were reached.<sup>128</sup>

With the knowledge of the general degree of polymerization needed to induce phase separation, efforts were directed toward synthesizing high molecular weight block copolymers (see Section 2.2.1 for synthetic details). As mentioned in the previous section, attempts at higher molecular weight triblock copolymers (polymers **13b** and **14b**) were unsuccessful. However, the diblock copolymers were successfully polymerized up to molecular weights targeted at 200 kDa. Therefore, the thermal properties of diblock copolymers targeted at 25 kDa (**10b**), 50 kDa (**10c**), 60 kDa (**10d**), and 75 kDa (**10e**) per block were analyzed (Table 2.10). Although no significant changes were



**Scheme 2.5.** Polymerization of random copolymer **15**.

**Table 2.8.** Catalyst loading and yields for the series of random copolymer **15**.

Entry	M/C <sup>a</sup>	Target M <sub>n</sub> (kDa)	M <sub>n</sub> <sup>b, c</sup> (kDa)	M <sub>w</sub> <sup>b, c</sup> (kDa)	Đ	Yield (%)
<b>15a</b>	<b>102</b>	<b>20.0</b>	<b>23.5</b>	<b>23.6</b>	<b>1.1</b>	<b>84</b>
<b>15b</b>	<b>382</b>	<b>75.0</b>	<b>62.8</b>	<b>69.8</b>	<b>1.1</b>	<b>82</b>

<sup>a</sup> Monomer to catalyst ratios (M/C) were calculated using the total amount of monomer. <sup>b</sup> Values were determined relative to poly(styrene) standards in tetrahydrofuran. <sup>c</sup> See Appendix C for GPC chromatograms.

observed in the decomposition temperatures between the copolymers, diblock copolymers **10d** and **10e** (entries 6 and 7 in Table 2.10) exhibited two separate glass transition temperatures that aligned with the glass transition temperatures of homopolymers **8c** and **9c** (entries 1 and 2 Table 2.10). Thus, phase separation of two components that only differed in the stereochemistry of its substituents was found to be successful by increasing the degree of polymerization.

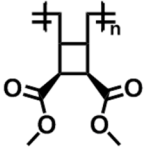
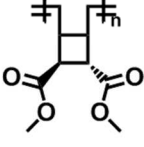
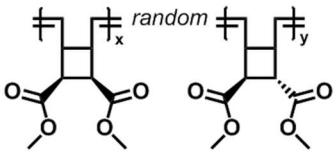
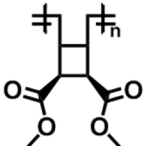
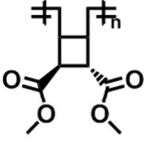
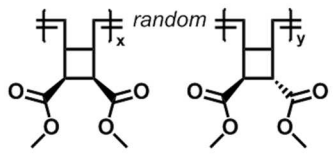
To confirm our hypothesis that the differences in glass transition temperatures were due to stereochemical influences within the polymer backbone, polymer **10e** was hydrogenated (Scheme 2.6). As previously mentioned, homopolymer **9** were believed to have a higher T<sub>g</sub> than **8** due to the steric hindrance of the ester group favoring monomer addition *trans* to the growing polymer chain. A higher *trans* content subsequently leads to closer interactions between the polymer chains, which results in a higher glass transition temperature. Saturation of the polymer backbone via hydrogenation however, would allow for rotation along the backbone, which would increase the movement of the polymer chains. Therefore, if the underlying cause for the observed differences in the T<sub>g</sub> are due to the stereochemistry of the polymer backbone, the glass transition temperatures of **10e** should not only decrease, but also exhibit only one T<sub>g</sub> after hydrogenation. Successful hydrogenation of polymer **10e** to polymer **16** using a palladium on carbon catalyst was confirmed via the disappearance of the olefinic signals ( $\delta$  5.5-6) in the <sup>1</sup>H NMR spectrum (see Appendix A) as well as the slight increase in molecular weight post hydrogenation (see Table 2.11). DSC measurements of **16** showed only a single glass transition temperature at ca. 70 °C (see Table 2.11). These results

strongly implied that the thermal properties of homopolymers **8** and **9** were due to the stereochemical differences within the polymer backbone.

### 2.3. Conclusions

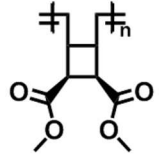
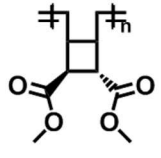
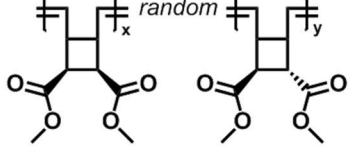
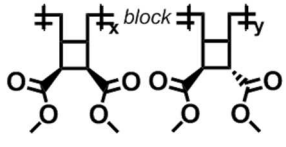
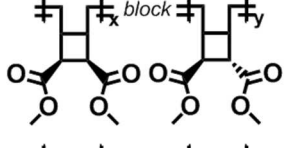
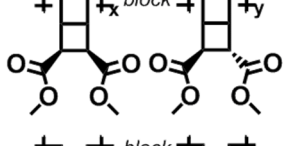
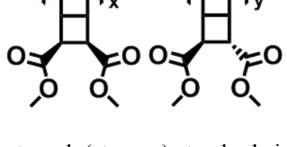
Homopolymers exhibiting different thermal properties as well as diblock copolymers being able to phase separate were successfully polymerized at high molecular weights with narrow molecular weight distributions from monomers with compact structures differing only in the stereochemistry of their substituents. Although the addition of large bulky functional groups and the utilization of polymers that are incompatible with each other are often employed to invoke different thermal properties and phase separation respectively, the polymers presented here require no additional functionalization to exhibit similar differences. These properties were attributed to differences within the stereochemistry of the polymer backbone, as confirmed by hydrogenation of a phase separated diblock copolymer. Although the same catalyst was used for the polymerization of **5** and **7**, stereochemical differences within the polymer backbone occurred due to the influence of the stereochemistry of the disubstituted functional groups. Thus, the thermal properties exhibited in the polymers presented here are the product of a stereochemical effect, which is the result of a different stereochemical effect. As such, compact monomers with the same chemical formula and similar structures can be utilized to form homopolymers and diblock copolymers that possess different thermal properties and can phase separate due to influences originating from stereochemistry.

**Table 2.9.** Glass transition temperature ( $T_g$ ) and decomposition temperature ( $T_d$ ) values for homopolymers, physical mixtures of homopolymers, and random copolymers of different molecular weights.

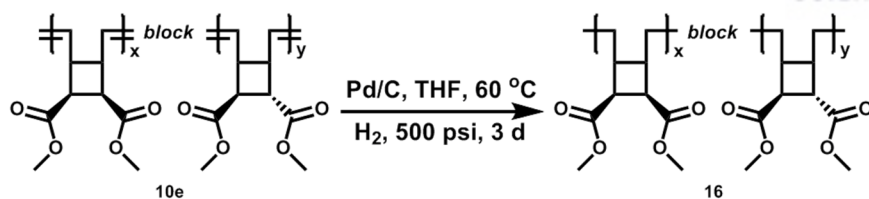
Entry	Polymer	Structure	$M_n^a$ (kDa)	$T_d^b$ (°C)	$T_g^c$ (°C)
1	8b		23.6	221.0	67.8
2	9b		20.3	241.1	94.1
3	15a		20.5	233.2	78.9
4	-	Physical Mixture of Polymers 8b & 9b	-	-	74.7
5	8c		66.4	224.1	72.6
6	9c		50.5	240.4	99.5
7	15b		62.8	236.5	87.3
8	-	Physical Mixture of Polymers 8c & 9c	-	-	77.1 97.3

<sup>a</sup>  $M_n$  values were determined relative to poly(styrene) standards in THF. <sup>b</sup> Thermal decomposition ( $T_d$ ) measurements were done at a heating rate of 10 °C min<sup>-1</sup> under a nitrogen atmosphere. The  $T_d$  was determined to be the temperature of the inflection point between 0-50% weight loss. <sup>c</sup> Samples underwent two heating and cooling cycles at a rate of 20 °C min<sup>-1</sup> under a nitrogen atmosphere prior to determination of the glass transition temperature ( $T_g$ ). The  $T_g$  values were determined from the DSC traces of the third heating cycle.

**Table 2.10.** Glass transition temperature ( $T_g$ ) and decomposition temperature ( $T_d$ ) values for diblock copolymers of different molecular weights.<sup>129</sup>

Entry	Polymer	Structure	$M_n^a$ (kDa)	$T_d^b$ (°C)	$T_g^c$ (°C)
1	8c		66.4	224.1	72.6
2	9c		50.5	241.1	99.5
3	15b		62.8	236.6	87.3
4	10b		44.9	232.6	82.1
5	10c		92.8	232.5	86.6
6	10d		111.3	234.8	74.5 90.9
7	10e		118.7	239.6	75.8 92.6

<sup>a</sup>  $M_n$  values were determined relative to poly(styrene) standards in THF. <sup>b</sup> Thermal decomposition ( $T_d$ ) measurements were done at a heating rate of 10 °C min<sup>-1</sup> under a nitrogen atmosphere. The  $T_d$  was determined to be the temperature of the inflection point between 0-50% weight loss. <sup>c</sup> Samples underwent two heating and cooling cycles at a rate of 20 °C min<sup>-1</sup> under a nitrogen atmosphere prior to determination of the glass transition temperature ( $T_g$ ). The  $T_g$  values were determined from the DSC traces of the third heating cycle.



**Scheme 2.6.** Synthetic scheme toward the hydrogenation of diblock copolymers.

**Table 2.11.** Molecular weights and glass transition temperatures ( $T_g$ ) before and after hydrogenation of diblock copolymer **10e**.

Polymer	Target $M_n$ (kDa)	$M_n^{a,b}$ (kDa)	$M_w^{a,b}$ (kDa)	$\bar{D}$	Yield (%)	$T_g^c$ ( $^\circ\text{C}$ )
<b>10e</b>	<b>150.0</b>	<b>118.7</b>	<b>133.1</b>	<b>1.1</b>	<b>-</b>	<b>75.8, 92.6</b>
<b>16</b>	<b>151.5</b>	<b>135.5</b>	<b>151.5</b>	<b>1.1</b>	<b>91</b>	<b>69.6</b>

<sup>a</sup> Values were determined relative to poly(styrene) standards in tetrahydrofuran. <sup>b</sup> See Appendix C for GPC chromatograms.

<sup>c</sup> Samples underwent two heating and cooling cycles at a rate of  $20 \text{ }^\circ\text{C min}^{-1}$  under a nitrogen atmosphere prior to determination of the glass transition temperature ( $T_g$ ). The  $T_g$  values were determined from the DSC traces of the third heating cycle.

## 2.4. Experimental

### Chemicals and Materials

Phthalic acid, sodium acetate, mercury, Grubbs 2<sup>nd</sup> Generation catalyst, palladium on carbon (10 weight %), and anhydrous dichloromethane were supplied by Sigma Aldrich Inc. Sulfuric acid, hydrochloric acid, acetic anhydride, and sodium metal were supplied by Samchun Chemical Company. 3-bromopyridine was supplied by Tokyo Chemical Inc. All solvents were supplied by Daejung Chemical unless otherwise noted.

Photoirradiation for the electrocyclic [2+2] reaction was performed using a 450-watt mercury lamp connected to a photo reactor purchased from Ace Glass Inc. All photoreactions were done in quartz vessels.

### Synthesis of Monomers **5** and **7**

Monomers were synthesized following modifications to previously reported procedures<sup>110-111</sup> (see Scheme 2.1). Briefly, **1** (16.6 g, 100 mmol) was reduced using a 3 weight % sodium amalgam (28.7 g, 350 mmol) to afford **2**, which was purified by recrystallization in aqueous sulfuric acid and isolated in 70% yield. Dehydration of the 1,3-cyclohexadiene derivative using acetic anhydride (13.24 mL, 140 mmol) at 95 °C for 2 hours afforded the corresponding anhydride **3**, which was purified by sublimation and collected in 75% yield as a white crystalline solid. With **3** in hand, photochemical isomerization was carried out in diethyl ether at room temperature over 27 hours, as monitored for completion by <sup>1</sup>H NMR spectroscopy, to afford **4**. Following removal of the residual solvent under reduced pressure, the crude product (**4**) was directly esterified with methyl alcohol in the presence of a catalytic amount of sulfuric acid to afford the corresponding diester **5** as a colorless liquid, which was subsequently purified via column chromatography (24% yield over two steps). Epimerization of **5** (1 g, 5 mmol) using methyl alcohol (0.2 M) and sodium methoxide (2.73 g, 50 mmol), followed by acidification and extraction via H<sub>3</sub>O<sup>+</sup>/ethyl acetate produced **6** with a 98% yield. The dicarboxylic acid (**6**) was then esterified with methyl alcohol in the presence of a catalytic amount of sulfuric acid and extracted via H<sub>3</sub>O<sup>+</sup>/dichloromethane to afford **7** in 97% yield. Prior to polymerization, both **5** and **7** were distilled at a pressure of 0.05 torr and temperature of 95 °C. <sup>1</sup>H NMR for **5** (400 MHz, CDCl<sub>3</sub>): δ 6.51 – 6.26 (m, 1H), 3.69 (s, 3H), 3.62 (t, *J* = 1.4 Hz, 1H), 3.17 (t, *J* = 1.3 Hz, 1H). <sup>13</sup>C NMR (100 MHz, CDCl<sub>3</sub>): δ 173.67, 142.48, 52.37, 44.87, 43.13. <sup>1</sup>H NMR for **7** (400 MHz, CDCl<sub>3</sub>): δ 6.39 (t, *J* = 2.3 Hz, 1H), 6.23 (t, *J* = 2.4 Hz, 1H), 3.73 (s, 3H), 3.71-3.65f (m,



4H), 3.59 (dt,  $J = 2.5$  Hz, 1H), 3.39 (q,  $J = 2.5$  Hz, 1H), 3.19 (dd,  $J = 2.4$  Hz, 1H).  $^{13}\text{C}$  NMR (100 MHz,  $\text{CDCl}_3$ ):  $\delta$  174.19, 172.91, 142.18, 139.65, 52.28, 51.94, 44.38, 43.43, 43.36, 40.11.

#### Synthesis of Grubbs 3<sup>rd</sup> Generation Catalyst (G3)

Grubbs 3<sup>rd</sup> generation catalyst was synthesized following a previously reported procedure.<sup>130</sup> Briefly, in a nitrogen atmosphere glove box, a 10 mL vial was charged with Grubbs 2<sup>nd</sup> generation catalyst (G2) (200 mg, 0.235 mmol). 3-bromopyridine (450 microliters, 4.67 mmol) was then injected and the reaction was allowed to proceed under stirring for 1 hour. While stirring, a color change from dark red to bright green is observed. The catalyst was then washed and filtered multiple times with anhydrous pentane and dried under reduced pressure overnight to afford G3 as a green powder in 97% yield.

#### Polymerization of Homopolymers **8** and **9**

All glassware was flame dried before usage. Monomer **5** (100 mg, 0.51 mmol) was dissolved in anhydrous dichloromethane (0.2 M) and injected under positive nitrogen flow into a 25 mL Schlenk tube. G3 (see Table 2.2 for monomer to catalyst ratios) was then dissolved in a minimal amount of anhydrous dichloromethane and immediately injected under positive nitrogen flow. The reaction was allowed to proceed under stirring at 25 °C under a  $\text{N}_2$  atmosphere for 0.5 hours, with monomer consumption being monitored by thin layer chromatography. Upon complete monomer consumption, the reaction was quenched with ethyl vinyl ether and the polymer was precipitated in excess cold hexane. Subsequent washing and filtering of the polymer with hexane followed by drying at 75 °C under reduced pressure afforded homopolymer **8**. The *trans* analog **9** was synthesized under the same conditions outlined above with monomer **7** being utilized instead of monomer **5**. All polymerizations afforded yields equal to or over 87%.  $^1\text{H}$  NMR for **8** (400 MHz,  $\text{CDCl}_3$ ):  $\delta$  5.82-5.29 (br, CH), 3.75-2.87 (br, CH, CH,  $\text{CH}_3$ ).  $^1\text{H}$  NMR for **9** (400 MHz,  $\text{CDCl}_3$ ):  $\delta$  5.82-5.30 (br, CH), 3.87-2.87 (br, CH, CH,  $\text{CH}_3$ ).

#### Polymerization of Diblock Copolymers **10** and **11**

All glassware was flame dried before usage. Monomer **5** (100 mg, 0.51 mmol) was dissolved in anhydrous dichloromethane (0.2 M) and injected under positive nitrogen flow into a 25 mL Schlenk tube. G3 (see Table 2.3 for monomer to catalyst ratios) was then dissolved in a minimal amount of anhydrous dichloromethane and immediately injected under positive nitrogen flow. The

reaction was allowed to proceed under stirring at 25 °C under a N<sub>2</sub> atmosphere for 0.5 hours, with monomer consumption being monitored by thin layer chromatography. Upon complete monomer consumption, a small aliquot was removed and precipitated in a hexane/ethyl vinyl ether mixture. Monomer **7** (100 mg, 0.51 mmol) was then dissolved in a minimal amount of anhydrous dichloromethane and immediately injected under positive nitrogen flow. The reaction was then allowed to proceed under stirring at 25 °C under a N<sub>2</sub> atmosphere for an additional 0.5 hours, with monomer consumption being monitored by thin layer chromatography. Upon complete monomer consumption the reaction was quenched with ethyl vinyl ether and the polymer was precipitated in excess cold hexane. Subsequent washing and filtering of the polymer with hexane followed by drying at 75 °C under reduced pressure afforded diblock copolymer **10**. Diblock copolymer **11** was synthesized under the same conditions outlined above except monomer **7** was added first, followed by monomer **5**. All polymerizations afforded yields over 80%. <sup>1</sup>H NMR for **10** (400 MHz, CDCl<sub>3</sub>): δ 5.61-5.49 (br, CH), 3.62-2.79 (br, CH, CH, CH<sub>3</sub>). <sup>1</sup>H NMR for **11** (400 MHz, CDCl<sub>3</sub>): δ 5.78-5.33 (br, CH), 3.78-2.93 (br, CH, CH, CH<sub>3</sub>).

#### Polymerization of Diblock Copolymer **12**

Polymer **12** was synthesized using a slightly modified version of the procedure used to polymerize **10**. All glassware was flame dried prior to usage. Monomer **5** (100 mg, 0.51 mmol) was dissolved in anhydrous dichloromethane (0.2 M) and injected under positive nitrogen flow into a 25 mL Schlenk tube. G3 (see Table 2.3 for monomer to catalyst ratios) was then dissolved in a minimal amount of anhydrous dichloromethane and immediately injected under positive nitrogen flow. The reaction was allowed to proceed under stirring at 25 °C under a N<sub>2</sub> atmosphere for 0.5 hours, with monomer consumption being monitored by thin layer chromatography. Upon complete monomer consumption, a small aliquot was removed and precipitated in a hexane/ethyl vinyl ether mixture. Triphenyl phosphine (6.69 mg, 0.025 mmol) was then dissolved in a minimal amount of anhydrous dichloromethane and injected under positive nitrogen flow. The reaction was then stirred at 25 °C under a N<sub>2</sub> atmosphere for 0.1 hours. Monomer **7** (100 mg, 0.51 mmol) was then dissolved in a minimal amount of anhydrous dichloromethane and immediately injected under positive nitrogen flow. The reaction was allowed to proceed under stirring at 25 °C under a N<sub>2</sub> atmosphere for an additional 2 hours, with monomer consumption being monitored by thin layer chromatography. Upon complete monomer consumption the reaction was quenched with ethyl vinyl ether and the polymer was precipitated in excess cold hexane. Subsequent washing and filtering of the polymer with hexane followed by drying at 75 °C under reduced pressure afforded diblock copolymer **12**. All polymerizations afforded yields over 80%. <sup>1</sup>H NMR for **12** (400 MHz, CDCl<sub>3</sub>): δ 5.94-5.24 (br, CH),

4.04-2.93 (br, CH, CH, CH<sub>3</sub>).

#### Synthesis of Triblock Copolymers **13** and **14**

All glassware was flame dried prior to usage. Monomer **5** (100 mg, 0.51 mmol) was dissolved in anhydrous dichloromethane (0.2 M) and injected under positive nitrogen flow into a 25 mL Schlenk tube. G3 (see Table 2.4 for monomer to catalyst ratios) was then dissolved in a minimal amount of anhydrous dichloromethane and immediately injected under positive nitrogen flow. The reaction was allowed to proceed under stirring at 0 °C under a N<sub>2</sub> atmosphere for 1 hour, with monomer consumption being monitored by thin layer chromatography. Upon complete monomer consumption, a small aliquot was removed and precipitated in a hexane/ethyl vinyl ether mixture. Monomer **7** (100 mg, 0.51 mmol) was then dissolved in a minimal amount of anhydrous dichloromethane and immediately injected under positive nitrogen flow. The reaction was then allowed to proceed under stirring at 0 °C under a N<sub>2</sub> atmosphere for an additional hour, with monomer consumption being monitored by thin layer chromatography. Upon complete monomer consumption, a small aliquot was removed and precipitated in a hexane/ethyl vinyl ether mixture. Monomer **5** (100 mg, 0.51 mmol) was then dissolved in a minimal amount of anhydrous dichloromethane and immediately injected under positive nitrogen flow. The reaction was then allowed to proceed under stirring at 0 °C under a N<sub>2</sub> atmosphere for an additional hour, with monomer consumption being monitored by thin layer chromatography. Upon complete monomer consumption the reaction was quenched with ethyl vinyl ether and the polymer was precipitated in excess cold hexane. Subsequent washing and filtering of the polymer with hexane followed by drying at 75 °C under reduced pressure afforded triblock copolymer **13**. Triblock copolymer **14** was synthesized under the same conditions outlined above with the caveat of monomer **7** being utilized first, followed by monomer **5**, and finally monomer **7**. All polymerizations afforded yields over 80%. <sup>1</sup>H NMR for **13** (400 MHz, CDCl<sub>3</sub>): δ 5.99-5.22 (br, CH), 3.89-2.85 (br, CH, CH, CH<sub>3</sub>). <sup>1</sup>H NMR for **14** (400 MHz, CDCl<sub>3</sub>): δ 5.83-5.31 (br, CH), 3.91-2.87 (br, CH, CH, CH<sub>3</sub>).

#### Synthesis of Random Copolymers **15**

All glassware was flame dried prior to usage. Monomers **5** (100 mg, 0.51 mmol) and **7** (100 mg, 0.51 mmol) were dissolved in anhydrous dichloromethane (0.2 M) and injected under positive nitrogen flow into a 25 mL Schlenk tube. G3 (see Table 2.8 for monomer to catalyst ratios) was then dissolved in a minimal amount of anhydrous dichloromethane and immediately injected under positive nitrogen flow. The reaction was allowed to proceed under stirring at 25 °C under a N<sub>2</sub>

atmosphere for 0.5 hours, with monomer consumption being monitored by thin layer chromatography. Upon complete monomer consumption, the reaction was quenched with ethyl vinyl ether and the polymer was precipitated in excess cold hexane. Subsequent washing and filtering of the polymer with hexane followed by drying at 75 °C under reduced pressure afforded random copolymer **15**. All polymerizations afforded yields over 80%. <sup>1</sup>H NMR for **15** (400 MHz, CDCl<sub>3</sub>): δ 5.83-5.33 (br, CH), 3.97-2.94 (br, CH, CH, CH<sub>3</sub>).

#### Hydrogenation of Diblock Copolymer **10e** to **16**

20 mg (0.1 mmol) of **10e** was dissolved in 250 mL of tetrahydrofuran and added to a Parr reactor along with 20 mg of palladium on carbon. The Parr reactor was then purged with argon gas for five minutes before being pressurized up to 500 psi with hydrogen gas and heated to 60 °C under stirring. The reaction was monitored by <sup>1</sup>H NMR spectroscopy and allowed to proceed until the complete disappearance of the signals in the olefinic region (approximately 3 days). After cooling to room temperature, the solution was filtered to remove the palladium on carbon. Tetrahydrofuran was then removed under reduced pressure and the remaining solute was precipitated in cold hexane. The polymer was washed and filtered multiple times with hexane and dried under reduced pressure to afford a white powder **16** in 91% yield. <sup>1</sup>H NMR for **16** (400 MHz, CDCl<sub>3</sub>): δ 3.68 (br, CH<sub>3</sub>), 3.40-2.26 (br, CH, CH, CH).

#### Physical Mixing of Homopolymers

Homopolymers in a 1:1 weight ratio were dissolved in dichloromethane and precipitated in cold hexane. The precipitate was washed and filtered with hexane multiple times and dried under reduced pressure overnight.

#### Physical Characterization

Nuclear magnetic resonance (NMR) spectra were recorded at ambient temperature (22.0(±1.0) °C, unless stated otherwise) on a Bruker Avance III HD spectrometer (operating at 400 MHz for <sup>1</sup>H). Chemical shifts are given in ppm relative to tetramethylsilane (TMS) using the residual, non-deuterated solvent as an internal standard. For <sup>1</sup>H NMR: CDCl<sub>3</sub>, 7.26 ppm.<sup>131</sup> For <sup>13</sup>C NMR: CDCl<sub>3</sub>, 77.16 ppm.<sup>131</sup> Abbreviations used for the description of the spectra are: s = singlet, d = doublet, t = triplet, q = quartet, dd = doublet of doublets, dt = doublet of triplets and m = multiplet. Coupling constants (J) are expressed in hertz (Hz).

Gel permeation chromatography (GPC) was performed on a Malvern GPCmax system. Two fluorinated poly(styrene) columns (IMBHW-3078 and I-MBHMW-3078) were used in series and maintained at 35 °C. Tetrahydrofuran was used as the mobile phase at a flow rate of 0.8 mL/min. Detection was performed using a Viscotek VE3580 RI Detector. Molecular weight and polydispersity data are reported relative to poly(styrene) standards in THF.

Differential scanning calorimetry (DSC) data were recorded using a TA Q2000 Differential Scanning Calorimeter (TA Instruments, New Castle, DE, USA). Measurements were taken under an atmosphere of nitrogen (50 mL min<sup>-1</sup>) over a temperature range of -80 °C to 150 °C. The samples underwent two heating and cooling cycles at rates of up to 20 °C min<sup>-1</sup> prior to recording of the data.

Thermal gravimetric analysis (TGA) data were recorded under nitrogen (60 mL min<sup>-1</sup>) on a TA Instruments TGA Q500 module at a heating rate of 10 °C min<sup>-1</sup> and using a platinum sample pan. The quantity of sample analyzed was typically 3–10 mg. High-purity nickel was used as a standard for temperature calibration (based on its Curie temperature).

Attenuated total reflectance infrared spectroscopy (ATR-IR) measurements were taken using a diamond crystal on a Cary 630 FT-IR Spectrometer supplied by Agilent Technologies Inc.

## 2.5. Acknowledgements

The synthetic scheme for the synthesis of monomers **5** and **7** were done in collaboration with Jinwon Seo and Professor Christopher W. Bielawski. GPC measurements were taken with the assistance of Dr. Songsu Kang and Dr. Tang Tang.

## Chapter 3: Determining the Stereochemical Influences on the Electronic Properties of Strained Poly(alkenamer)s

### 3.1. Introduction

Due to the multitude of reactions that can be catalyzed by simple exposure to light, the field of photochemistry has continued to grow and find applications throughout various fields. Reactions including isomerization of molecules,<sup>132-133</sup> activation/deactivation of catalysts,<sup>134</sup> cleavage of bonds,<sup>135</sup> and bond formation,<sup>136</sup> have all been shown to be possible and reversible through simple control over the wavelength of the irradiating light. The process that a molecule undergoes upon absorption of light can be generally explained through the Jablonski diagram.<sup>137</sup> As shown in Figure 3.1, electrons can be excited from the ground state ( $S_0$ ) to a higher energy state ( $S_2$ ) upon light absorption. The excited electron can then return back to the ground state ( $S_0$ ) with the excess energy released as fluorescence or can undergo intersystem crossing to the triplet state ( $T_2$ ). Subsequent relaxation to the ground state releases the excess energy via phosphorescence.<sup>137</sup>

Photochemistry is able to facilitate reactions that normally do not proceed at ambient temperatures since the absorption of light excites electrons to a higher energetic state.<sup>138</sup> Molecules that possess a cyclic transition state when undergoing a reaction, such as the retro [2+2] cycloaddition of cyclobutane, are classified as pericyclic reactions and proceed in a concerted fashion.<sup>139</sup> Determining the stereochemistry of pericyclic reactions were initially proposed by Robert Woodward and Roald Hoffmann, and now are commonly known as the Woodward-Hoffmann rules.<sup>140-141</sup> Based off of frontier molecular orbital theory, the Woodward-Hoffmann rules predict that in order for a pericyclic reaction to proceed in a concerted fashion, the bonds will rotate in a manner to allow for continuous overlap.<sup>140-141</sup> These rotations, termed conrotatory and disrotatory, were found to be dependent on the number of electrons involved in the reaction as well as if the reaction was being catalyzed by heat or light (Table 3.1). When an even number of electrons were involved, a conrotatory rotation, where the bonds rotate in the same direction, was found to be necessary under thermal conditions in order for the molecular orbitals to align and for the new sigma bond to form (see Figure 3.2). However, exposure to light excites an electron into what was formerly the lowest unoccupied molecular orbital (LUMO) of a molecule to create a single occupied molecular orbital (SOMO). Therefore, under photochemical conditions, a disrotatory rotation, where the bonds rotate in opposite directions, was found to be necessary for the molecular orbitals to align and form a new bond (see Figure 3.3).

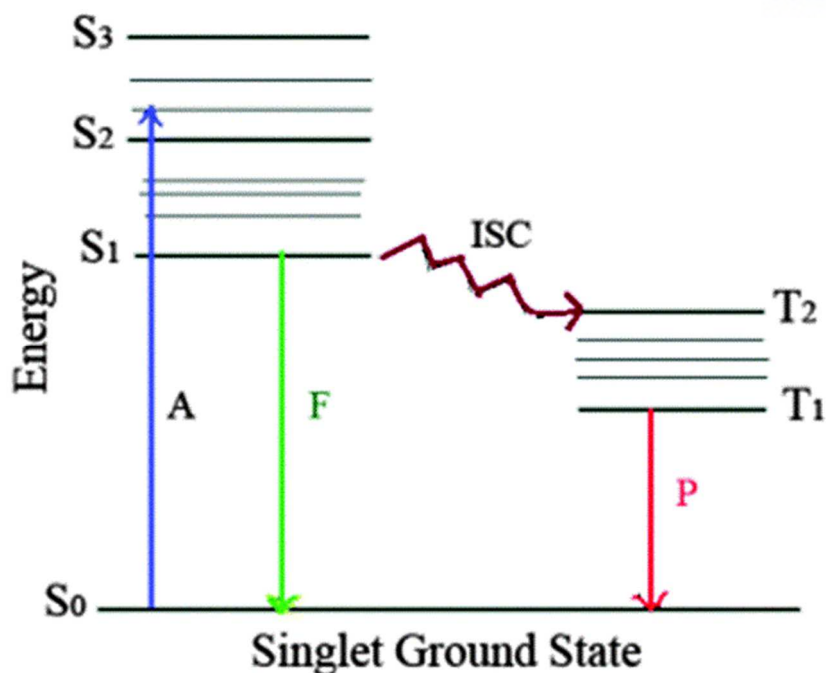


**Figure 3.1.** Simplified Jablonski diagram outlining the possible electronic states and transitions that can occur upon photoirradiation. The symbols A, F, and P represent absorption, fluorescence, and phosphorescence respectively. Adapted from reference 142.

**Table 3.1.** Woodward-Hoffmann rules for bond rotation during electrocyclic ring opening and closing.

# of Electron Pairs	$\Delta$	$h\nu$
Even	Conrotatory	Disrotatory
Odd	Disrotatory	Conrotatory

Since significant differences in the thermal properties were observed with a simple change in stereochemistry, investigations into whether these same differences could elicit changes in the electronic properties as well were investigated. As shown in Figure 3.4, orbital mismatch between the HOMO and LUMO under thermal conditions forbids the formation of cyclobutane from two ethylene molecules. However, photoirradiation promotes an electron to a higher energy state, leading to the formation of a single occupied molecular orbital (SOMO). Therefore, the molecular orbitals are able to align, and both the [2+2] and the retro [2+2] cycloaddition reactions become possible. Since the polymers presented in this work, possess a cyclobutane ring, we hypothesized that photoirradiation of the polymer would induce the retro [2+2] reaction on cyclobutane.<sup>135, 143</sup> Due to the differences in stereochemistry, the resulting products were expected to differ as the reaction was expected to proceed in a concerted manner (see Scheme 3.1).<sup>140-141</sup>

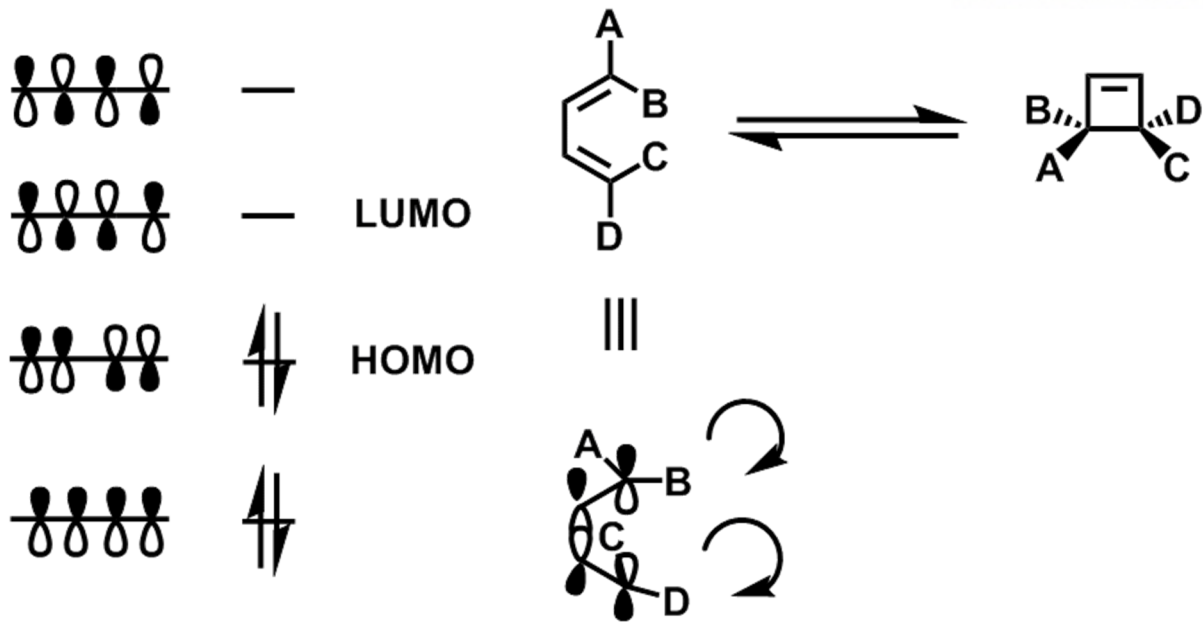


**Figure 3.2.** 1,3-Butadiene undergoing electrocyclic ring closing through conrotatory bond rotation when thermally driven.

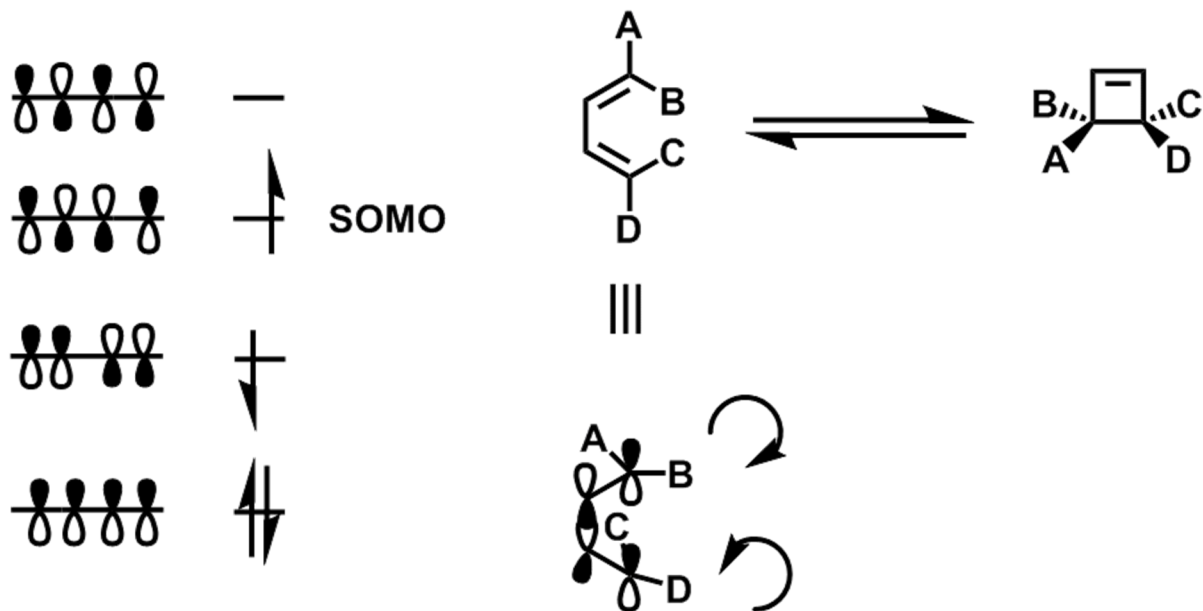


**Figure 3.3.** 1,3-Butadiene undergoing electrocyclic ring closing through disrotatory bond rotation when photochemically driven.



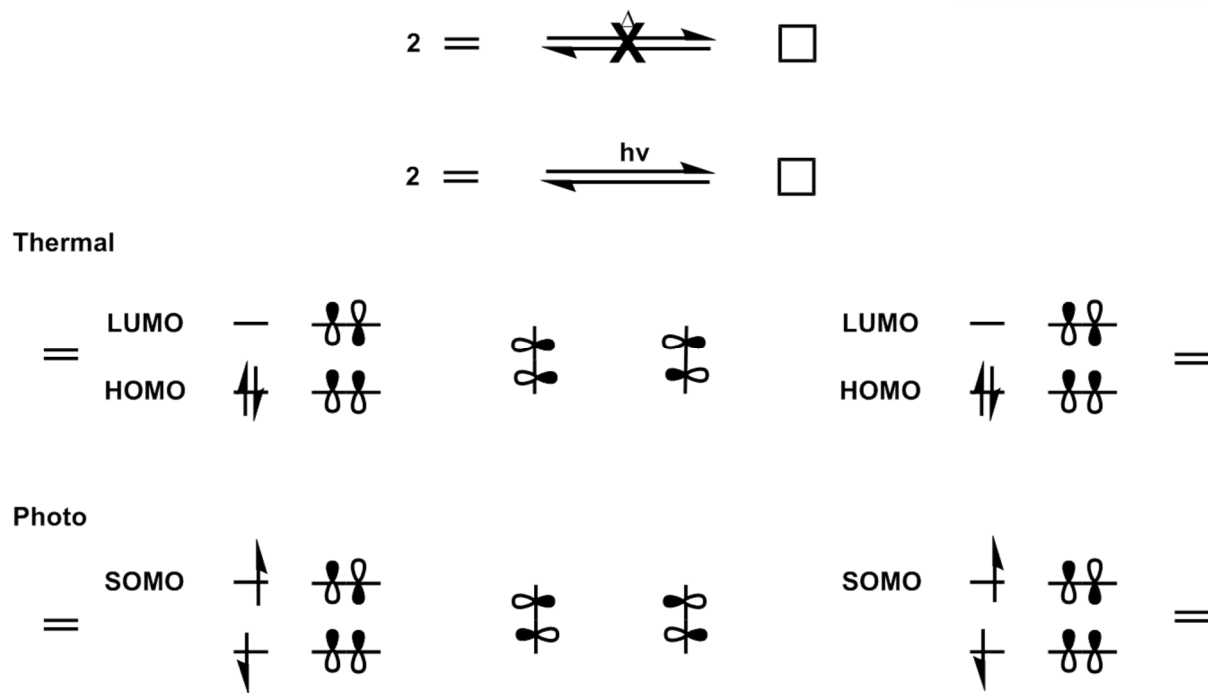
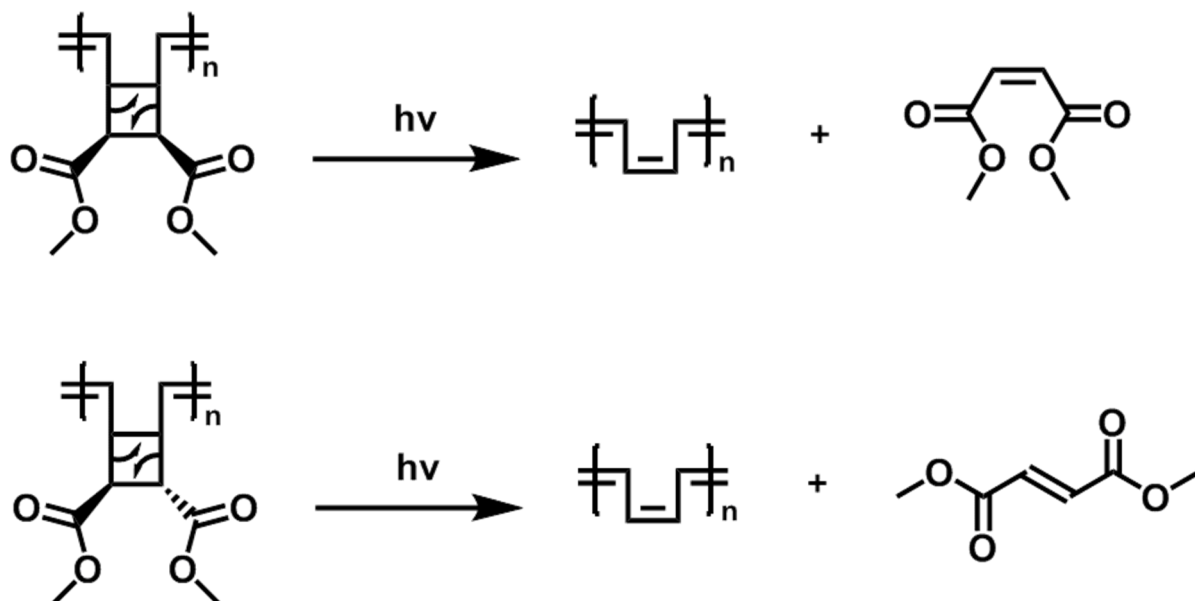


**Figure 3.4.** Frontier molecular orbitals for two ethylene molecules under thermal and photochemical conditions. The cycloaddition is forbidden under thermal conditions but allowed when photoirradiated.



**Scheme 3.1.** Proposed mechanism for the photodegradation of homopolymers **8** and **9**.

### 3.2. Results and Discussion

Analysis by gas chromatography-mass spectrometry (GC-MS) of diblock copolymer **10e** after photo-irradiation for 30 hours showed the appearance of new signals at 6.68 and 8.00 minutes in the GC chromatogram (Figure 3.5) and were confirmed to be dimethyl fumarate and dimethyl maleate respectively by mass spectrometry. (Figure 3.6). The appearance of these products implied that the cyclobutyl group within the polymer underwent a retro [2+2] reaction to afford poly(acetylene), and either dimethyl fumarate or dimethyl maleate depending on the block component. (see Scheme 3.1) As mentioned in the introduction, retentions in stereochemistry should occur if the reactions proceed in a concerted manner.<sup>140-141</sup> Therefore, photoirradiation should lead to the formation of poly(acetylene) along with the components of **10e** originating from monomer **5** degrading to dimethyl maleate and the sections of the polymer originating from monomer **7** degrading to dimethyl fumarate. As these two components within the block copolymer existed in a one to one ratio, an equal amount of dimethyl maleate and dimethyl fumarate was expected. However, based off the signals in the GC chromatogram and also by analysis of <sup>1</sup>H NMR of the crude photodegraded product (see Appendix A), dimethyl maleate was found to be in much higher concentrations than dimethyl fumarate.

In order to determine the reason for the difference in concentration, homopolymers **8a** and **9a** were subjected to the same photodegradation conditions. As **8a** has the diester substituents *cis* to each other and **9a** has the diester substituents *trans* to each other, it was hypothesized that photodegradation of **8a** and **9a** would lead to the exclusive formation of dimethyl maleate and dimethyl fumarate respectively. Contrary to our hypothesis, although the GC chromatogram for the photodegraded product of **8a** did show a signal corresponding to dimethyl maleate (Figures 3.7 and 3.8), the photodegradation of **9a** produced a mixture of dimethyl fumarate and dimethyl maleate with dimethyl fumarate being present in higher concentrations. (Figures 3.9 and 3.10).

Although reports of molecules undergoing isomerization from the *cis* conformation to the more thermodynamically stable *trans* configuration has been well reported,<sup>144-145</sup> previous research involving the UV irradiation of stilbene<sup>132</sup> and azobenzene<sup>133</sup> have shown these molecules undergoing *trans* to *cis* isomerization. In addition, reports involving the isomerization of fumaric acid to maleic acid when irradiated have also been shown, though no explanation for this occurrence was found.<sup>146</sup> Similar to what was found to occur with stilbene, we believe that an isomerization reaction is occurring through a diabatic photoreaction,<sup>137</sup> which ultimately leads to the formation of dimethyl maleate as the major product. As shown in Figure 3.11, once a molecule is excited to the S<sub>1</sub> state, it is a biradical state and thus no longer restricted to a planar conformation. As the molecule rotates to

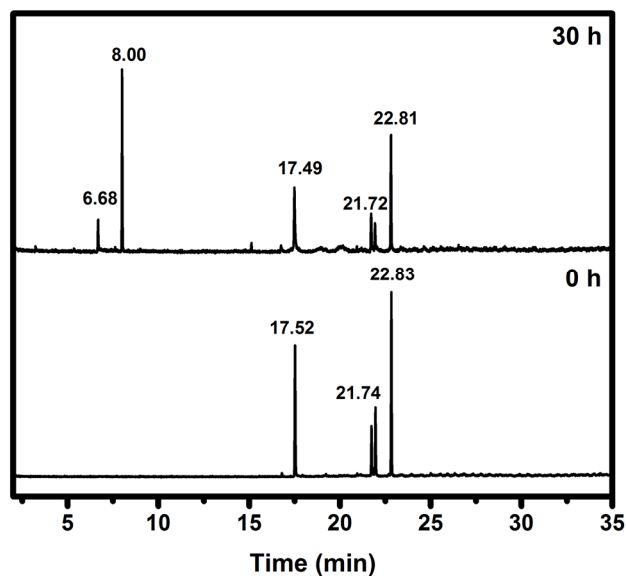


**Figure 3.5.** GC chromatograms for diblock polymer **10f** before and after 30 hours of irradiation with 300 nm light.

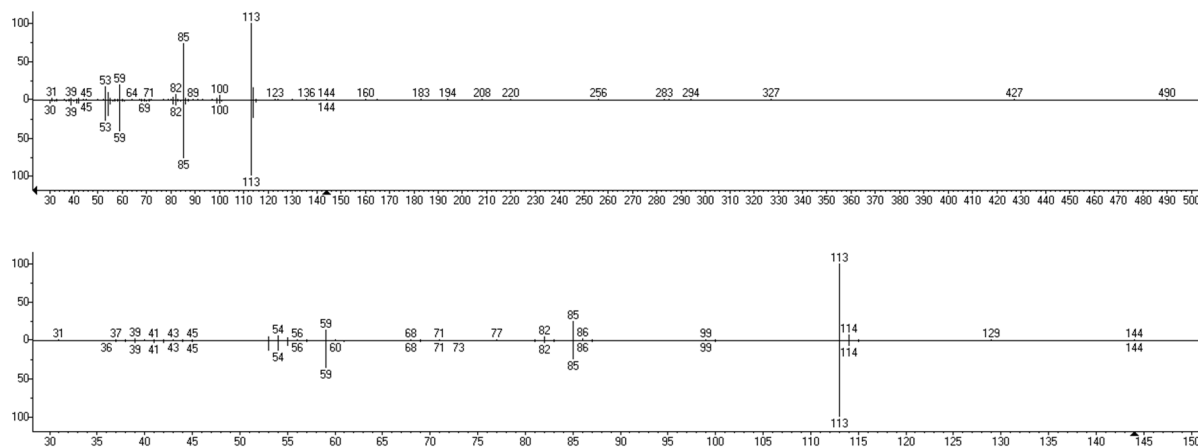


**Figure 3.6.** Mass spectra for the signals seen at 6.68 (top) and 8.00 minutes (bottom) in Figure 3.5. The spectrum seen on the positive Y-axis represents the measured data while the negative Y-axis shows the spectrum for the fragmentation pattern of dimethyl fumarate (6.68 minutes) and dimethyl maleate (8.00 minutes). The spectra for dimethyl maleate and dimethyl fumarate were taken from the NIST standard reference database (<https://webbook.nist.gov/chemistry/name-ser/>).

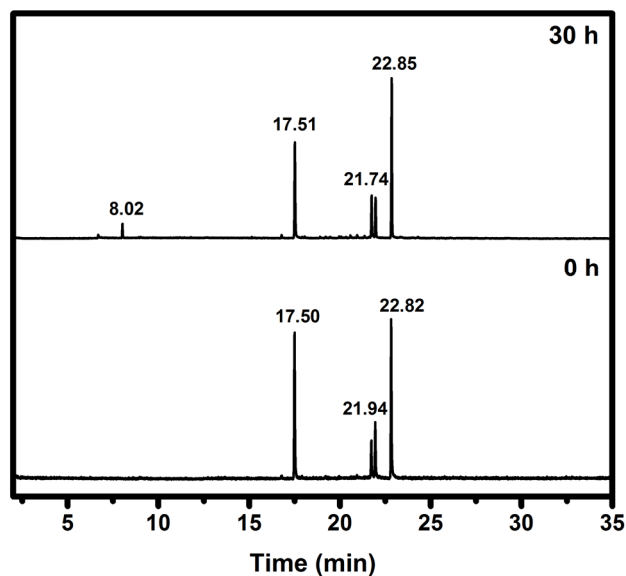


**Figure 3.7.** GC chromatograms for homopolymer **8a** before and after 30 hours of irradiation with 300 nm light.

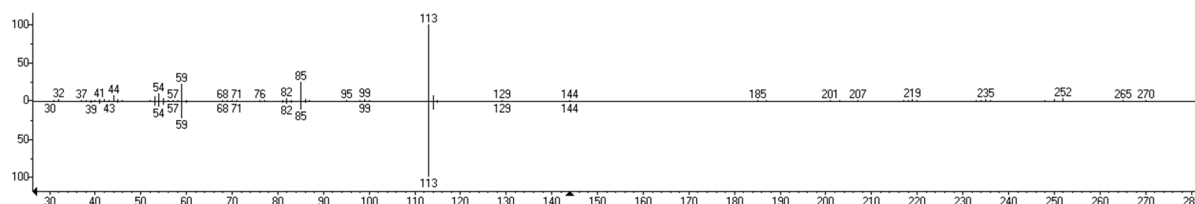


**Figure 3.8.** Mass spectrum for the signal seen at 8.02 minutes in Figure 3.7. The spectrum seen on the positive Y-axis represents the measured data while the negative Y-axis shows the spectrum for the fragmentation pattern of dimethyl maleate. The spectrum for dimethyl maleate was taken from the NIST standard reference database (<https://webbook.nist.gov/chemistry/name-ser/>).

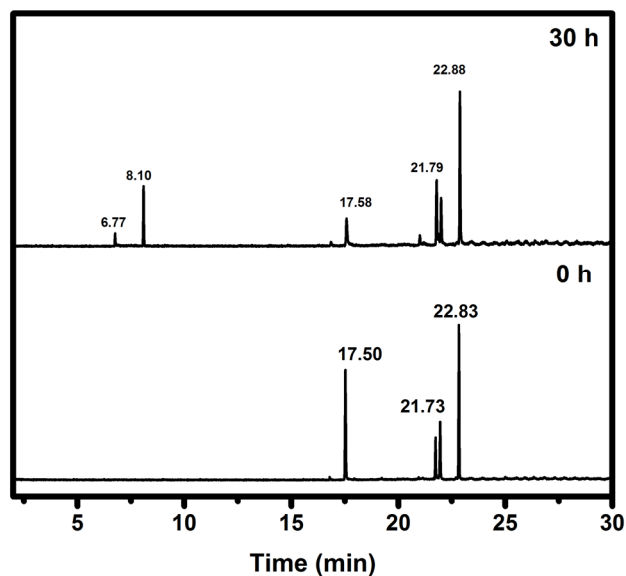


**Figure 3.9.** GC chromatograms for homopolymer **9a** before and after 30 hours of irradiation with 300 nm light.

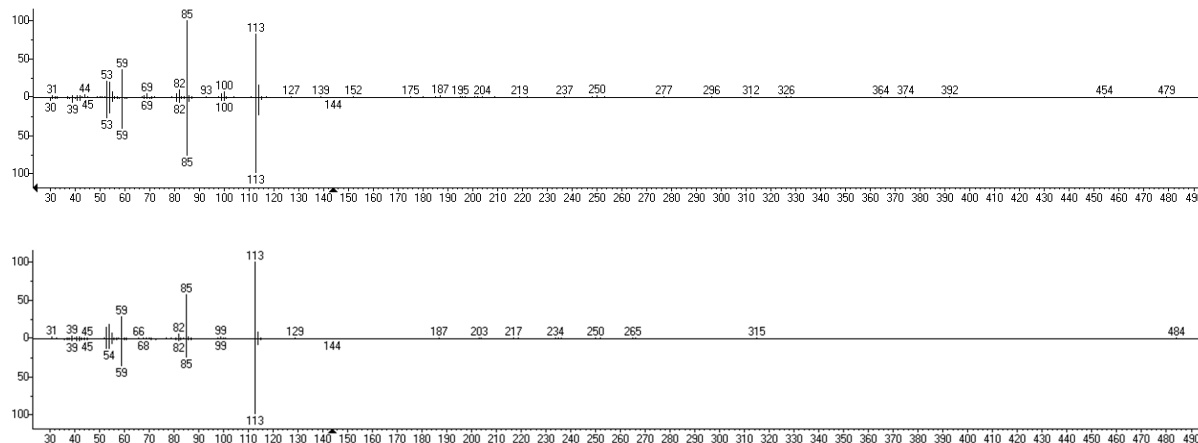


**Figure 3.10.** Mass spectra for the signals seen at 6.77 minutes (top) and at 8.10 minutes (bottom) in Figure 3.9. The spectrum seen on the positive Y-axis represents the measured data while the negative Y-axis shows the spectrum for the fragmentation pattern of dimethyl fumarate (6.77 minutes) and dimethyl maleate (8.10 minutes). The spectra for dimethyl maleate and dimethyl fumarate were taken from the NIST standard reference database (<https://webbook.nist.gov/chemistry/name-ser/>).

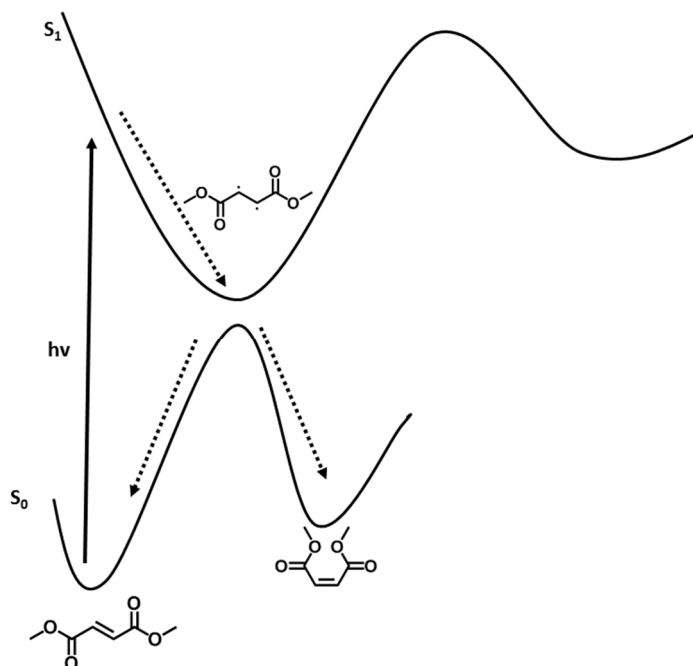


**Figure 3.11.** Representative image for the diabatic photoreaction of dimethyl fumarate to dimethyl maleate upon irradiation with UV light. Figure adapted from reference 137.

adapt a favorable structure, it relaxes down the minimum of  $S_1$ , where it can further “hop” down through vibrational motion to the maximum of  $S_0$  if the relative energy levels are close enough.<sup>137</sup> At this point, there are two potential energy surfaces that can be attained as the molecule relaxes, *cis* and *trans*. If the excited molecule adopts the *trans* configuration, dimethyl fumarate is recreated. However, if the excited molecule adopts the *cis* configuration, dimethyl maleate is formed.

A small energy gap between the  $S_1$  and  $S_0$  states is crucial for diabatic photoreactions since it provides a funneling effect for the molecule to return to the ground state.<sup>137</sup> When irradiated with a light source possessing a wide range of wavelengths, both the *cis* and *trans* product can be excited and repeatedly undergo isomerization. In this situation, the thermodynamically favored product will ultimately be favored<sup>137</sup> and lead to dimethyl fumarate being the expected major product since *trans* isomers are most often the thermodynamically favored molecule.<sup>144-145</sup> However, in theory, the full isomerization of dimethyl fumarate to dimethyl maleate could occur if a specific wavelength of light could excite only dimethyl fumarate. In this type of scenario, although both dimethyl fumarate and dimethyl maleate could form upon excitation and isomerization, the process will only repeat itself with dimethyl fumarate. Therefore, over time, only dimethyl maleate would be present. Although theoretically possible, the fact that both isomers in these situations are usually photo active and also have overlapping absorption regions make complete isomerization to one conformer difficult.

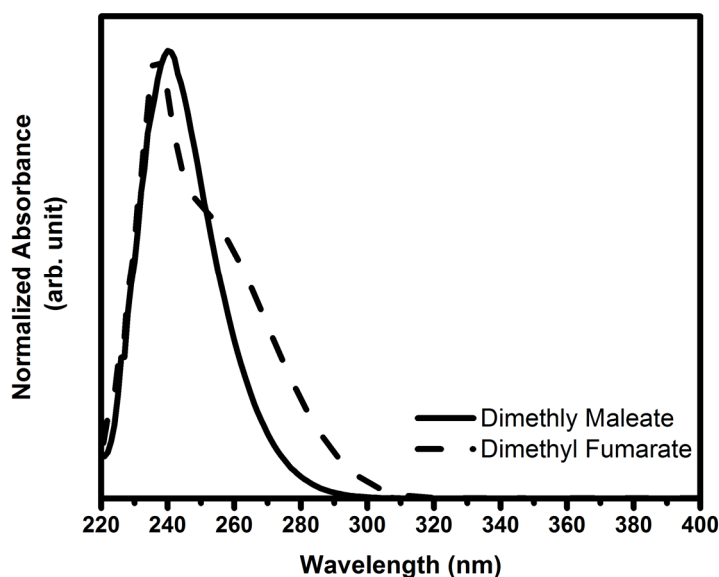


**Figure 3.12.** UV-Vis spectra for dimethyl maleate (solid line) and dimethyl fumarate (dashed line). All measurements were taken in acetonitrile.

However, continued irradiation with a specific wavelength of light could lead to an equilibrium point where one conformation is favored over the other.<sup>137</sup> This equilibrium state, called the photostationary state, is defined as the point where the ratio of the two products are in equilibrium and further isomerization does not occur. Irradiation with a wavelength of light favored towards one of the stereochemical isomers would lead to more excitation of molecules in that conformation and the subsequent “funneling” towards the formation of its stereochemical analog. As can be seen for the UV spectra for dimethyl fumarate and dimethyl maleate (Figure 3.12), even though there are many overlapping regions, the absorption bands are distinctly different. Therefore, when irradiated with a specific wavelength of light, in this case 300 nm, excitation of dimethyl fumarate is favored over dimethyl maleate, which pushes the photostationary state towards the formation of dimethyl maleate.

With a plausible explanation for why the formation of dimethyl maleate is favored over that of dimethyl fumarate, efforts toward determining the differences in the efficiency of degradation between **8a** and **9a** were analyzed in further detail. Although the GPC traces of the photodegraded products showed significant losses in molecular weight, integration of the protons corresponding to the olefins in dimethyl fumarate and dimethyl maleate to that of the olefins in the polymer backbone in the <sup>1</sup>H NMR spectra only showed a conversion of approximately 20% for **9a** and barely any conversion for **8a** (see Appendix A). Initially, these differences were thought to be due to differences

in UV absorption between the two polymers. However, subsequent UV-Vis measurements showed no discernable differences between **8a** and **9a** (Figure 3.13). Alternatively, investigations involving the degradation patterns of substituted cyclobutanes have shown that the stereochemistry of substituted functional groups plays a role in determining the direction in which the retro [2+2] reaction proceeds.<sup>135, 147</sup> As shown in Figure 3.14, the retro [2+2] reaction of substituted cyclobutanes can occur through two different pathways. Cyclobutanes having functional groups *cis* relative to each other weaken the bond between the two substituents due to repulsive forces. Therefore, upon irradiation, the weakened bond is favored to cleave and lead to the formation of a symmetric product. However, when the substituents are *trans* to each other, the repulsive forces are no longer existent, and asymmetric cleavage becomes the favored pathway.<sup>135, 147</sup> Thus, similar trends could be occurring with polymers **8a** and **9a**, which would favor **8a** undergoing degradation through an alternate pathway.

Subsequent analysis of the photodegraded products by UV-GPC with UV detection set at a wavelength of 300 nm, exhibited the appearance of a signal in line with the signal detected by refractive index (Figures 3.15 and 3.16). As such, one can conclude that as the retro [2+2] reaction proceeds, conjugation of what was formerly the backbone of the polymer begins to occur. If the reaction goes to completion, the end result should be the formation of poly(acetylene). However, analysis of the UV-vis spectra of the photodegraded products showed no absorption bands characteristic to that of poly(acetylene) (350-600 nm dependent on substitution and conjugation length).<sup>148-149</sup> Therefore, we believe that the photodegradation continues until a conjugation length that absorbs the irradiated light (300 nm) is reached. At that point, the partially conjugated poly(acetylene) begins to absorb the incoming light, hindering further degradation.

### 3.3. Conclusions and Future Outlooks

The photodegradation of diblock copolymers and homopolymers synthesized from monomers **5** and **7** was found to partially occur. Although only differing in the stereochemistry of their substituents, polymers **8** and **9** were found to have different absorption spectra, which influenced the efficiency of degradation. Contrary to what was expected, the *cis* isomer, dimethyl maleate, was found to be the major product over the more thermodynamically stable *trans* isomer, dimethyl fumarate. This unusual phenomenon was attributed to the photostationary effect, which led to the funneling of the molecules toward the formation of dimethyl maleate. Although photodegradation was found to be successful, further optimization is necessary to reach higher conversions. The low conversions were thought to be due to competition between different degradation pathways and/or the



formation of a conjugated molecule as a product of photodegradation led to the absorption of the irradiating light, ultimately hindering further degradation. These issues may be mitigated through the use of photosensitizers<sup>150-151</sup> or through photoirradiation using a different wavelength of light. Nevertheless, these findings display how the incorporation of photochemically active functional groups can tailor polymers to not only undergo photodegradation, but also to drive the photodegraded products to favor a certain conformation. In addition, the photodegradation of polymer **9a** to poly(acetylene) offers intriguing potential applications in photolithography. The utilization of photolithographic techniques to create well defined patterns for usages in materials such as circuit boards has been well documented.<sup>152</sup> Naturally, the progression of this field to create micropatterns composed of conducting polymers has been attempted but due to conducting polymers usually being insoluble,<sup>153</sup> successful implementation has been limited. Methods involving the use of a conducting polymer film to coat a micropatterned structure post photolithography<sup>154</sup> or the photolithography of a photoresist comprised of a conducting polymer blend have been shown to be possible.<sup>155-156</sup> However, these methods suffer from difficulties arising with adhesion and blend ratio optimization respectively. As the homopolymers presented in this study are completely soluble, films could be easily formed, and subsequently converted to poly(acetylene) upon photoirradiation. Thus, one can imagine that with optimization, photolithography of the homopolymers would lead to the formation of micropatterns comprised of poly(acetylene) that would curtail all the issues that have plagued previously reported methods.

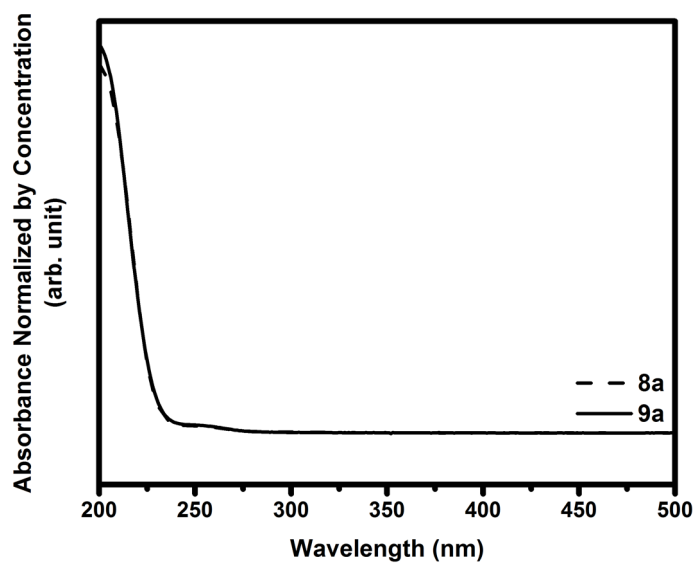


**Figure 3.13.** UV-Vis spectra for homopolymer **8a** and homopolymer **9a**. All measurements were taken in acetonitrile.

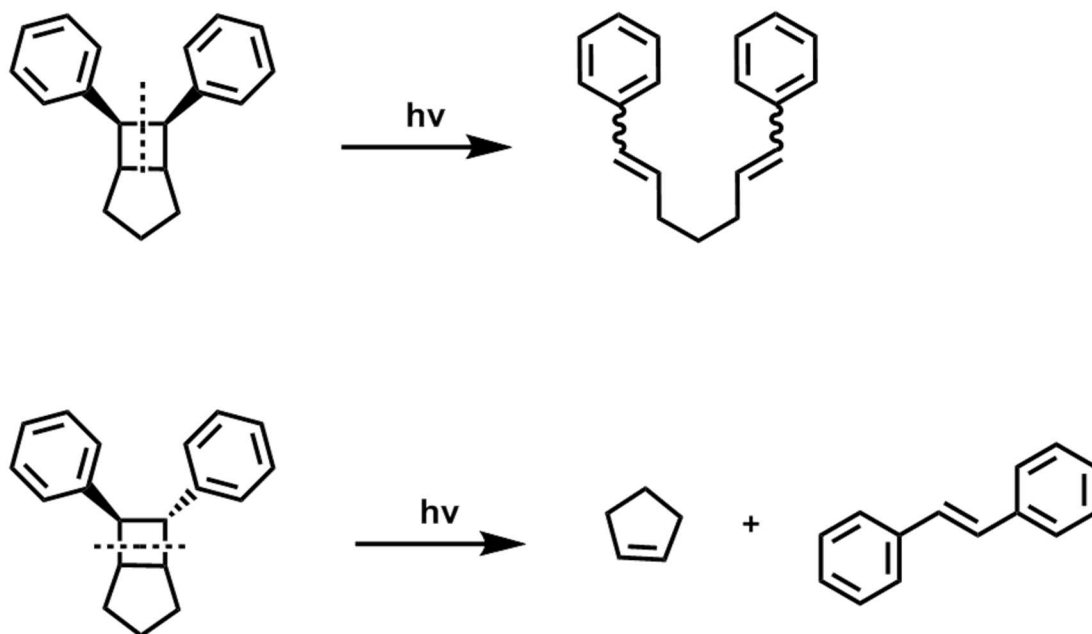


**Figure 3.14.** Representative example for how the stereochemistry of the functional groups influence the pathway in which the retro [2+2] reaction proceeds. Adapted from reference 147.

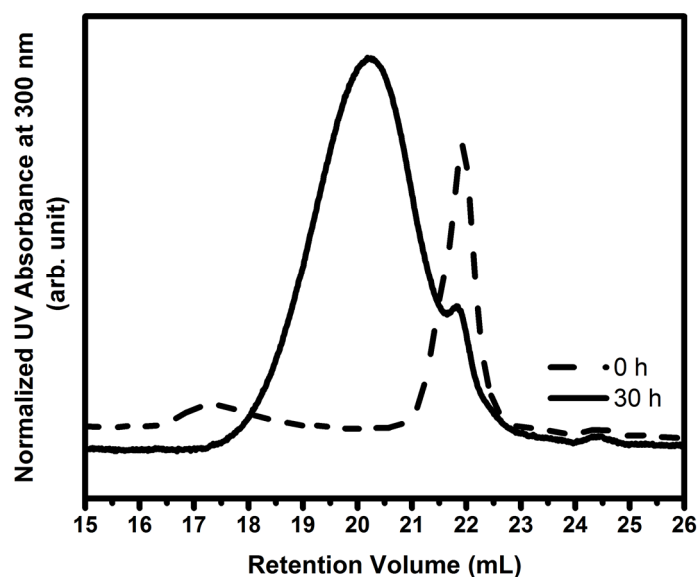


**Figure 3.15.** UV-Vis GPC chromatograms for homopolymer **8a** before and after photoirradiation with 300 nm light. The UV detector was calibrated to detect signals at 300 nm. Absorbance was normalized by the concentration (1 mg/mL).

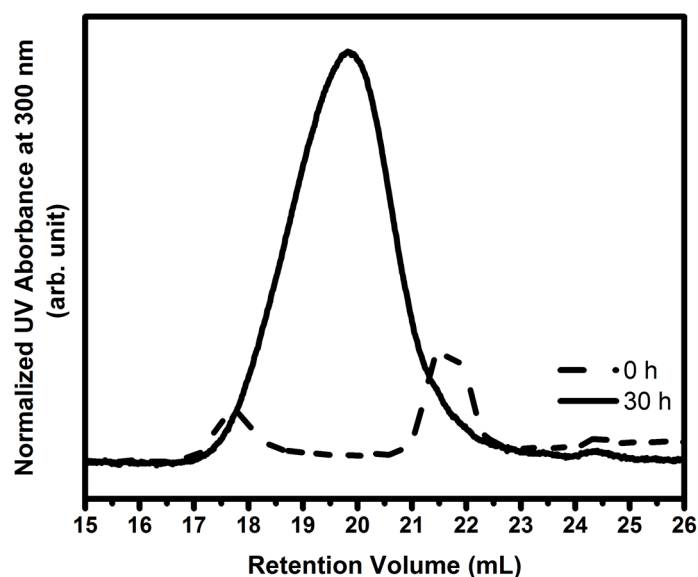


**Figure 3.16.** UV-Vis GPC chromatograms for homopolymer **9a** before and after photoirradiation with 300 nm light. The UV detector was calibrated to detect signals at 300 nm. Absorbance was normalized by the concentration (1 mg/mL).

### 3.4. Experimental

#### Chemicals and Materials

All solvents were supplied by Daejung Chemical unless otherwise noted.

The synthesis and polymerization of polymers were done following the procedures outline in Chapter 2.4.

Photodegradation experiments were performed using 300 nm wavelength lamps connected to a Rayonet RPR-200 photochemical reactor purchased from The Southern New England Ultraviolet Co. All photoreactions were done in quartz vessels.

#### Physical Characterization

Ultraviolet-visibility (UV-vis) spectroscopy measurements were taken using a Cary Series UV-Vis Spectrophotometer supplied by Agilent Technologies Inc. Samples were dissolved in acetonitrile and measurements were taken in a quartz cell with a path length of 1 cm. Baseline measurements were subtracted from the measured spectra.

Gel permeation chromatography (GPC) was performed on a Malvern GPCmax system. Two fluorinated poly(styrene) columns (IMBHW-3078 and I-MBHMW-3078) were used in series and maintained at 35 °C. THF was used as the mobile phase at a flow rate of 0.8 mL/min. Detection was performed using a Viscotek VE3580 RI Detector. UV detection was performed using a Viscotek UV Detector 2600 with the UV detection set at a 300 nm wavelength. Molecular weight and polydispersity data are reported relative to poly(styrene) standards in THF.

Gas chromatography-mass spectrometry (GC-MS) measurements were taken using a Perkin Elmer Clarus 680 Gas Chromatograph and a Clarus SQ 8 S mass spectrometer. Samples were dissolved in acetonitrile in a concentration of 2 mg ml<sup>-1</sup> and ionized at 290 °C.

## Chapter 4: Ascertaining the Hybridization State of Carbon Based Materials and Polymers by *D*-Parameter Values

### 4.1. Introduction

Orbital hybridization is a fundamental determinant of the properties displayed by carbon-based materials. For example, materials rich in  $sp^2$ -hybridized carbon atoms (e.g., graphite) are often soft and exhibit good electrical conductivity properties whereas those containing relatively large amounts of interlinked,  $sp^3$ -hybridized carbon atoms (i.e., diamond) are hard and insulating. As such, quantifying the carbon hybridization states of carbon-based materials is of high importance for determining the suitability of use in various applications. Methods such as solid-state nuclear magnetic resonance (ssNMR) spectroscopy,<sup>157-158</sup> Fourier-transformed infrared (FT-IR) spectroscopy,<sup>159</sup> Raman spectroscopy,<sup>160</sup> X-ray photoelectron spectroscopy (XPS),<sup>161-162</sup> and near-edge X-ray absorption fine structure (NEXAFS) spectroscopy<sup>163</sup> have been previously reported as techniques for such purposes. Although the  $sp^2$ - and/or  $sp^3$ - hybridized carbons can be distinguished using these methods, the use of subjective techniques (e.g., peak fitting) is often required which can challenge accurate quantification.<sup>164</sup>

X-ray photoelectron spectroscopy (XPS) involves the detection of ejected core electrons due to excitation by x-rays (Figure 4.1). Following ejection, electrons from the outer shells relax to fill the empty hole created by the emitted electron. As the electron relaxes, the excess energy can be dissipated through two different processes, fluorescence or Auger emission.<sup>165</sup> Fluorescence involves the excess energy being released in the form of light whereas Auger emission involves transfer of the energy and the subsequent ejection of another electron in a higher lying orbital. The pathway in which the excess energy is dissipated was found to depend on the atomic number of the element being analyzed; higher atomic number elements were found to favor fluorescence emission while lower atomic number elements favored Auger electron ejection (see Figure 4.2).<sup>165-166</sup>

Analysis of the shapes and linewidths of the carbon KLL Auger signals obtained using X-ray Auger induced electron spectroscopy (XAES) has been reported as an alternative method for determining the hybridization states of carbon atoms present in various types of synthetic and natural materials.<sup>161, 167-168</sup> In addition to benefits that include relatively short analysis times, minimal sample quantities and a relatively low sensitivity to charging effects,<sup>169</sup> XAES can be utilized to

quantify the hybridization state of carbon atoms present in insoluble materials.

An Auger signal can be described according to the following equation:

$$E_k = C(1s) - V_i - V_j,$$

where  $E_k$  is the kinetic energy of the Auger electron,  $C(1s)$  is the binding energy of the core 1s band, and  $V_i$  and  $V_j$  represent the binding energies of the valence states involved.<sup>161, 170</sup> Although methods to utilize the structure of the Auger signal as a “fingerprint” of the carbon hybridization states present within a material have been attempted, factors such as low signal to noise ratios and damage from electron irradiation have led to varying results.<sup>168, 171</sup> Therefore, calculations involving measuring the separation degree between the maxima and minima of the first derivatives of the carbon KLL Auger peaks and correlating the separation degree to the ratio of  $sp^2$ -to- $sp^3$ -hybridized atoms are often used instead. Determining the hybridization states of carbon atoms by this separation value, known as the  $D$ -parameter, is advantageous when compared to other methods since factors that result in signal losses, such as incomplete relaxation, which is typical in solid-state NMR experiments,<sup>172</sup> are not an issue; as such, the method may be broadly applicable. For example, previous reports have successfully calculated the hybridization states in mixtures of graphite and diamond<sup>161, 173-174</sup> as well as in block copolymers of styrene and ethylene<sup>169</sup> by measurement of the corresponding  $D$ -parameters.

Our efforts were focused on extending the technique described above to facilitate the quantification of the hybridization states of a broad range of carbon-based materials and to ultimately realize a ‘universal’ calibration method.<sup>169, 175</sup> Since the density of states in the valence band and thus the shapes of corresponding C KLL Auger signals are affected by the physical properties and chemical structures displayed by the samples under study,<sup>169, 176-177</sup> efforts were directed toward the analysis of a systematic series of polymers and related small molecules containing carbon atoms with varying degrees of hybridization states.

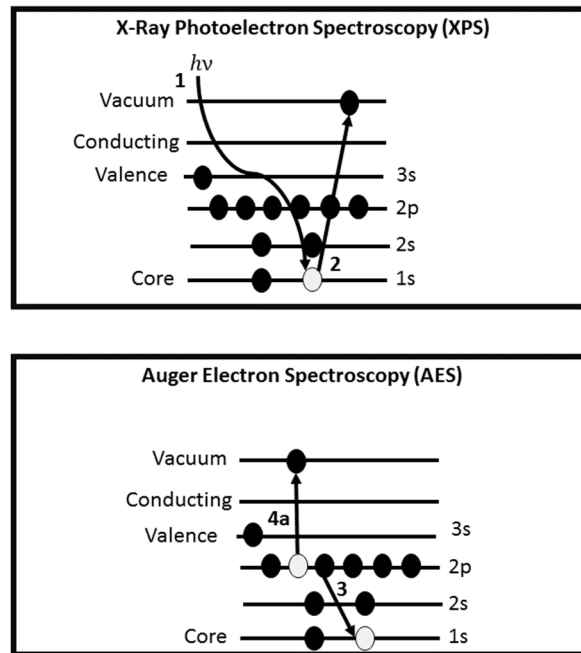


**Figure 4.1.** Depiction of electron ejection due to excitation (top) and subsequent auger electron emission (bottom) for x-ray photoelectron spectroscopy (XPS) and auger electron spectroscopy (AES) analysis.

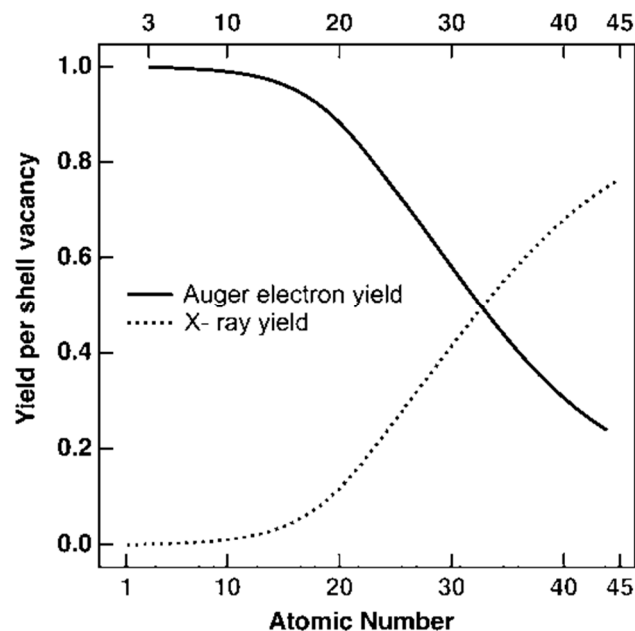


**Figure 4.2.** The correlation between an element's atomic number and auger emission or fluorescence. Taken from reference 165.

## 4.2. Results and Discussion

### 4.2.1. Correlating Orbital Hybridization to *D*-Parameter Values

Our efforts began by acquiring C 1s spectra of mixtures containing known ratios of graphite and diamond using XPS. In accordance with previous results,<sup>161, 173-174</sup> two distinct signals that corresponded to the relative quantities of diamond and graphite in the mixture were observed (see Figure 4.3). While peak fitting may be used to quantify the relative amounts of each material present, such methods can be challenging due to charging effects<sup>178</sup> and signal assignment, particularly for diamond have been proved to vary.<sup>179</sup> Instead, analysis of the first derivative of the C KLL Auger spectra avoids signal deconvolution and assignment,<sup>168, 174, 177</sup> particularly in samples that result in poor signal-to-noise ratios,<sup>174</sup> and/or suffer from charging effects.<sup>169</sup> Following procedures outlined in the literature,<sup>173-174</sup> *D*-parameters were calculated from the first derivatives of the C KLL Auger signals recorded for the aforementioned mixtures and the ratios of *sp*<sup>2</sup>-to-*sp*<sup>3</sup>-hybridized carbons were determined (see Figures 4.3 and 4.4). As summarized in Table 4.1 and Figure 4.5, a linear correlation similar to previously reported results was observed.<sup>161, 174, 180</sup>

To determine if the analysis technique described above could be extended to other carbon-based materials, a systematic series of polymers comprised of carbons with varying ratios of *sp*<sup>2</sup>-to-*sp*<sup>3</sup> hybridization states were synthesized utilizing the ring-opening metathesis polymerization (ROMP) reaction and analyzed (see Table 4.2 and Figure 4.6). ROMP was selected because the ratio of *sp*<sup>2</sup>-to-*sp*<sup>3</sup> hybridization present in the monomer unit is preserved in the repeat unit of the corresponding products,<sup>48</sup> which in turn allowed us to synthesize polymers with tunable compositions. As shown in Figure 4.6 and summarized in Table 4.2, a good correlation between the *D*-parameter and the percentage of *sp*<sup>3</sup>-hybridized carbons within a given material was observed. For example, poly(acetylene) was found to exhibit a larger *D*-parameter than poly(ethylene) (c.f.,  $17.30 \pm 0.51$  vs.  $12.70 \pm 0.17$ ). In addition to the different hybridization states, the larger *D*-parameter values were attributed in part to expanded peak widths that may arise from electronic transitions within the unhybridized *p*-orbitals.<sup>161, 174</sup>



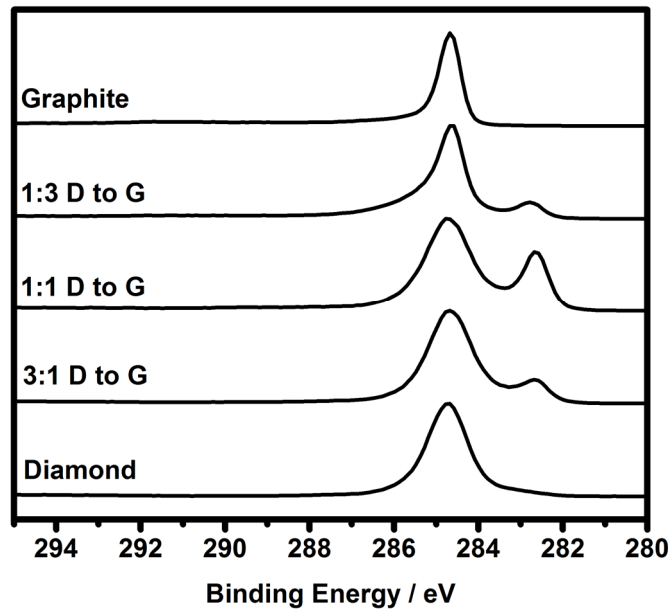


**Figure 4.3.** Representative carbon 1s spectra recorded by XPS for graphite, diamond and various physical mixtures of graphite (G) and diamond (D).

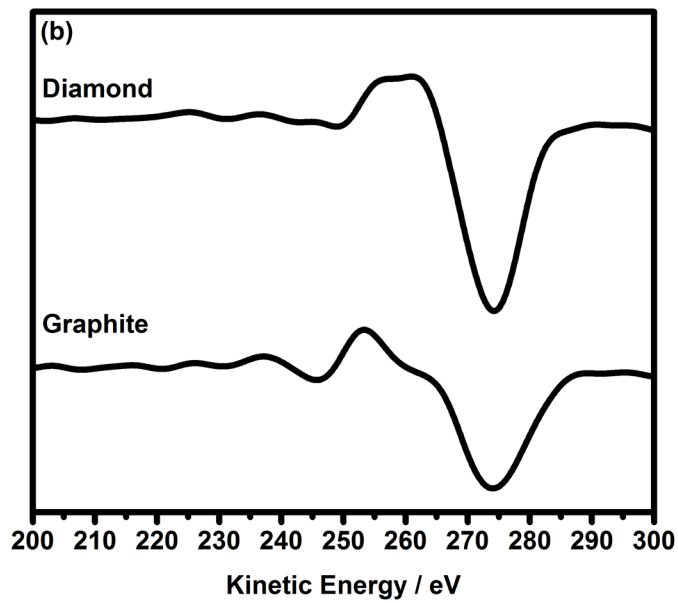
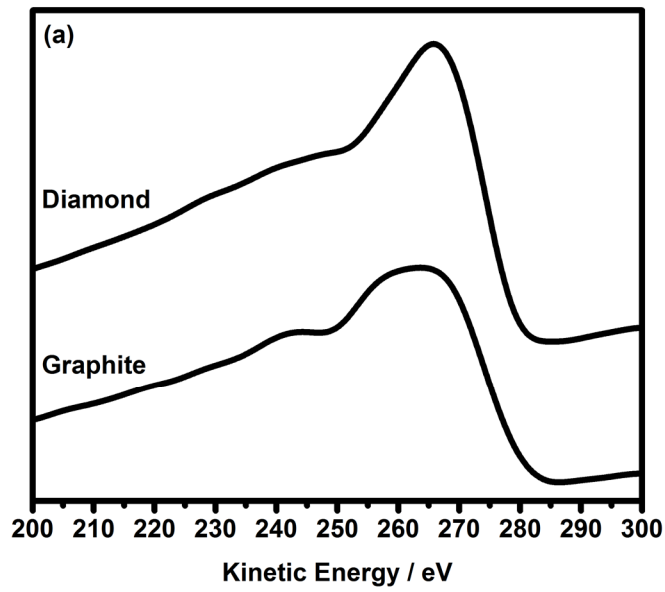


**Figure 4.4.** Representative C KLL Auger (a) and first-derivative C KLL Auger (b) spectra of diamond and graphite powder.

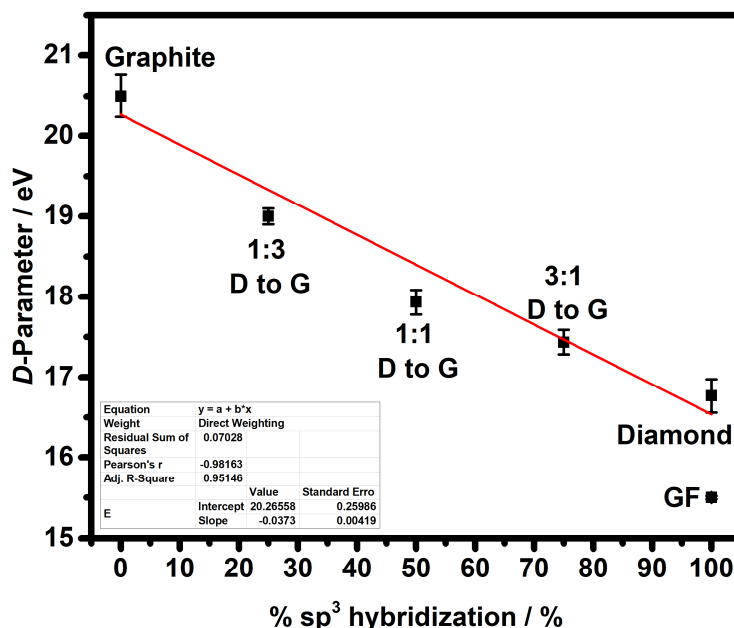


**Figure 4.5.** Plot of  $D$ -parameter values versus the percentage of  $sp^3$  hybridized carbons in graphite, diamond, various physical mixtures of graphite (G) and diamond (D), and graphite fluoride.<sup>181</sup>

**Table 4.1.** Summary of  $D$ -parameter values and standard errors calculated for diamond, graphite, various physical mixtures of those two carbon materials, and graphite fluoride (as a control sample<sup>182</sup>).

Diamond to Graphite Ratio	Amount of Diamond (mg)	Amount of Graphite (mg)	% $sp^2$	% $sp^3$	$D$ -Parameter (eV) <sup>a</sup>	Standard Error <sup>b</sup>
1:0	100	0	0	100	16.8	0.2
3:1	75	25	25	75	17.4	0.2
1:1	50	50	50	50	17.9	0.2
1:3	25	75	75	25	19	0.1
0:1	0	100	100	0	20.5	0.3
Graphite Fluoride	-	-	-	-	15.5	0.0

<sup>a</sup> The  $D$ -parameter values represent the average value from a minimum of three different measurements taken at different locations on the sample. <sup>b</sup> The standard errors were calculated from a minimum of three different measurements taken at different locations on the sample.

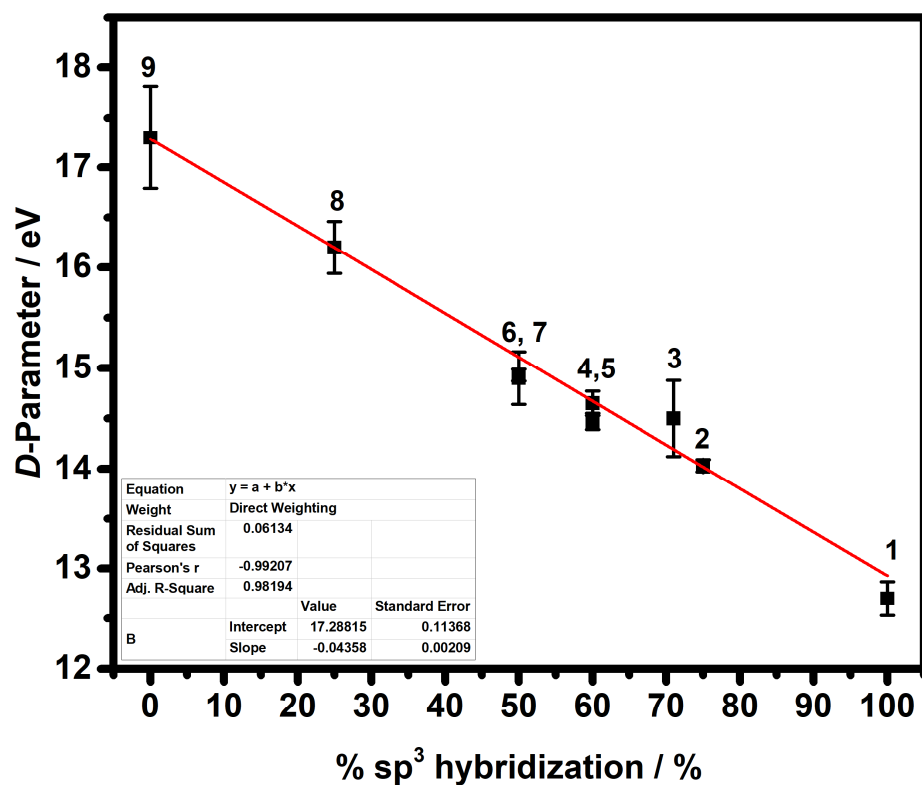


**Figure 4.6.** Plot of  $D$ -parameter values versus the percentage of  $sp^3$  hybridized carbons found in various polymers. The percentages were calculated from the formal repeat unit of each polymer analyzed. The numbers shown refer to a particular sample and are defined in Table 4.2.

**Table 4.2.** Summary of *D*-parameter values, and standard errors measured for various polymers.

Entry	Polymer	Structure	% sp <sup>2</sup>	% sp <sup>3</sup>	D-Parameter (eV) <sup>a</sup>	Standard Error <sup>b</sup>
1	Poly(ethylene)		0	100	12.7	0.2
2	Poly(cyclooctene)		25	75	14.0	0.1
3	Poly(norbornene)		29	71	14.5	0.4
4	Poly(cyclopentene)		40	60	14.5	0.1
5	Poly(dicyclopentadiene)		40	60	14.7	0.1
6	Poly(cyclooctadiene) a.k.a Poly(butadiene)		50	50	14.9	0.1
7	<i>cis</i> -1,4-Poly(butadiene)		50	50	14.9	0.3
8	Poly(styrene)		75	25	16.2	0.3
9	Poly(cyclooctatetraene) a.k.a Polyacetylene		100	0	17.3	0.5

<sup>a</sup> The *D*-parameter values represent the average value from a minimum of three different measurements taken at different locations on the sample. <sup>b</sup> The standard errors were calculated from a minimum of three different measurements taken at different locations on the sample.

#### 4.2.2. Extension of the *D*-Parameter via a Calibration Curve based on $\pi$ -to- $\sigma$ -Bonding Ratios

Next, polymers containing *sp*-hybridized carbon atoms and/or heteroatoms were analyzed; key results are shown in Figure 4.7 and summarized in Table 4.3. Unfortunately, it proved challenging to extract useful trends between the *D*-parameters measured for polymers containing *sp*<sup>2</sup>- and/or *sp*<sup>3</sup>-hybridized carbons to those containing *sp*-hybridized carbons. For example, no correlation was observed between poly(styrene), a polymer that contains *sp*<sup>2</sup>- and *sp*<sup>3</sup>- hybridized carbons, poly(phenylene ethynylene), a polymer that is comprised of *sp*- and *sp*<sup>2</sup>-hybridized carbons, and poly(vinyl acetylene), a polymer containing only *sp*- and *sp*<sup>3</sup>-hybridized carbons (see Table 4.3).

This limitation prompted the development of an alternative calibration curve that correlated the calculated *D*-parameters to the ratio of canonical  $\pi$ -to- $\sigma$ -bonds within the formal repeat unit of the polymer. Such a comparison resulted in a linear correlation between the calculated *D*-parameter values and the  $\pi$ -to- $\sigma$ -bond ratio for polymers consisting of only carbon and hydrogen, with the exception of poly(vinyl acetylene). This discrepancy was attributed to the high reactivity of the terminal alkynes which may have undergone crosslinking via addition over the course of the analysis and thus resulted in a change in the measured hybridization state of the corresponding carbon atoms. In contrast, linear trends were not observed with polymers containing heteroatoms, which may be due to charging effects.<sup>183</sup> Electronegative heteroatoms (e.g., nitrogen and oxygen) may facilitate the buildup of positive charge on adjoining carbon atoms which effectively alters the hybridization states and thus the corresponding *D*-parameter values of the latter.

Finally, a series of small molecule analogues of graphite were analyzed. As shown in Figure 4.7 and summarized in Table 4.3, the *D*-parameters measured for pentacene as well as coronene were less than that of graphite, which may be due to localization effects<sup>184</sup> and/or properties intrinsic to graphite (i.e., high surface area or extended conjugation) that are not present in its small molecule analogues. In contrast, calculation of the ratio of  $\pi$ -to- $\sigma$ -bonds using the method described above resulted in a good correlation with the calibration curve constructed from the carbon-based polymers.

Although linear relationships between the *D*-parameter and degree of hybridization for the mixtures of graphene and diamond mixtures as well as for the hydrocarbons were observed, the trends and underlying *D*-parameter values calculated for similar degrees of hybridization were not identical.<sup>185</sup> For example, the *D*-parameter measured for a 1:1 mixture of graphite and diamond was found to be 17.90 whereas the value measured for poly(cyclooctadiene) was determined to be 14.93, even though both samples were comprised of stoichiometric ratios of *sp*<sup>2</sup>- and *sp*<sup>3</sup>-hybridized carbons.

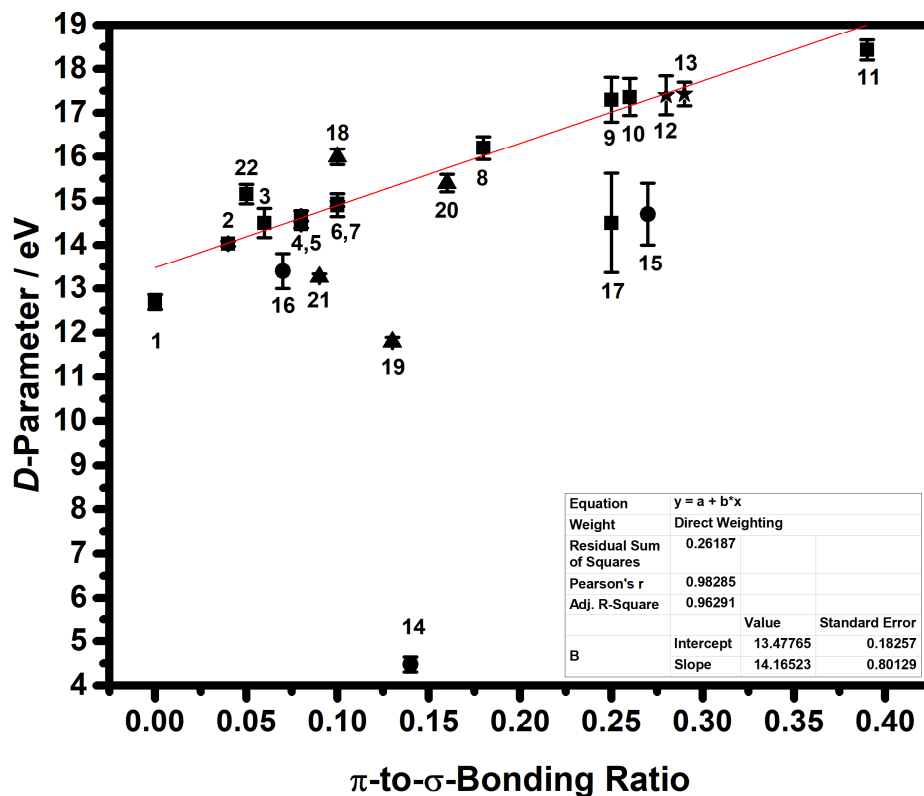


**Figure 4.7.** Plot of the *D*-parameter values to the canonical  $\pi$ -to- $\sigma$  bonding ratios of polymers containing carbons in different hybridization states (squares), small molecules (stars), polymers containing heteroatoms (circles), and polymer blends (triangles). The hybridization ratios were calculated from the formal repeat units of the respective polymers. The numbers shown refer to a particular sample and are defined in Table 4.3.

**Table 4.3.**  $\pi$ -to- $\sigma$ -bond ratios and  $D$ -parameter values for various polymers, blends and small molecules.

Entry	Polymer	Structure	# of $\sigma$ Bonds	# of $\pi$ Bonds	$\pi$ to $\sigma$ Ratio <sup>a</sup>	D-Parameter Average (eV) <sup>b</sup>	Standard Error <sup>c</sup>
1	Poly(ethylene)		6	0	0.00	12.70	0.17
2	Poly(cyclooctene)		23	1	0.04	14.03	0.06
3	Poly(norbornene)		18	1	0.06	14.50	0.33
4	Poly(cyclopentene)		13	1	0.08	14.47	0.08
5	Poly(dicyclopentadiene)		24	2	0.08	14.65	0.12
6	Poly(cyclooctadiene) a.k.a Poly(butadiene)		20	2	0.10	14.93	0.06
7	cis-1,4-Polybutadiene		10	1	0.10	14.90	0.26
8	Poly(styrene)		17	3	0.18	16.20	0.26
9	Poly(cyclooctatetraene) a.k.a. poly(acetylene)		16	4	0.25	17.30	0.51
10	Poly(vinyl phenyl acetylene)		19	5	0.26	17.36	0.42
11	Poly(phenylene ethynylene)		13	5	0.39	18.43	0.23
12	Pentacene		40	11	0.28	17.40	0.44
13	Coronene		41	12	0.29	17.43	0.27
14	Poly(acrylonitrile)		7	1	0.14	4.48	0.17
15	Poly(4-vinyl pyridine)		11	3	0.27	14.70	0.7
16	Poly(methyl methacrylate)		14	1	0.07	13.43	0.4
17	Poly(vinyl acetylene)		8	2	0.25	14.50	1.13
18	PE : PA 1 : 1	-	10	1	0.10	16.00	0.18
19	PS : PE 1 : 1	-	3	23	0.13	11.80	0.1
20	PS : PE 3 : 1	-	57	9	0.16	15.40	0.2
21	PS : PE 1 : 3	-	35	3	0.09	13.27	0.06
22 <sup>d</sup>	PS- <i>b</i> -PE- <i>b</i> -PS		65	3	0.05	15.15	0.22

<sup>a</sup> The  $\pi$ -to- $\sigma$ -bond ratio was calculated from the repeat unit of the polymer. <sup>b</sup> The  $D$ -parameter values represent the average value obtained from a minimum of three different measurements taken at different locations on a sample. <sup>c</sup> Standard errors were calculated from a minimum of three different measurements taken at different locations on a sample. <sup>d</sup> The ratio of poly(styrene) to poly(ethylene) present in the block copolymers was determined to be 1:4 by <sup>1</sup>H NMR spectroscopy.



In contrast, the  $D$ -parameter values measured for poly(cyclooctadiene) and *cis*-1,4-poly(butadiene), which also contained a 1:1 ratio of  $sp^2$ - and  $sp^3$ -hybridized carbons, were found to be nearly identical (14.93 versus 14.90). Turgeon et al. also observed different linear correlations when comparing graphite/diamond mixtures with block copolymers of styrene and ethylene, and attributed the differences to the presence of hydrogen in the latter.<sup>169</sup> Although the presence of C–H bonds in synthetic polymers compared to the absence of C–H bonds in graphite / diamond mixtures is a plausible explanation for the different linear relationships, it does not explain why the  $D$ -parameter values for the block copolymer and the mixtures of poly(styrene) and poly(ethylene) do not correlate to the  $\pi$ -to- $\sigma$ -bonding calibration curve described above.

In order to elucidate the reason behind these differences, the  $D$ -parameters for physical, stoichiometric mixtures of poly(ethylene) and poly(acetylene) as well as blends of poly(styrene) and poly(ethylene) were measured. As shown in Figure 4.8, the first-derivative Auger spectrum that was recorded for the former exhibited a wider valley and featured two different minima that aligned with the minima that were independently measured for poly(acetylene) and poly(ethylene). A similar observation was made when comparing the first-derivative Auger spectra of the blends of poly(styrene) and poly(ethylene) (Figure 4.9). As expected, the poly(styrene) / poly(ethylene) blends and the poly(ethylene) / poly(acetylene) mixtures did not show correlations between the  $D$ -parameter values and the corresponding  $\pi$ -to- $\sigma$ -bond ratios (c.f. Figure 4.7 and Table 4.3). We concluded from these results that the hydrocarbon calibration curve presented herein may be applicable to materials with constituents that are connected through a common backbone.

Further examination of the 1:1 blend of poly(styrene) and poly(ethylene) by differential scanning calorimetry (DSC) revealed distinct peaks that corresponded to the glass transition temperature ( $T_g$ ) of poly(styrene) (ca. 100 °C) and the melting temperature of poly(ethylene) (ca. 130 °C) (see Appendix E).<sup>186</sup> These signals are in line with literature values reported for homopolymers of styrene<sup>187</sup> and ethylene.<sup>188</sup> Likewise, DSC data recorded for the poly(styrene)-*block*-poly(ethylene)-*block*-poly(styrene) showed signals that corresponded to a glass transition and a melting temperature (see Appendix E). Collectively, the data indicated that the 1:1 blend of poly(styrene) and poly(ethylene) as well as the block copolymer were phase separated.<sup>189</sup> As such, the poly(styrene) and poly(ethylene) components have limited interaction with each other, and thus may not be representative of a homogenous blend. These results also explain why the blends and the block copolymers exhibited relatively wide minima in the first-derivative spectra because each signal may stem from the respective homopolymers (c.f., Figure 4.9).

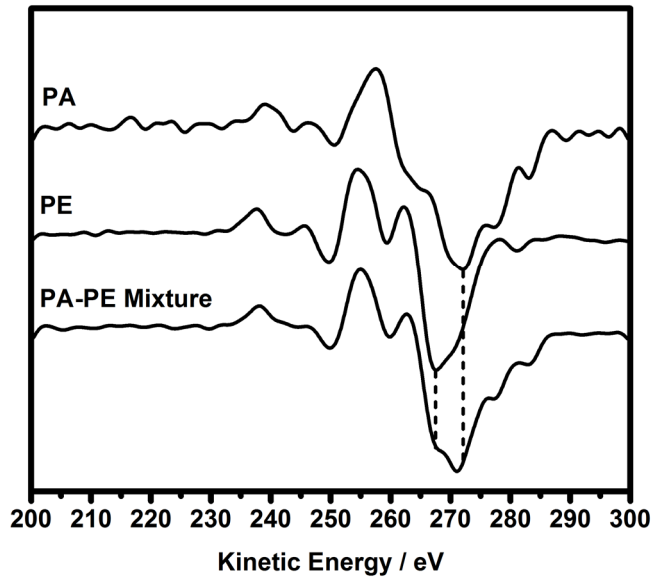


**Figure 4.8.** First-derivative Auger spectra recorded for poly(ethylene) (PE), poly(acetylene) (PA) and a stoichiometric, physical mixture of poly(ethylene) and poly(acetylene).

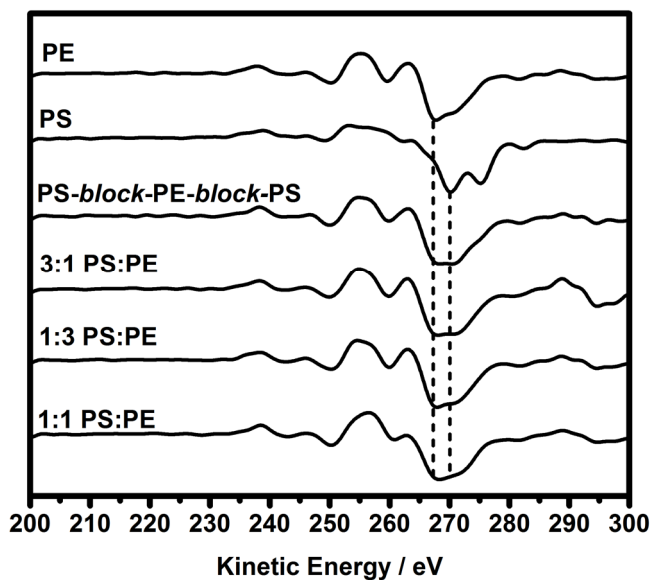


**Figure 4.9.** First-derivative Auger spectra recorded for poly(ethylene) (PE), poly(styrene) (PS), a poly(styrene)-block-poly(ethylene)-block-poly(styrene) block copolymer, and various poly(ethylene)/poly(styrene) blends (ratios are indicated).

### 4.3. Conclusions

Herein we report the use of XAES as a method to ascertain the hybridization states of the carbon atoms in various synthetic polymers. In addition to only requiring minimal amounts of sample and being robust to factors that often result in signal loss, the method is not dependent on the use of peak-fitting procedures. Utilization of this method was found to be successful for quantifying the relative amounts of  $sp^2$ - and  $sp^3$ -hybridized carbon atoms in various hydrocarbons and was extended to polymers containing  $sp$ -hybridized carbons by utilizing the ratio of formal  $\pi$ -to- $\sigma$  bonds present within the polymer repeat unit. Indeed, the methodology is not only applicable to materials containing  $sp^2$ - and  $sp^3$ -hybridized carbons, but also enables measurement of those that are  $sp$ -hybridized which, to the best of our knowledge, is unprecedented. The technique may be limited to polymer samples that consist exclusively of carbon and hydrogen, are not phase-separated, and are connected via a backbone of carbon atoms. Nevertheless, the quantification of hybridization states in synthetic polymers by XAES provides an alternative technique to assess a wide range of macromolecular materials and enables the rapid quantification of their relative ratios of  $sp$ -,  $sp^2$ - and  $sp^3$ -hybridized carbon atoms.

#### 4.4. Experimental

##### Chemicals and Materials

Poly(ethylene), cyclooctadiene, poly(styrene), poly(acrylonitrile), poly(4-vinylpyridine), Grubbs 1<sup>st</sup> generation catalyst, Grubbs 2<sup>nd</sup> generation catalyst, diamond powder, 1,4-diethynylbenzene, poly(styrene)-*block*-poly(butadiene)-*block*-poly(styrene), and graphite fluoride were purchased from Sigma-Aldrich Inc. Cyclooctene and ethyl vinyl ether were purchased from Alfa Aesar. *cis*-1,4-poly(butadiene) was purchased from Scientific Polymer Products. Cyclooctatetraene was purchased from Matrix Scientific. Graphite powder was purchased from Bay Carbon (Bay Carbon Inc., Bay City, Michigan, USA). Cyclopentene, coronene, and pentacene were purchased from Tokyo Chemical Industry.

##### Synthesis of Polymers for XAES Analysis

Poly(cyclooctene),<sup>75</sup> poly(cyclopentene),<sup>75</sup> poly(dicyclopentadiene)<sup>190</sup>, poly(cyclooctadiene),<sup>75</sup> poly(acetylene),<sup>31</sup> poly(vinyl acetylene),<sup>191</sup> poly(vinyl phenylacetylene),<sup>192-193</sup> poly(phenylene ethynylene)<sup>194</sup> and poly(styrene)-*block*-poly(ethylene)-*block*-poly(styrene)<sup>195</sup> were synthesized following previously reported procedures.

##### Mixtures of Graphite and Diamond for XAES Analysis

Graphite (particle size: ca. 69  $\mu\text{m}$ ) and diamond powder (ca 1  $\mu\text{m}$ ) were mixed in known ratios using a mortar and pestle, and then dried under reduced pressure.

##### Blends of Poly(styrene) and Poly(ethylene) for XAES Analysis

Various combinations of poly(styrene) and poly(ethylene) were blended according to a previously reported method.<sup>196</sup> Briefly, 1:1 (5.00 g, 48 mmol poly(styrene) and 1.35 g, 48 mmol poly(ethylene)), 1:3 (3.00 g, 29 mmol poly(styrene) and 2.42 g, 87 mmol poly(ethylene)), and 3:1 (5.00 g, 48 mmol poly(styrene) and 0.45 g, 16 mmol poly(ethylene)) molar mixtures of poly(styrene) and poly(ethylene) were blended at 220 °C in a Haake Minilab II Twin Screw Extruder (Thermo Fisher Scientific, Waltham, MA, USA). The polymers were then extruded over the course of 10 min at a screw rotation of 90 rpm and then dried under reduced pressure at 100 °C.

## Mixtures of Poly(acetylene) and Poly(ethylene) for XAES Analysis

In a glove box filled with nitrogen, an analytical mill (IKA A-10, Staufen, Germany) was charged with poly(acetylene) (340 mg, 3.27 mmol) and poly(ethylene) (366 mg, 13.08 mmol), and then the resulting mixture was ground for 2 min. The resulting material was loaded onto an XPS sample holder and transferred to an XPS analysis chamber using an air-free vessel to minimize oxidation of the poly(acetylene) component.

## Physical Characterization

XPS and XAES data were recorded over a spot size of 500  $\mu\text{m}$  using an Escalab 250Xi (Thermo Fisher Scientific, Waltham, MA, USA) equipped with a monochromated aluminum  $K\alpha$  source (1486.6 eV). All samples were dried under vacuum before analysis. All measurements were recorded at a normal angle from the surface using charge compensation via a combined ion/flood gun operating at a current of 50  $\mu\text{A}$  and an ion voltage of 2 V. Carbon 1s spectra were taken at a pass energy of 20 eV (100 scans). XAES of the C KLL Auger measurements were taken at a retard ratio of 4 s (100 scans). Following previously reported procedures,<sup>197-198</sup> all spectra were calibrated by initially recording the gold  $4f_{7/2}$  spectrum of a gold foil under the same conditions outlined above. The spectrum was then shifted so that the peak position of the gold  $4f_{7/2}$  spectrum was equal to 84.0 eV. The shifted value was applied to all subsequent C1s and Auger spectra.

XPS and Auger data were processed using the Avantage software package (version 5.966). A 23-point Savitzky-Golay filter was applied to the XAES data before applying the first derivative. The  $D$ -parameter was calculated as the distance between the maximum and minimum points in the derivative spectra. For each sample analyzed, measurements were acquired at three different locations.

DSC data were recorded using a TA Q2000 Differential Scanning Calorimeter (TA Instruments, New Castle, DE, USA). Measurements were taken under an atmosphere of nitrogen (50 mL  $\text{min}^{-1}$  over a temperature range of  $-80\text{ }^{\circ}\text{C}$  to  $150\text{ }^{\circ}\text{C}$ . The samples underwent two heating and cooling cycles at rates of up to  $20\text{ }^{\circ}\text{C min}^{-1}$  prior to recording of the data.

TGA traces were recorded under nitrogen (60 mL  $\text{min}^{-1}$ ) on a TA Instruments TGA Q500 module at a heating rate of  $10\text{ }^{\circ}\text{C min}^{-1}$  and using a platinum sample pan. The quantity of sample

analyzed was typically 5–10 mg. High-purity nickel was used as a standard for temperature calibration (based on its Curie temperature).

#### 4.5. Acknowledgements

Portions of this chapter were reproduced in part with permission from Lee, S. Y.; Lyu, J.; Kang, S.; Lu, S. J.; Bielawski, C. W., Ascertaining the Carbon Hybridization States of Synthetic Polymers with X-ray Induced Auger Electron Spectroscopy. *Journal of Physical Chemistry C* **2018**, *122* (22), 11855-11861. Copyright 2018. American Chemical Society

Poly(vinyl acetylene) and poly(vinyl phenylacetylene) were synthesized with the assistance of Lyu, J. Blends of poly(styrene) and poly(ethylene) were made with assistance of Lu, S. Synthesis of poly(phenylene ethynylene) was done with the assistance of Kang, S.

## Chapter 5: Conclusions and Future Outlooks

### 5.1. Conclusions

The merging of synthetic methods derived from organic chemistry with polymer science has resulted in the rapid advancement of both polymerization methods and applications. Although organic chemistry and polymer chemistry initially began as two divisive areas, these two fields now share a symbiotic relationship as concepts and mechanisms from both disciplines have led to groundbreaking discoveries. The field of macromolecular research has advanced to the point where polymers can be polymerized to exhibit specific morphologies and properties; concepts and ideas that probably were not even entertained during the infancy stages of polymer chemistry. With polymers finding new applications on a daily basis, research into the continued progression of polymerization methods and also modifications to introduce new properties is inevitable.

The rapid evolution of polymer synthesis has led to a direct correlation to the advancement in polymer analysis. Analysis techniques such as size exclusion chromatography (SEC), nuclear magnetic resonance (NMR) spectroscopy, thermal gravimetric analysis (TGA), and differential scanning calorimetry (DSC), have been instrumental in identifying polymer properties and attributing those properties to specific functionalities within the polymer. As polymers exhibiting new traits and morphologies continue to be discovered, challenges such as insolubility are bound to arise. Therefore, research into developing novel and/or alternative methods to analyze these properties, such as the Auger electron spectroscopy technique outlined in this dissertation, must continue in order for polymer chemists to be able to pinpoint the influence of specific functionalities on a polymer's properties, and thus, tailor polymers for specific applications.

### 5.2. Future Outlooks

The advancements in polymerization methods coupled with the development of analytical methods has led to a meteoric rise in the field of polymer chemistry, which in turn, has led to widespread utilization of polymers in everyday common items. Less publicized however are the problems related to removal or disposal of polymeric materials. Traits that make polymers so useful, such as durability and toughness, are also the same reasons why disposal or recycling of polymeric materials remains a daunting task. A representative example of the severity of the situation would be the Great Pacific Garbage Patch (GPGP) located between Hawaii and California. As the GPGP is

located in a relatively stationary region, debris collected from multiple currents is deposited in this region, leading to accumulation. Although it has been difficult to get exact data of the size and weight of this patch, estimates place the GPGP to be 1.6 million km<sup>2</sup> in size and weigh 80,000 metric tons, with 99% of it being plastic debris.<sup>199</sup>

Difficulties with disposing of polymers such as poly(ethylene) arise due to degradation leading to lower molecular weight products instead of small molecules. Although decreasing the molecular weight of a polymer can lead to changes in the polymer's properties, the degraded material is still a polymer in the case of poly(ethylene). However, as a testament to how fast the field of polymer research has developed, methods aimed at addressing these issues are already ongoing. As shown in this dissertation, incorporation of functional groups that can undergo pericyclic reactions (i.e. cyclobutane) can be degraded to small molecules when exposed to light. In the field of biomedicine, similar concepts have already been utilized for drug transport and delivery.<sup>98</sup> The drug could be transported via a polymeric vessel and delivered once it reaches its destination through the photodegradation of the polymer vessel. Therefore, it doesn't seem far-fetched that designed polymers possessing properties similar to polymers used in everyday common applications (i.e. poly(ethylene)) but containing functional groups that can undergo degradation to small molecules when exposed to an external stimulus will be synthesized in the near future. These polymers could be utilized in everyday applications but could be degraded and recycled once they had served their purpose.

The results presented here only show a glimpse into the potential that the field of polymer chemistry possesses. Although no one can predict the future, the historical discoveries that have shaped polymer chemistry into what it is today were all made by pushing to and exceeding the limits of macromolecular chemistry. The results of these discoveries have revolutionized the world we live in as polymers have been incorporated into a multitude of everyday materials that people use on a daily basis. Though this has led to its own set of issues, continued exploration of the macromolecular frontier is bound to lead to solutions as well as usher in the next generation of polymers. No longer is polymer chemistry in a "pioneering period" full of turbulence and chaos. Rather, similar to how concepts derived from organic chemistry ignited the evolution of polymer chemistry, the field of macromolecular science is at the point where its principles and concepts may serve as a spark towards the development of other research fields currently in their early developmental stages. Looking back at the multitude of milestones that have occurred in just under a 100 years since Staudinger first theorized the concept of macromolecules displays how far the field of polymer chemistry has evolved through the efforts of countless researchers. As such, the field of



polymer research will continue to grow as long as it is fueled by scientists who are willing to explore the macromolecular frontier and “boldly go where no man has gone before.”<sup>200</sup>

## References

1. Ringsdorf, H., Hermann Staudinger and the Future of Polymer Research Jubilees-Beloved Occasions for Cultural Piety. *Angew. Chem. Int. Ed.* **2004**, *43*, 1064-76.
2. Mark, H. F., Aus Den Frhen Tagen Der Makromolekularen Chemie. *Naturwissenschaften* **1980**, *67*, 477-483.
3. Staudinger, H., Über Polymerisation. **1920**, *53*, 1073-1085.
4. Berzelius, J., Unterscheidung Von Damit Analogen Verhältnissen. *Jahres-Bericht* **1833**, *12*, 63-67.
5. Graham, T., Liquid Diffusion Applied to Analysis. *Philosophical Transactions of the Royal Society of London* **1861**, *151*, 183-224.
6. Grubbs, R. B.; Grubbs, R. H., 50<sup>th</sup> Anniversary Perspective: Living Polymerization—Emphasizing the Molecule in Macromolecules. *Macromolecules* **2017**, *50*, 6979-6997.
7. Ren, J. M.; McKenzie, T. G.; Fu, Q.; Wong, E. H.; Xu, J.; An, Z.; Shanmugam, S.; Davis, T. P.; Boyer, C.; Qiao, G. G., Star Polymers. *Chem. Rev.* **2016**, *116*, 6743-836.
8. Yoshida, M.; Fresco, Z. M.; Ohnishi, S.; Fréchet, J. M. J., Efficient Divergent Synthesis of Dendronized Polymers with Extremely High Molecular Weight: Structural Characterization by SEC-MALLS and SFM and Novel Organic Gelation Behavior. *Macromolecules* **2005**, *38*, 334-344.
9. Milner, S. T., Polymer Brushes. *Science* **1991**, *251*, 905-14.
10. Xia, Y.; Olsen, B. D.; Kornfield, J. A.; Grubbs, R. H., Efficient Synthesis of Narrowly Dispersed Brush Copolymers and Study of Their Assemblies: The Importance of Side Chain Arrangement. *J. Am. Chem. Soc.* **2009**, *131*, 18525-32.
11. Gaucher, G.; Dufresne, M. H.; Sant, V. P.; Kang, N.; Maysinger, D.; Leroux, J. C., Block Copolymer Micelles: Preparation, Characterization and Application in Drug Delivery. *J Control Release* **2005**, *109*, 169-88.
12. Chen, T.; Xu, W. F.; Huang, Z. H.; Peng, H. M.; Ke, Z. Y.; Lu, X. W.; Yan, Y. C.; Liu, R. Y., Poly(Phenyleneethynylene) Nanoparticles: Preparation, Living Cell Imaging and Potential Application as Drug Carriers. *J. Mater. Chem. B* **2015**, *3*, 3564-3572.

13. Reisch, A.; Klymchenko, A. S., Fluorescent Polymer Nanoparticles Based on Dyes: Seeking Brighter Tools for Bioimaging. *Small* **2016**, *12*, 1968-92.
14. Odian, G., *Principles of Polymerization*; John Wiley & Sons, Inc., 2004.
15. Van Krevelen, D. W.; Te Nijenhuis, K., Polymer Properties. In *Properties of Polymers*, Van Krevelen, D. W.; Te Nijenhuis, K., Eds. Elsevier: Amsterdam, 2009; pp 3-5.
16. Nunes, R. W.; Martin, J. R.; Johnson, J. F., Influence of Molecular Weight and Molecular Weight Distribution on Mechanical Properties of Polymers. *Polym. Eng. Sci.* **1982**, *22*, 205-228.
17. Merz, E. H.; Nielsen, L. E.; Buchdahl, R., Influence of Molecular Weight on the Properties of Polystyrene. *Ind. Eng. Chem.* **1951**, *43*, 1396-1401.
18. Flory, P. J., Tensile Strength in Relation to Molecular Weight of High Polymers. *J. Am. Chem. Soc.* **1945**, *67*, 2048-2050.
19. Sookne, A. M.; Harris, M., Polymolecularity and Mechanical Properties of Cellulose Acetate. *Ind. Eng. Chem.* **1945**, *37*, 478-482.
20. Nguyen, T. Q.; Kausch, H. H., Molecular Weight Distribution and Mechanical Properties. In *Mechanical Properties and Testing of Polymers*, Springer Netherlands: Dordrecht, 1999; pp 143-150.
21. Szwarc, M., 'Living' Polymers. *Nature* **1956**, *178*, 1168-1169.
22. Klumperman, B., Reversible Deactivation Radical Polymerization. In *Encyclopedia of Polymer Science and Technology*, 2015; pp 1-27.
23. Matyjaszewski, K., Atom Transfer Radical Polymerization: From Mechanisms to Applications. *Isr. J. Chem.* **2012**, *52*, 206-220.
24. Matyjaszewski, K.; Xia, J., Atom Transfer Radical Polymerization. *Chem. Rev.* **2001**, *101*, 2921-90.
25. Curran, D. P., The Design and Application of Free Radical Chain Reactions in Organic Synthesis. Part 1. *Synthesis* **1988**, *1988*, 417-439.
26. Curran, D. P., The Design and Application of Free Radical Chain Reactions in Organic Synthesis. Part 2. *Synthesis* **1988**, *1988*, 489-513.

27. Kharasch, M. S.; Jensen, E. V.; Urry, W. H., Addition of Carbon Tetrachloride and Chloroform to Olefins. *Science* **1945**, *102*, 128.
28. Calderon, N., Olefin Metathesis Reaction. *Acc. Chem. Res.* **1972**, *5*, 127-&.
29. Chauvin, Y., Olefin Metathesis: The Early Days (Nobel Lecture). *Angew. Chem. Int. Ed.* **2006**, *45*, 3740-7.
30. Hawker, C. J.; Wooley, K. L., The Convergence of Synthetic Organic and Polymer Chemistries. *Science* **2005**, *309*, 1200-5.
31. Scherman, O. A.; Grubbs, R. H., Polycyclooctatetraene (Polyacetylene) Produced with a Ruthenium Olefin Metathesis Catalyst. *Synth. Met.* **2001**, *124*, 431-434.
32. Saxman, A. M.; Liepins, R.; Aldissi, M., Polyacetylene: Its Synthesis, Doping and Structure. *Prog. Polym. Sci.* **1985**, *11*, 57-89.
33. Gorman, C. B.; Ginsburg, E. J.; Grubbs, R. H., Soluble, Highly Conjugated Derivatives of Polyacetylene from the Ring-Opening Metathesis Polymerization of Monosubstituted Cyclooctatetraenes - Synthesis and the Relationship between Polymer Structure and Physical-Properties. *J. Am. Chem. Soc.* **1993**, *115*, 1397-1409.
34. Furlani, A.; Napoletano, C.; Paolesse, R.; Russo, M. V., Conductivity Measurements on Doped Poly(Substituted) Acetylenes. *Synth. Met.* **1987**, *21*, 337-342.
35. Edwards, J. H.; Feast, W. J., A New Synthesis of Poly(Acetylene). *Polymer* **1980**, *21*, 595-596.
36. Feast, W. J.; Tsibouklis, J.; Pouwer, K. L.; Groenendaal, L.; Meijer, E. W., Synthesis, Processing and Material Properties of Conjugated Polymers. *Polymer* **1996**, *37*, 5017-5047.
37. Swager, T. M.; Dougherty, D. A.; Grubbs, R. H., Strained Rings as a Source of Unsaturation - Polybenzvalene, a New Soluble Polyacetylene Precursor. *J. Am. Chem. Soc.* **1988**, *110*, 2973-2974.
38. Chen, Z.; Mercer, J. A. M.; Zhu, X.; Romaniuk, J. A. H.; Pfattner, R.; Cegelski, L.; Martinez, T. J.; Burns, N. Z.; Xia, Y., Mechanochemical Unzipping of Insulating Poly(ladderene) to Semiconducting Polyacetylene. *Science* **2017**, *357*, 475-479.
39. Roth, S.; Filzmoser, M., Conducting Polymers-Thirteen Years of Polyacetylene Doping. *Adv. Mater.* **1990**, *2*, 356-360.

40. Helms, B.; Mynar, J. L.; Hawker, C. J.; Frechet, J. M., Dendronized Linear Polymers via "Click Chemistry". *J. Am. Chem. Soc.* **2004**, *126*, 15020-1.
41. Tsarevsky, N. V.; Bernaerts, K. V.; Dufour, B.; Du Prez, F. E.; Matyjaszewski, K., Well-Defined (Co)Polymers with 5-Vinyltetrazole Units Via Combination of Atom Transfer Radical (Co)Polymerization of Acrylonitrile and "Click Chemistry"-Type Postpolymerization Modification. *Macromolecules* **2004**, *37*, 9308-9313.
42. Das, A.; Theato, P., Activated Ester Containing Polymers: Opportunities and Challenges for the Design of Functional Macromolecules. *Chem. Rev.* **2016**, *116*, 1434-95.
43. Quirk, R. P.; Lee, B., Experimental Criteria for Living Polymerizations. *Polym. Int.* **1992**, *27*, 359-367.
44. Yoon, K. Y.; Lee, I. H.; Kim, K. O.; Jang, J.; Lee, E.; Choi, T. L., One-Pot in Situ Fabrication of Stable Nanocaterpillars Directly from Polyacetylene Diblock Copolymers Synthesized by Mild Ring-Opening Metathesis Polymerization. *J. Am. Chem. Soc.* **2012**, *134*, 14291-4.
45. Matson, J. B.; Grubbs, R. H., ROMP-ATRP Block Copolymers Prepared from Monotelechelic Poly(Oxa)Norbornenes Using a Difunctional Terminating Agent. *Macromolecules* **2008**, *41*, 5626-5631.
46. Runge, M. B.; Dutta, S.; Bowden, N. B., Synthesis of Comb Block Copolymers by ROMP, ATRP, and ROP and Their Assembly in the Solid State. *Macromolecules* **2006**, *39*, 498-508.
47. Bielawski, C. W.; Benitez, D.; Morita, T.; Grubbs, R. H., Synthesis of End-Functionalized Poly(Norbornene)s via Ring-Opening Metathesis Polymerization. *Macromolecules* **2001**, *34*, 8610-8618.
48. Bielawski, C. W.; Grubbs, R. H., Living Ring-Opening Metathesis Polymerization. *Prog. Polym. Sci.* **2007**, *32*, 1-29.
49. Grubbs, R. H.; Carr, D. D.; Hoppin, C.; Burk, P. L., Consideration of the Mechanism of the Metal Catalyzed Olefin Metathesis Reaction. *J. Am. Chem. Soc.* **1976**, *98*, 3478-3483.
50. Grubbs, R. H.; Burk, P. L.; Carr, D. D., Mechanism of the Olefin Metathesis Reaction. *J. Am. Chem. Soc.* **1975**, *97*, 3265-3267.
51. Katz, T. J.; Rothchild, R., Mechanism of the Olefin Metathesis of 2,2'-Divinylbiphenyl. *J. Am. Chem. Soc.* **1976**, *98*, 2519-2526.

52. Lapinte, V.; de Fremont, P.; Montembault, V. R.; Fontaine, L., Ring Opening Metathesis Polymerization (ROMP) of *cis*- and *trans*-3,4-Bis(Acetyloxymethyl)Cyclobut-1-enes and Synthesis of Block Copolymers. *Macromol. Chem. Phys.* **2004**, *205*, 1238-1245.
53. Morandi, G.; Montembault, V.; Pascual, S.; Legoupy, S.; Fontaine, L., Well-Defined Graft Copolymers Issued from Cyclobutenyl Macromonomers by Combination of ATRP and ROMP. *Macromolecules* **2006**, *39*, 2732-2735.
54. Grubbs, R. B.; Khosravi, E., *Handbook of Metathesis Volume 3: Polymer Synthesis*; Wiley, 2015.
55. Sutthasupa, S.; Shiotsuki, M.; Sanda, F., Recent Advances in Ring-Opening Metathesis Polymerization, and Application to Synthesis of Functional Materials. *Polym. J.* **2010**, *42*, 905-915.
56. Li, S.; Burns, A. B.; Register, R. A.; Bell, A., Poly(Phenylnorbornene) from Ring-Opening Metathesis and its Hydrogenated Derivatives. *Macromol. Chem. Phys.* **2012**, *213*, 2027-2033.
57. Bishop, J. P.; Register, R. A., Poly(Phenylethylnorbornene)s and Their Hydrogenated Derivatives. *Macromol. Rapid Commun.* **2008**, *29*, 713-718.
58. Nishihara, Y.; Inoue, Y.; Nakayama, Y.; Shiono, T.; Takagi, K., Comparative Reactivity of *Exo*- and *Endo*-Isomers in the Ru-Initiated Ring-Opening Metathesis Polymerization of Doubly Functionalized Norbornenes with Both Cyano and Ester Groups. *Macromolecules* **2006**, *39*, 7458-7460.
59. Khosravi, E.; Al-Hajaji, A. A., Ring Opening Metathesis Polymerisation of N-Alkyl Norbornene Dicarboxyimides Using Well-Defined Initiators. *Polymer* **1998**, *39*, 5619-5625.
60. Raptopoulos, G.; Kyriakou, K.; Mali, G.; Scarpellini, A.; Anyfantis, G. C.; Mavromoustakos, T.; Pitsikalis, M.; Paraskevopoulou, P., Copolymerization of Norbornene and Norbornadiene Using a *cis*-Selective Bimetallic W-Based Catalytic System. *Polymers-Basel* **2017**, *9*, 141.
61. Sutthasupa, S.; Shiotsuki, M.; Sanda, F., Recent Advances in Ring-Opening Metathesis Polymerization, and Application to Synthesis of Functional Materials. *Polym. J.* **2010**, *42*, 905.
62. Crabtree, R., *The Organometallic Chemistry of the Transition Metals*, 4th ed.; Wiley, 2005.
63. Schrock, R. R.; Hoveyda, A. H., Molybdenum and Tungsten Imido Alkylidene Complexes as Efficient Olefin-Metathesis Catalysts. *Angew. Chem. Int. Ed.* **2003**, *42*, 4592-633.

64. Schrock, R. R.; DePue, R. T.; Feldman, J.; Schaverien, C. J.; Dewan, J. C.; Liu, A. H., Preparation and Reactivity of Several Alkylidene Complexes of the Type  $W(\text{Chr}')(\text{N}-2,6\text{-C}_6\text{H}_3\text{-Iso-Pr}_2)(\text{or})_2$  and Related Tungstacyclobutane Complexes. Controlling Metathesis Activity through the Choice of Alkoxide Ligand. *J. Am. Chem. Soc.* **1988**, *110*, 1423-1435.
65. Hoveyda, A. H.; Schrock, R. R., Catalytic Asymmetric Olefin Metathesis. *Chemistry* **2001**, *7*, 945-50.
66. Feast, W. J.; Gibson, V. C.; Marshall, E. L., A Remarkable Ancillary Ligand Effect in Living Ring-Opening Metathesis Polymerization. *J. Chem. Soc. Chem. Comm.* **1992**, 1157-1158.
67. Bazan, G. C.; Khosravi, E.; Schrock, R. R.; Feast, W. J.; Gibson, V. C.; O'Regan, M. B.; Thomas, J. K.; Davis, W. M., Living Ring-Opening Metathesis Polymerization of 2,3-Difunctionalized Norbornadienes by  $\text{Mo}(\text{Ch-}t\text{-bu})(\text{N}-2,6\text{-C}_6\text{H}_3\text{-}i\text{-Pr}_2)(\text{O-}t\text{-Bu})_2$ . *J. Am. Chem. Soc.* **1990**, *112*, 8378-8387.
68. Grubbs, R. H., Olefin-Metathesis Catalysts for the Preparation of Molecules and Materials (Nobel Lecture). *Angew. Chem. Int. Ed.* **2006**, *45*, 3760-5.
69. Michelotti, F. W.; Keaveney, W. P., Coordinated Polymerization of the Bicyclo-[2.2.1]-Heptene-2 Ring System (Norbornene) in Polar Media. *J. Polym. Sci. Part A: General Papers* **1965**, *3*, 895-905.
70. Novak, B. M.; Grubbs, R. H., Catalytic Organometallic Chemistry in Water - the Aqueous Ring-Opening Metathesis Polymerization of 7-Oxanorbornene Derivatives. *J. Am. Chem. Soc.* **1988**, *110*, 7542-7543.
71. Novak, B. M.; Grubbs, R. H., The Ring-Opening Metathesis Polymerization of 7-Oxabicyclo[2.2.1]Hept-5-Ene Derivatives - a New Acyclic Polymeric Ionophore. *J. Am. Chem. Soc.* **1988**, *110*, 960-961.
72. Schwab, P.; France, M. B.; Ziller, J. W.; Grubbs, R. H., A Series of Well-Defined Metathesis Catalysts—Synthesis of  $[\text{RuCl}_2(=\text{CHR}')(\text{Pr}_3)_2]$  and Its Reactions. *Angew. Chem. Int. Ed.* **1995**, *34*, 2039-2041.
73. Lynn, D. M.; Kanaoka, S.; Grubbs, R. H., Living Ring-Opening Metathesis Polymerization in Aqueous Media Catalyzed by Well-Defined Ruthenium Carbene Complexes. *J. Am. Chem. Soc.* **1996**, *118*, 784-790.
74. Scholl, M.; Ding, S.; Lee, C. W.; Grubbs, R. H., Synthesis and Activity of a New Generation of Ruthenium-Based Olefin Metathesis Catalysts Coordinated with 1,3-Dimesityl-4,5-Dihydroimidazol-2-Ylidene Ligands. *Org. Lett.* **1999**, *1*, 953-6.

75. Bielawski, C. W.; Grubbs, R. H., Highly Efficient Ring-Opening Metathesis Polymerization (ROMP) Using New Ruthenium Catalysts Containing *N*-Heterocyclic Carbene Ligands. *Angew. Chem. Int. Ed.* **2000**, *39*, 2903-2906.
76. Robson, D. A.; Gibson, V. C.; Davies, R. G.; North, M., A New and Highly Efficient Grubbs Initiator for Ring-Opening Metathesis Polymerization. *Macromolecules* **1999**, *32*, 6371-6373.
77. Bielawski, C. W.; Grubbs, R. H., Increasing the Initiation Efficiency of Ruthenium-Based Ring-Opening Metathesis Initiators: Effect of Excess Phosphine. *Macromolecules* **2001**, *34*, 8838-8840.
78. Love, J. A.; Morgan, J. P.; Trnka, T. M.; Grubbs, R. H., A Practical and Highly Active Ruthenium-Based Catalyst That Effects the Cross Metathesis of Acrylonitrile. *Angew. Chem. Int. Ed.* **2002**, *41*, 4035-4037.
79. Beck, D. L.; Hiltz, A. A.; Knox, J. R., Glass Transitions in Polypropylene. *Spe. Trans.* **1963**, *3*, 279-285.
80. Bekkedahl, N.; Tryon, M., Review - Natural and Synthetic Rubbers. *Anal. Chem.* **1955**, *27*, 589-598.
81. Mark, J., *Polymer Data Handbook*; Oxford University Press, 1999.
82. Flory, P. J., *Principles of Polymer Chemistry*; Cornell University Press: Ithaca, NY, 1953.
83. Karasz, F. E.; MacKnight, W. J., The Influence of Stereoregularity on the Glass Transition Temperatures of Vinyl Polymers. *Macromolecules* **1968**, *1*, 537-540.
84. Gargallo, L.; Soto, E.; Tagle, L. H.; Radić, D., Effect of the Side Chain Structure on the Glass Transition Temperature. *Thermochim. Acta* **1988**, *130*, 289-297.
85. Yazdani-Pedram, M.; Soto, E.; Tagle, L. H.; Diaz, F. R.; Gargallo, L.; Radić, D., Effect of the Side Chain Structure on the Glass Transition Temperatures of Some Poly(Thiocarbonate)S. *Thermochim. Acta* **1986**, *105*, 149-160.
86. Negash, S.; Tatek, Y. B.; Tsige, M., Effect of Tacticity on the Structure and Glass Transition Temperature of Polystyrene Adsorbed onto Solid Surfaces. *J. Chem. Phys.* **2018**, *148*, 134705.
87. Huang, C. L.; Chen, Y. C.; Hsiao, T. J.; Tsai, J. C.; Wang, C., Effect of Tacticity on Viscoelastic Properties of Polystyrene. *Macromolecules* **2011**, *44*, 6155-6161.



88. Liu, F.; Zhang, J. W.; Wang, J. G.; Liu, X. Q.; Zhang, R. Y.; Hu, G. H.; Na, H. N.; Zhu, J., Soft Segment Free Thermoplastic Polyester Elastomers with High Performance. *J. Mater. Chem. A* **2015**, *3*, 13637-13641.
89. Berti, C.; Binassi, E.; Celli, A.; Colonna, M.; Fiorini, M.; Marchese, P.; Marianucci, E.; Gazzano, M.; Di Credico, F.; Brunelle, D. J., Poly(1,4-Cyclohexylenedimethylene 1,4-Cyclohexanedicarboxylate): Influence of Stereochemistry of 1,4-Cyclohexylene Units on the Thermal Properties. *J. Polym. Sci. Pol. Phys.* **2008**, *46*, 619-630.
90. Berti, C.; Celli, A.; Marchese, P.; Marianucci, E.; Barbiroli, G.; Di Credico, F., Influence of Molecular Structure and Stereochemistry of the 1,4-Cyclohexylene Ring on Thermal and Mechanical Behavior of Poly(Butylene 1,4-Cyclohexanedicarboxylate). *Macromol. Chem. Phys.* **2008**, *209*, 1333-1344.
91. Wang, J. G.; Liu, X. Q.; Jia, Z.; Sun, L. Y.; Zhang, Y. J.; Zhu, J., Modification of Poly(ethylene 2,5-Furandicarboxylate) (PEF) with 1, 4-Cyclohexanedimethanol: Influence of Stereochemistry of 1,4-Cyclohexylene Units. *Polymer* **2018**, *137*, 173-185.
92. Morton, M.; Mcgrath, J. E.; Juliano, P. C., Structure-Property Relationships for Styrene-Diene Thermoplastic Elastomers. *J. Polym. Sci. Pol. Symp.* **1969**, *26*, 99-&.
93. Drobny, J. G., 5 - Styrenic Block Copolymers. In *Handbook of Thermoplastic Elastomers (Second Edition)*, Drobny, J. G., Ed. William Andrew Publishing: Oxford, 2014; pp 175-194.
94. Letchford, K.; Burt, H., A Review of the Formation and Classification of Amphiphilic Block Copolymer Nanoparticulate Structures: Micelles, Nanospheres, Nanocapsules and Polymersomes. *Eur. J. Pharm. Biopharm.* **2007**, *65*, 259-69.
95. Cui, H.; Chen, Z.; Zhong, S.; Wooley, K. L.; Pochan, D. J., Block Copolymer Assembly via Kinetic Control. *Science* **2007**, *317*, 647-50.
96. Zhang, L.; Eisenberg, A., Multiple Morphologies of "Crew-Cut" Aggregates of Polystyrene-B-Poly(Acrylic Acid) Block Copolymers. *Science* **1995**, *268*, 1728-31.
97. Choi, Y. K.; Bae, Y. H.; Kim, S. W., Star-Shaped Poly(ether-ester) Block Copolymers: Synthesis, Characterization, and Their Physical Properties. *Macromolecules* **1998**, *31*, 8766-8774.
98. Jeong, B.; Bae, Y. H.; Lee, D. S.; Kim, S. W., Biodegradable Block Copolymers as Injectable Drug-Delivery Systems. *Nature* **1997**, *388*, 860-2.
99. Zhong-wei, G.; Wei-ping, Y.; Ji-yuan, Y.; You-xin, L.; Xian-li, C.; Ge-wen, Z.; Xin-de, F., Biodegradable Block Copolymer Matrices for Long-Acting Contraceptives with Constant Release. *J. Controlled Release* **1992**, *22*, 3-14.

100. Gallardo, A.; Roman, J. S., Effect of Large Polar Side-Groups on the Glass-Transition Temperature of Acrylic Copolymers. *Macromolecules* **1993**, *26*, 3681-3686.
101. Trnka, T. M.; Grubbs, R. H., The Development of  $L_2X_2Ru=CHR$  Olefin Metathesis Catalysts: An Organometallic Success Story. *Acc. Chem. Res.* **2001**, *34*, 18-29.
102. Furstner, A.; Thiel, O. R.; Lehmann, C. W., Study Concerning the Effects of Chelation on the Structure and Catalytic Activity of Ruthenium Carbene Complexes. *Organometallics* **2002**, *21*, 331-335.
103. Sivaram, S., Giulio Natta and the Origins of Stereoregular Polymers. *Resonance* **2017**, *22*, 1007-1023.
104. Natta, G.; Corradini, P., The Crystalline Structure of a New Type of Polypropylene. In *Stereoregular Polymers and Stereospecific Polymerizations*, Natta, G.; Danusso, F., Eds. Pergamon: 1967; pp 19-20.
105. Jones, T. D.; Chaffin, K. A.; Bates, F. S.; Annis, B. K.; Hagan, E. W.; Kim, M. H.; Wignall, G. D.; Fan, W.; Waymouth, R., Effect of Tacticity on Coil Dimensions and Thermodynamic Properties of Polypropylene. *Macromolecules* **2002**, *35*, 5061-5068.
106. Burfield, D. R.; Doi, Y., Differential Scanning Calorimetry Characterization of Polypropylene - Dependence of Tg on Polymer Tacticity and Molecular-Weight. *Macromolecules* **1983**, *16*, 702-704.
107. Grohens, Y.; Brogly, M.; Labbe, C.; David, M. O.; Schultz, J., Glass Transition of Stereoregular Poly(Methyl Methacrylate) at Interfaces. *Langmuir* **1998**, *14*, 2929-2932.
108. Jha, K. C.; Zhu, H.; Dhinojwala, A.; Tsige, M., Molecular Structure of Poly(Methyl Methacrylate) Surface Ii: Effect of Stereoregularity Examined through All-Atom Molecular Dynamics. *Langmuir* **2014**, *30*, 12775-85.
109. Geng, K.; Tsui, O. K. C., Effects of Polymer Tacticity and Molecular Weight on the Glass Transition Temperature of Poly(Methyl Methacrylate) Films on Silica. *Macromolecules* **2016**, *49*, 2671-2678.
110. McDonald, R. N.; Reineke, C. E., Strained-Ring Systems. The Synthesis and Solvolysis of *Exo*-Bicyclo[2.2.0]Hex-2-Yl Tosylate. *J. Org. Chem.* **1967**, *32*, 1878-1887.
111. van Tamelen, E. E.; Pappas, B., The 9,10-Dihydronaphthalene Cyclodecapentaene Valence Bond Isomer System. *J. Am. Chem. Soc.* **1963**, *85*, 3296-3297.

112. Patton, P. A.; Lillya, C. P.; Mccarthy, T. J., Olefin Metathesis of Cyclohexene. *Macromolecules* **1986**, *19*, 1266-1268.

113. Hlil, A. R.; Balogh, J.; Moncho, S.; Su, H. L.; Tuba, R.; Brothers, E. N.; Al-Hashimi, M.; Bazzi, H. S., Ring Opening Metathesis Polymerization (ROMP) of Five-to Eight-Membered Cyclic Olefins: Computational, Thermodynamic, and Experimental Approach. *J. Polym. Sci. Pol. Chem.* **2017**, *55*, 3137-3145.

114. Further attempts with lower concentrations of triphenyl phosphine (20 equivalents and 10 equivalents) led to higher molecular weights than polymer 12, but were still well below the targeted values.

115. Ashirov, R. V.; Zemlyakov, D. I.; Lyapkov, A. A.; Kiselev, S. A., Kinetics of the Metathesis Polymerization of 5,6-Di(Methoxycarbonyl)Bicyclo[2.2.1]Hept-2-Enes on an Original Hoveyda-Grubbs II Type Catalyst. *Kinet. and Catal.* **2013**, *54*, 469-474.

116. Kiselev, S. A.; Lenev, D. A.; Lyapkov, A. A.; Semakin, S. V.; Bozhenkova, G.; Verpoort, F.; Ashirov, R. V., Reactivity of Norbornene Esters in Ring-Opening Metathesis Polymerization Initiated by a N-Chelating Hoveyda II Type Catalyst. *RSC Adv.* **2016**, *6*, 5177-5183.

117. Kanaoka, S.; Grubbs, R. H., Synthesis of Block-Copolymers of Silicon-Containing Norbornene Derivatives Via Living Ring-Opening Metathesis Polymerization Catalyzed by a Ruthenium Carbene Complex. *Macromolecules* **1995**, *28*, 4707-4713.

118. Seehof, N.; Grutke, S.; Risse, W., Selective Reaction with *Exo*-Isomers in Ring-Opening Olefin Metathesis Polymerization (ROMP) of Fluoroalkyl-Substituted Norbornene Derivatives. *Macromolecules* **1993**, *26*, 695-700.

119. The position of the protons attached to the carbon alpha to the olefins was confirmed through proton NMR coupling constants, measurements of the dihedral angle, and the Karplus equation.

120. Antoniadis, S. J.; Samara, C. T.; Theodorou, D. N., Effect of Tacticity on the Molecular Dynamics of Polypropylene Melts. *Macromolecules* **1999**, *32*, 8635-8644.

121. Lohse, D. J.; Hadjichristidis, N., Microphase Separation in Block Copolymers. *Curr. Opin. Colloid. Interface Sci.* **1997**, *2*, 171-176.

122. Leibler, L., Theory of Microphase Separation in Block Copolymers. *Macromolecules* **1980**, *13*, 1602-1617.

123. Stuparu, M. C.; Khan, A.; Hawker, C. J., Phase Separation of Supramolecular and Dynamic Block Copolymers. *Polym. Chem.* **2012**, *3*, 3033-3044.

124. Krappe, U.; Stadler, R.; Voigt-Martin, I., Chiral Assembly in Amorphous ABC Triblock Copolymers. Formation of a Helical Morphology in Polystyrene-Block-Polybutadiene-Block-Poly(Methyl Methacrylate) Block Copolymers. *Macromolecules* **1995**, *28*, 4558-4561.

125. Khandpur, A. K.; Forster, S.; Bates, F. S.; Hamley, I. W.; Ryan, A. J.; Bras, W.; Almdal, K.; Mortensen, K., Polyisoprene-Polystyrene Diblock Copolymer Phase Diagram near the Order-Disorder Transition. *Macromolecules* **1995**, *28*, 8796-8806.

126. Bates, F. S.; Bair, H. E.; Hartney, M. A., Block Copolymers near the Microphase Separation Transition .1. Preparation and Physical Characterization of a Model System. *Macromolecules* **1984**, *17*, 1987-1993.

127. Londono, J. D.; Narten, A. H.; Wignall, G. D.; Honnell, K. G.; Hsieh, E. T.; Johnson, T. W.; Bates, F. S., Composition Dependence of the Interaction Parameter in Isotopic Polymer Blends. *Macromolecules* **1994**, *27*, 2864-2871.

128. Hill, M. J.; Barham, P. J.; Keller, A., Phase Segregation in Blends of Linear with Branched Polyethylene - The Effect of Varying the Molecular-Weight of the Linear Polymer. *Polymer* **1992**, *33*, 2530-2541.

129. The glass transition temperatures for polymers **10f** and **12** were measured and can be viewed in Appendix C. Although polymer **10f** exhibited two separate glass transition temperatures, the presence of a shoulder in the GPC trace made discerning if the glass temperatures were due to the diblock copolymer or the "dead" homopolymer. Although polymer **12** was targeted at a molecular weight of 200 kDa, only one glass transition temperature was seen. This may be in part because the actual  $M_n$  value was 94 kDa, which may not have been enough to cross the critical value for phase separation.

130. Love, J. A.; Morgan, J. P.; Trnka, T. M.; Grubbs, R. H., A Practical and Highly Active Ruthenium-Based Catalyst That Effects the Cross Metathesis of Acrylonitrile. *Angew. Chem. Int. Ed.* **2002**, *41*, 4035-4037.

131. Fulmer, G. R.; Miller, A. J. M.; Sherden, N. H.; Gottlieb, H. E.; Nudelman, A.; Stoltz, B. M.; Bercaw, J. E.; Goldberg, K. I., NMR Chemical Shifts of Trace Impurities: Common Laboratory Solvents, Organics, and Gases in Deuterated Solvents Relevant to the Organometallic Chemist. *Organometallics* **2010**, *29*, 2176-2179.

132. Beale, R. N.; Roe, E. M. F., 554. Ultra-Violet Absorption Spectra of *trans*- and *cis*-Stilbenes and Their Derivatives. Part I. *trans*- and *cis*-Stilbenes. *J. Chem. Soc.* **1953**, 2755-2763.

133. Tiberio, G.; Muccioli, L.; Berardi, R.; Zannoni, C., How Does the *trans-cis* Photoisomerization of Azobenzene Take Place in Organic Solvents? *Chemphyschem* **2010**, *11*, 1018-28.

134. Teator, A. J.; Lastovickova, D. N.; Bielawski, C. W., Switchable Polymerization Catalysts. *Chem. Rev.* **2015**.

135. Yonezawa, N.; Yoshida, T.; Hasegawa, M., Symmetric and Asymmetric Photocleavage of the Cyclobutane Rings in Head-to-Head Coumarin Dimers and Their Lactone-Opened Derivatives. *J. Chem. Soc. Perkin Trans. 1* **1983**, 1083-1086.

136. Andrew, D.; Hastings, D. J.; Weedon, A. C., The Mechanism of the Photochemical Cycloaddition Reaction between 2-Cyclopentenone and Polar Alkenes - Trapping of Triplet 1,4-Biradical Intermediates with Hydrogen Selenide. *J. Am. Chem. Soc.* **1994**, *116*, 10870-10882.

137. Anslyn, E.; Dougherty, D., *Modern Physical Organic Chemistry*; University Science Books, 2006.

138. Chatani, S.; Kloxin, C. J.; Bowman, C. N., The Power of Light in Polymer Science: Photochemical Processes to Manipulate Polymer Formation, Structure, and Properties. *Polym. Chem.* **2014**, *5*, 2187-2201.

139. Houk, K. N.; Gonzalez, J.; Li, Y., Pericyclic Reaction Transition-States - Passions and Punctilios, 1935-1995. *Acc. Chem. Res.* **1995**, *28*, 81-90.

140. Woodward, R. B.; Hoffmann, R., The Conservation of Orbital Symmetry. *Angew. Chem. Int. Ed.* **1969**, *8*, 781-853.

141. Woodward, R. B.; Hoffmann, R., Stereochemistry of Electrocyclic Reactions. *J. Am. Chem. Soc.* **1965**, *87*, 395-&.

142. Basak, S.; Chattopadhyay, K., Studies of Protein Folding and Dynamics Using Single Molecule Fluorescence Spectroscopy. *PCCP* **2014**, *16*, 11139-49.

143. Gromov, S. P.; Vedernikov, A. I.; Lobova, N. A.; Kuz'mina, L. G.; Dmitrieva, S. N.; Strelenko, Y. A.; Howard, J. A., Synthesis, Structure, and Properties of Supramolecular Photoswitches Based on Ammonioalkyl Derivatives of Crown Ether Styryl Dyes. *J. Org. Chem.* **2014**, *79*, 11416-30.

144. Dugave, C.; Demange, L., Cis-Trans Isomerization of Organic Molecules and Biomolecules: Implications and Applications. *Chem. Rev.* **2003**, *103*, 2475-532.

145. Wade, L. G., *Organic Chemistry*, 8th ed.; Pearson, 2014.

146. Macoas, E. M. S.; Fausto, R.; Lundell, J.; Pettersson, M.; Khriachtchev, L.; Rasanen, M., A Matrix Isolation Spectroscopic and Quantum Chemical Study of Fumaric and Maleic Acid. *J. Phys. Chem. A* **2001**, *105*, 3922-3933.

147. Schaumann, E.; Ketcham, R., [2+2]-Cycloreversions. *Angew. Chem. Int. Ed.* **1982**, *21*, 225-247.
148. Drury, M. R.; Bloor, D., The Optical Constants of Isotropic Durham Polyacetylene. *Synth. Met.* **1989**, *32*, 33-41.
149. Qu, J. Q.; Kawasaki, R.; Shiotsuki, M.; Sanda, F.; Masuda, T., Synthesis and Properties of Polyacetylenes Carrying N-Phenylcarbazole and Triphenylamine Moieties. *Polymer* **2006**, *47*, 6551-6559.
150. Prier, C. K.; Rankic, D. A.; MacMillan, D. W., Visible Light Photoredox Catalysis with Transition Metal Complexes: Applications in Organic Synthesis. *Chem. Rev.* **2013**, *113*, 5322-63.
151. Koike, T.; Akita, M., Visible-Light Radical Reaction Designed by Ru- and Ir-Based Photoredox Catalysis. *Inorg. Chem. Front.* **2014**, *1*, 562-576.
152. Acikgoz, C.; Hempenius, M. A.; Huskens, J.; Vancso, G. J., Polymers in Conventional and Alternative Lithography for the Fabrication of Nanostructures. *Eur. Polym. J.* **2011**, *47*, 2033-2052.
153. Wilson, L., Conducting Polymers and Applications. In *Mater. Sci. and Technol.*, 2006.
154. Ma, Y.; Thiele, J.; Abdelmohsen, L.; Xu, J.; Huck, W. T., Biocompatible Macro-Initiators Controlling Radical Retention in Microfluidic on-Chip Photo-Polymerization of Water-in-Oil Emulsions. *Chem. Commun.* **2014**, *50*, 112-4.
155. Cho, N.; Diekhans, J.; Steward, M.; Bakr, O. M.; Choi, S., A Facile Micropatterning Method for a Highly Flexible PEDOT:PSS on SU-8. *Org. Electron.* **2016**, *34*, 75-78.
156. Abargues, R.; Rodriguez-Canto, P. J.; Garcia-Calzada, R.; Martinez-Pastor, J., Patterning of Conducting Polymers Using UV Lithography: The *in-situ* Polymerization Approach. *J. Phys. Chem. C* **2012**, *116*, 17547-17553.
157. Kaplan, S.; Jansen, F.; Machonkin, M., Characterization of Amorphous Carbon Hydrogen Films by Solid State Nuclear Magnetic Resonance. *Appl. Phys. Lett.* **1985**, *47*, 750-753.
158. Jarman, R. H.; Ray, G. J.; Standley, R. W.; Zajac, G. W., Determination of Bonding in Amorphous Carbon Films: A Quantitative Comparison of Core Electron Energy Loss Spectroscopy and <sup>13</sup>C Nuclear Magnetic Resonance Spectroscopy. *Appl. Phys. Lett.* **1986**, *49*, 1065-1067.
159. Grill, A.; Patel, V., Characterization of Diamondlike Carbon by Infrared Spectroscopy? *Appl. Phys. Lett.* **1992**, *60*, 2089-2091.

160. Whitener, K. E.; Lee, W. K.; Campbell, P. M.; Robinson, J. T.; Sheehan, P. E., Chemical Hydrogenation of Single-Layer Graphene Enables Completely Reversible Removal of Electrical Conductivity. *Carbon* **2014**, *72*, 348-353.
161. Lascovich, J. C.; Giorgi, R.; Scaglione, S., Evaluation of the  $sp^2/sp^3$  Ratio in Amorphous Carbon Structure by XPA and XAES. *Appl. Surf. Sci.* **1991**, *47*, 17-21.
162. Haerle, R.; Riedo, E.; Pasquarello, A.; Baldereschi, A.,  $sp^2/sp^3$  Hybridization Ratio in Amorphous Carbon from C 1s Core-Level Shifts: X-Ray Photoelectron Spectroscopy and First-Principles Calculation. *Phys. Rev. B: Condens. Matter* **2001**, *65*, 045101.
163. Jaouen, M.; Tourillon, G.; Delafond, J.; Junqua, N.; Hug, G., A NEXAFS Characterization of Ion-Beam-Assisted Carbon-Sputtered Thin Films. *Diamond Relat. Mater.* **1995**, *4*, 200-206.
164. Singh, B.; Diwan, A.; Jain, V.; Herrera-Gomez, A.; Terry, J.; Linford, M. R., Uniqueness Plots: A Simple Graphical Tool for Identifying Poor Peak Fits in X-Ray Photoelectron Spectroscopy. *Appl. Surf. Sci.* **2016**, *387*, 155-162.
165. Thompson, M.; Baker, M. D.; Christie, A.; Tyson, J. F., *Auger Electron Spectroscopy*; John Wiley & Sons: Chichester, 1985.
166. Wagner, C. D.; Riggs, W. M.; Davis, L. E.; Moulder, J. F., *Handbook of X-Ray Photoelectron Spectroscopy*, 1979.
167. Lascovich, J. C.; Scaglione, S., Comparison among XAES, PELS and XPS Techniques for Evaluation of  $sp^2$  Percentage in a-C-H. *Appl. Surf. Sci.* **1994**, *78*, 17-23.
168. Mizokawa, Y.; Miyasato, T.; Nakamura, S.; Geib, K. M.; Wilmsen, C. W., Comparison of the C KLL First-Derivative Auger Spectra from XPS and AES Using Diamond, Graphite, SiC and Diamond-Like-Carbon Films. *Surf. Sci.* **1987**, *182*, 431-438.
169. Turgeon, S.; Paynter, R. W., On the Determination of Carbon  $sp^2/sp^3$  Ratios in Polystyrene–Polyethylene Copolymers by Photoelectron Spectroscopy. *Thin Solid Films* **2001**, *394*, 43-47.
170. Lascovich, J. C.; Santoni, A., Study of the Occupied Electronic Density of States of Carbon Samples by Using Second Derivative Carbon KVV Auger Spectra. *Appl. Surf. Sci.* **1996**, *103*, 245-253.
171. David, E. R., Auger Line Shapes as a Probe of Electronic Structure in Covalent Systems. *Phys. Scr.* **1992**, *1992*, 77.

172. Freitas, J. C. C.; Cipriano, D. F.; Zucolotto, C. G.; Cunha, A. G.; Emmerich, F. G., Solid-State  $^{13}\text{C}$  NMR Spectroscopy Applied to the Study of Carbon Blacks and Carbon Deposits Obtained by Plasma Pyrolysis of Natural Gas. *J. Spectro.* **2016**, *2016*, 1-6.

173. Mezzi, A.; Kaciulis, S., Surface Investigation of Carbon Films: From Diamond to Graphite. *Surf. Interface Anal.* **2010**, *42*, 1082-1084.

174. Mizokawa, Y.; Miyasato, T.; Nakamura, S.; Geib, K. M.; Wilmsen, C. W., The C KLL First Derivative X Ray Photoelectron Spectroscopy Spectra as a Fingerprint of the Carbon State and the Characterization of Diamondlike Carbon Films. *J. Vac. Sci. Technol., A* **1987**, *5*, 2809-2813.

175. Mérel, P.; Tabbal, M.; Chaker, M.; Moisa, S.; Margot, J., Direct Evaluation of the  $sp^3$  Content in Diamond-Like-Carbon Films by XPS. *Appl. Surf. Sci.* **1998**, *136*, 105-110.

176. Ramaker, D. E., Chemical Effects in the Carbon KVV Auger Line-Shapes. *J. Vac. Sci. Technol., A* **1989**, *7*, 1614-1622.

177. Lesiak, B.; Zemek, J.; Houdkova, J.; Jiricek, P.; Jozwik, A., XPS and XAES of Polyethylenes Aided by Line Shape Analysis: The Effect of Electron Irradiation. *Polym. Degrad. Stab.* **2009**, *94*, 1714-1721.

178. Nansé, G.; Papirer, E.; Fioux, P.; Moguet, F.; Tressaud, A., Fluorination of Carbon Blacks: An X-Ray Photoelectron Spectroscopy Study: I. A Literature Review of XPS Studies of Fluorinated Carbons. XPS Investigation of Some Reference Compounds. *Carbon* **1997**, *35*, 175-194.

179. Fujimoto, A.; Yamada, Y.; Koinuma, M.; Sato, S., Origins of  $sp^3$  C Peaks in C 1s X-Ray Photoelectron Spectra of Carbon Materials. *Anal. Chem.* **2016**, *88*, 6110-4.

180. Fuchs, A.; Scherer, J.; Jung, K.; Ehrhardt, H., Determination of  $sp^2/sp^3$  Carbon Bonding Ratio in  $a\text{-C:H}$  Including Irradiation Damage by Factor Analysis of Auger Electron Spectra. *Thin Solid Films* **1993**, *232*, 51-55.

181. The  $D$ -parameter measured for graphite fluoride was lower than that measured for diamond even though both materials consist of  $sp^3$  hybridized carbon.

182. The  $D$ -parameter measured for graphite fluoride was lower than that measured for diamond even though both materials consist of  $sp^3$  hybridized carbon.

183. The  $D$ -parameter measured for graphite fluoride was lower than that measured for diamond even though both materials consist of  $sp^3$  hybridized carbon.

184. Clar, E., *Polycyclic Hydrocarbons*; Springer Science & Business Media, 2013; Vol. 1.



185. The slope (14.16523) and intercept (13.47765) for the p-to-s-calibration curve could not be directly compared with the calibration curves shown in Figures 4.5 and 4.6 since the X-axis's were different

186. The block copolymer showed glass transition temperatures lower than the values reported for the homopolymers, which was attributed to increases in segmental motion. For further information please see Morèse-Séguéla, B.; St-Jacques, M.; Renaud, J. M.; Prod'homme, J., *Macromolecules* **1980**, *13*, 100-106.

187. Rieger, J., The Glass Transition Temperature of Polystyrene - Results of a Round Robin Test. *J. Therm. Anal.* **1996**, *46*, 965-972.

188. Brown, R. G.; Eby, R. K., Effect of Crystallization Conditions and Heat Treatment on Polyethylene: Lamellar Thickness, Melting Temperature, and Density. *J. Appl. Phys.* **1964**, *35*, 1156-1161.

189. Furukawa, T.; Sato, H.; Kita, Y.; Matsukawa, K.; Yamaguchi, H.; Ochiai, S.; Siesler, H. W.; Ozaki, Y., Molecular Structure, Crystallinity and Morphology of Polyethylene/Polypropylene Blends Studied by Raman Mapping, Scanning Electron Microscopy, Wide Angle X-Ray Diffraction, and Differential Scanning Calorimetry. *Polym. J.* **2006**, *38*, 1127-1136.

190. Rule, J. D.; Moore, J. S., Romp Reactivity of Endo- and Exo-Dicyclopentadiene. *Macromolecules* **2002**, *35*, 7878-7882.

191. Helms, B.; Mynar, J. L.; Hawker, C. J.; Frechet, J. M., Dendronized Linear Polymers Via "Click Chemistry". *J. Am. Chem. Soc.* **2004**, *126*, 15020-15021.

192. Sonogashira, K.; Tohda, Y.; Hagihara, N., A Convenient Synthesis of Acetylenes: Catalytic Substitutions of Acetylenic Hydrogen with Bromoalkenes, Iodoarenes and Bromopyridines. *Tetrahedron Lett.* **1975**, *16*, 4467-4470.

193. Ochiai, B.; Tomita, I.; Endo, T., Investigation on Radical Polymerization Behavior of 4-Substituted Aromatic Enynes. Experimental, ESR, and Computational Studies. *Macromolecules* **2001**, *34*, 1634-1639.

194. Bunz, U. H., Poly(Aryleneethynylene)S: Syntheses, Properties, Structures, and Applications. *Chem. Rev.* **2000**, *100*, 1605-1644.

195. Kang, S.; Ono, R. J.; Bielawski, C. W., Synthesis of Poly(3-Hexylthiophene)-Block-Poly(Ethylene)-Block-Poly(3-Hexylthiophene) Via a Combination of Ring-Opening Olefin Metathesis Polymerization and Grignard Metathesis Polymerization. *J. Polym. Sci., Part A: Polym. Chem.* **2013**, *51*, 3810-3817.

196. Tang, J.; Tang, W.; Yuan, H.; Jin, R., Mechanical Behaviors of Ethylene/Styrene Interpolymer Compatibilized Polystyrene/Polyethylene Blends. *J. Appl. Polym. Sci.* **2007**, *104*, 4001-4007.

197. Anthony, M. T.; Seah, M. P., Xps - Energy Calibration of Electron Spectrometers .1. An Absolute, Traceable Energy Calibration and the Provision of Atomic Reference Line Energies. *Surf. Interface Anal.* **1984**, *6*, 95-106.

198. Anthony, M. T.; Seah, M. P., XPS - Energy Calibration of Electron Spectrometers .2. Results of an Interlaboratory Comparison. *Surf. Interface Anal.* **1984**, *6*, 107-115.

199. Lebreton, L., et al., Evidence That the Great Pacific Garbage Patch Is Rapidly Accumulating Plastic. *Sci. Rep.* **2018**, *8*, 4666.

200. Quote from Star Trek: The Final Frontier.

## Acknowledgements

It's amazing how fast time flies. It still baffles me how it's already been four years since I joined the Bielawski Lab. At that time, the lab was still in its infancy and therefore, the initial stages of my PhD career involved dealing with the intricacies of setting up a lab from scratch. Looking at how far the lab has come since then and being able to be a part of its evolution from the near beginning has been a rewarding experience and a testament to all the fellow graduate students and post-doctorates who helped make the lab what it is today.

The fact that I am even at a point to receive a PhD would not have been possible without the help and support of a multitude of people. First and foremost, I would like to thank my advisor, Professor Christopher Bielawski for taking a chance on me four years ago and for your patience and guidance since then. There were probably many times where I tested your patience and drove you mad but thank you for constantly motivating me and also for always making time no matter how busy you were, to sit down and discuss what was on my mind. I'm not the type of person who necessarily vocalizes my thoughts and ideas. However, having worked in other laboratories, I truly understand how much of a rarity it was that you always had the door to your office always open and how I could walk in anytime to discuss chemistry. Through your guidance, I've learned to not be afraid to go against the norm and to explore ideas and concepts that others may think are crazy. I graduate a better researcher than when I first joined the lab and I look forward to working with you in the future.

I would also like to thank my former advisor, Professor Yung-Eun Sung at Seoul National University and my mentor at the time Kwang Hyun Choi. Although there were probably many reasons to not accept an international student who had no real expertise in your area of study, thank you for allowing me to join your lab and guiding me throughout my master's degree. Joining your lab started my graduate career in Korea and if I hadn't joined your lab, I probably would not have met my current advisor and be in the position that I am in today. To my mentor Kwang Hyun, thank you for teaching me the ropes when I first joined the lab and for being a good friend throughout. I miss you and hope that wherever you are, you're happy and in a better place devoid of pain and suffering.

Special thanks is also merited for my former undergraduate advisor Professor Russell Monson and my mentor at the time, Dr. Nicole Trahan. Working in your lab with Nicole ignited my interest in graduate school and pursuing research after graduation. The experiences I had working with Nicole served me well and the lessons I learned helped prepare me to survive graduate school.

To Nicole, thank you for taking the time to introduce me to what life as a graduate student would be like. I'm sure there were plenty of times where it probably felt like you were teaching a kid how to walk but thank you for sticking with me. All those times hiking up to the Mountain Research Center in the snow to collect data helped prepare me for trials and tribulations of graduate school. We'll definitely have to go snowboarding and grab a beer the next time we are both in Colorado.

My warmest regards go out to both my PhD committee members (Professor Hyeon-Suk Shin, Professor Jong-Beom Baek, Professor Zonghoon Lee, and Professor Feng Ding) as well as to the members who served on my qualifying exam committee (Professor Hoi Ri Moon and Professor Young S. Park). Thank you for taking the time out of your busy schedules to serve as committee members and provide valuable feedback and advice. What I realized with graduate school is that at times, you can get mired in your research and forget to step back and tackle things from a different perspective. However, the advice and comments I received from all of you helped me view my research from a different point of view and ultimately resulted in strengthening the scope of my projects.

I'll always be eternally grateful to my loving and supportive family (my parents Jintae and Hyokyung, my brother James, and my sister Annabel) who were instrumental in helping me become the person that I am now. None of us thought that I would be gone this long when I left for Korea nearly 9 years ago to be an English teacher. I know that being this far apart is difficult but thank you for always letting me follow my own path, even though you may not have necessarily agreed with all of my life choices. In hindsight, I didn't always necessarily make the right decision, but I could always count on all of you to be there to pick me back up and make sure I didn't give up. I will try to visit more often, and I look forward to our future family trips, even though they all usually involve some degree of chaos and disaster.

Along the same lines, I'd also like to express my gratitude toward my extended family in Korea, especially to 지애 고모 and 고모부 Paul along with their kids Aaron and Clarise. I know I said this 4 years ago when I graduated from SNU, but I wanted to give my heartfelt thanks once again for acting as my surrogate family during my time in Korea. Anyone who has lived in a foreign country for an extended amount of time knows the difficulties that arise with missing the comforts of home. However, I was fortunate to always have all of you, who welcomed me into your home, fed me, had Aaron bring me a beer (the bell will always be ringing Aaron), and treated me as one of your own. Although we missed our chance to see Peyton Manning, we will still have to take a trip to Denver in the near future and catch a Broncos game at Mile High.

Big thanks go out to Jose Alejandro Rosales and the rest of the Oregon crew. Even though we are all far apart from each other, thank you for taking the time to catch up and for always welcoming me back whenever I was home or had a chance to meet up. All of you always have a place to stay out here in Korea and I look forward to meeting up with all of you back in the US in the near future.

My heartfelt gratitude and appreciation also goes out to Minjae Cho, who has been by my side throughout most of my graduate career. Thank you for your patience and understanding throughout all the time that we have been together. I know that seeing each other once every few weeks for nearly five years now was not easy, but even though I may not have shown it, I always appreciated that you remained positive and tried to make the most of the time we were together. As anyone who has gone through the toils of graduate school knows, things almost never go as planned and unexpected events frequently occur. However, what is not so common is having someone like you who was always understanding of my situation, and never got angry even when I had to suddenly cancel things because something came up in the lab. I'm very lucky to have met you and you've helped me keep my sanity through some of the more stressful times of my graduate career.

Finally, my warmest regards go out to all the former and current Bielawski Lab members. As I mentioned in the beginning, it's rewarding to see how far the lab has come in such a short amount of time through the hard work and efforts of both former and current members. I would like to especially thank Jinwon Seo, Hyosic Jung, and Jihong Lyu who were there with me from when I first joined the Bielawski Lab and are still here at the end of it. Thank you for all the times you've helped me whenever I've come to any of you and asked for help with filling out documents in Korean. More importantly, thank you for always taking the time to discuss chemistry related issues and/or going out and grabbing a beer with me when we couldn't resolve those said issues.

Graduate school, let alone graduate school in a foreign country, was a crazy ride full of ups and downs. However, thanks to all of you, I was able to survive it in a relatively intact manner and leave the lab a much better researcher and a significantly better person than when I joined. Thank you once again for everything and take care.

Sincerely,  
Stanfield Lee  
이영원 올림

December 4<sup>th</sup>, 2018

## Appendix A: NMR Spectra

### Table of Contents

<b>Figure A1.</b>	$^1\text{H}$ NMR of <b>5</b> .....	106
<b>Figure A2.</b>	$^{13}\text{C}$ NMR of <b>5</b> .....	107
<b>Figure A3.</b>	$^1\text{H}$ NMR of <b>7</b> .....	108
<b>Figure A4.</b>	$^{13}\text{C}$ NMR of <b>7</b> .....	109
<b>Figure A5.</b>	$^1\text{H}$ NMR for the series of homopolymer <b>8</b> .....	110
<b>Figure A6.</b>	$^1\text{H}$ NMR for the series of homopolymer <b>9</b> .....	111
<b>Figure A7.</b>	$^1\text{H}$ NMR for the series of diblock copolymers <b>10-12</b> .....	112
<b>Figure A8.</b>	$^1\text{H}$ NMR for the series of triblock copolymers <b>13</b> and <b>14</b> .....	113
<b>Figure A9.</b>	$^1\text{H}$ NMR for the series of random copolymers <b>15</b> .....	114
<b>Figure A10.</b>	$^1\text{H}$ NMR for diblock copolymer <b>10e</b> before and after hydrogenation.....	115
<b>Figure A11.</b>	$^1\text{H}$ NMR of polymer <b>8a</b> after irradiation with 300 nm light for 30 hours.....	116
<b>Figure A12.</b>	$^1\text{H}$ NMR of polymer <b>9a</b> after irradiation with 300 nm light for 30 hours.....	117

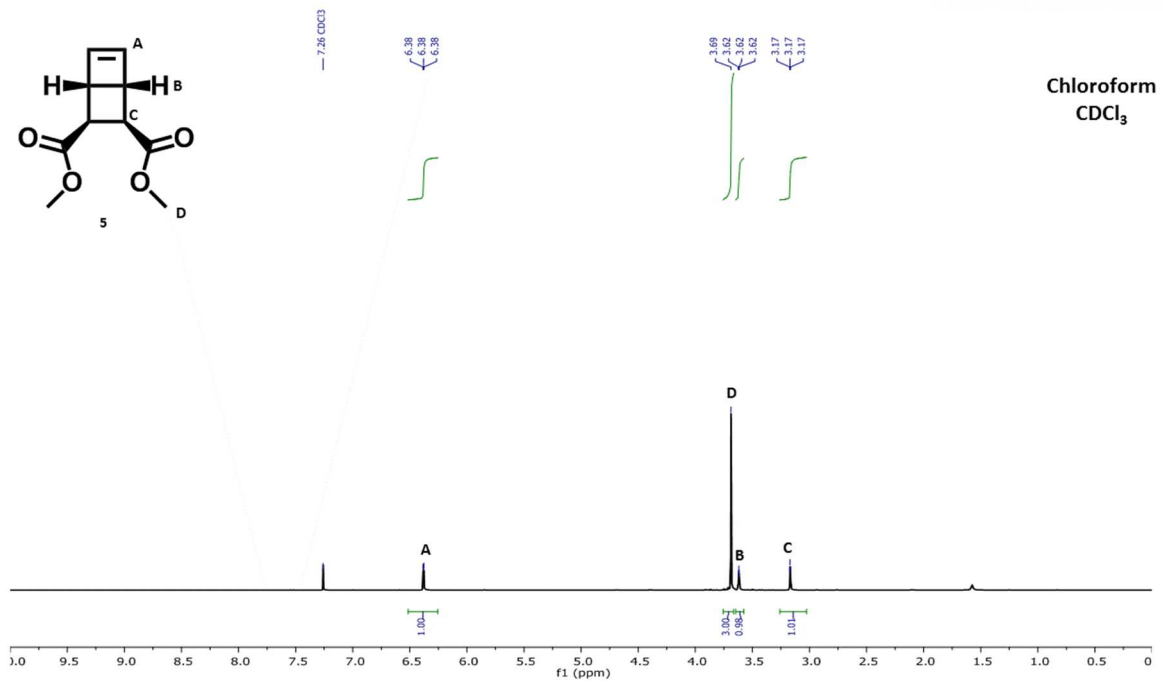


**Figure A1.**  $^1\text{H}$  NMR of **5**. All measurements were taken at ambient temperature in deuterated chloroform ( $\text{CDCl}_3$ ).

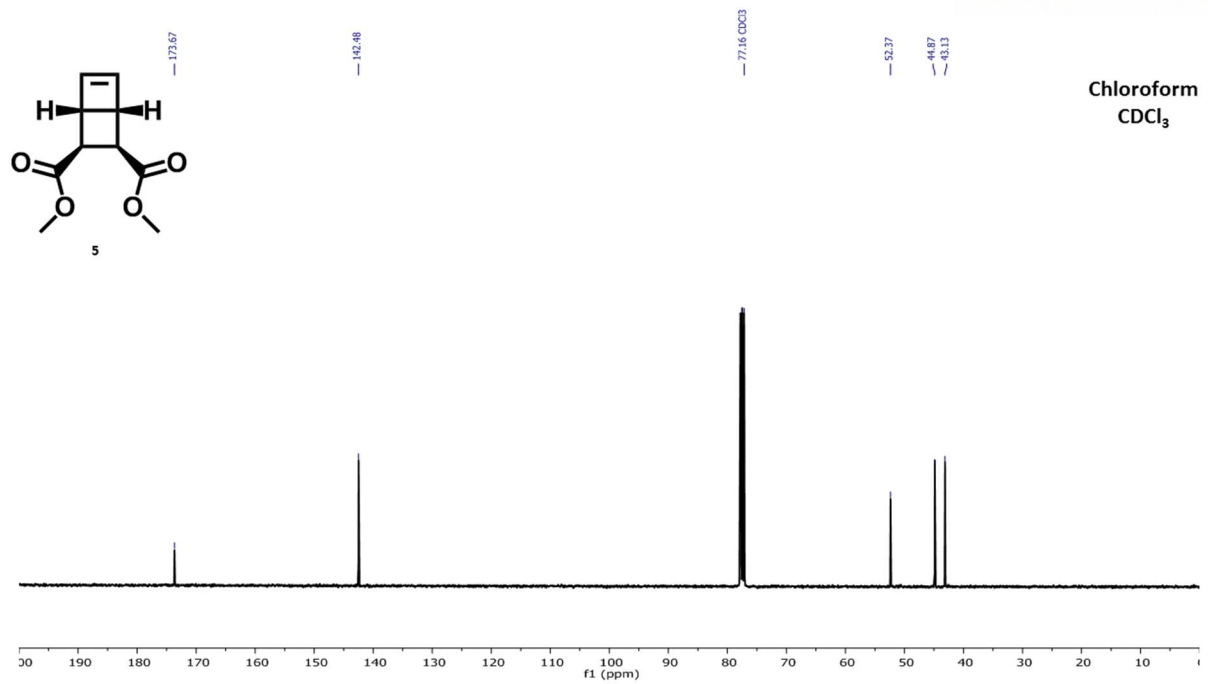


**Figure A2.**  $^{13}\text{C}$  NMR of **5**. All measurements were taken at ambient temperature in deuterated chloroform ( $\text{CDCl}_3$ ).



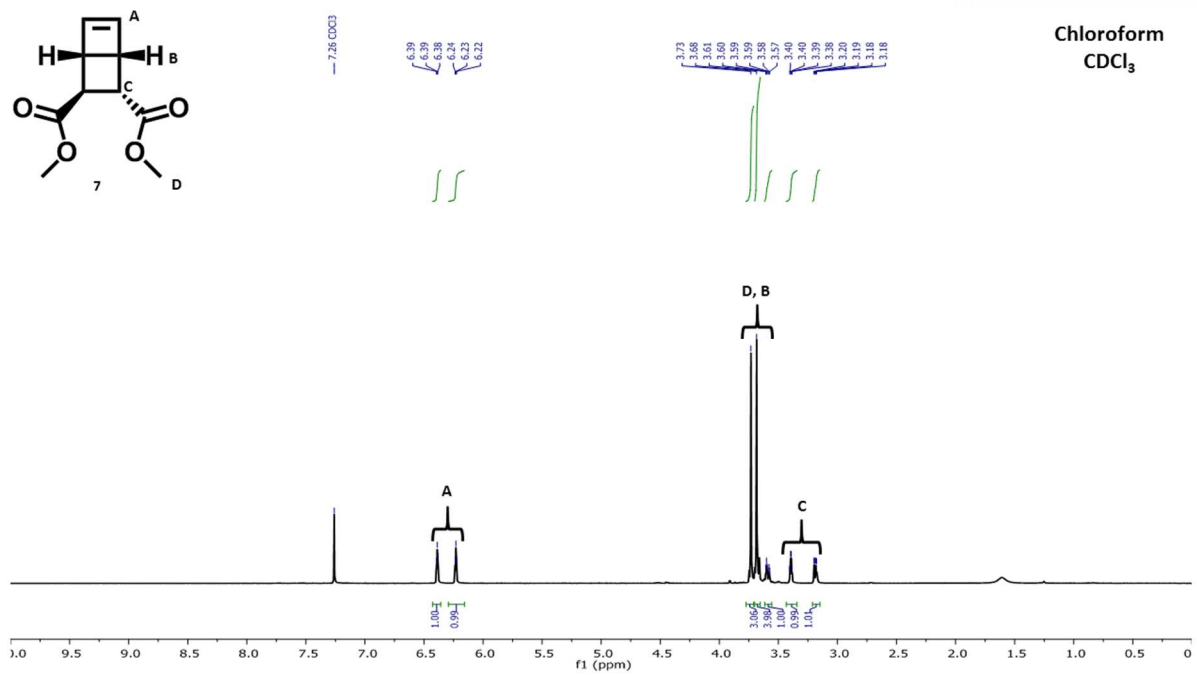


**Figure A3.**  $^1\text{H}$  NMR of 7. All measurements were taken at ambient temperature in deuterated chloroform ( $\text{CDCl}_3$ ).

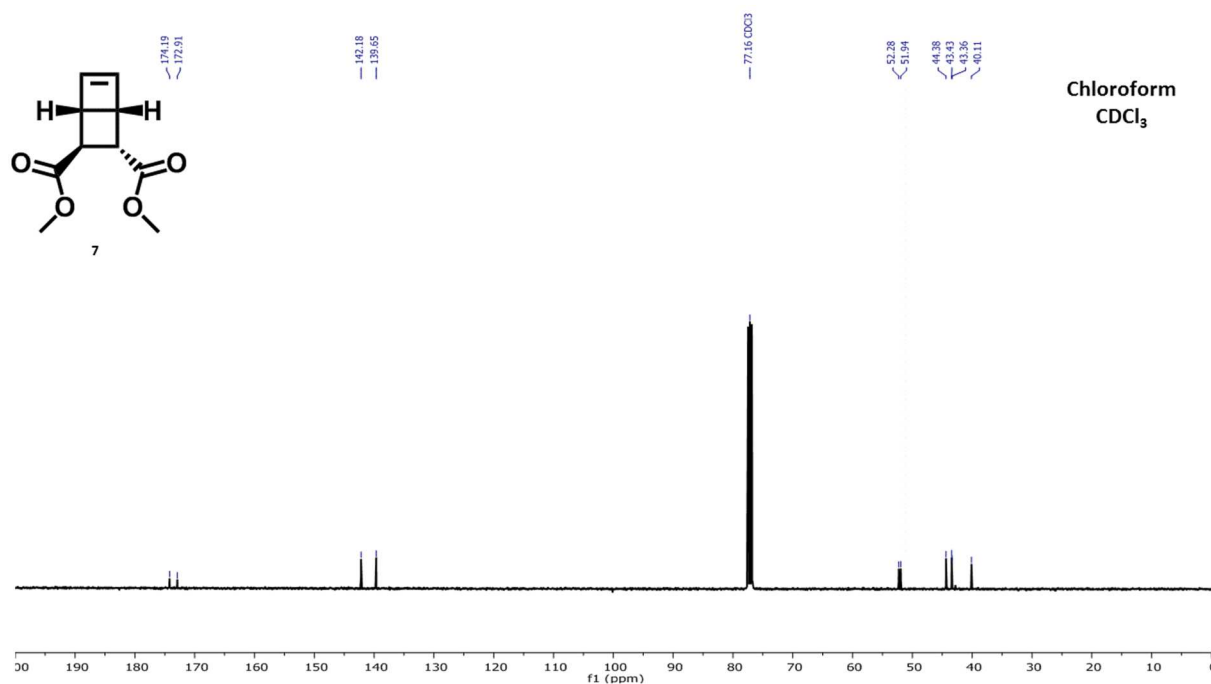


**Figure A4.**  $^{13}\text{C}$  NMR of 7. All measurements were taken at ambient temperature in deuterated chloroform ( $\text{CDCl}_3$ ).

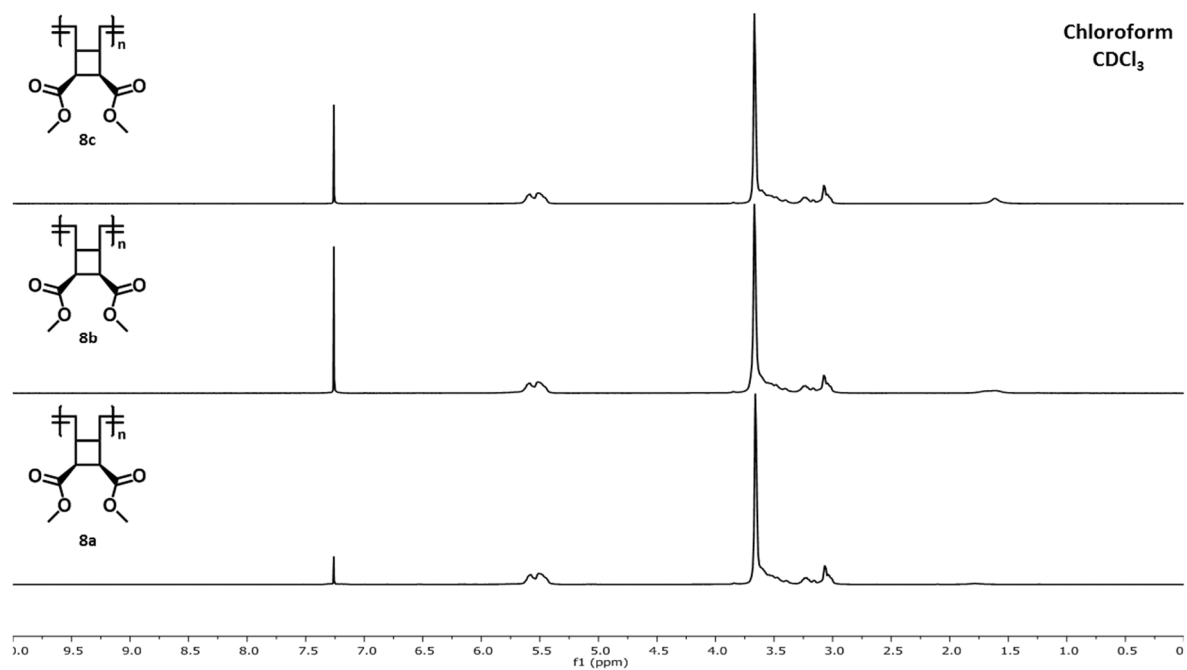


**Figure A5.** <sup>1</sup>H NMR for the series of homopolymer **8**. All measurements were taken at ambient temperature in deuterated chloroform (CDCl<sub>3</sub>).

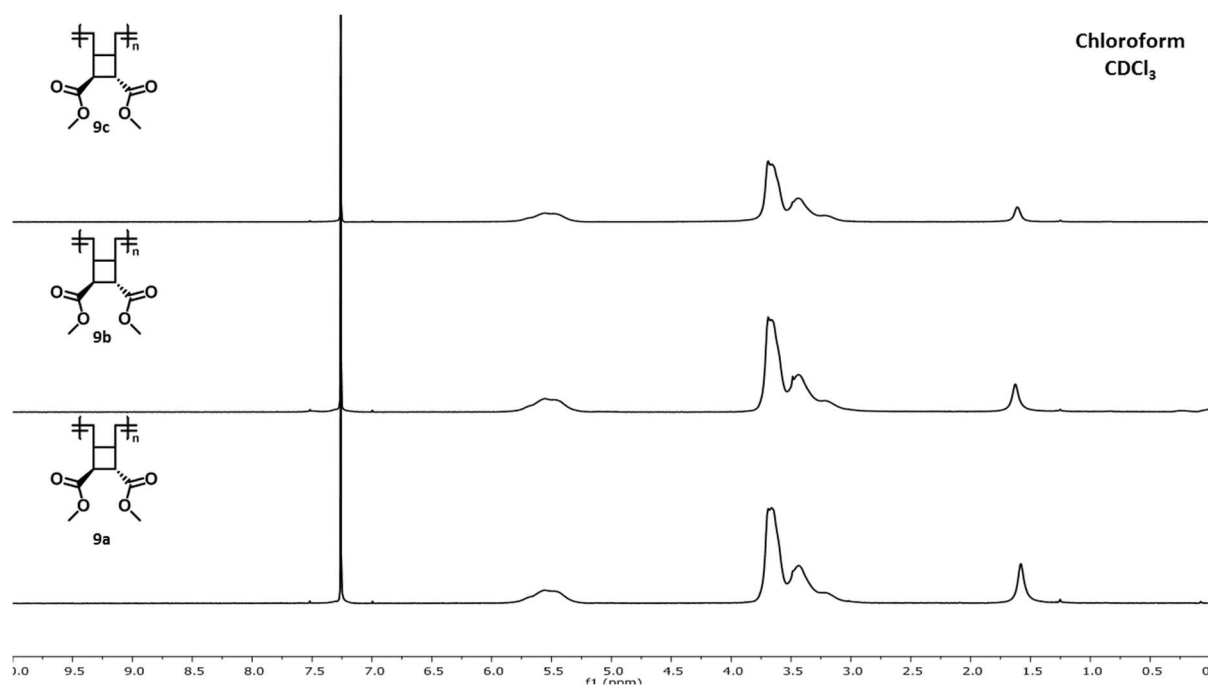


**Figure A6.** <sup>1</sup>H NMR for the series of homopolymer **9**. All measurements were taken at ambient temperature in deuterated chloroform (CDCl<sub>3</sub>).

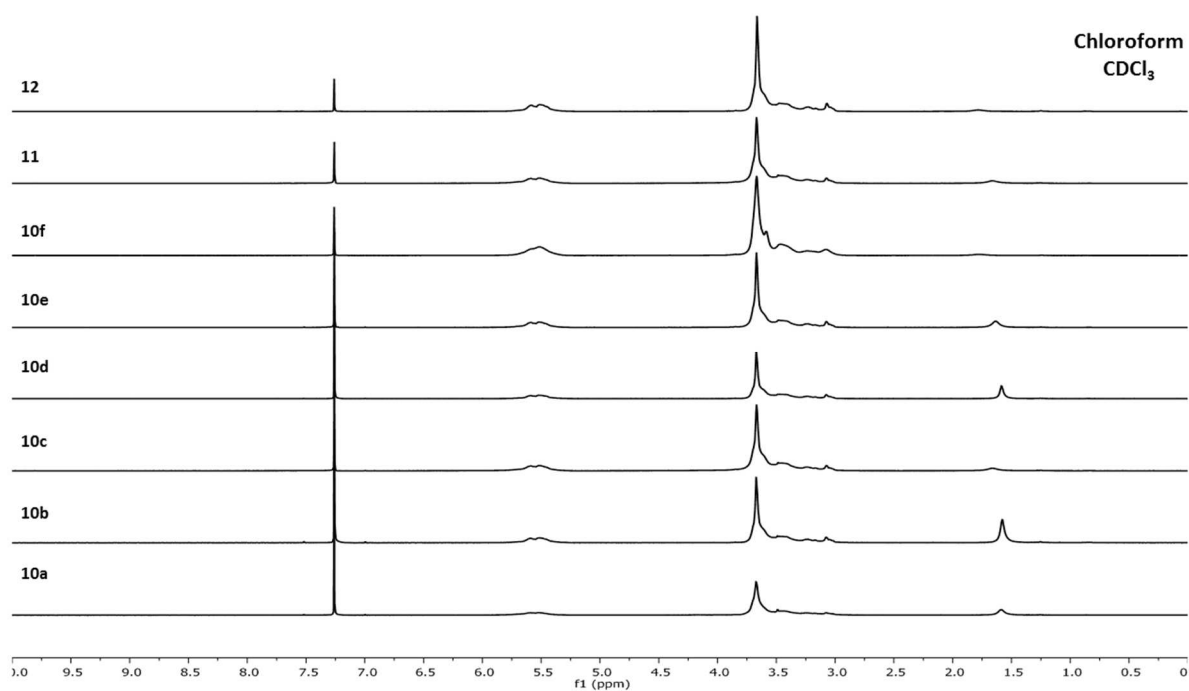


**Figure A7.** <sup>1</sup>H NMR for the series of diblock copolymers **10-12**. All measurements were taken at ambient temperature in deuterated chloroform (CDCl<sub>3</sub>).

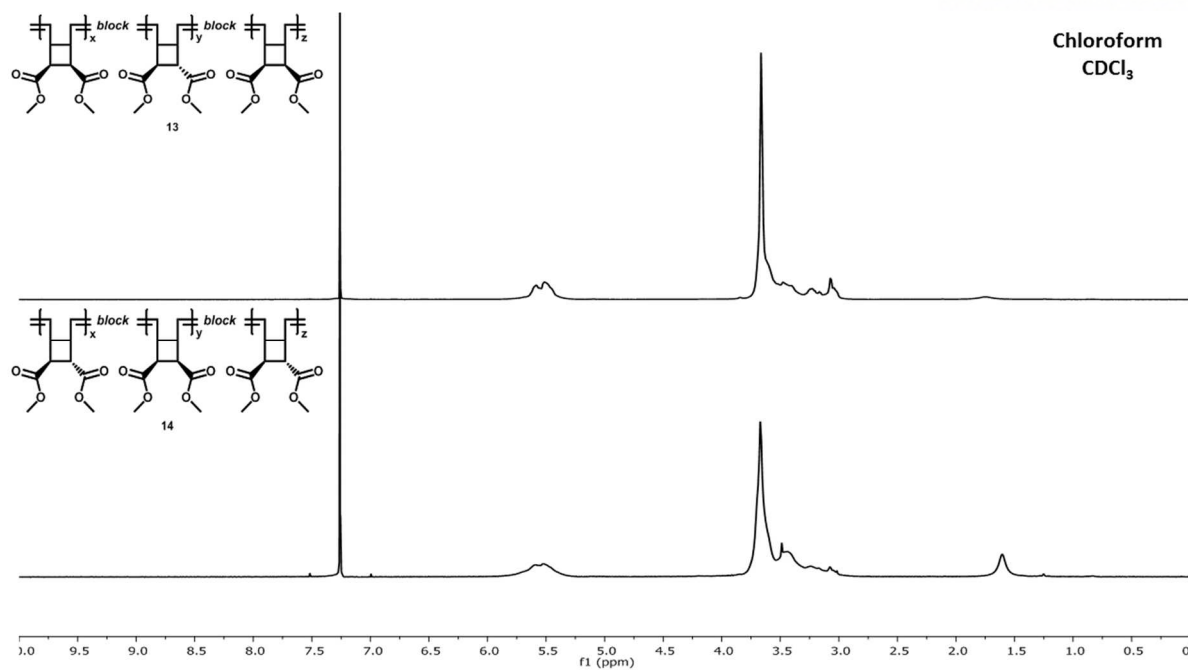


**Figure A8.**  $^1\text{H}$  NMR for the series of triblock copolymers **13** and **14**. All measurements were taken at ambient temperature in deuterated chloroform ( $\text{CDCl}_3$ ).

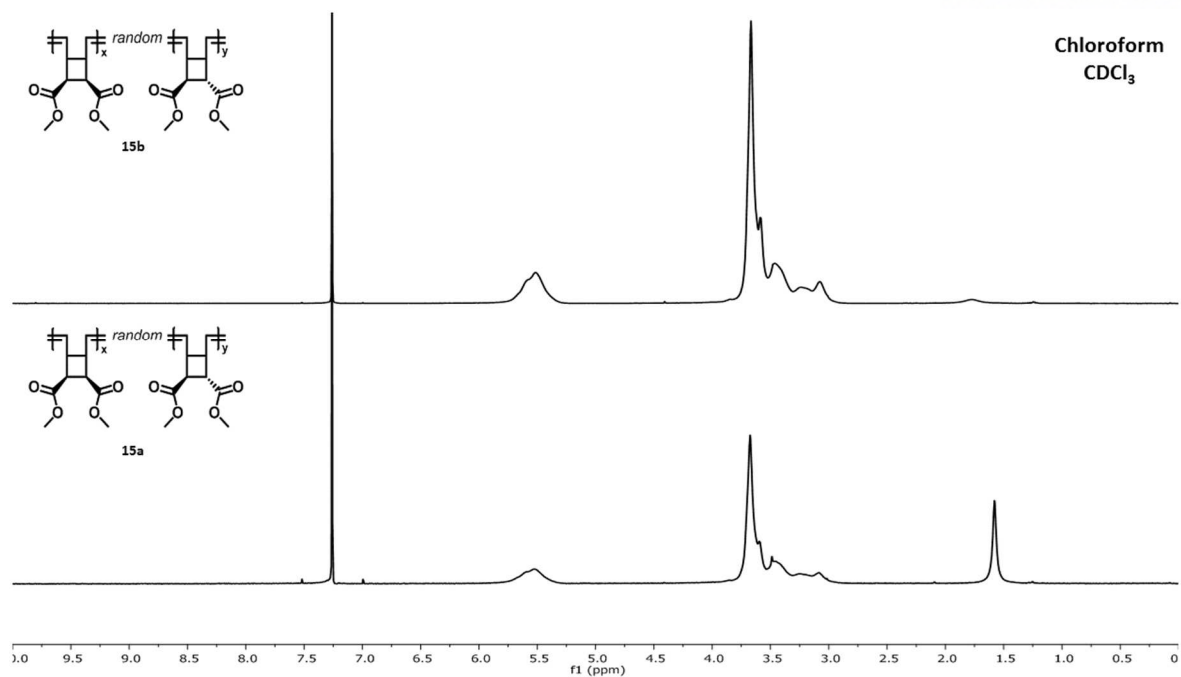


**Figure A9.** <sup>1</sup>H NMR for the series of random copolymers **15**. All measurements were taken at ambient temperature in deuterated chloroform (CDCl<sub>3</sub>).

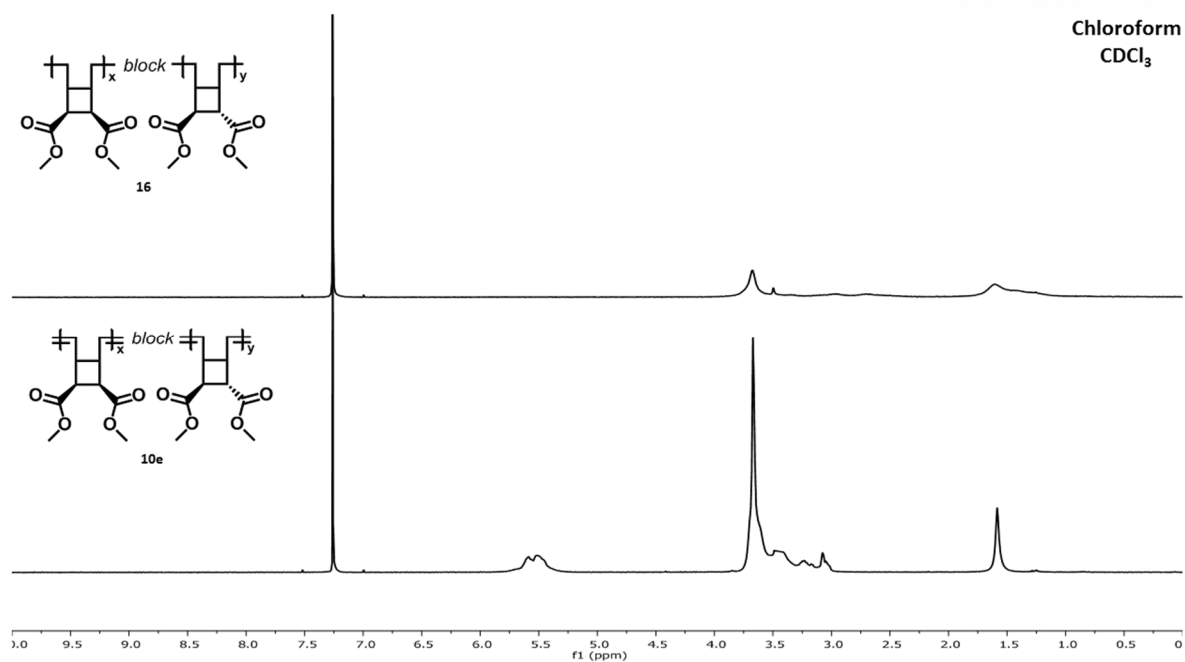


**Figure A10.** <sup>1</sup>H NMR for diblock copolymer **10e** before and after hydrogenation. All measurements were taken at ambient temperature in deuterated chloroform (CDCl<sub>3</sub>).



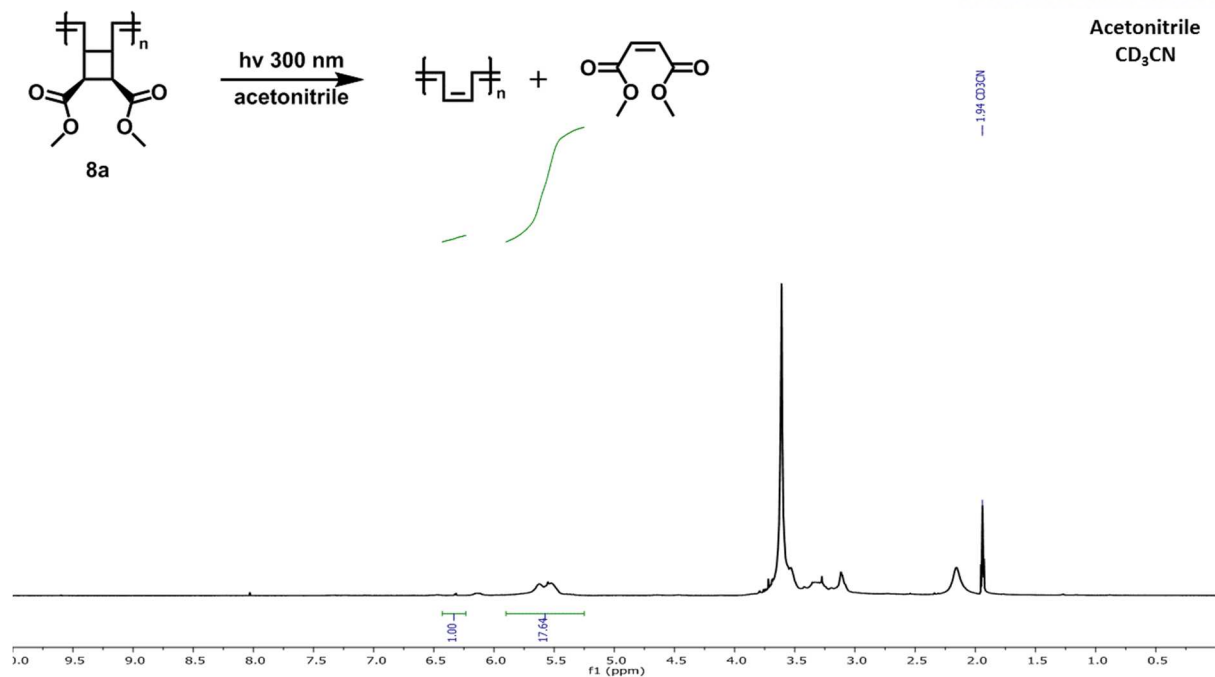


**Figure A11.** <sup>1</sup>H NMR of polymer **8a** after irradiation with 300 nm light for 30 hours. A 1:18 ratio was observed when the conversions were calculated from the proton signals corresponding to dimethyl maleate and fumarate were integrated to the proton signals corresponding to the olefins in the polymer backbone. All measurements were taken at ambient temperature in deuterated acetonitrile (CD<sub>3</sub>CN).

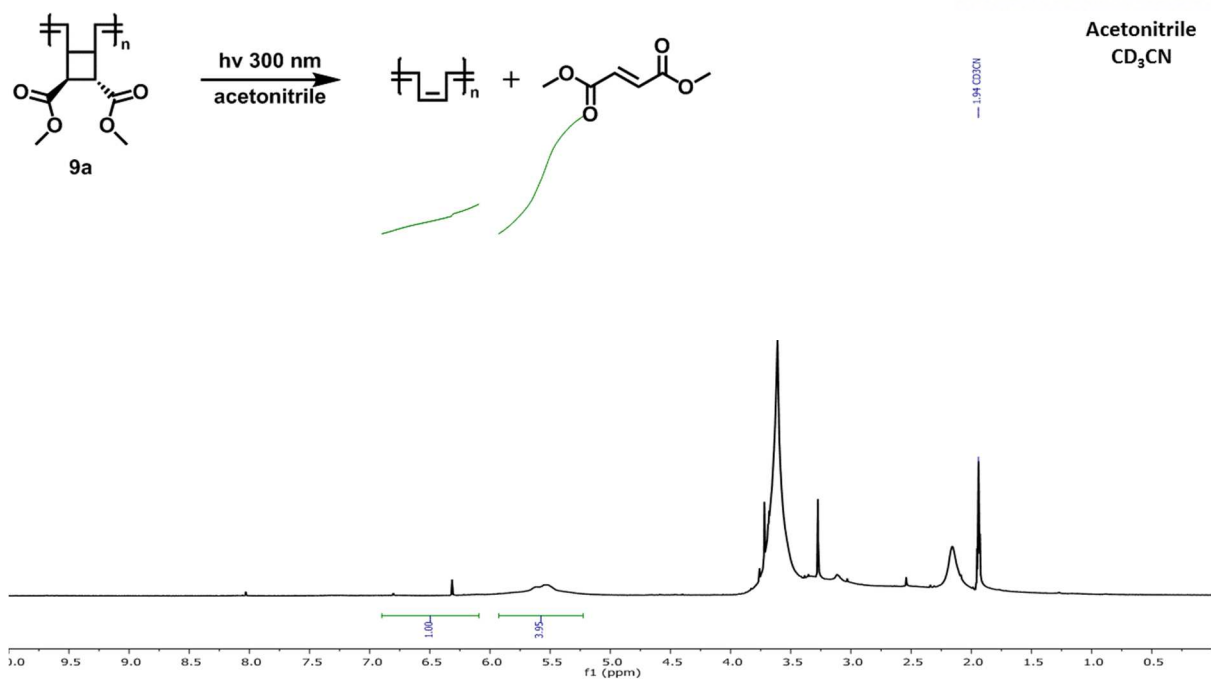


**Figure A12.** <sup>1</sup>H NMR of polymer **9a** after irradiation with 300 nm light for 30 hours. A 1:4 ratio was observed when the conversions were calculated from the proton signals corresponding to dimethyl maleate and fumarate were integrated to the proton signals corresponding to the olefins in the polymer backbone. All measurements were taken at ambient temperature in deuterated acetonitrile (CD<sub>3</sub>CN)

## **Appendix B: ATR-IR Spectra**

### **Table of Contents**

<b>Figure B1.</b> Representative IR spectra of homo-, di-, and triblock copolymers polymerized from monomers <b>5</b> and <b>7</b> .....	119
<b>Figure B2.</b> IR spectra of the series of diblock copolymers <b>10</b> .....	120
<b>Figure B3.</b> IR spectra of homopolymers and random copolymers.....	121

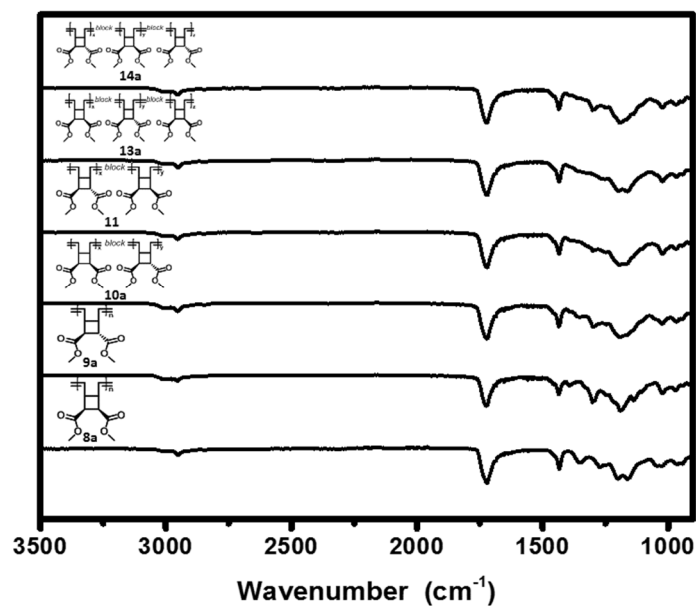


**Figure B1.** Representative IR spectra of homo-, di-, and triblock copolymers polymerized from monomers **5** and **7**. All measurements were taken at ambient temperature using a diamond ATR-IR.

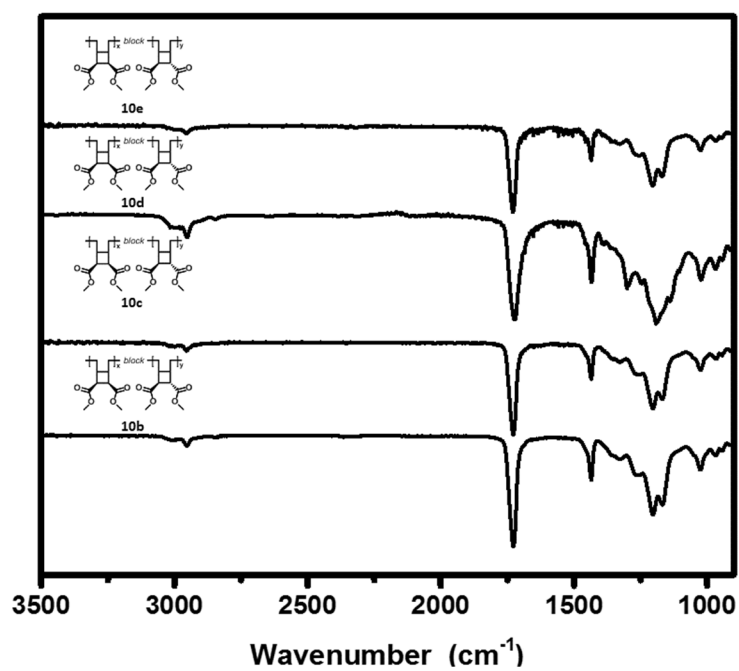


**Figure B2.** IR spectra of the series of diblock copolymers **10**. All measurements were taken at ambient temperature using a diamond ATR-IR.

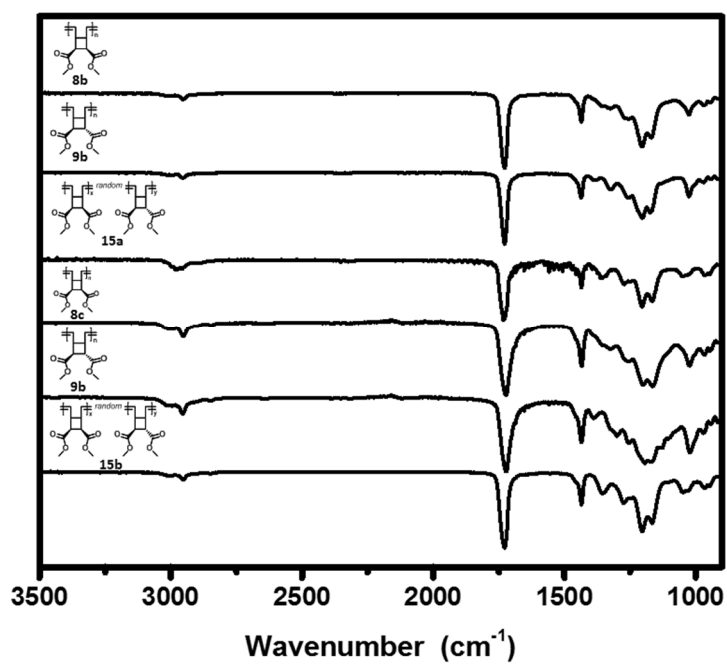
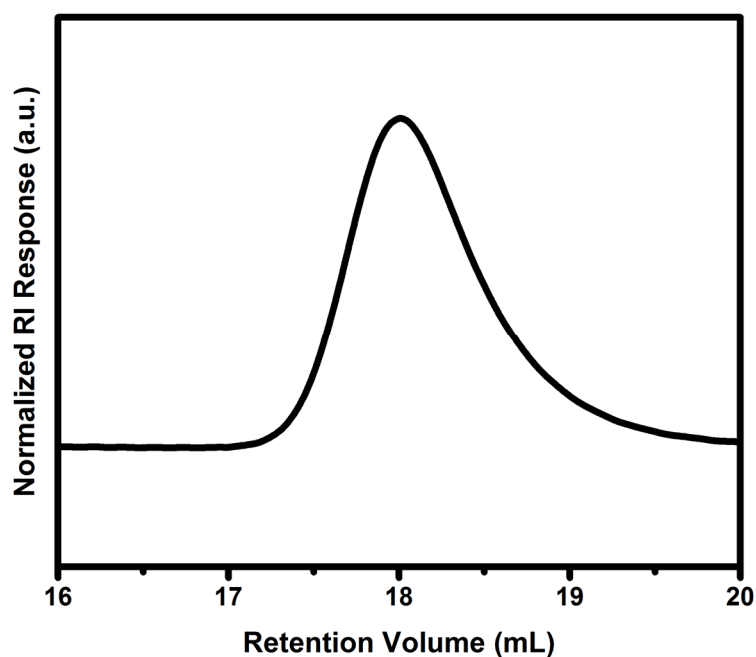
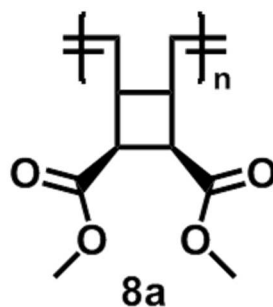


**Figure B3.** IR spectra of homopolymers and random copolymers of different molecular weights. All measurements were taken at ambient temperature using a diamond ATR-IR.

## Appendix C: GPC Chromatograms

### Table of Contents

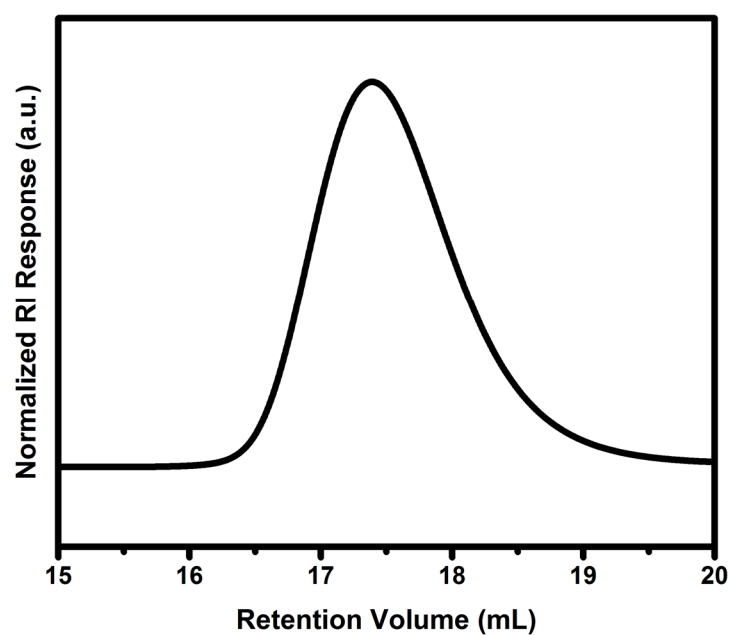
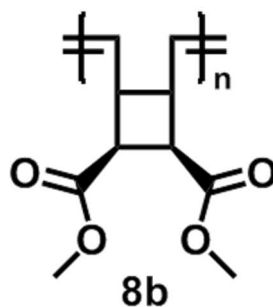
<b>Figure C1.</b>	GPC chromatogram for homopolymer <b>8a</b> .....	123
<b>Figure C2.</b>	GPC chromatogram for homopolymer <b>8b</b> .....	124
<b>Figure C3.</b>	GPC chromatogram for homopolymer <b>8c</b> .....	125
<b>Figure C4.</b>	GPC chromatogram for homopolymer <b>9a</b> .....	126
<b>Figure C5.</b>	GPC chromatogram for homopolymer <b>9b</b> .....	127
<b>Figure C6.</b>	GPC chromatogram for homopolymer <b>9c</b> .....	128
<b>Figure C7.</b>	GPC chromatograms for diblock copolymer <b>10a</b> .....	129
<b>Figure C8.</b>	GPC chromatograms for diblock copolymer <b>10b</b> .....	130
<b>Figure C9.</b>	GPC chromatograms for diblock copolymer <b>10c</b> .....	131
<b>Figure C10.</b>	GPC chromatograms for diblock copolymer <b>10d</b> .....	132
<b>Figure C11.</b>	GPC chromatograms for diblock copolymer <b>10e</b> .....	133
<b>Figure C12.</b>	GPC chromatograms for diblock copolymer <b>10f</b> .....	134
<b>Figure C13.</b>	GPC chromatograms for diblock copolymer <b>11</b> .....	135
<b>Figure C14.</b>	GPC chromatograms for diblock copolymer <b>12</b> .....	136
<b>Figure C15.</b>	GPC chromatograms for the triblock copolymer <b>13a</b> .....	137
<b>Figure C16.</b>	GPC chromatograms for the triblock copolymer <b>13b</b> .....	138
<b>Figure C17.</b>	GPC chromatograms for the triblock copolymer <b>14a</b> .....	139
<b>Figure C18.</b>	GPC chromatograms for the triblock copolymer <b>14b</b> .....	140
<b>Figure C19.</b>	GPC chromatogram for random copolymer <b>15a</b> .....	141
<b>Figure C20.</b>	GPC chromatogram for random copolymer <b>15b</b> .....	142
<b>Figure C21.</b>	GPC chromatograms for diblock copolymer <b>10e</b> pre and post hydrogenation.....	143
<b>Figure C22.</b>	GPC chromatograms for polymer <b>8a</b> before and after irradiation .....	144
<b>Figure C23.</b>	GPC chromatograms for polymer <b>9a</b> before and after irradiation .....	145



Monomer to Catalyst Ratio	Target $M_n$ (kDa)	$M_n$ (kDa)	$M_w$ (kDa)	$\bar{D}$	Yield (%)
76	15.0	14.6	17.1	1.2	95

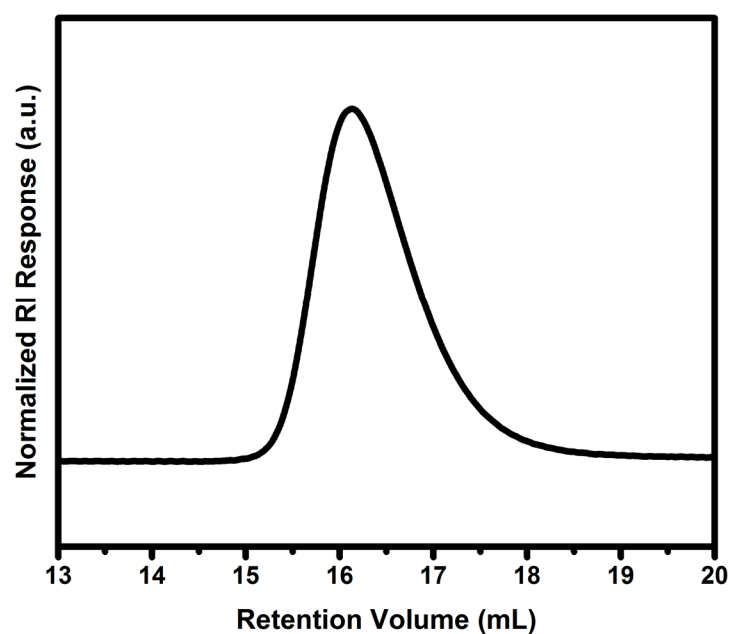
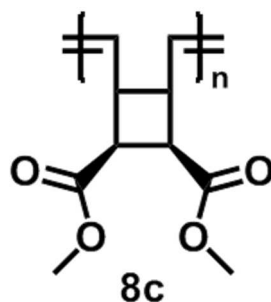
**Figure C1.** GPC chromatogram for homopolymer **8a**. All measurements were taken using tetrahydrofuran as the mobile phase at a flow rate of 0.8 mL/min. Molecular weights and polydispersity were determined relative to poly(styrene) standards in tetrahydrofuran.





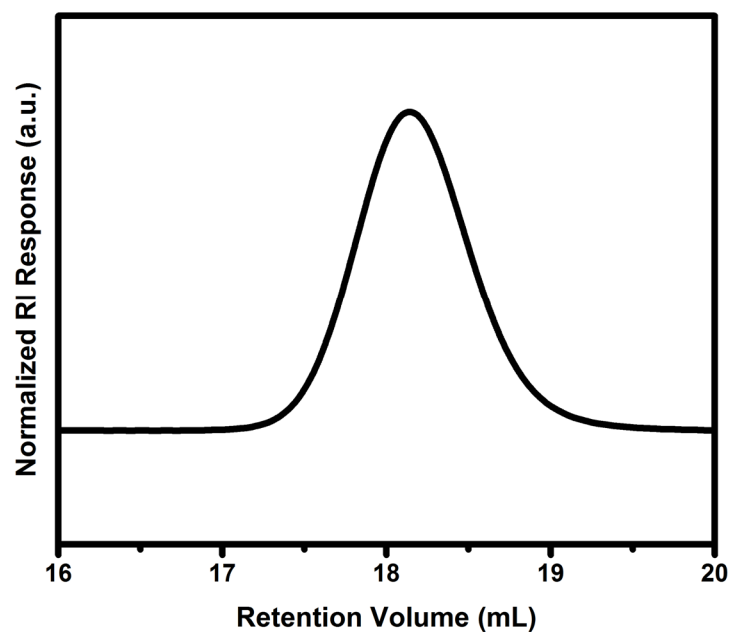
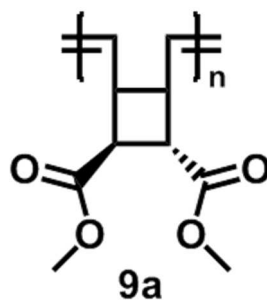
Monomer to Catalyst Ratio	Target $M_n$ (kDa)	$M_n$ (kDa)	$M_w$ (kDa)	$\bar{D}$	Yield (%)
102	20.0	23.6	29.4	1.2	87

**Figure C2.** GPC chromatogram for homopolymer **8b**. All measurements were taken using tetrahydrofuran as the mobile phase at a flow rate of 0.8 mL/min. Molecular weights and polydispersity were determined relative to poly(styrene) standards in tetrahydrofuran.



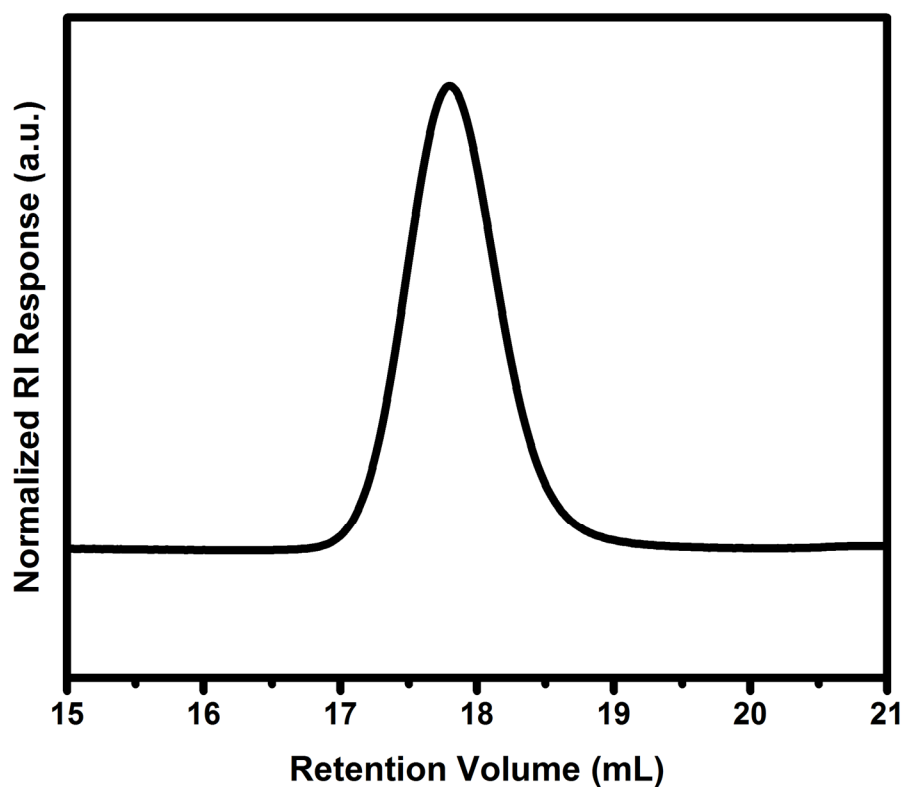
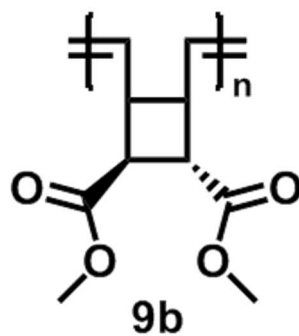
Monomer to Catalyst Ratio	Target $M_n$ (kDa)	$M_n$ (kDa)	$M_w$ (kDa)	$\bar{D}$	Yield (%)
382	75.0	66.4	82.8	1.2	87

**Figure C3.** GPC chromatogram for homopolymer **8c**. All measurements were taken using tetrahydrofuran as the mobile phase at a flow rate of 0.8 mL/min. Molecular weights and polydispersity were determined relative to poly(styrene) standards in tetrahydrofuran.



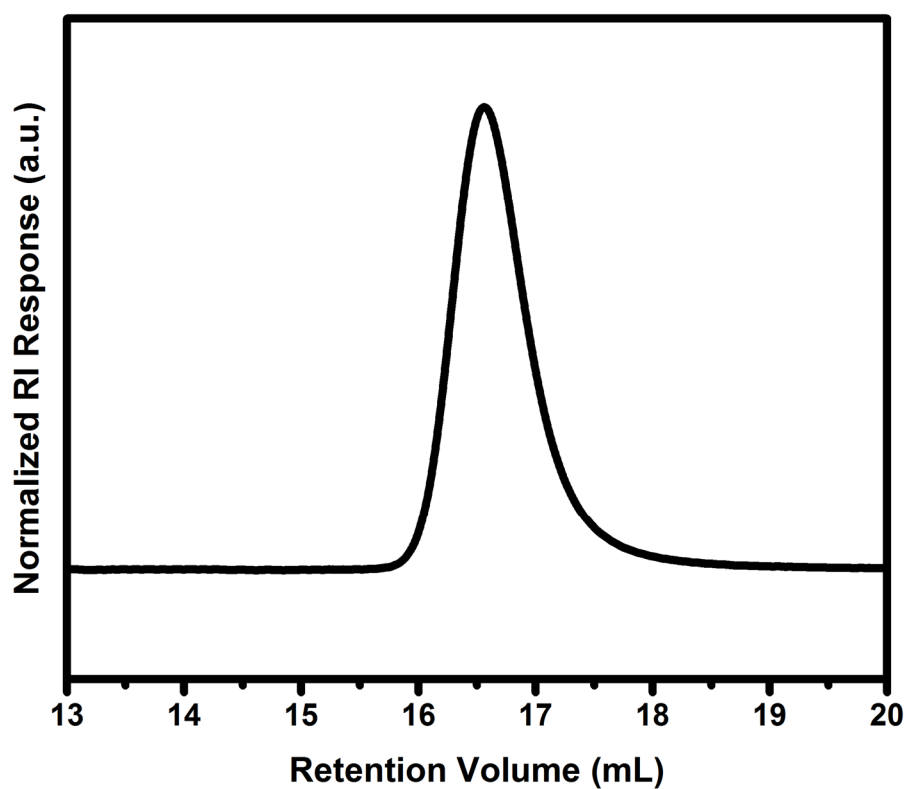
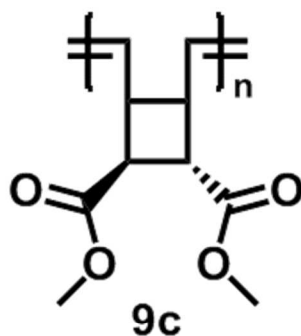
Monomer to Catalyst Ratio	Target $M_n$ (kDa)	$M_n$ (kDa)	$M_w$ (kDa)	$\bar{D}$	Yield (%)
76	15.0	16.6	18.6	1.1	89

**Figure C4.** GPC chromatogram for homopolymer **9a**. All measurements were taken using tetrahydrofuran as the mobile phase at a flow rate of 0.8 mL/min. Molecular weights and polydispersity were determined relative to poly(styrene) standards in tetrahydrofuran.



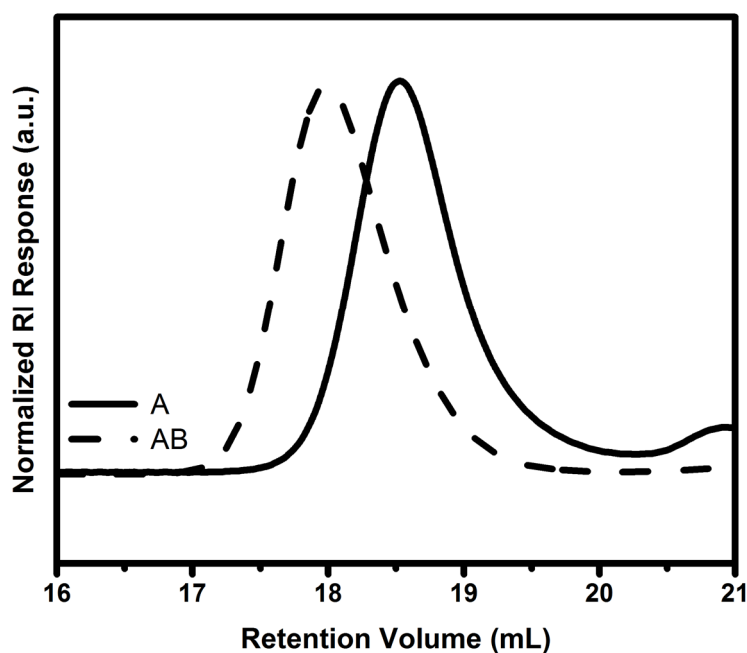
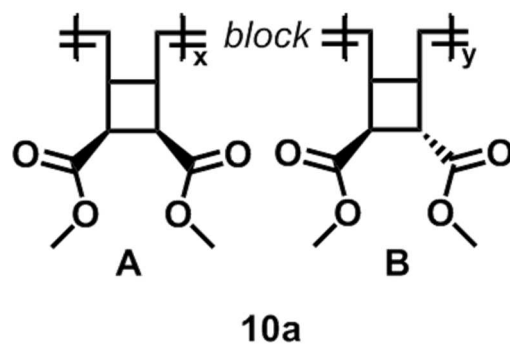
Monomer to Catalyst Ratio	Target $M_n$ (kDa)	$M_n$ (kDa)	$M_w$ (kDa)	$\bar{D}$	Yield (%)
102	20.0	20.3	22.2	1.1	87

**Figure C5.** GPC chromatogram for homopolymer **9b**. All measurements were taken using tetrahydrofuran as the mobile phase at a flow rate of 0.8 mL/min. Molecular weights and polydispersity were determined relative to poly(styrene) standards in tetrahydrofuran.



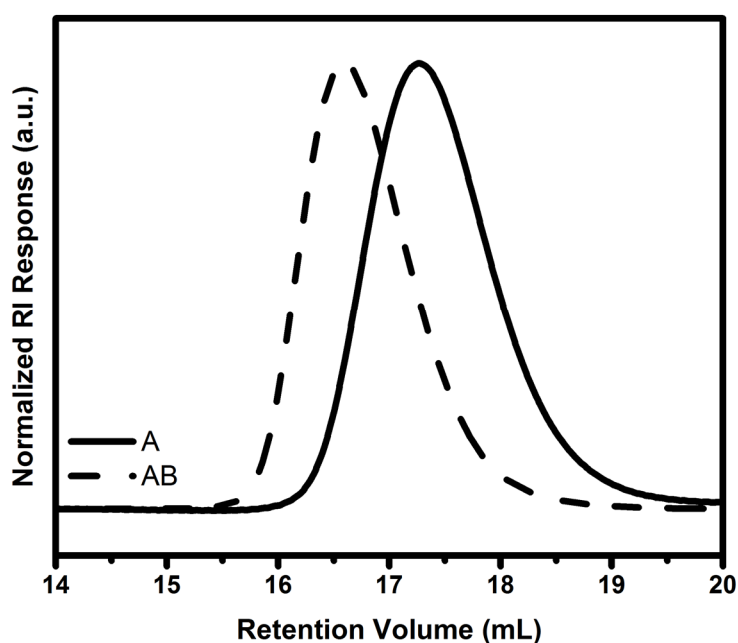
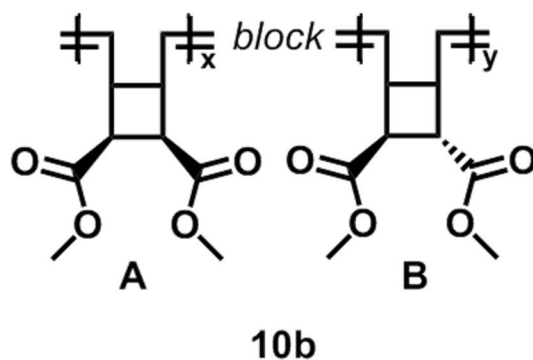
Monomer to Catalyst Ratio	Target $M_n$ (kDa)	$M_n$ (kDa)	$M_w$ (kDa)	$\mathcal{D}$	Yield (%)
382	75.0	50.5	55.6	1.1	87

**Figure C6.** GPC chromatogram for homopolymer **9c**. All measurements were taken using tetrahydrofuran as the mobile phase at a flow rate of 0.8 mL/min. Molecular weights and polydispersity were determined relative to poly(styrene) standards in tetrahydrofuran.



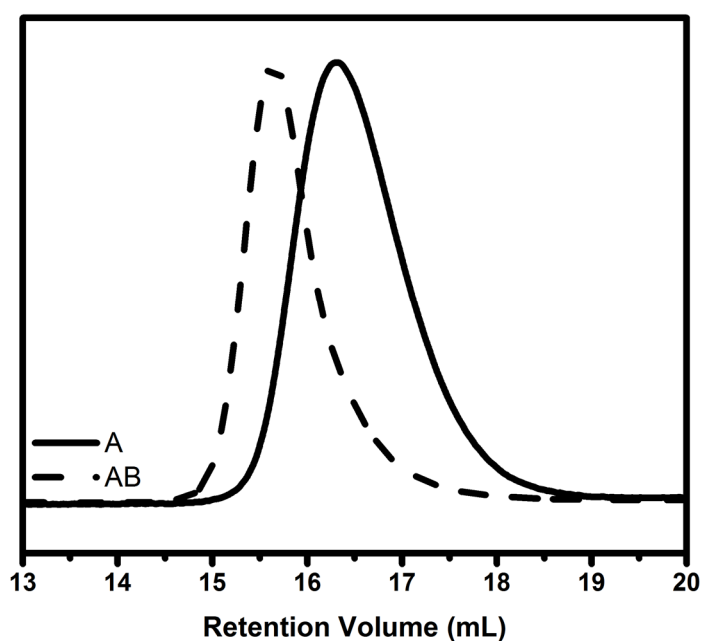
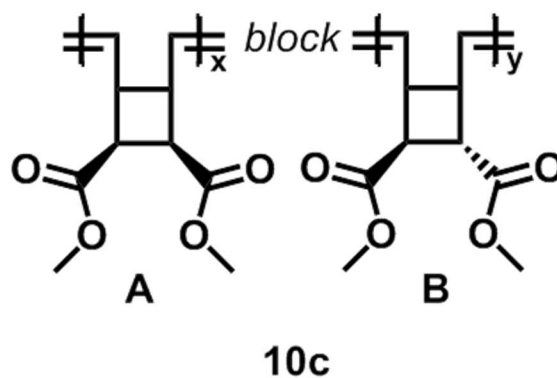
Block (Ratio)	Monomer to Catalyst Ratio	Target $M_n$ (kDa)	$M_n$ (kDa)	$M_w$ (kDa)	$\bar{D}$	Yield (%)
A	38	7.5	9.4	11.3	1.2	-
AB (1:1)	-	15.0	15.7	18.0	1.2	98

**Figure C7.** GPC chromatograms for diblock copolymer **10a**. All measurements were taken using tetrahydrofuran as the mobile phase at a flow rate of 0.8 mL/min. Molecular weights and polydispersity were determined relative to poly(styrene) standards in tetrahydrofuran.



Block (Ratio)	Monomer to Catalyst Ratio	Target $M_n$ (kDa)	$M_n$ (kDa)	$M_w$ (kDa)	$\bar{D}$	Yield (%)
A	127	25.0	25.9	32.5	1.3	-
AB (1:1)	-	50.0	44.9	53.2	1.2	93

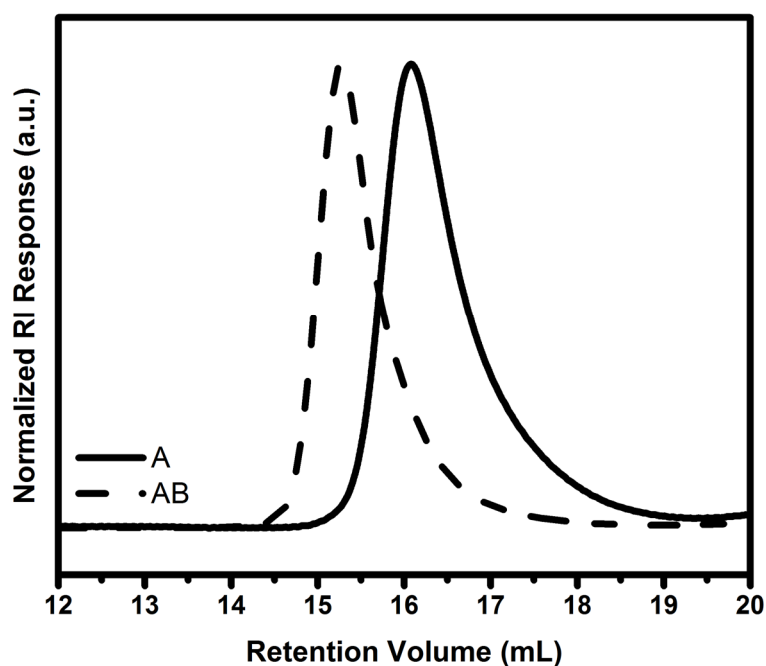
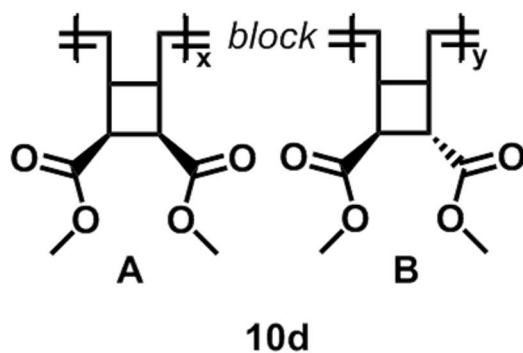
**Figure C8.** GPC chromatograms for diblock copolymer **10b**. All measurements were taken using tetrahydrofuran as the mobile phase at a flow rate of 0.8 mL/min. Molecular weights and polydispersity were determined relative to poly(styrene) standards in tetrahydrofuran.



Block (Ratio)	Monomer to Catalyst Ratio	Target $M_n$ (kDa)	$M_n$ (kDa)	$M_w$ (kDa)	$\bar{D}$	Yield (%)
A	255	50.0	53.9	65.7	1.2	-
AB (1:1)	-	100.0	92.8	106.3	1.2	89

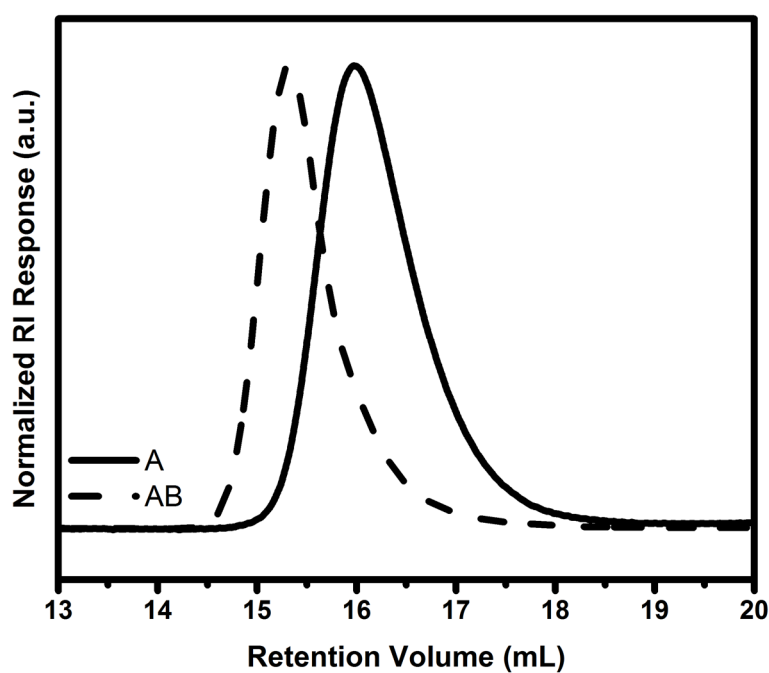
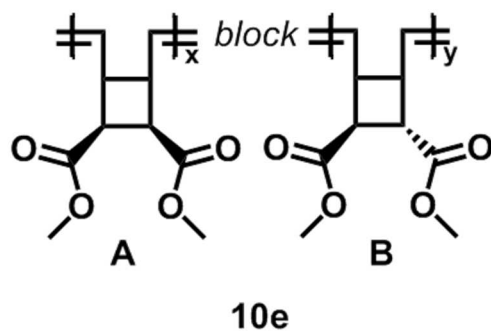
**Figure C9.** GPC chromatograms for diblock copolymer **10c**. All measurements were taken using tetrahydrofuran as the mobile phase at a flow rate of 0.8 mL/min. Molecular weights and polydispersity were determined relative to poly(styrene) standards in tetrahydrofuran.





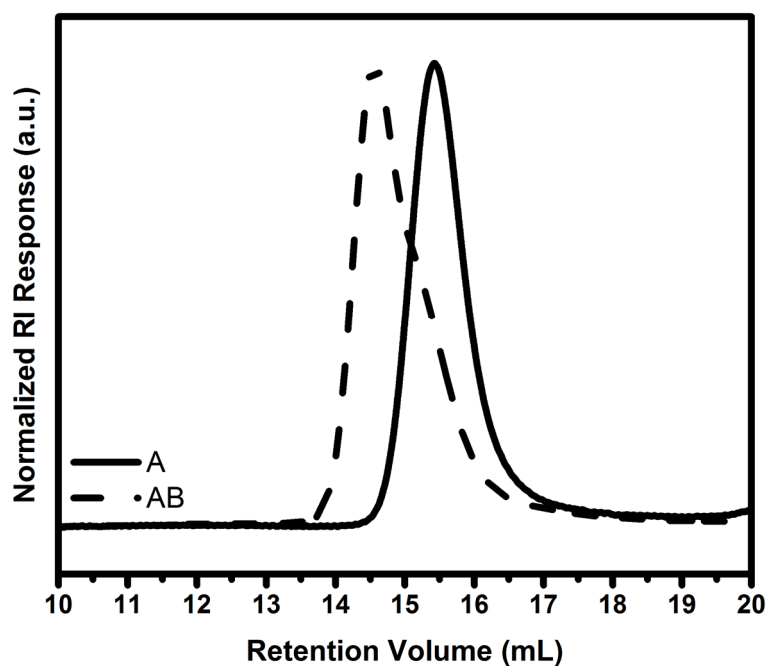
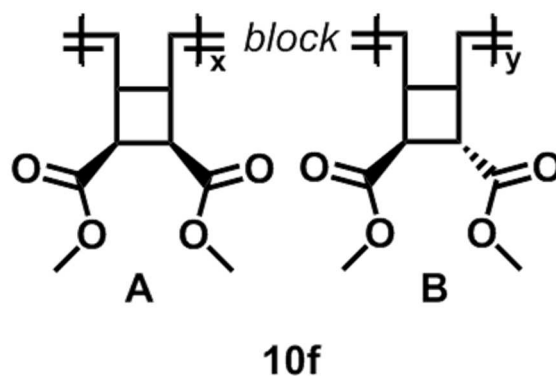
Block (Ratio)	Monomer to Catalyst Ratio	Target $M_n$ (kDa)	$M_n$ (kDa)	$M_w$ (kDa)	$D$	Yield (%)
A	306	60.0	58.4	72.3	1.2	-
AB (1:1)	-	120.0	111.3	133.2	1.2	98

**Figure C10.** GPC chromatograms for diblock copolymer **10d**. All measurements were taken using tetrahydrofuran as the mobile phase at a flow rate of 0.8 mL/min. Molecular weights and polydispersity were determined relative to poly(styrene) standards in tetrahydrofuran.



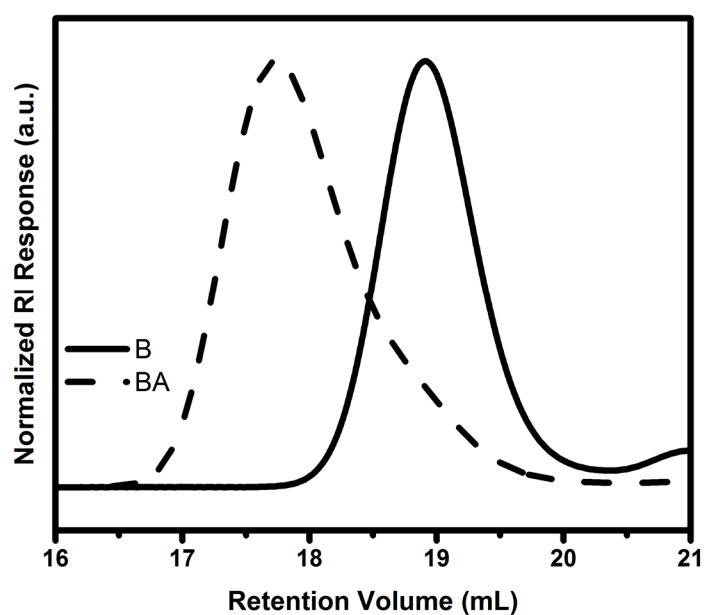
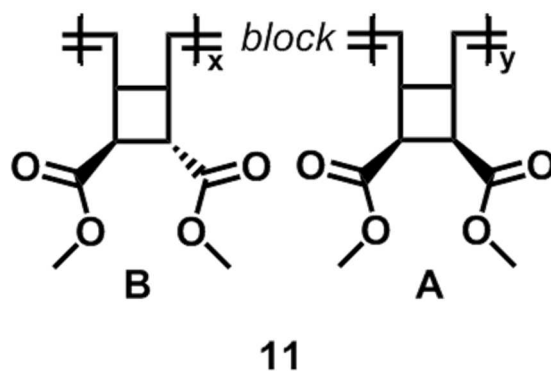
Block (Ratio)	Monomer to Catalyst Ratio	Target $M_n$ (kDa)	$M_n$ (kDa)	$M_w$ (kDa)	$\bar{D}$	Yield (%)
A	381	75.0	68.0	82.0	1.2	-
AB (1:1)	-	150.0	118.7	134.2	1.1	95

**Figure C11.** GPC chromatograms for diblock copolymer **10e**. All measurements were taken using tetrahydrofuran as the mobile phase at a flow rate of 0.8 mL/min. Molecular weights and polydispersity were determined relative to poly(styrene) standards in tetrahydrofuran.



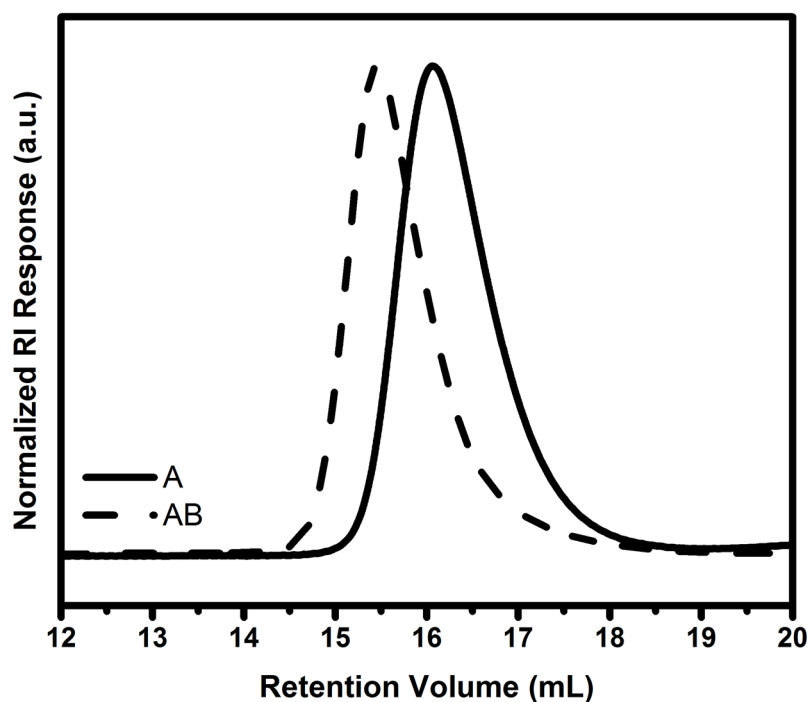
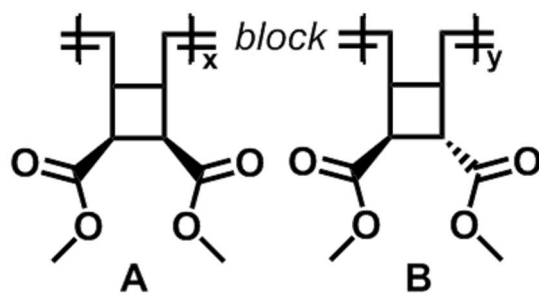
Block (Ratio)	Monomer to Catalyst Ratio	Target $M_n$ (kDa)	$M_n$ (kDa)	$M_w$ (kDa)	$\bar{D}$	Yield (%)
A	510	100.0	117.3	130.1	1.1	-
AB (1:1)	-	200.0	173.0	210.7	1.2	90

**Figure C12.** GPC chromatograms for diblock copolymer **10f**. All measurements were taken using tetrahydrofuran as the mobile phase at a flow rate of 0.8 mL/min. Molecular weights and polydispersity were determined relative to poly(styrene) standards in tetrahydrofuran.



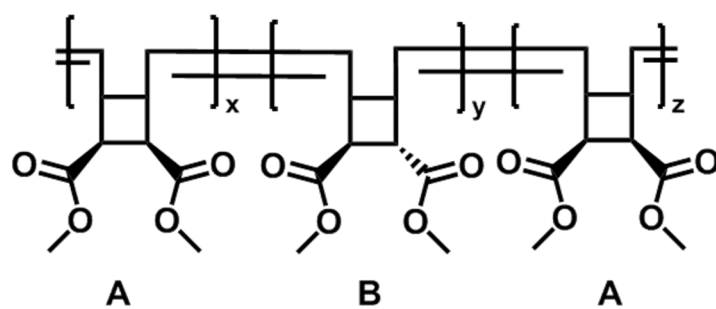
Block (Ratio)	Monomer to Catalyst Ratio	Target $M_n$ (kDa)	$M_n$ (kDa)	$M_w$ (kDa)	$\bar{D}$	Yield (%)
B	38	7.5	7.0	8.2	1.2	-
BA (1:1)	-	15.0	16.2	21.1	1.3	80

**Figure C13.** GPC chromatograms for diblock copolymer **11**. All measurements were taken using tetrahydrofuran as the mobile phase at a flow rate of 0.8 mL/min. Molecular weights and polydispersity were determined relative to poly(styrene) standards in tetrahydrofuran.

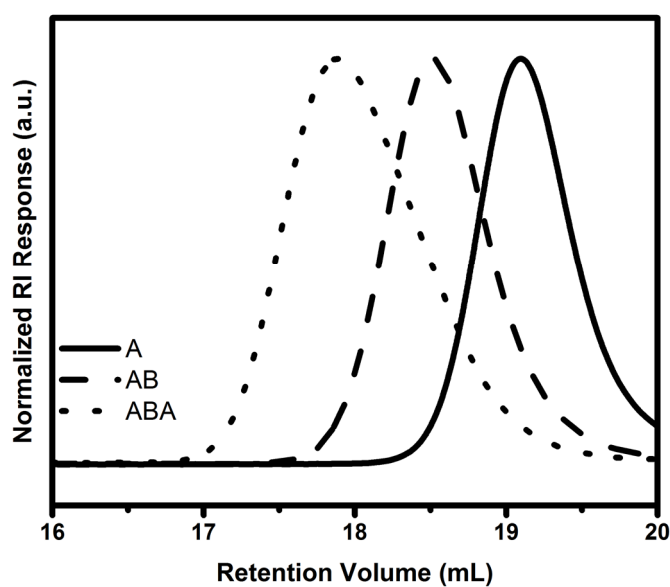


Block (Ratio)	Monomer to Catalyst Ratio	Target $M_n$ (kDa)	$M_n$ (kDa)	$M_w$ (kDa)	$\bar{D}$	Yield (%)
A	510	100.0	62.4	77.0	1.2	-
AB (1:1)	-	200.0	94.4	118.0	1.2	90

**Figure C14.** GPC chromatograms for diblock copolymer **12**. All measurements were taken using tetrahydrofuran as the mobile phase at a flow rate of 0.8 mL/min. Molecular weights and polydispersity were determined relative to poly(styrene) standards in tetrahydrofuran.

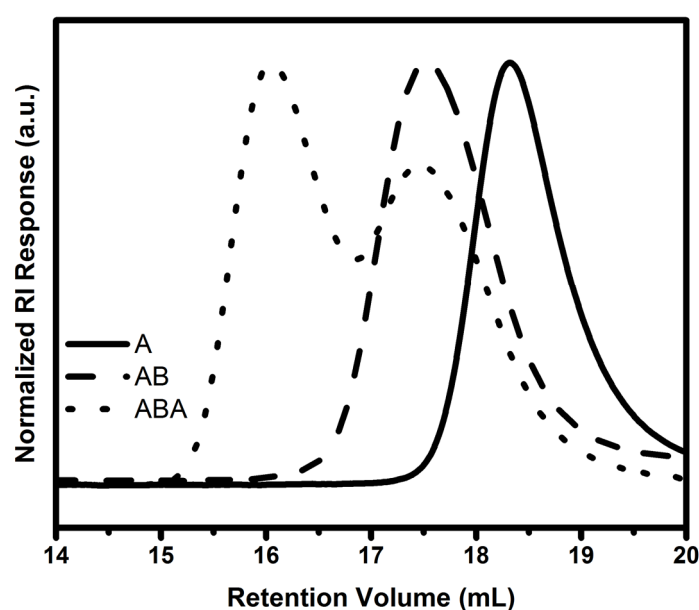
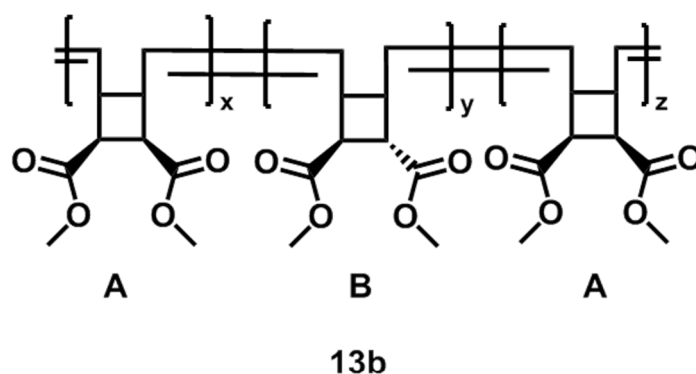


13a



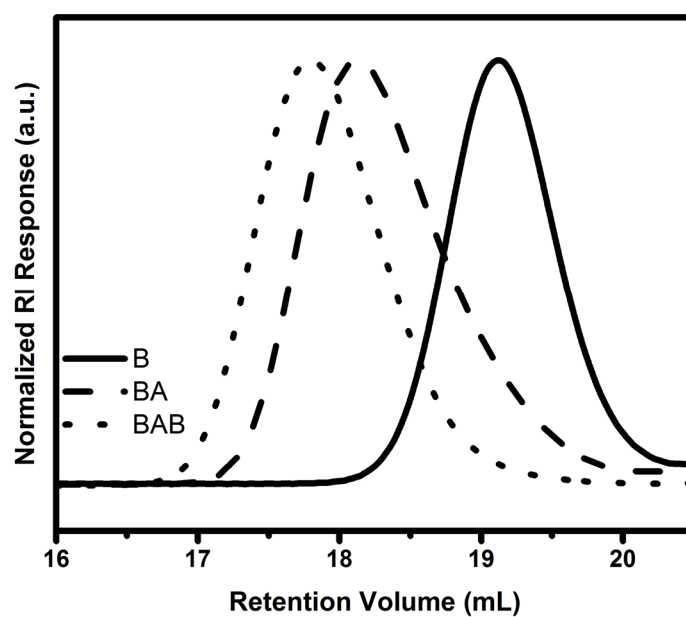
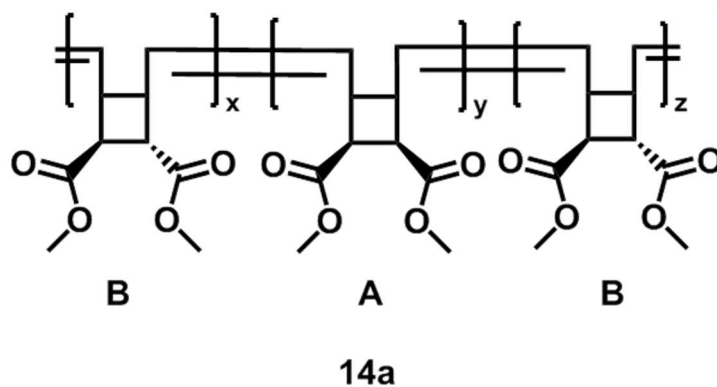
Block (Ratio)	Monomer to Catalyst Ratio	Target $M_n$ (kDa)	$M_n$ (kDa)	$M_w$ (kDa)	$D$	Yield (%)
A	25	5.0	5.9	6.7	1.1	-
AB (1:1)	-	10.0	10.5	11.7	1.1	-
ABA (1:1:1)	-	15.0	16.4	19.2	1.2	93

**Figure C15.** GPC chromatograms for the triblock copolymer **13a**. All measurements were taken using THF as the mobile phase at a flow rate of 0.8 mL/min. Molecular weights and polydispersity were determined relative to poly(styrene) standards in THF.



Block (Ratio)	Monomer to Catalyst Ratio	Target $M_n$ (kDa)	$M_n$ (kDa)	$M_w$ (kDa)	$D$	Yield (%)
A	51	10.0	10.0	12.7	1.2	-
AB (1:1)	-	20.0	21.3	26.2	1.2	-
ABA (1:1:1)	-	30.0	32.3	54.7	1.7	88

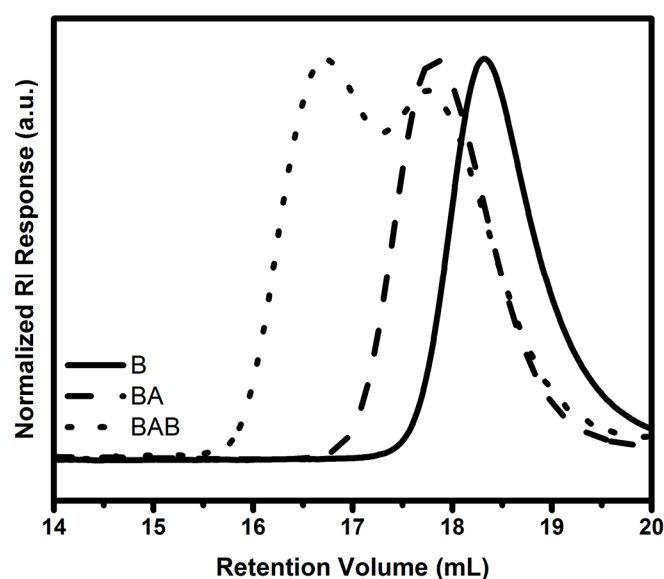
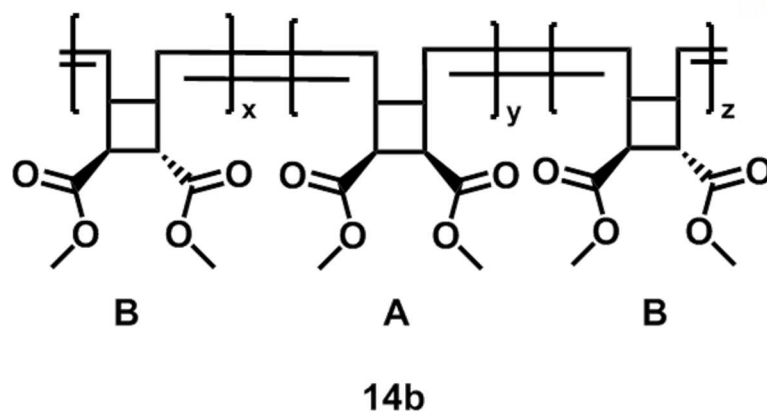
**Figure C16.** GPC chromatograms for the triblock copolymer **13b**. All measurements were taken using THF as the mobile phase at a flow rate of 0.8 mL/min. Molecular weights and polydispersity were determined relative to poly(styrene) standards in THF.



Block (Ratio)	Monomer to Catalyst Ratio	Target $M_n$ (kDa)	$M_n$ (kDa)	$M_w$ (kDa)	$\bar{D}$	Yield (%)
B	25	5.0	5.9	6.8	1.2	-
BA (1:1)	-	10.0	12.4	15.5	1.2	-
BAB (1:1:1)	-	15.0	18.7	21.7	1.2	80

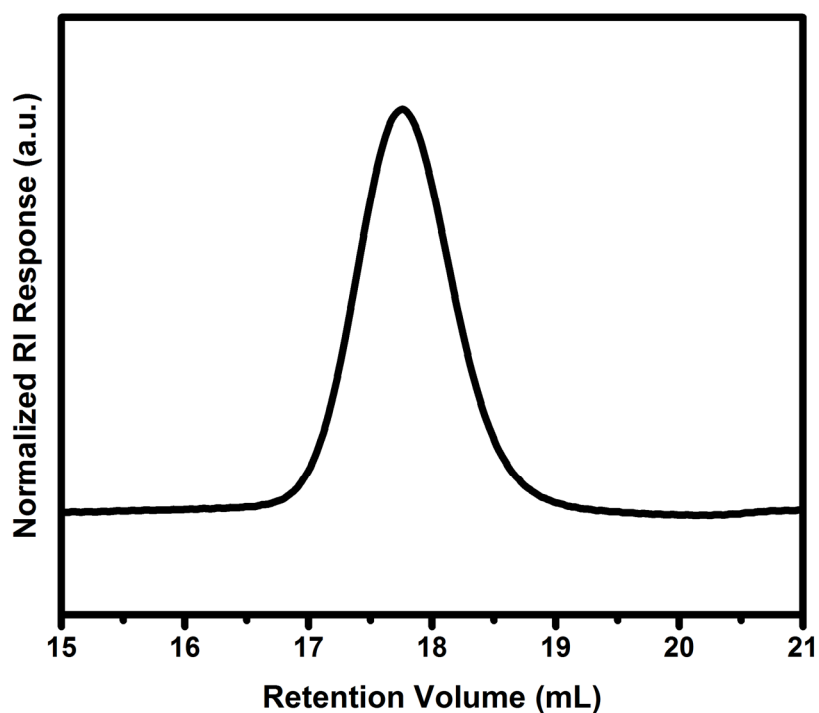
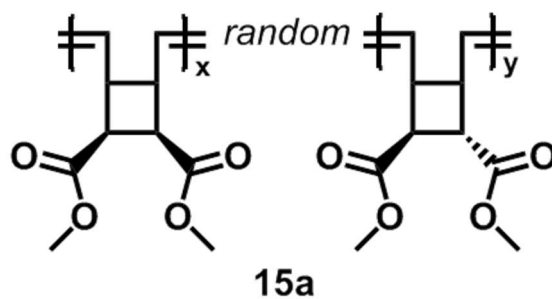
**Figure C17.** GPC chromatograms for the triblock copolymer **14a**. All measurements were taken using THF as the mobile phase at a flow rate of 0.8 mL/min. Molecular weights and polydispersity were determined relative to poly(styrene) standards in THF.





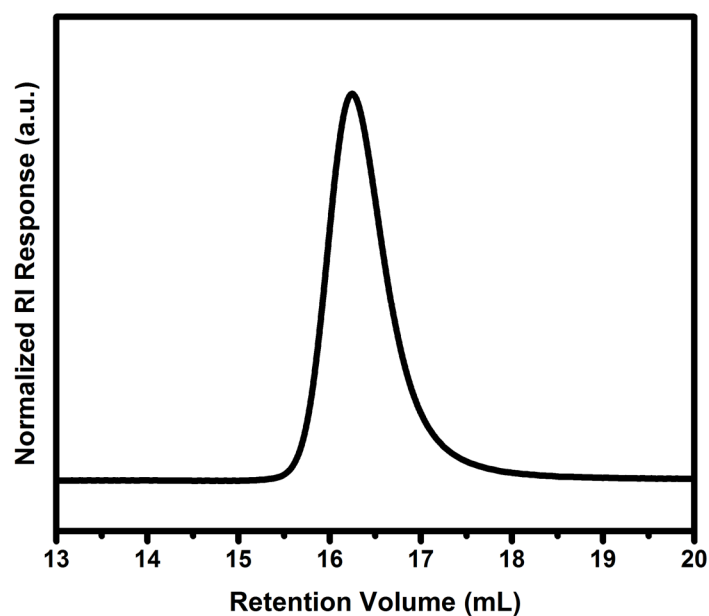
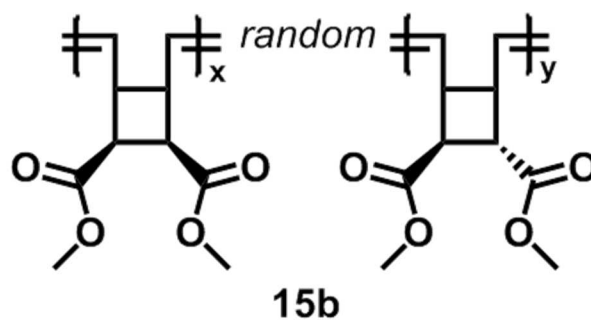
Block (Ratio)	Monomer to Catalyst Ratio	Target $M_n$ (kDa)	$M_n$ (kDa)	$M_w$ (kDa)	$\bar{D}$	Yield (%)
B	51	10.0	14.0	16.3	1.2	-
BA (1:1)	-	20.0	16.5	20.3	1.2	-
BAB (1:1:1)	-	30.0	23.7	36.5	1.5	91

**Figure C18.** GPC chromatograms for the triblock copolymer **14b**. All measurements were taken using THF as the mobile phase at a flow rate of 0.8 mL/min. Molecular weights and polydispersity were determined relative to poly(styrene) standards in THF.



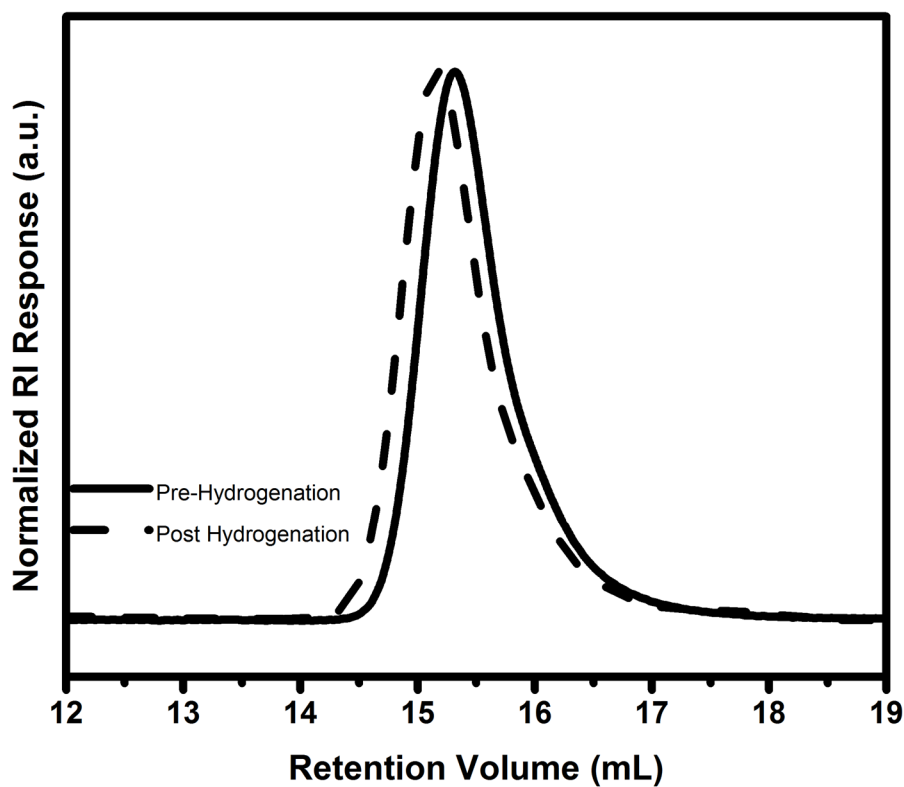
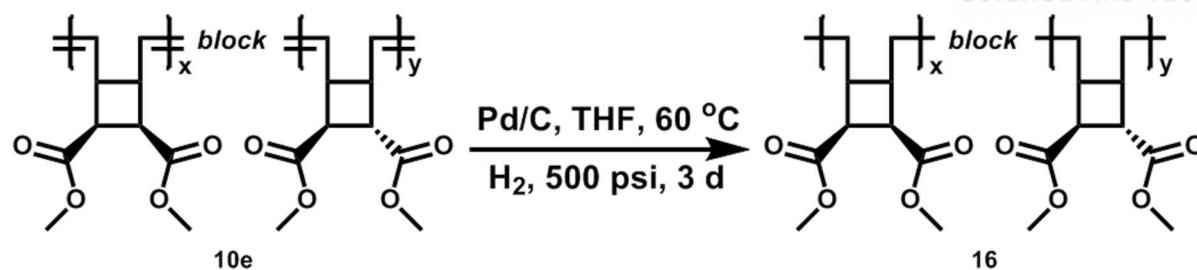
Monomer to Catalyst Ratio	Target $M_n$ (kDa)	$M_n$ (kDa)	$M_w$ (kDa)	$\bar{D}$	Yield (%)
102	20.0	23.5	23.6	1.1	84

**Figure C19.** GPC chromatogram for random copolymer **15a**. All measurements were taken using tetrahydrofuran as the mobile phase at a flow rate of 0.8 mL/min. Molecular weights and polydispersity were determined relative to poly(styrene) standards in tetrahydrofuran.



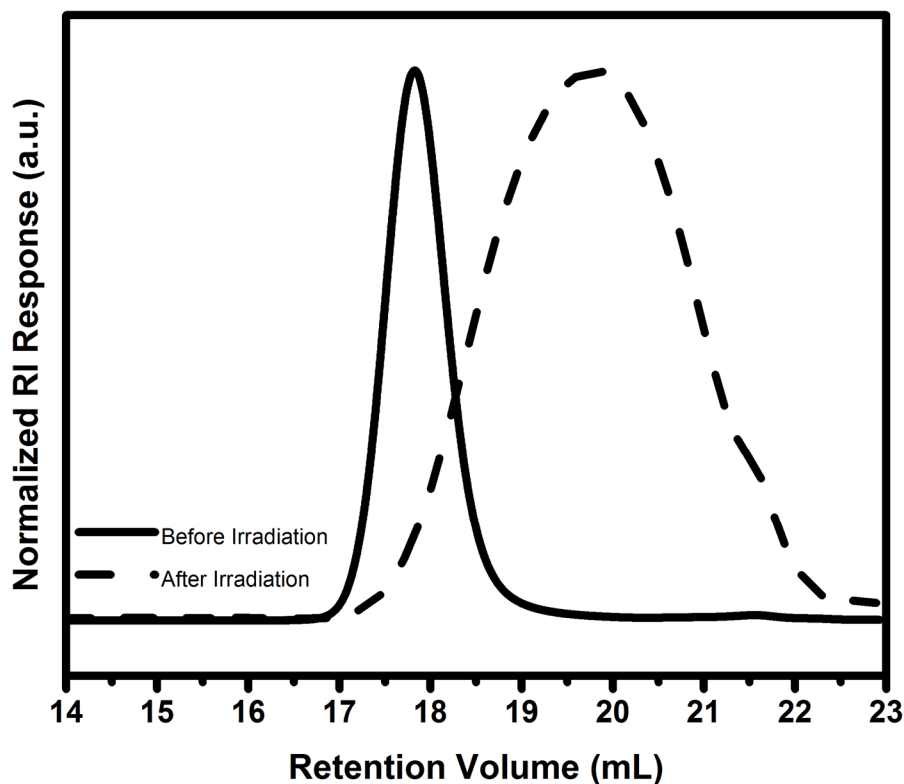
Monomer to Catalyst Ratio	Target $M_n$ (kDa)	$M_n$ (kDa)	$M_w$ (kDa)	$\bar{D}$	Yield (%)
382	75.0	62.8	69.8	1.1	82

**Figure C20.** GPC chromatogram for random copolymer **15b**. All measurements were taken using tetrahydrofuran as the mobile phase at a flow rate of 0.8 mL/min. Molecular weights and polydispersity were determined relative to poly(styrene) standards in tetrahydrofuran.



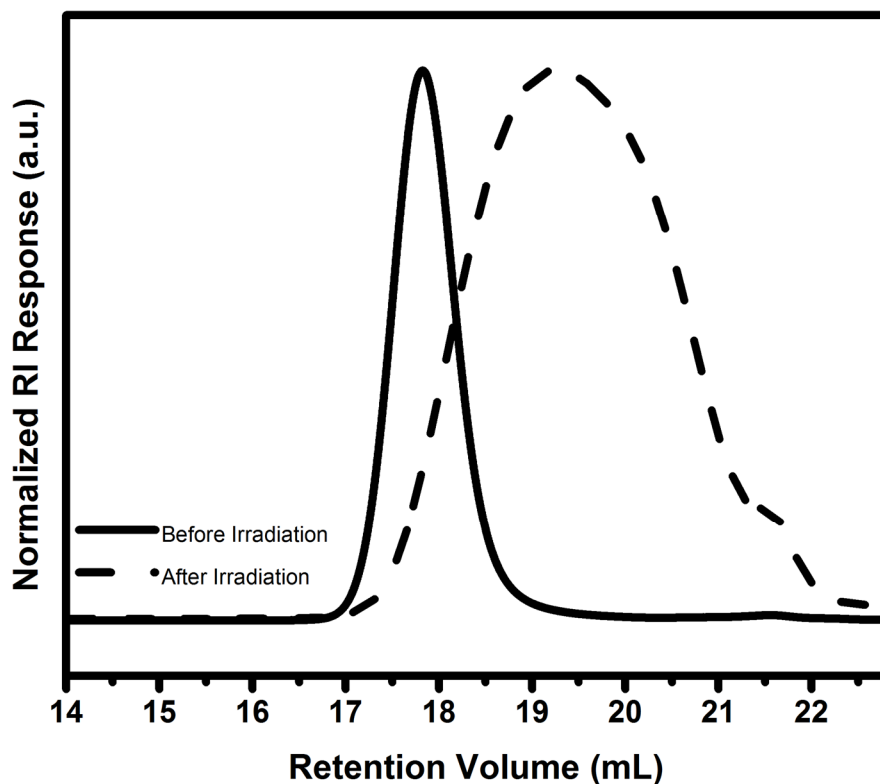
Polymer	Target $M_n$ (kDa)	$M_n$ (kDa)	$M_w$ (kDa)	$\bar{D}$	Yield (%)
<b>10e</b>	150.0	118.7	133.1	1.1	-
<b>16</b>	151.5	135.5	151.5	1.1	91

**Figure C21.** GPC chromatograms for diblock copolymer **10e** pre and post hydrogenation. All measurements were taken using THF as the mobile phase at a flow rate of 0.8 mL/min. Molecular weights and polydispersity were determined relative to poly(styrene) standards in tetrahydrofuran.



Polymer	Target $M_n$ (kDa)	$M_n$ (kDa)	$M_w$ (kDa)	$\bar{D}$
Before Irradiation	20.0	23.1	29.8	1.3
After Irradiation	5.3	1.7	5.2	3.0

**Figure C22.** GPC chromatograms for polymer **8a** before (black line) and after (dashed line) irradiation with 300 nm light for 30 hours. All measurements were taken using THF as the mobile phase at a flow rate of 0.8 mL/min. Molecular weights and polydispersity were determined relative to poly(styrene) standards in tetrahydrofuran.



Polymer	Target $M_n$ (kDa)	$M_n$ (kDa)	$M_w$ (kDa)	$\bar{D}$
Before Irradiation	20.0	19.1	21.5	1.1
After Irradiation	5.3	2.1	6.6	3.1

**Figure C23.** GPC chromatograms for polymer **9a** before (black line) and after (dashed line) irradiation with 300 nm light for 30 hours. All measurements were taken using THF as the mobile phase at a flow rate of 0.8 mL/min. Molecular weights and polydispersity were determined relative to poly(styrene) standards in tetrahydrofuran.

## Appendix D: TGA Curves

### Table of Contents

<b>Figure D1.</b>	TGA curves for the series of homopolymers <b>8</b> .....	147
<b>Figure D2.</b>	TGA curves for the series of homopolymers <b>9</b> .....	148
<b>Figure D3.</b>	TGA curves for the series of diblock copolymers <b>10-12</b> .....	149
<b>Figure D4.</b>	TGA curves for the series of triblock copolymers <b>13-14</b> .....	150
<b>Figure D5.</b>	TGA curves for the series of random copolymers <b>15</b> .....	151

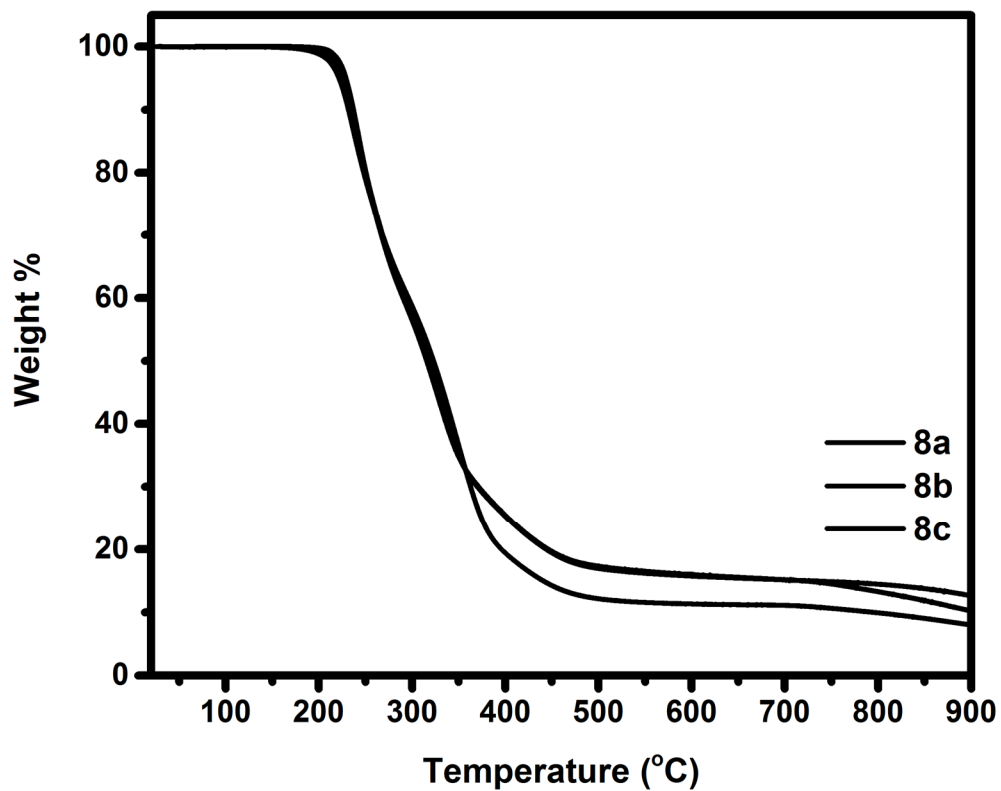


**Figure D1.** TGA curves for the series of homopolymers **8**. All TGA measurements were taken under a nitrogen atmosphere at a heating rate of 10 °C min<sup>-1</sup>.



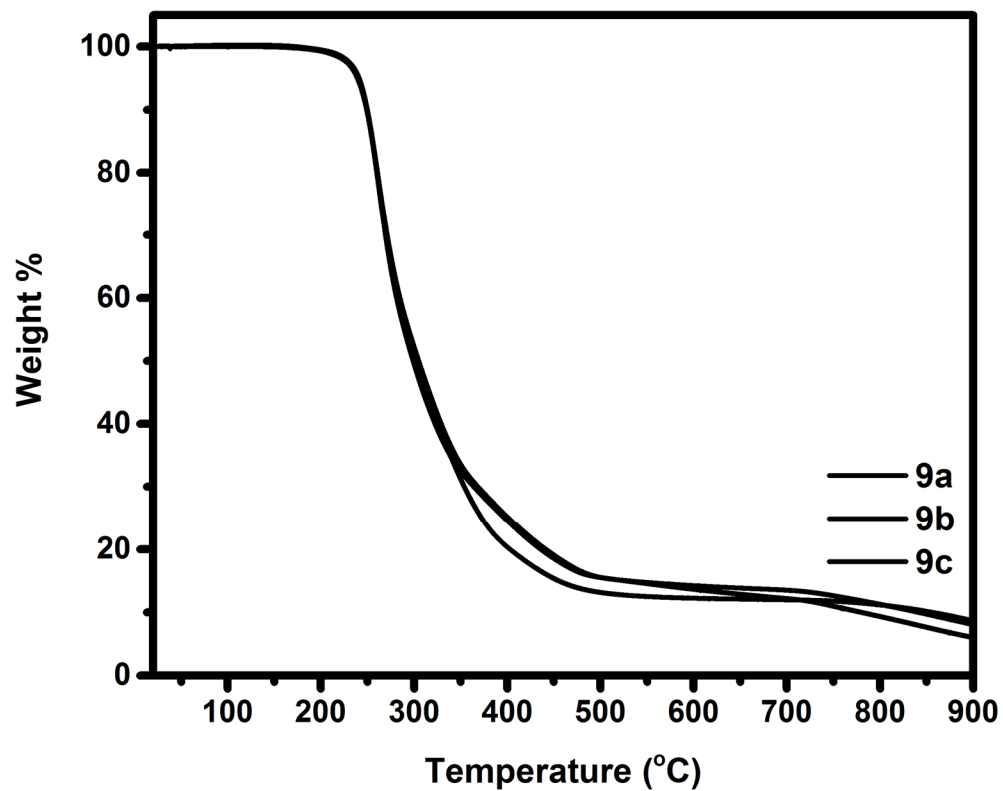


**Figure D2.** TGA curves for the series of homopolymers **9**. All TGA measurements were taken under a nitrogen atmosphere at a heating rate of  $10\text{ }^{\circ}\text{C min}^{-1}$ .

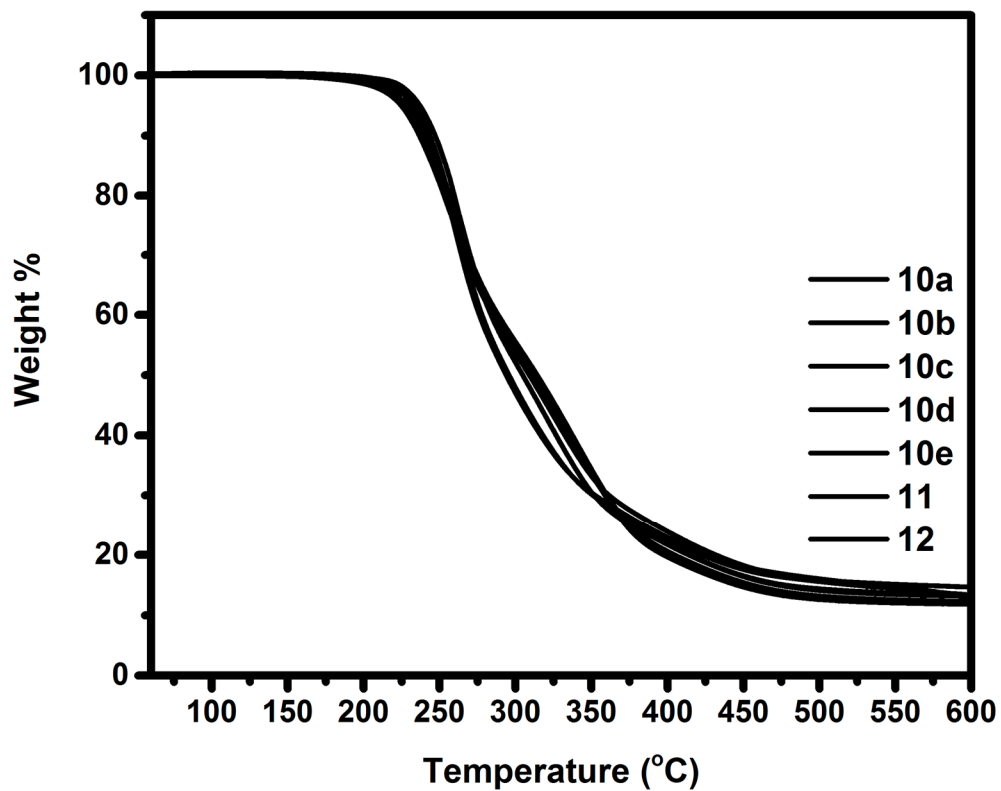


**Figure D3.** TGA curves for the series of diblock copolymers 10-12. All TGA measurements were taken under a nitrogen atmosphere at a heating rate of 10 °C min<sup>-1</sup>.

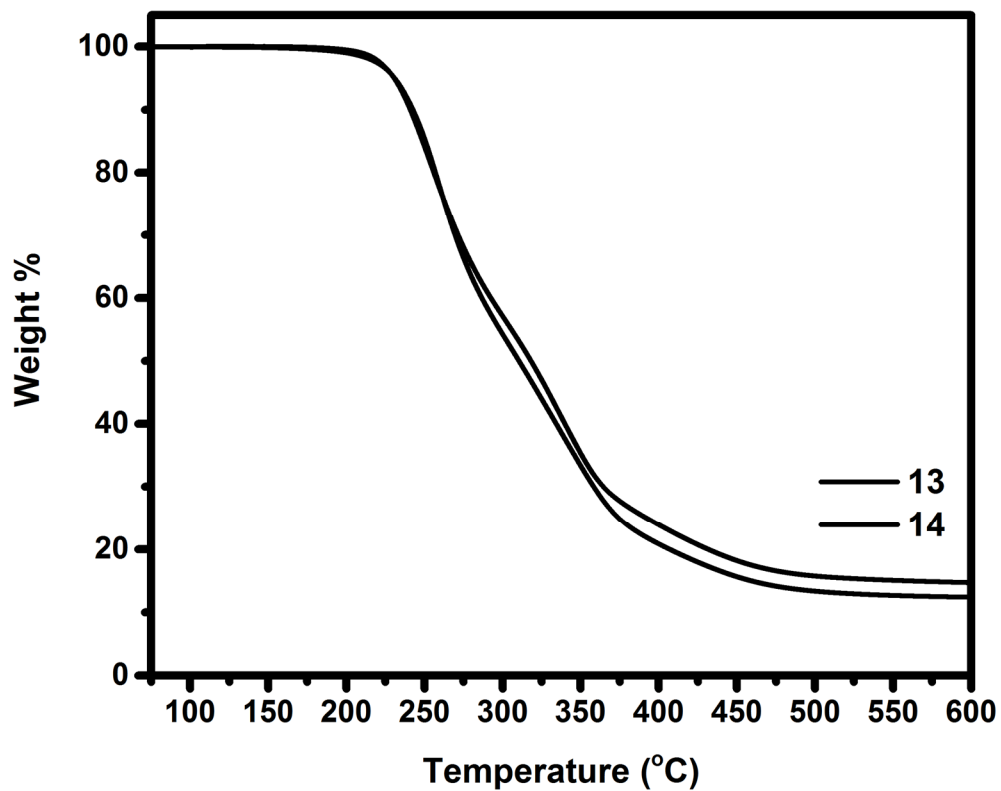


**Figure D4.** TGA curves for the series of triblock copolymers 13-14. All TGA measurements were taken under a nitrogen atmosphere at a heating rate of 10 °C min<sup>-1</sup>.

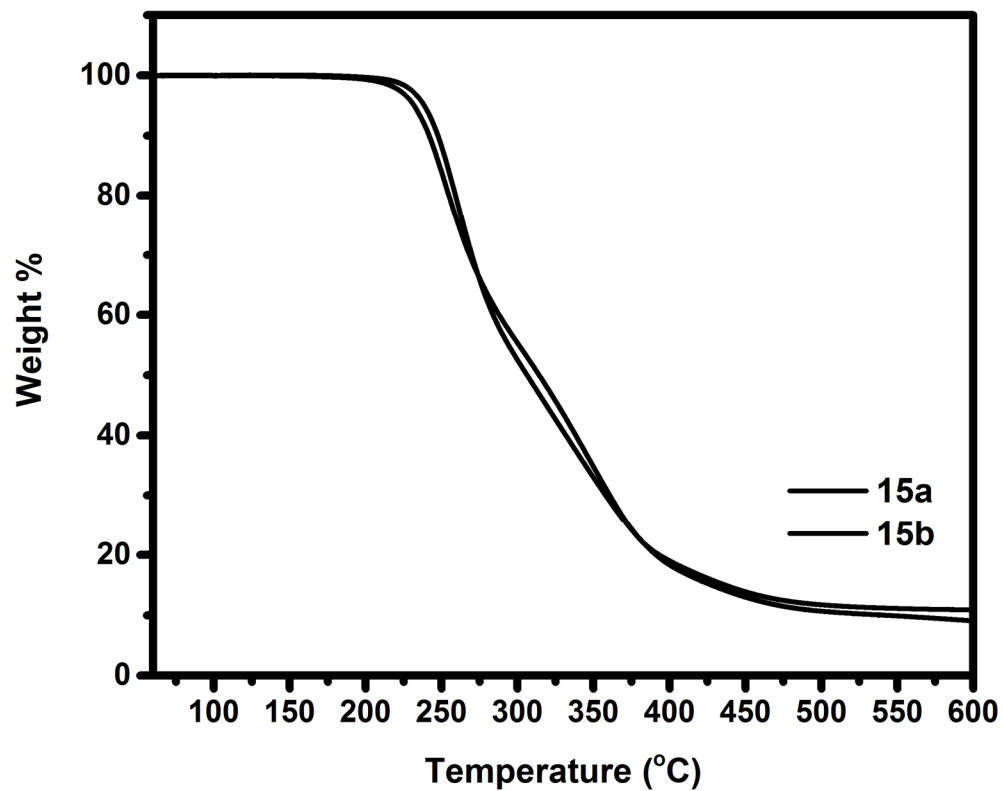


**Figure D5.** TGA curves for the series of random copolymers **15**. All TGA measurements were taken under a nitrogen atmosphere at a heating rate of  $10\text{ }^{\circ}\text{C min}^{-1}$ .

## Appendix E: DSC Traces

### Table of Contents

<b>Figure E1.</b>	DSC traces for homopolymers, diblock copolymers, and triblock copolymers.....	153
<b>Figure E2.</b>	DSC traces for homopolymers, random copolymers and physical mixtures .....	154
<b>Figure E3.</b>	DSC traces for homopolymers, random copolymers and diblock copolymers .....	155
<b>Figure E4.</b>	DSC trace for diblock copolymer <b>10f</b> .....	156
<b>Figure E5.</b>	DSC trace for diblock copolymer <b>12</b> .....	157
<b>Figure E6.</b>	DSC traces for block copolymer <b>10e</b> before and after hydrogenation .....	158
<b>Figure E7.</b>	DSC trace recorded for poly(styrene)- <i>block</i> -poly(ethylene)- <i>block</i> -poly(styrene) block copolymer and a 1:1 blend of poly(styrene) and poly(ethylene) .....	159

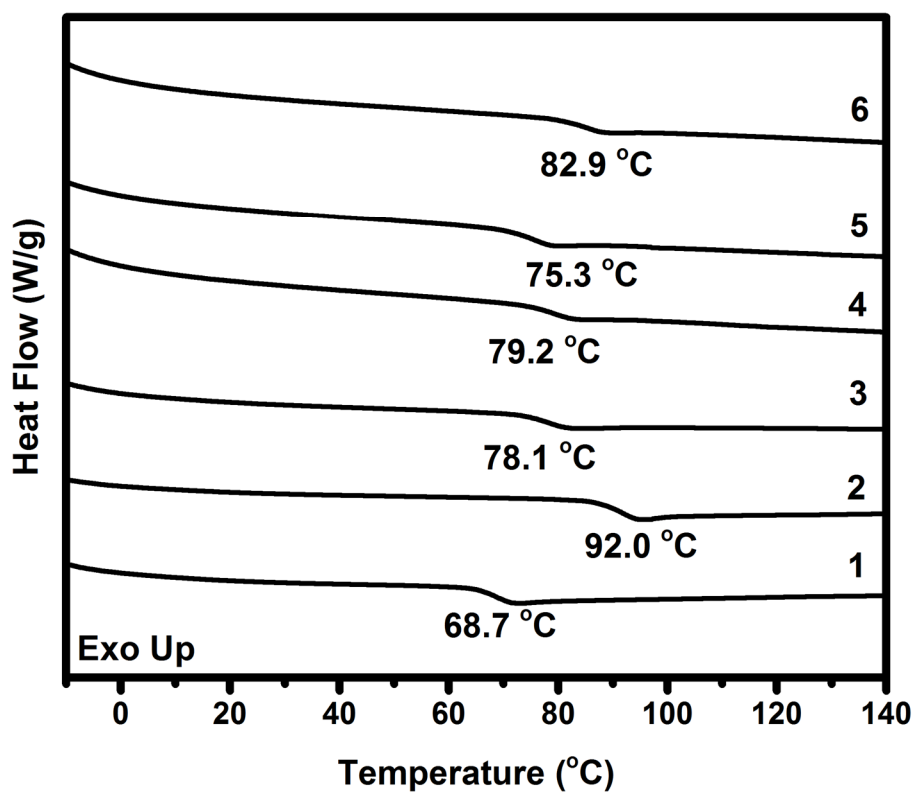


**Figure E1.** DSC traces for homopolymers, diblock copolymers, and triblock copolymers. Refer to Table 2.5 for further details. All DSC samples underwent two heating and cooling cycles under a nitrogen atmosphere at a rate of 20 °C min<sup>-1</sup> prior to recording of the data. The DSC traces presented in the figure were recorded during the third heating cycle.

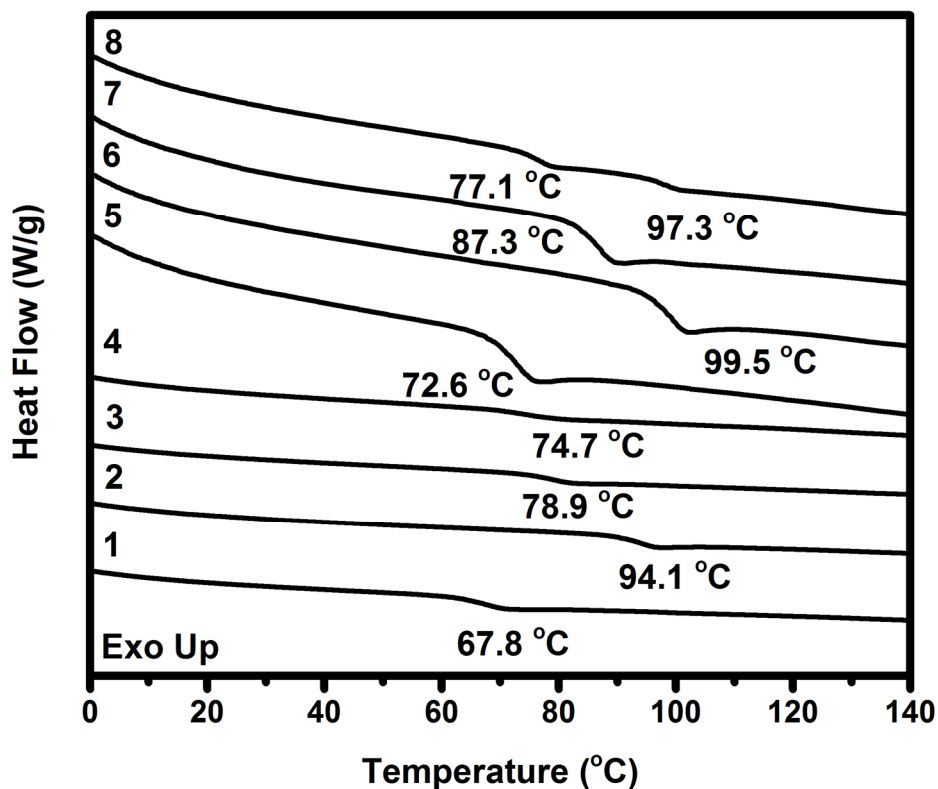


**Figure E2.** DSC traces for homopolymers, random copolymers and physical mixtures of homopolymers of different molecular weights. Refer to Table 2.9 for further details. All DSC samples underwent two heating and cooling cycles under a nitrogen atmosphere at a rate of 20 °C min<sup>-1</sup> prior to recording of the data. The DSC traces presented in the figure were recorded during the third heating cycle.

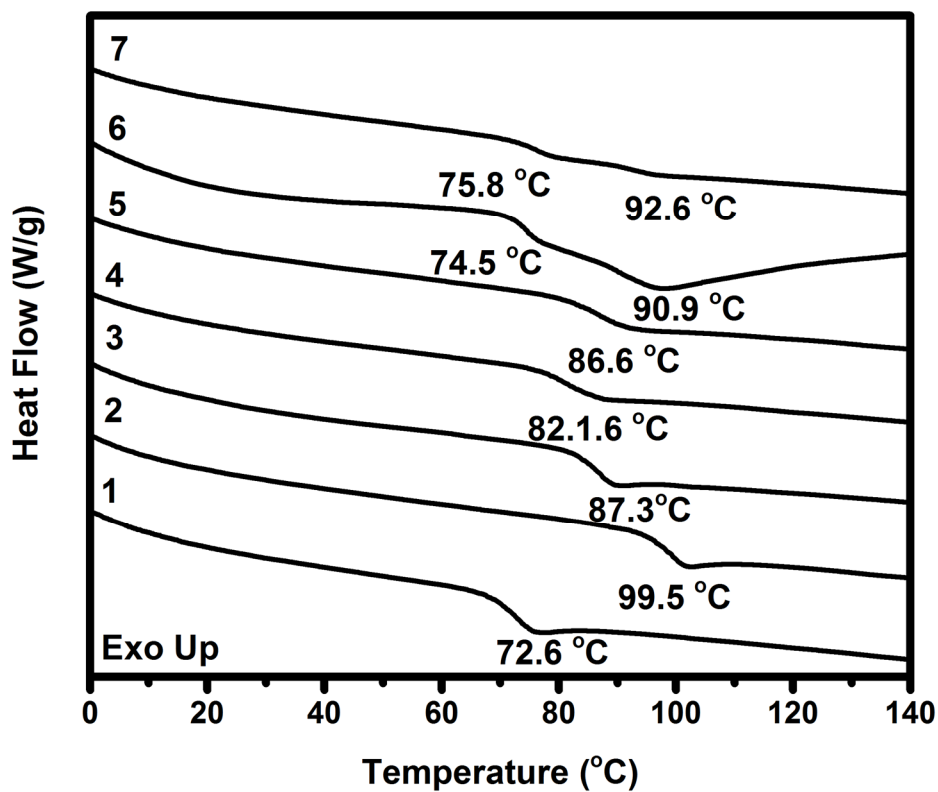


**Figure E3.** DSC traces for homopolymers, random copolymers and diblock copolymers of different molecular weights. Refer to Table 2.10 for further details. All DSC samples underwent two heating and cooling cycles under a nitrogen atmosphere at a rate of  $20\text{ }^{\circ}\text{C min}^{-1}$  prior to recording of the data. The DSC traces presented in the figure were recorded during the third heating cycle.



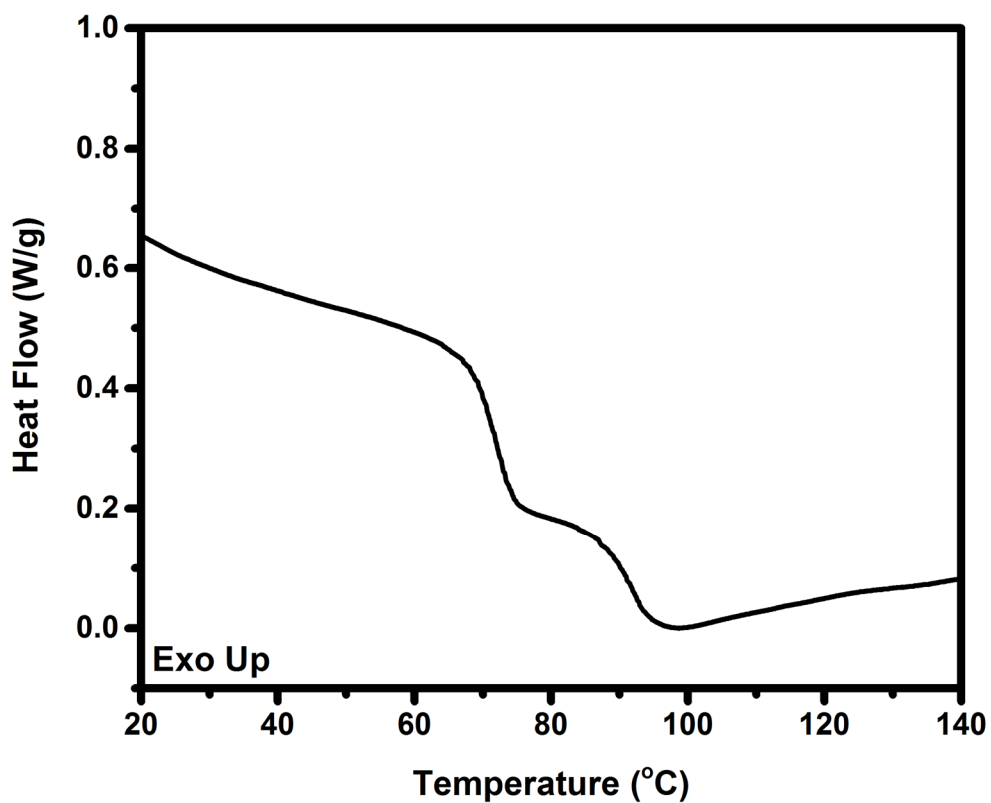


**Figure E4.** DSC trace for diblock copolymer **10f**. The sample underwent two heating and cooling cycles under a nitrogen atmosphere at a rate of  $20\text{ }^{\circ}\text{C min}^{-1}$  prior to recording of the data. The DSC trace presented in the figure was recorded during the third heating cycle.

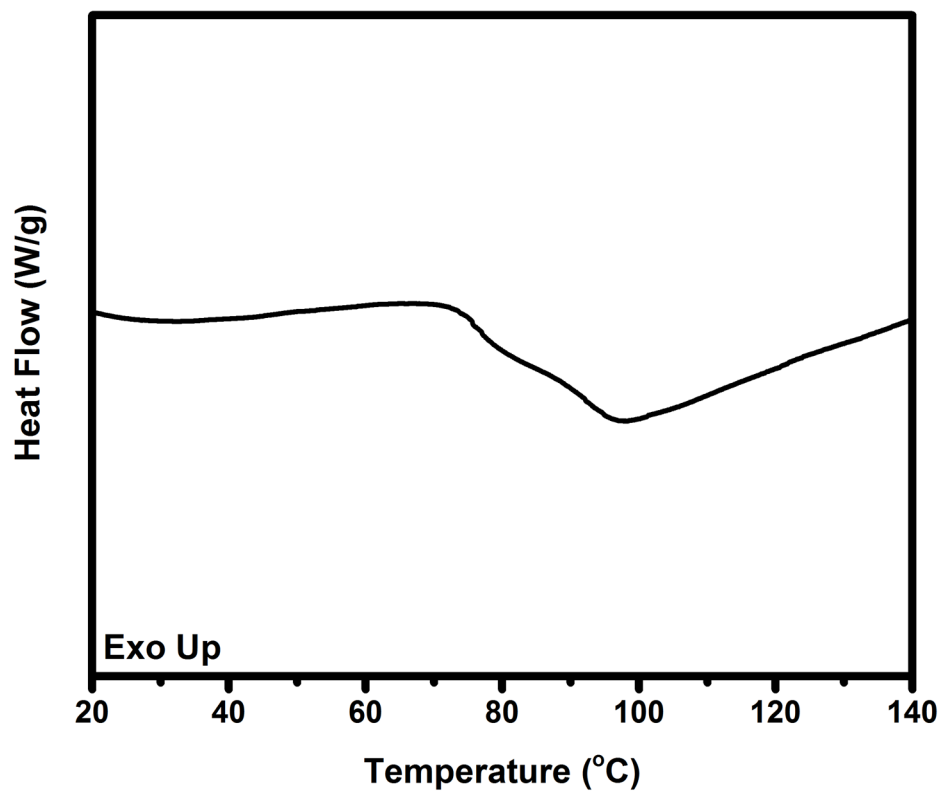


**Figure E5.** DSC trace for diblock copolymer 12. The sample underwent two heating and cooling cycles under a nitrogen atmosphere at a rate of 20 °C min<sup>-1</sup> prior to recording of the data. The DSC trace presented in the figure was recorded during the third heating cycle.

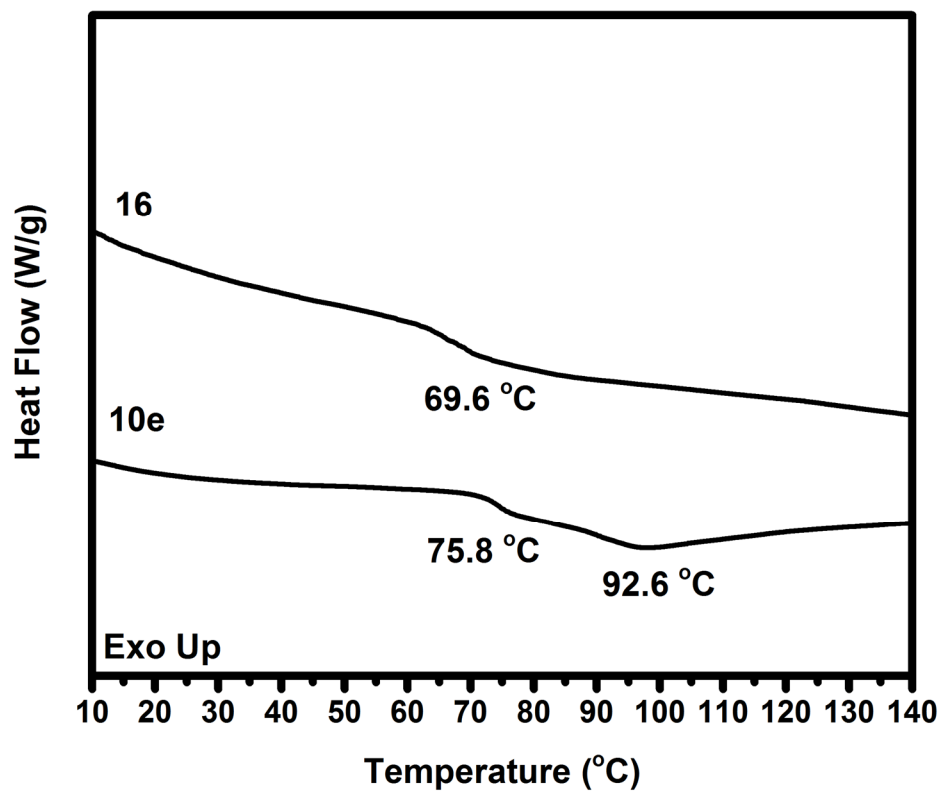


**Figure E6.** DSC traces for block copolymer **10e** before and after hydrogenation. All DSC samples underwent two heating and cooling cycles under a nitrogen atmosphere at a rate of 20 °C min<sup>-1</sup> prior to recording of the data. The DSC traces presented in the figure were recorded during the third heating cycle.

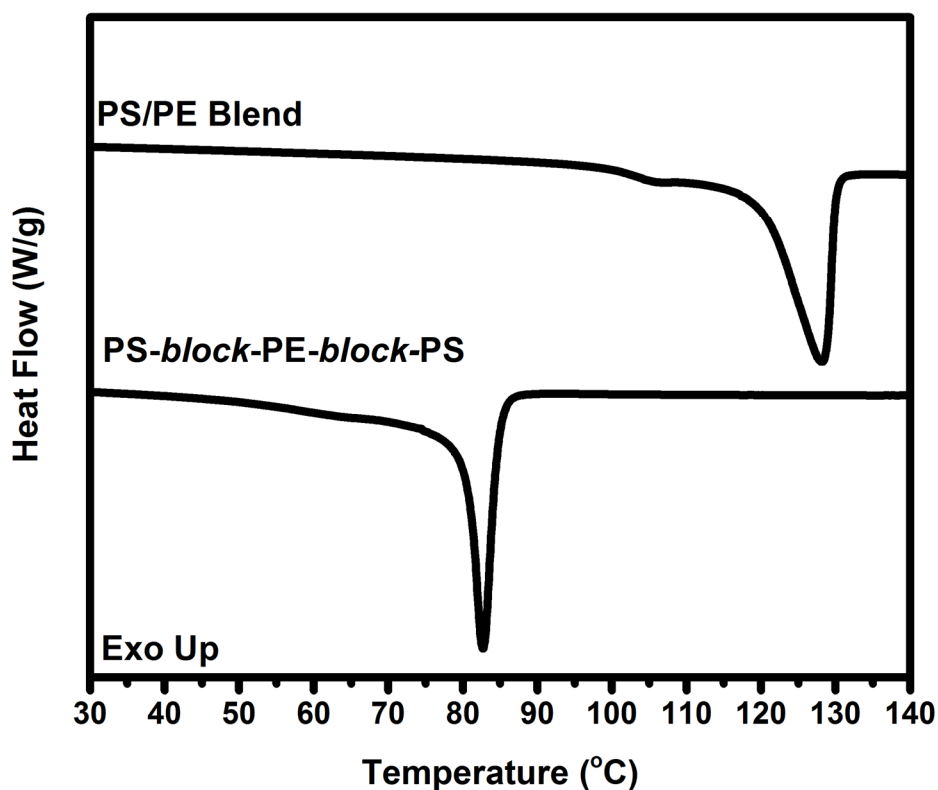


**Figure E7.** DSC trace recorded for poly(styrene)-*block*-poly(ethylene)-*block*-poly(styrene) block copolymer and a 1:1 blend of poly(styrene) and poly(ethylene). Samples underwent two heating and cooling cycles under a nitrogen atmosphere at a rate of 20 °C min<sup>-1</sup> prior to recording of the data. The DSC traces presented in the figure were recorded during the third heating cycle.

## Appendix F: Derivative and Auger Spectra

### Table of Contents

<b>Figure F1.</b> Representative Auger (top) and the first derivative Auger spectra (bottom) for graphite powder .....	162
<b>Figure F2.</b> Representative Auger (top) and the first derivative Auger spectra (bottom) for a one to three mixture of diamond and graphite powder .....	163
<b>Figure F3.</b> Representative Auger (top) and the first derivative Auger spectra (bottom) for a one to one mixture of diamond and graphite powder .....	164
<b>Figure F4.</b> Representative Auger (top) and the first derivative Auger spectra (bottom) for a three to one mixture of diamond and graphite powder .....	165
<b>Figure F5.</b> Representative Auger (top) and the first derivative Auger spectra (bottom) of diamond powder .....	166
<b>Figure F6.</b> Representative Auger (top) and the first derivative Auger spectra (bottom) of poly(ethylene) .....	167
<b>Figure F7.</b> Representative Auger (top) and the first derivative Auger spectra (bottom) of poly(cyclooctene).....	168
<b>Figure F8.</b> Representative Auger (top) and the first derivative Auger spectra (bottom) of poly(norbornene).....	169
<b>Figure F9.</b> Representative Auger (top) and the first derivative Auger spectra (bottom) of poly(cyclopentene).....	170
<b>Figure F10.</b> Representative Auger (top) and the first derivative Auger spectra (bottom) of poly(dicyclopentadiene).....	171
<b>Figure F11.</b> Representative Auger (top) and the first derivative Auger spectra (bottom) of poly(cyclooctadiene).....	172
<b>Figure F12.</b> Representative Auger (top) and the first derivative Auger spectra (bottom) of poly(cis-1,4-butadiene) .....	173
<b>Figure F13.</b> Representative Auger (top) and the first derivative Auger spectra (bottom) of poly(styrene) .....	174
<b>Figure F14.</b> Representative Auger (top) and the first derivative Auger spectra (bottom) of poly(acetylene).....	175
<b>Figure F15.</b> Representative Auger (top) and the first derivative Auger spectra (bottom) of poly(vinyl acetylene) .....	176

**Figure F16.** Representative Auger (top) and the first derivative Auger spectra (bottom) of poly(phenylene ethynylene)..... 177

**Figure F17.** Representative Auger (top) and the first derivative Auger spectra (bottom) of pentacene ..... 178

**Figure F18.** Representative Auger (top) and the first derivative Auger spectra (bottom) of coronene ..... 179

**Figure F19.** Representative Auger (top) and the first derivative Auger spectra (bottom) of poly(acrylonitrile) ..... 180

**Figure F20.** Representative Auger (top) and the first derivative Auger spectra (bottom) of poly(4-vinyl pyridine)..... 181

**Figure F21.** Representative Auger (top) and the first derivative Auger spectra (bottom) of poly(methyl methacrylate)..... 182

**Figure F22.** Representative Auger (top) and the first derivative Auger spectra (bottom) of poly(vinyl acetylene) ..... 183

**Figure F23.** Representative Auger (top) and the first derivative Auger spectra (bottom) of one to one physical mixture of poly(ethylene) and poly(acetylene)..... 184

**Figure F24.** Representative Auger (top) and the first derivative Auger spectra (bottom) of a one to one blend of poly(styrene) and poly(ethylene) ..... 185

**Figure F25.** Representative Auger (top) and the first derivative Auger spectra (bottom) of a three to one blend of poly(styrene) and poly(ethylene) ..... 186

**Figure F26.** Representative Auger (top) and the first derivative Auger spectra (bottom) of a one to three blend of poly(styrene) and poly(ethylene) ..... 187

**Figure F27.** Representative Auger (top) and the first derivative Auger spectra (bottom) of a poly(styrene)-*block*-poly(ethylene)-*block*-poly(styrene) ..... 188

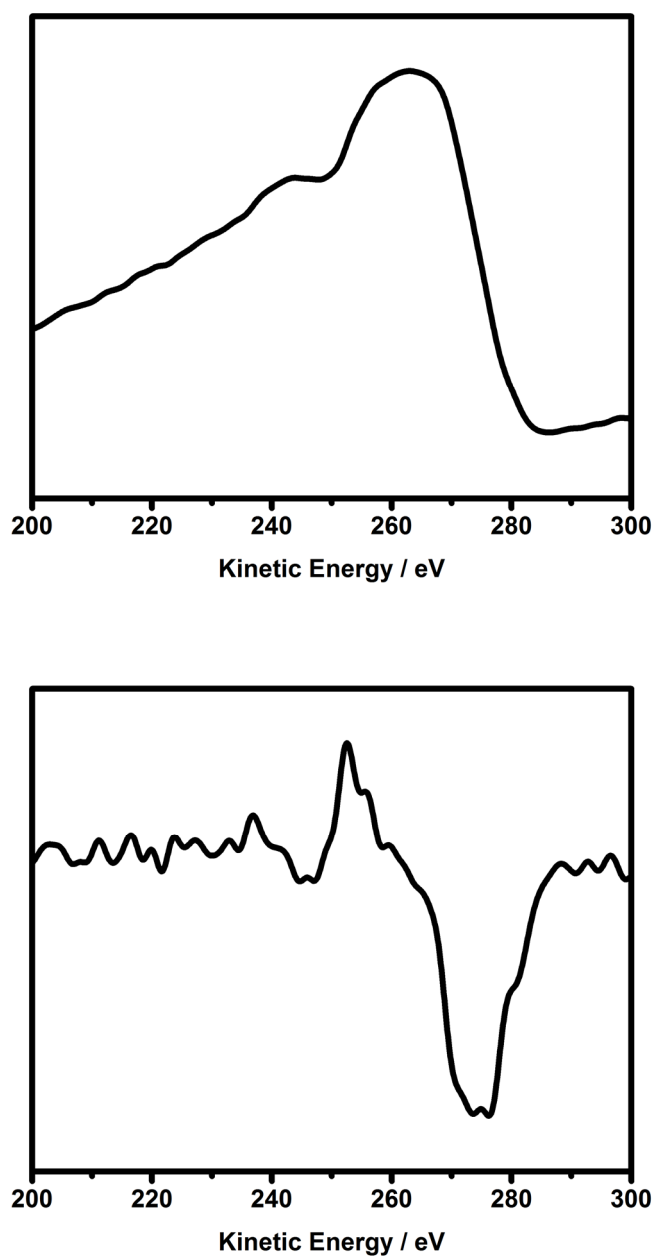


**Figure F1.** Representative Auger (top) and the first derivative Auger spectra (bottom) for graphite powder. The  $D$ -parameter was calculated from the distance between the maximum and minimum point on the derivative spectra.

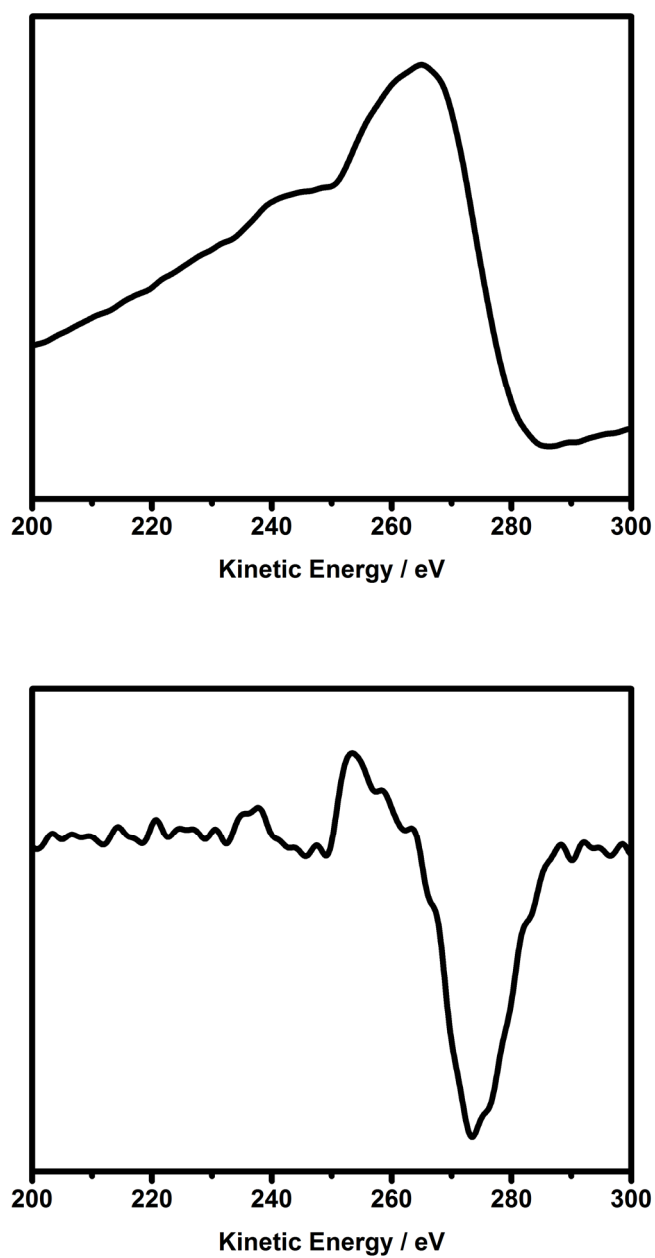


**Figure F2.** Representative Auger (top) and the first derivative Auger spectra (bottom) for a one to three mixture of diamond and graphite powder. The  $D$ -parameter was calculated from the distance between the maximum and minimum point on the derivative spectra.



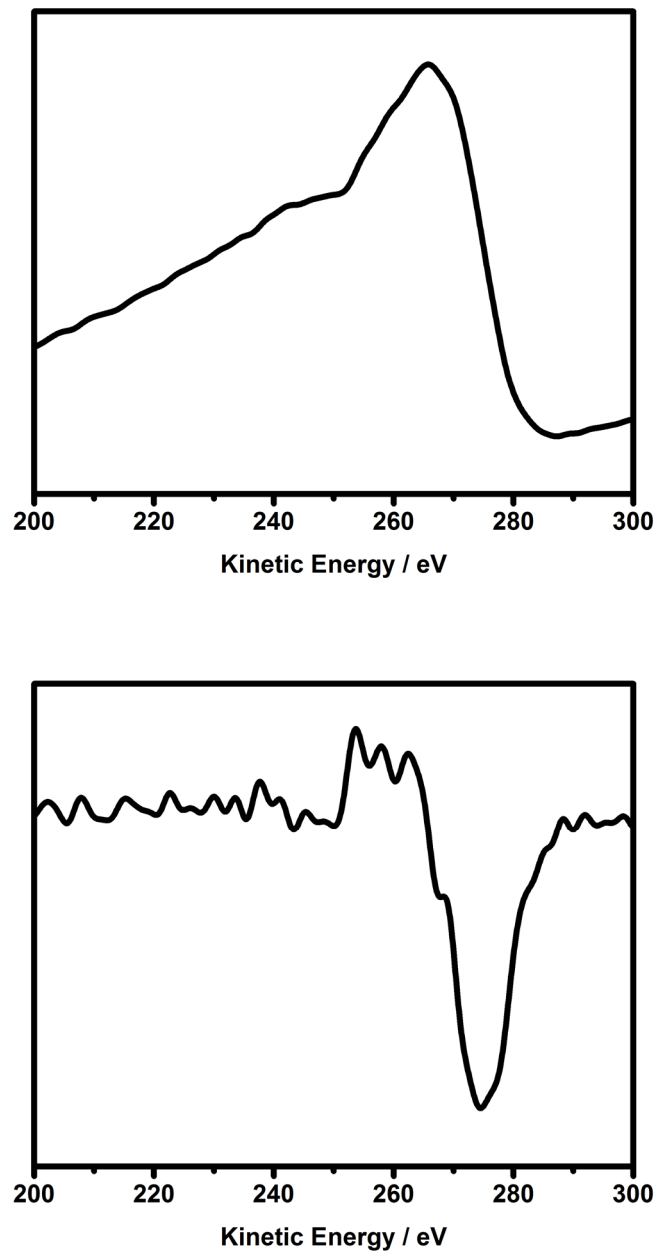


**Figure F3.** Representative Auger (top) and the first derivative Auger spectra (bottom) for a one to one mixture of diamond and graphite powder. The  $D$ -parameter was calculated from the distance between the maximum and minimum point on the derivative spectra.

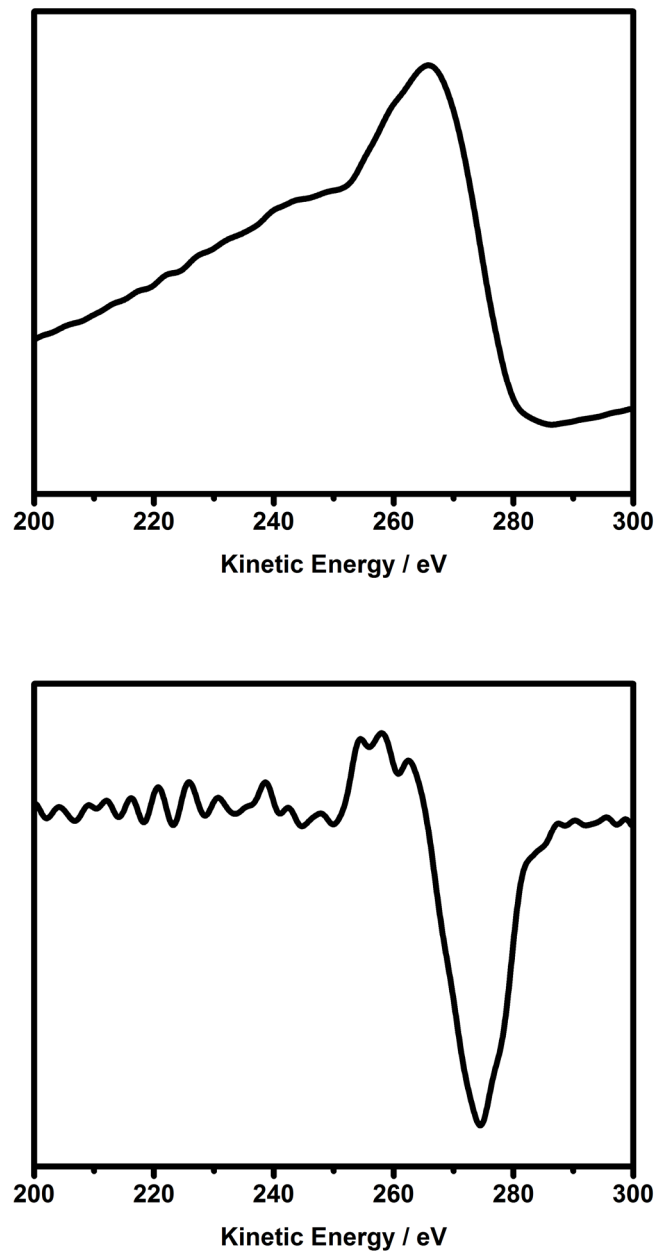


**Figure F4.** Representative Auger (top) and the first derivative Auger spectra (bottom) for a three to one mixture of diamond and graphite powder. The  $D$ -parameter was calculated from the distance between the maximum and minimum point on the derivative spectra.

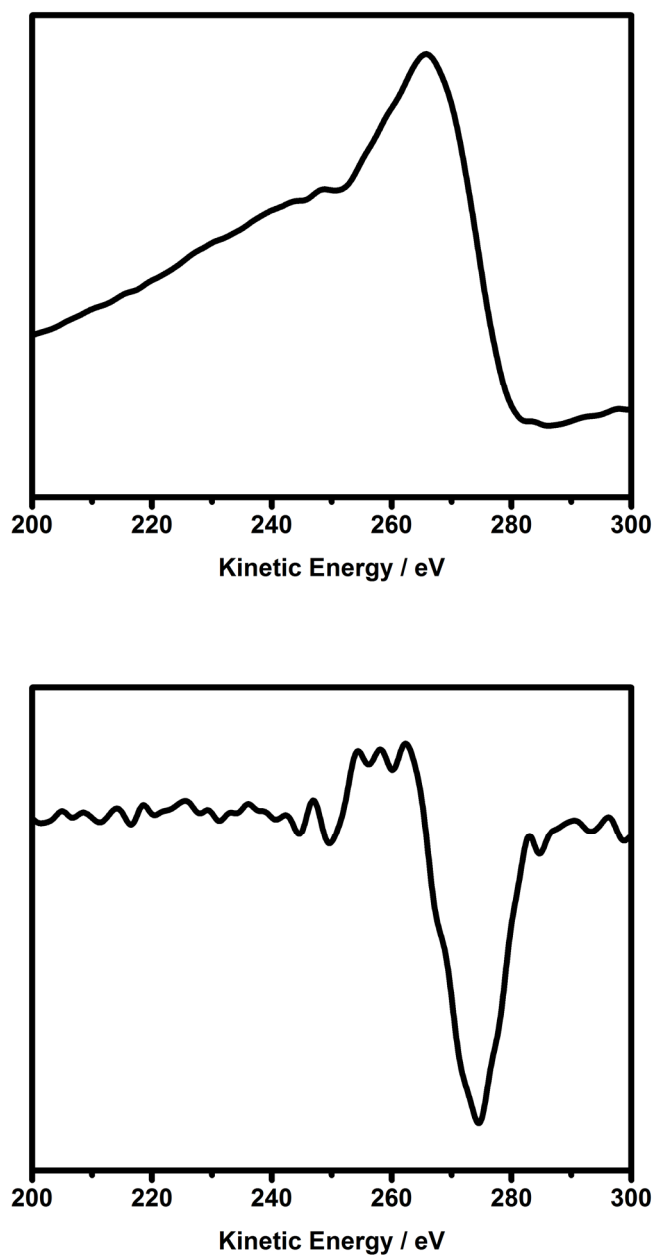


**Figure F5.** Representative Auger (top) and the first derivative Auger spectra (bottom) of diamond powder. The  $D$ -parameter was calculated from the distance between the maximum and minimum point on the derivative spectra.

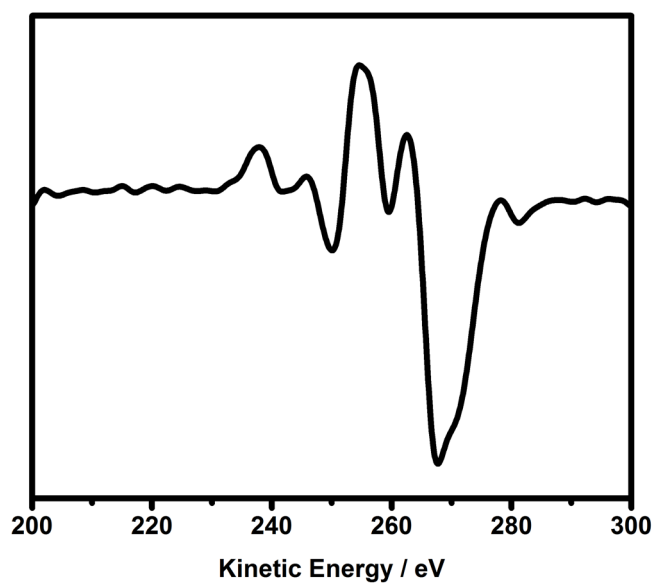
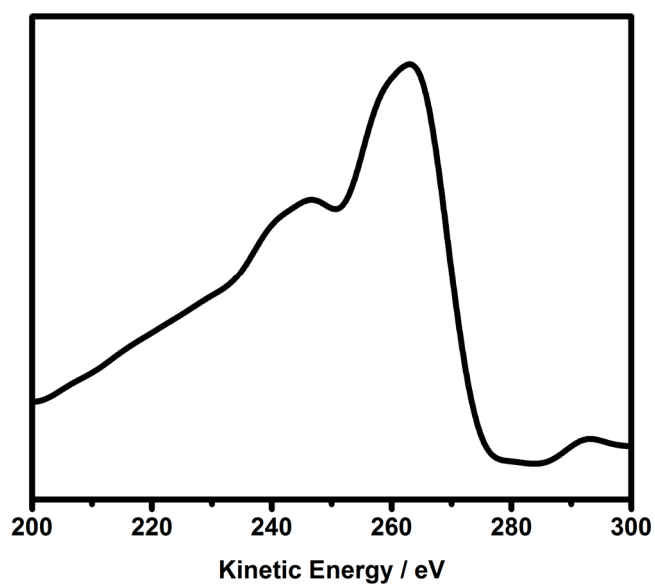


**Figure F6.** Representative Auger (top) and the first derivative Auger spectra (bottom) of poly(ethylene). The  $D$ -parameter was calculated from the distance between the maximum and minimum point on the derivative spectra.

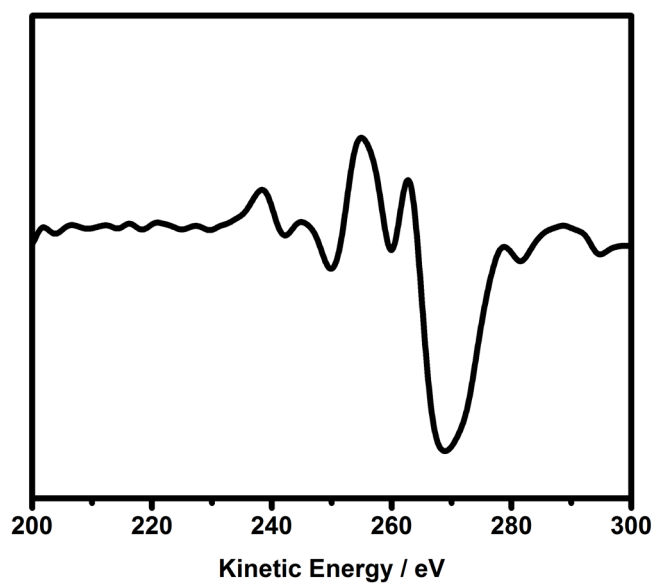
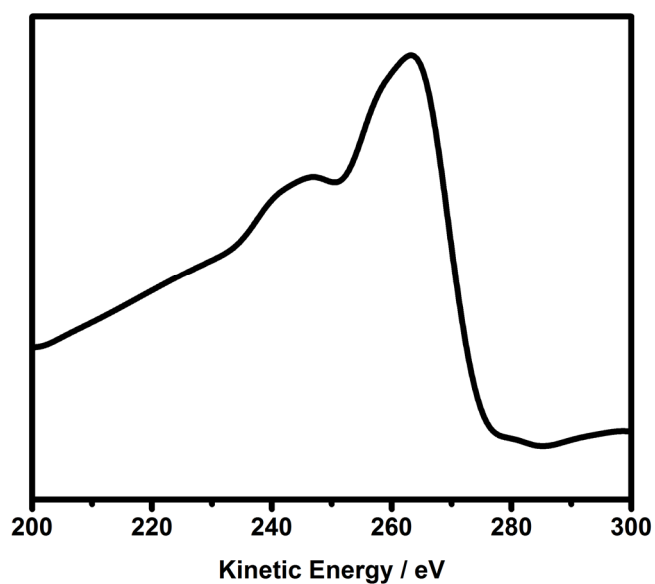


**Figure F7.** Representative Auger (top) and the first derivative Auger spectra (bottom) of poly(cyclooctene). The *D*-parameter was calculated from the distance between the maximum and minimum point on the derivative spectra.

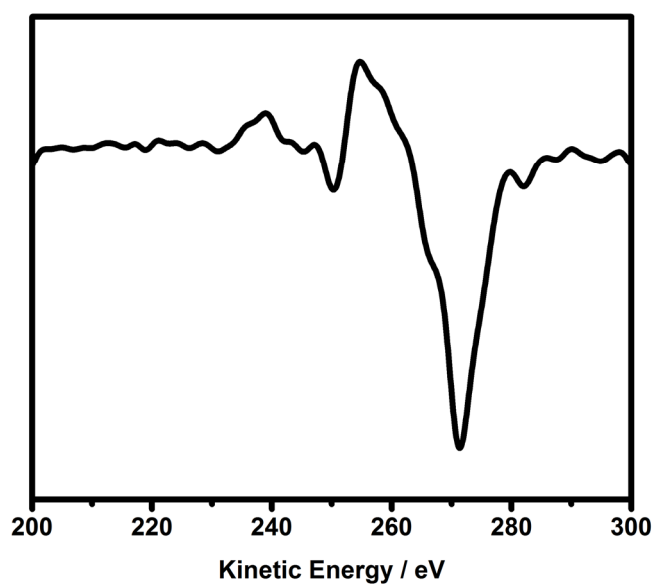
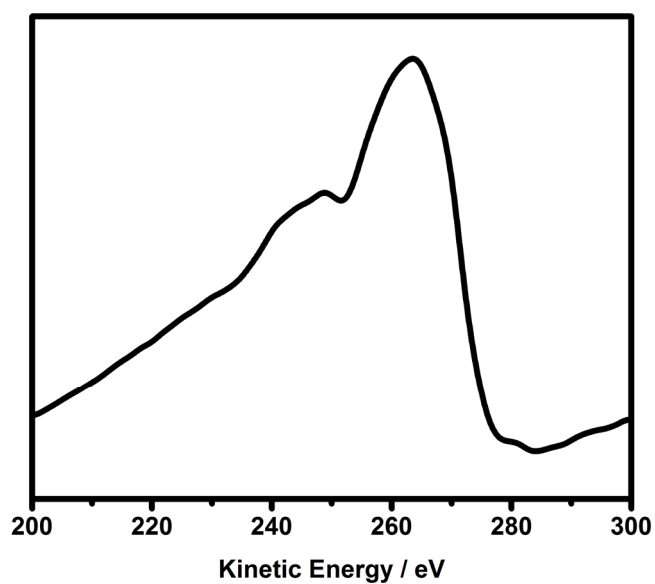


**Figure F8.** Representative Auger (top) and the first derivative Auger spectra (bottom) of poly(norbornene). The  $D$ -parameter was calculated from the distance between the maximum and minimum point on the derivative spectra.

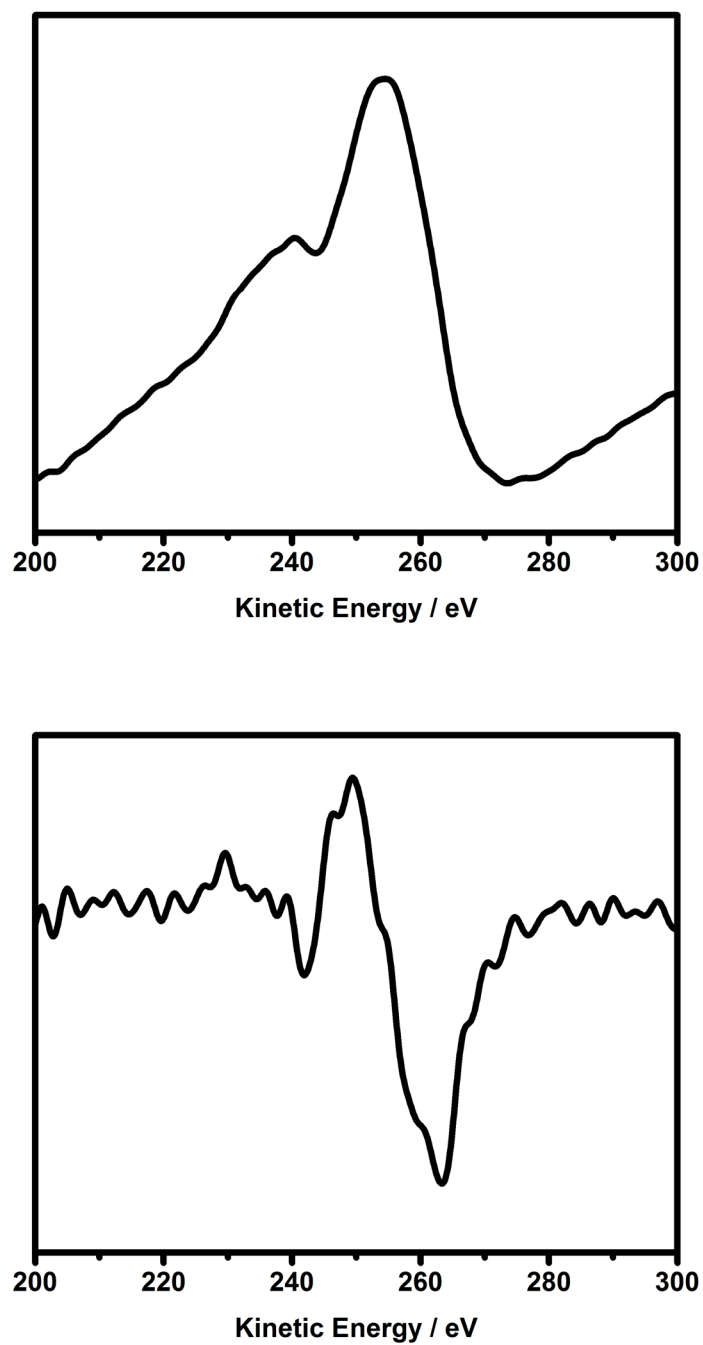


**Figure F9.** Representative Auger (top) and the first derivative Auger spectra (bottom) of poly(cyclopentene). The  $D$ -parameter was calculated from the distance between the maximum and minimum point on the derivative spectra.

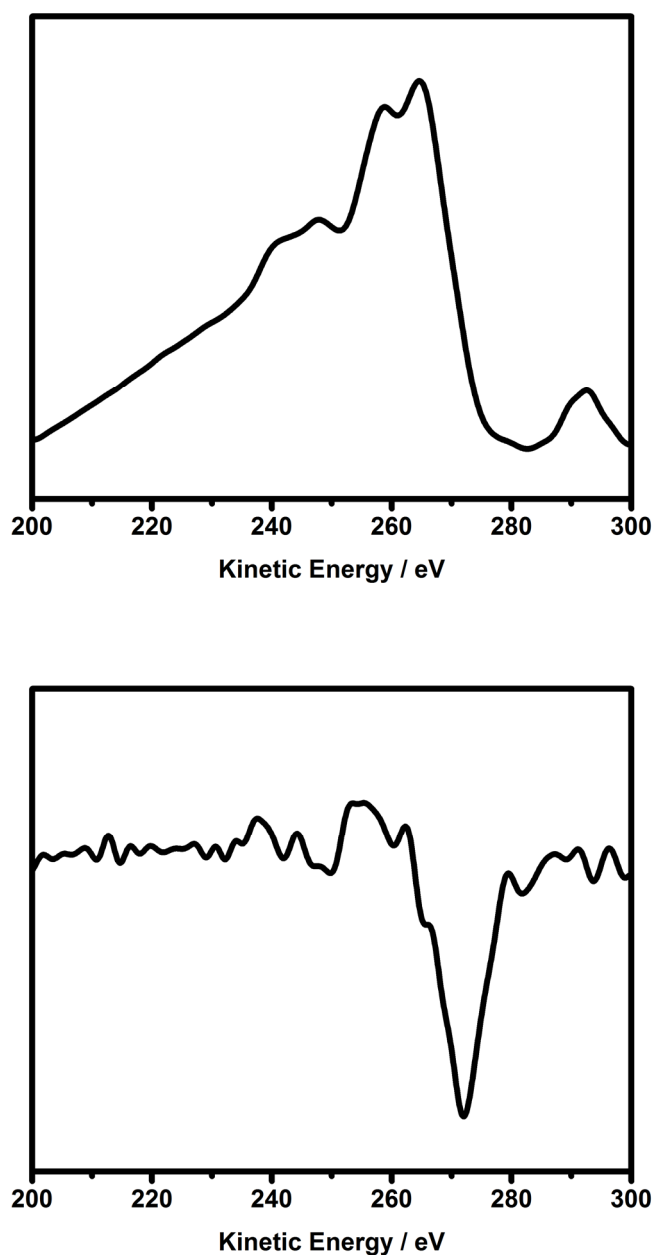


**Figure F10.** Representative Auger (top) and the first derivative Auger spectra (bottom) of poly(dicyclopentadiene). The  $D$ -parameter was calculated from the distance between the maximum and minimum point on the derivative spectra.



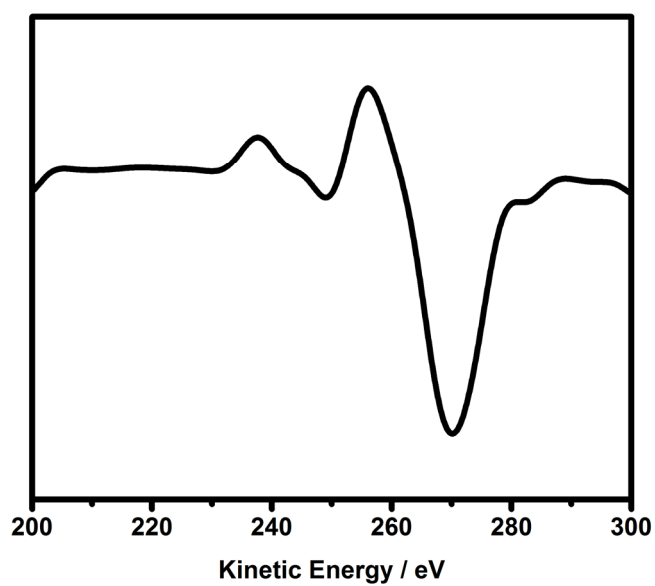
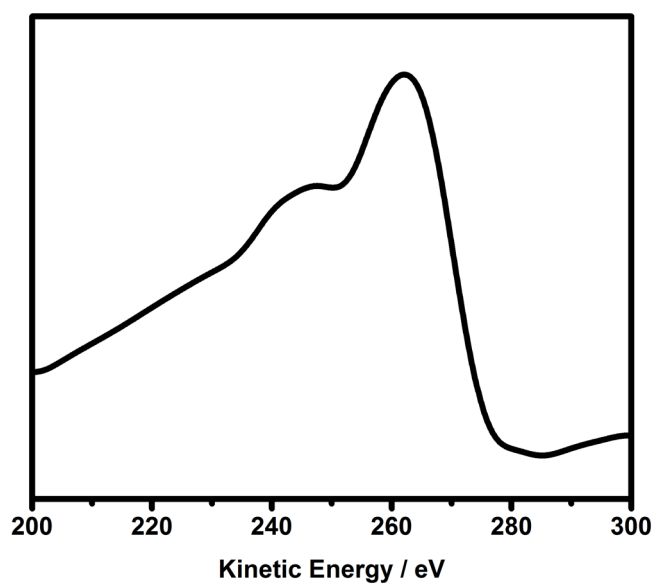


**Figure F11.** Representative Auger (top) and the first derivative Auger spectra (bottom) of poly(cyclooctadiene). The  $D$ -parameter was calculated from the distance between the maximum and minimum point on the derivative spectra.

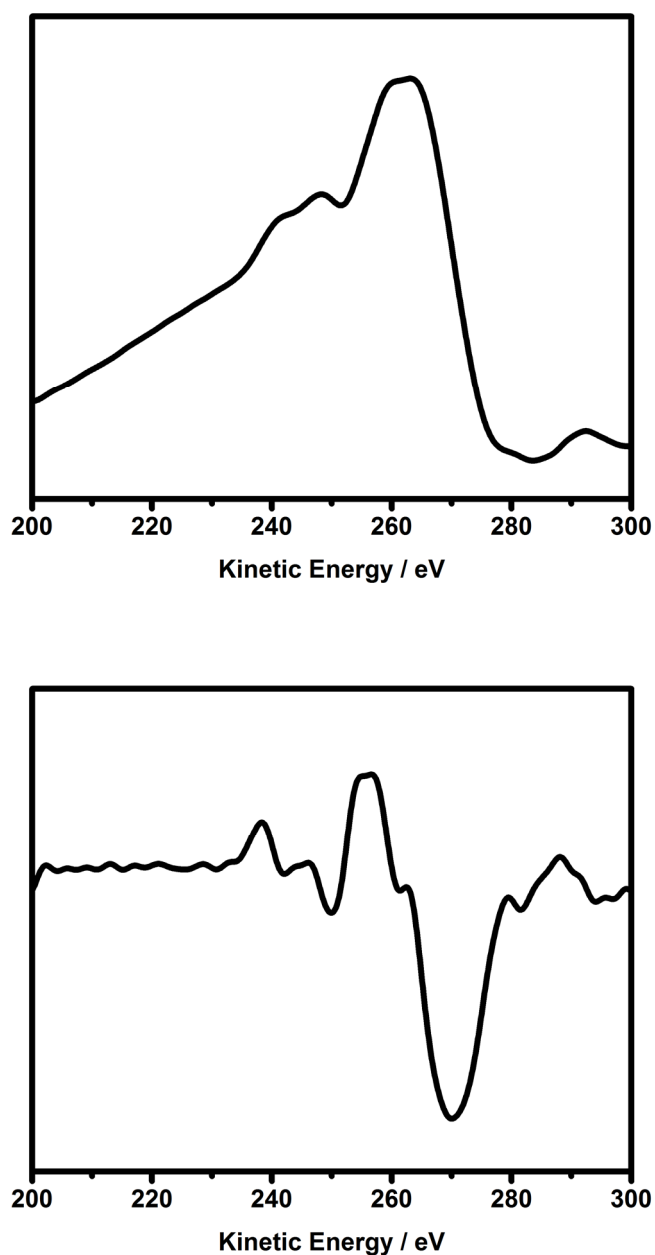


**Figure F12.** Representative Auger (top) and the first derivative Auger spectra (bottom) of poly(cis-1,4-butadiene). The  $D$ -parameter was calculated from the distance between the maximum and minimum point on the derivative spectra.

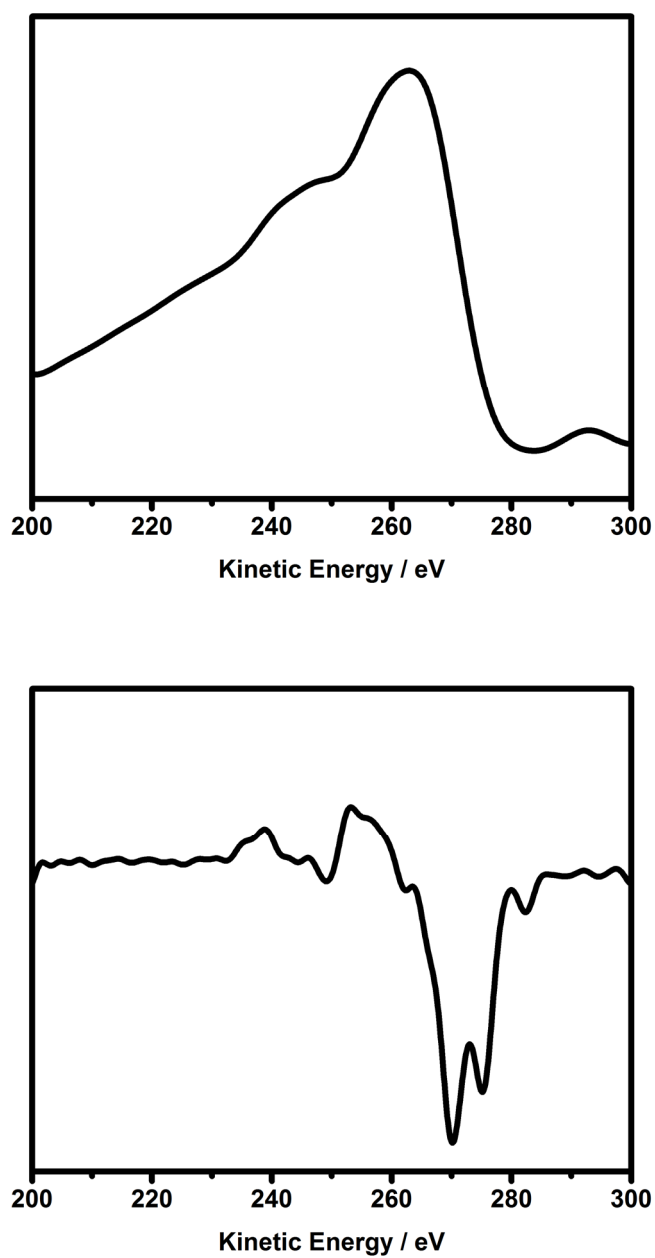


**Figure F13.** Representative Auger (top) and the first derivative Auger spectra (bottom) of poly(styrene). The  $D$ -parameter was calculated from the distance between the maximum and minimum point on the derivative spectra.

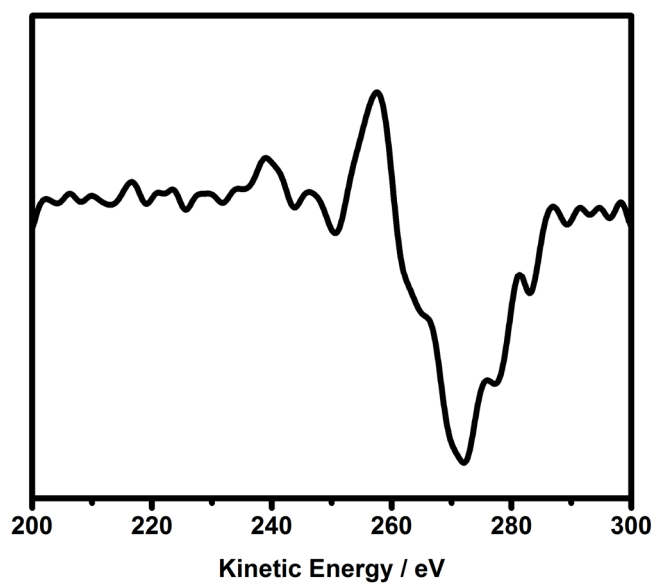
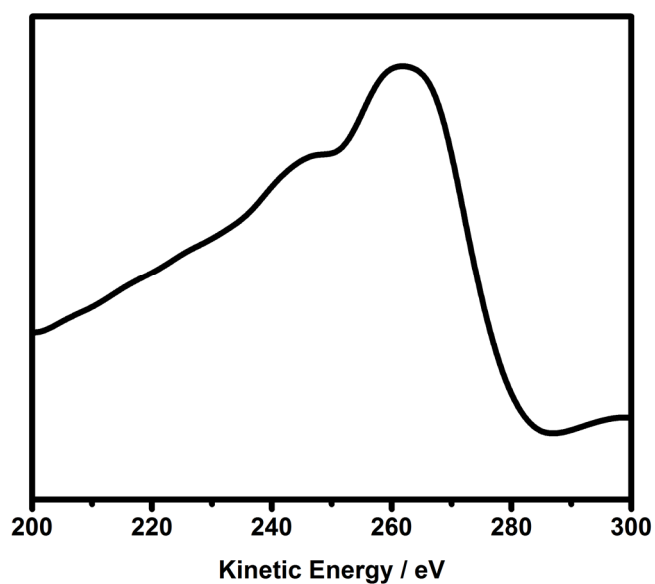


**Figure F14.** Representative Auger (top) and the first derivative Auger spectra (bottom) of poly(acetylene). The  $D$ -parameter was calculated from the distance between the maximum and minimum point on the derivative spectra.

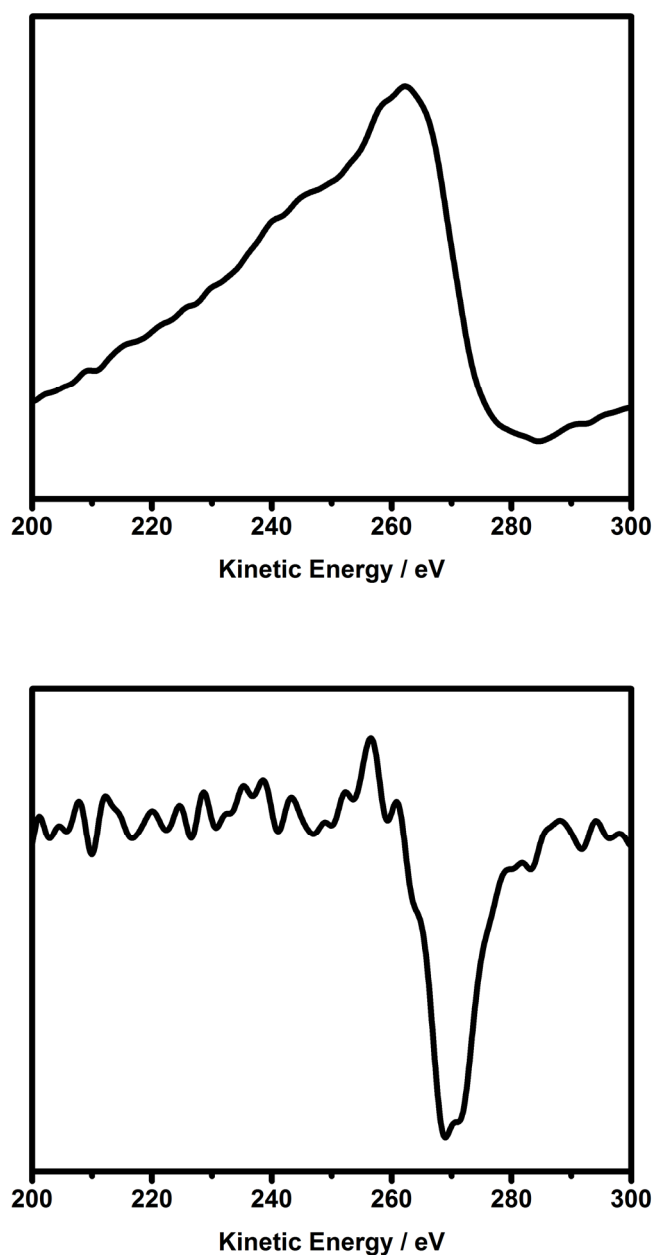


**Figure F15.** Representative Auger (top) and the first derivative Auger spectra (bottom) of poly(vinyl acetylene). The  $D$ -parameter was calculated from the distance between the maximum and minimum point on the derivative spectra.

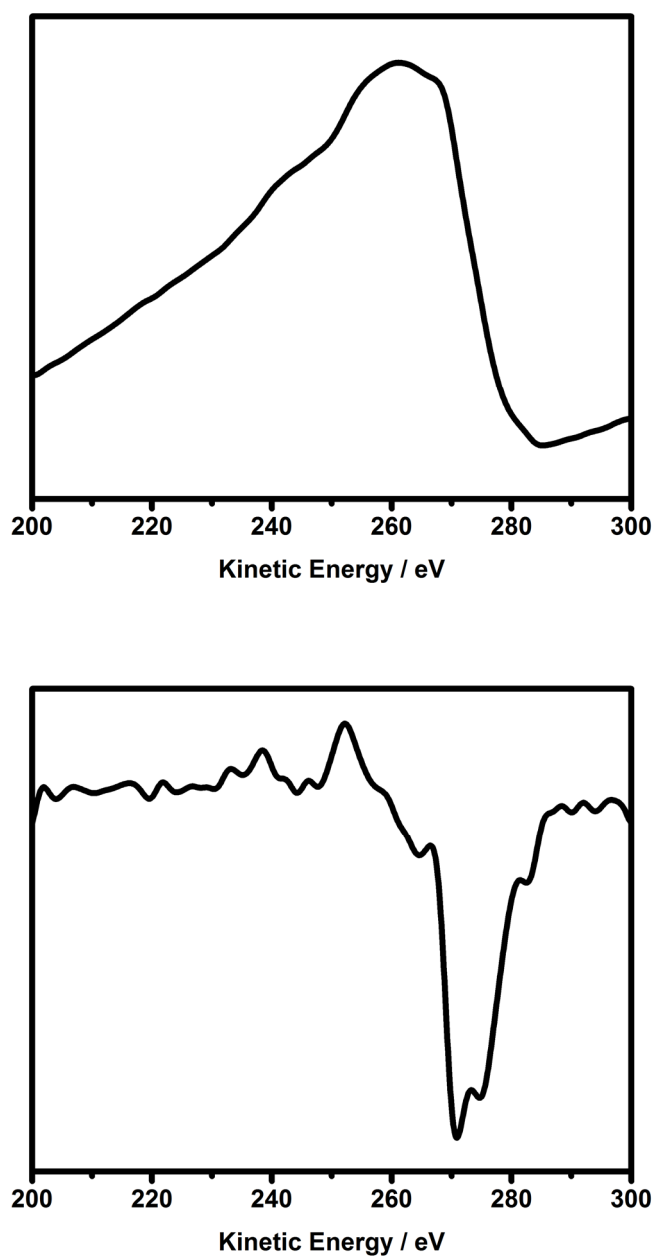


**Figure F16.** Representative Auger (top) and the first derivative Auger spectra (bottom) of poly(phenylene ethynylene). The *D*-parameter was calculated from the distance between the maximum and minimum point on the derivative spectra.

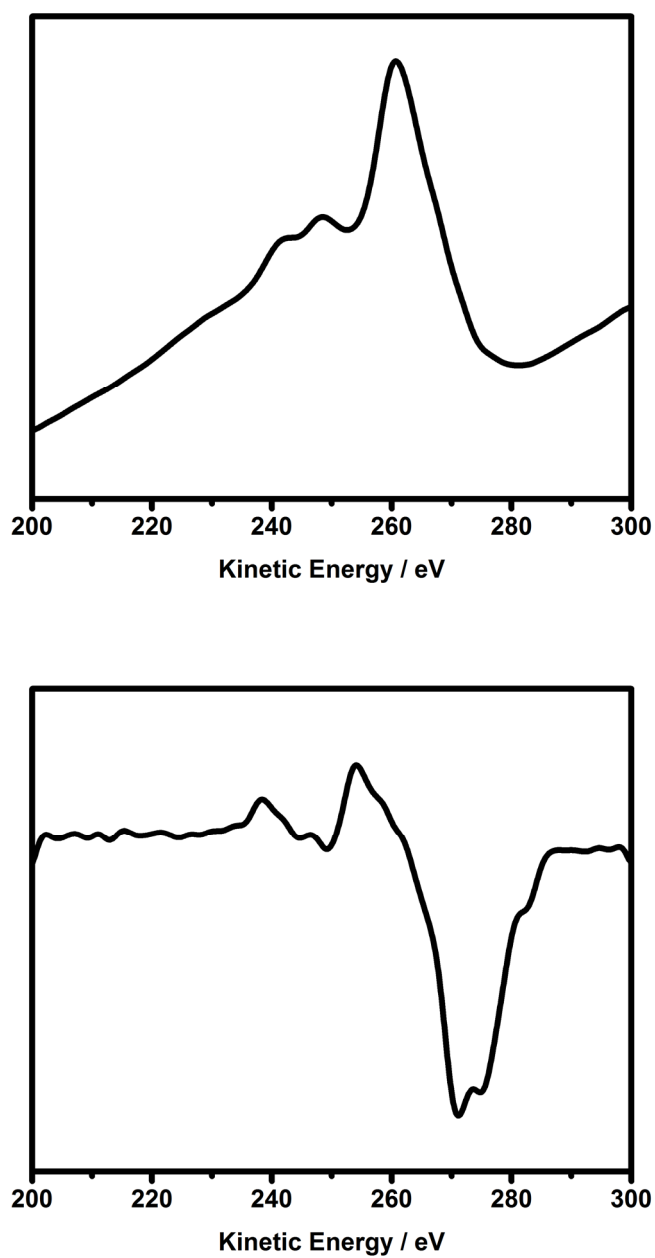


**Figure F17.** Representative Auger (top) and the first derivative Auger spectra (bottom) of pentacene. The  $D$ -parameter was calculated from the distance between the maximum and minimum point on the derivative spectra.

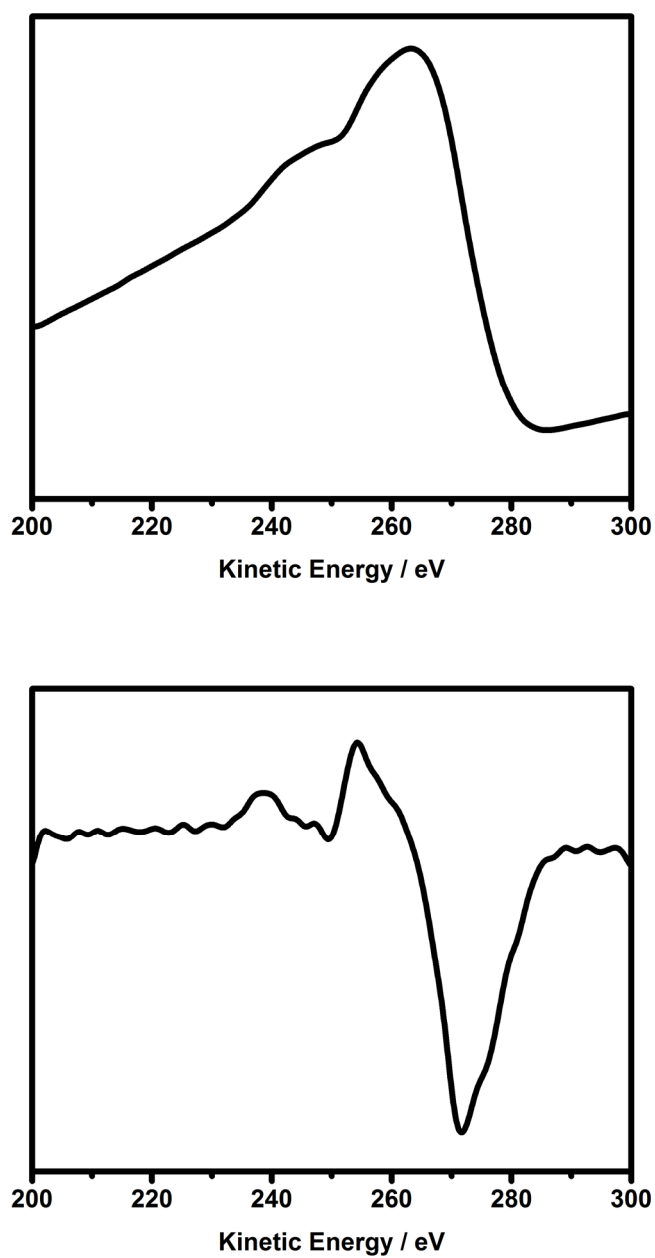


**Figure F18.** Representative Auger (top) and the first derivative Auger spectra (bottom) of coronene. The  $D$ -parameter was calculated from the distance between the maximum and minimum point on the derivative spectra.



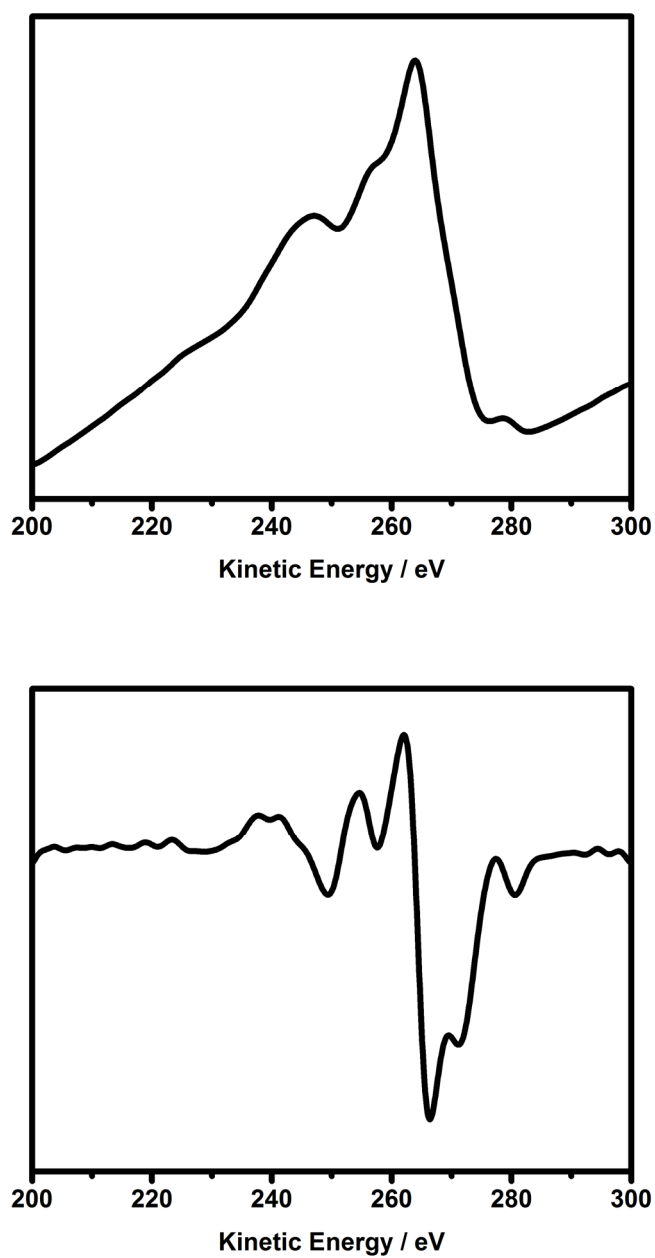


**Figure F19.** Representative Auger (top) and the first derivative Auger spectra (bottom) of poly(acrylonitrile). The  $D$ -parameter was calculated from the distance between the maximum and minimum point on the derivative spectra.

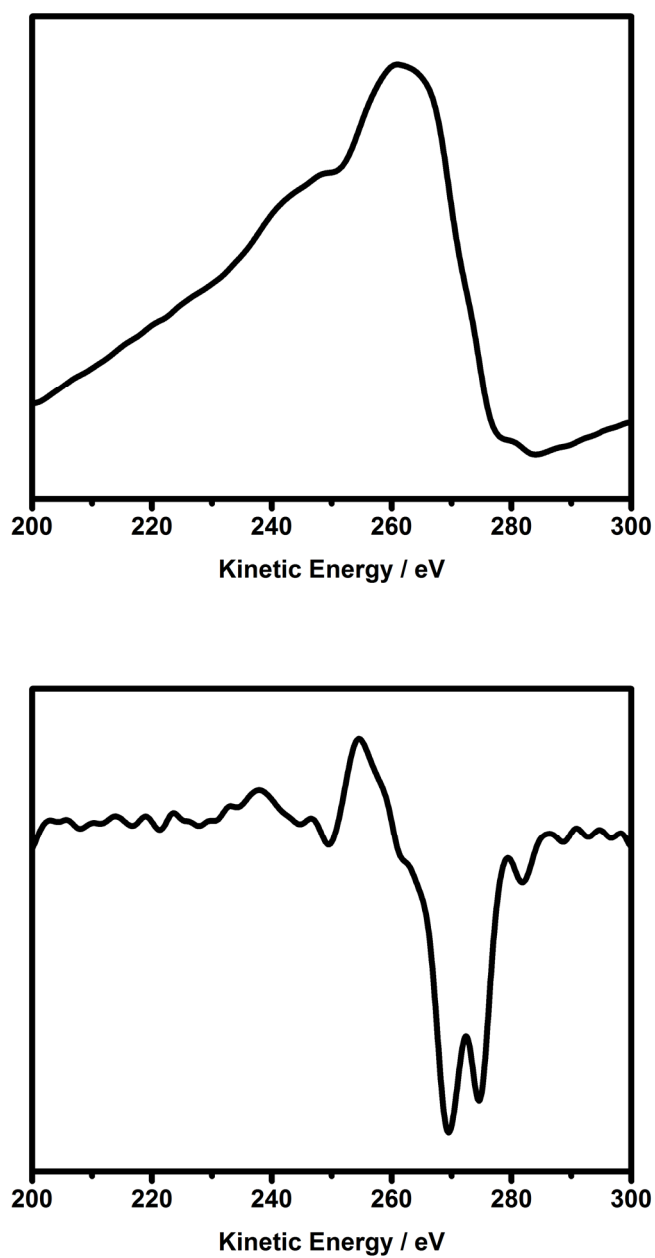


**Figure F20.** Representative Auger (top) and the first derivative Auger spectra (bottom) of poly(4-vinyl pyridine). The  $D$ -parameter was calculated from the distance between the maximum and minimum point on the derivative spectra.

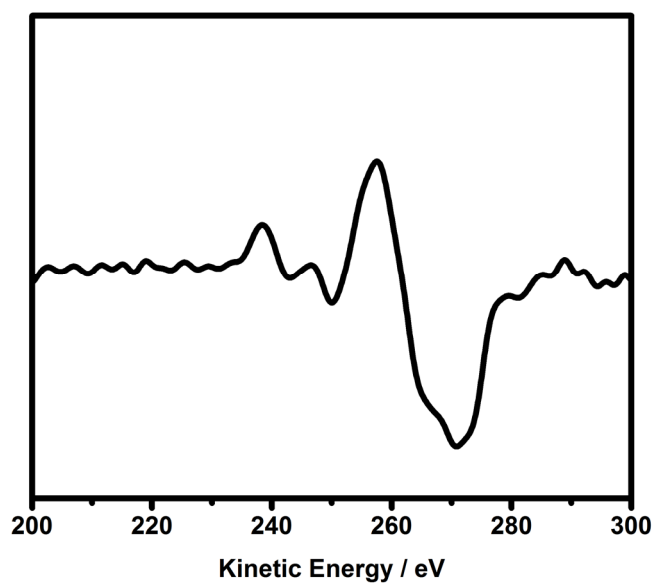
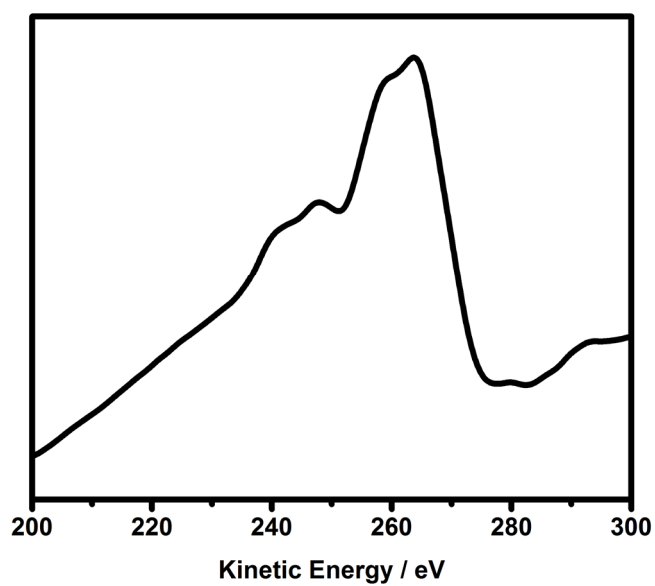


**Figure F21.** Representative Auger (top) and the first derivative Auger spectra (bottom) of poly(methyl methacrylate). The  $D$ -parameter was calculated from the distance between the maximum and minimum point on the derivative spectra.

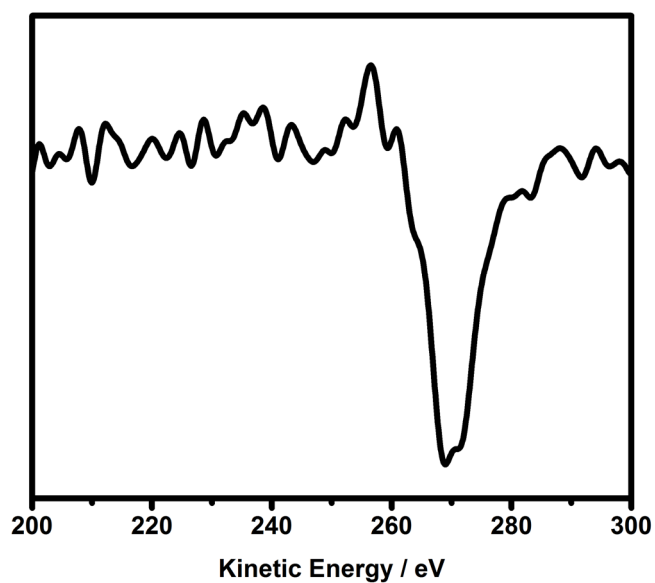
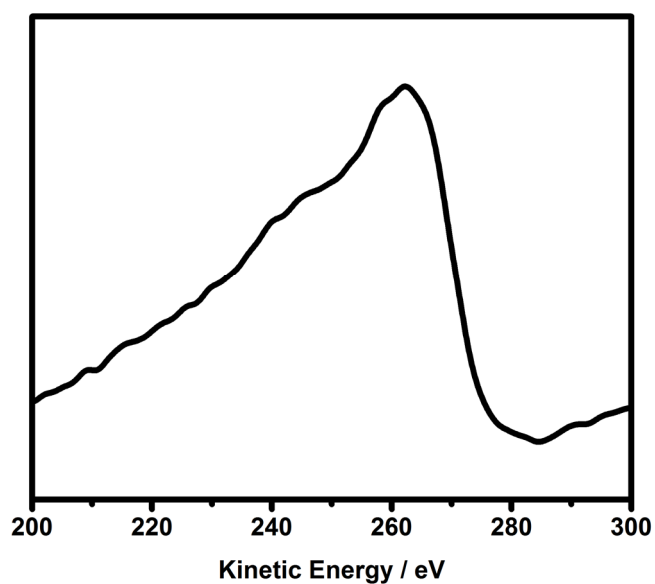


**Figure F22.** Representative Auger (top) and the first derivative Auger spectra (bottom) of poly(vinyl acetylene). The  $D$ -parameter was calculated from the distance between the maximum and minimum point on the derivative spectra.

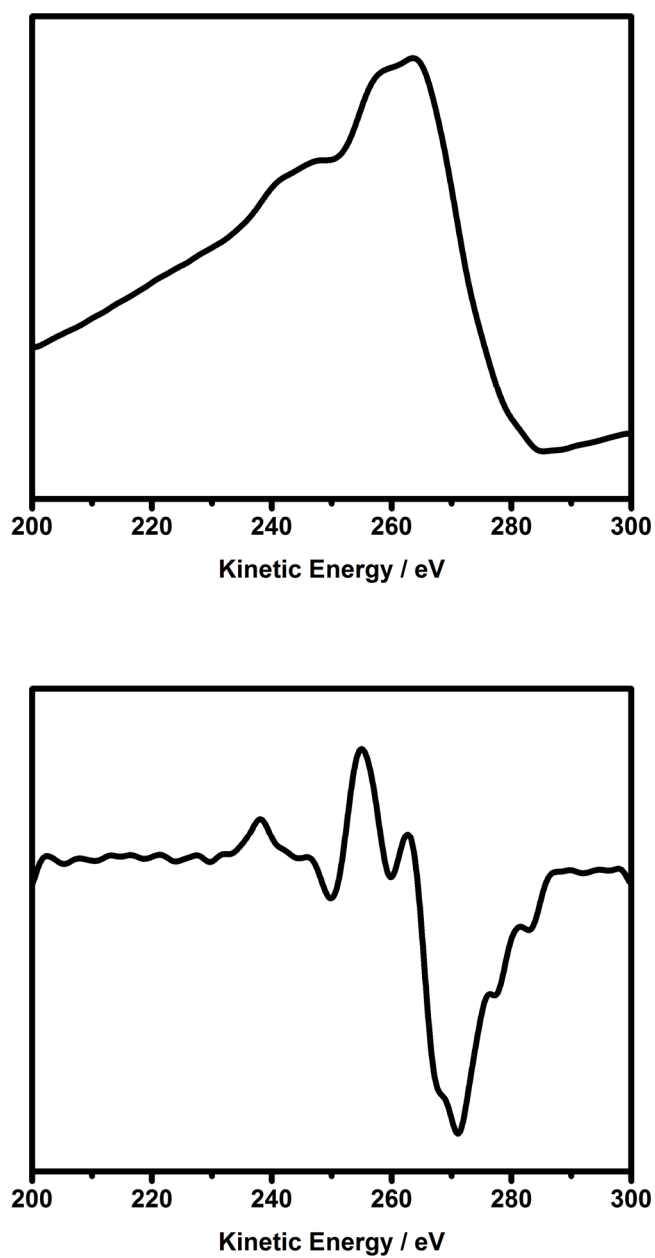


**Figure F23.** Representative Auger (top) and the first derivative Auger spectra (bottom) of one to one physical mixture of poly(ethylene) and poly(acetylene). The  $D$ -parameter was calculated from the distance between the maximum and minimum point on the derivative spectra.

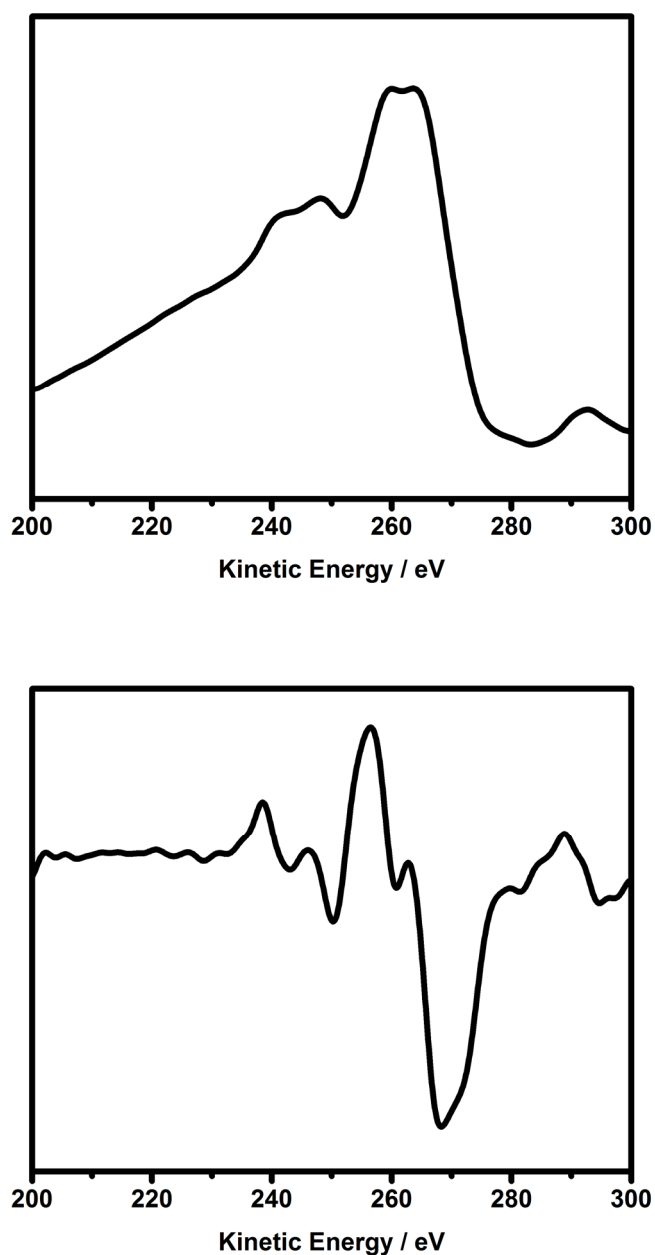


**Figure F24.** Representative Auger (top) and the first derivative Auger spectra (bottom) of a one to one blend of poly(styrene) and poly(ethylene). The  $D$ -parameter was calculated from the distance between the maximum and minimum point on the derivative spectra.

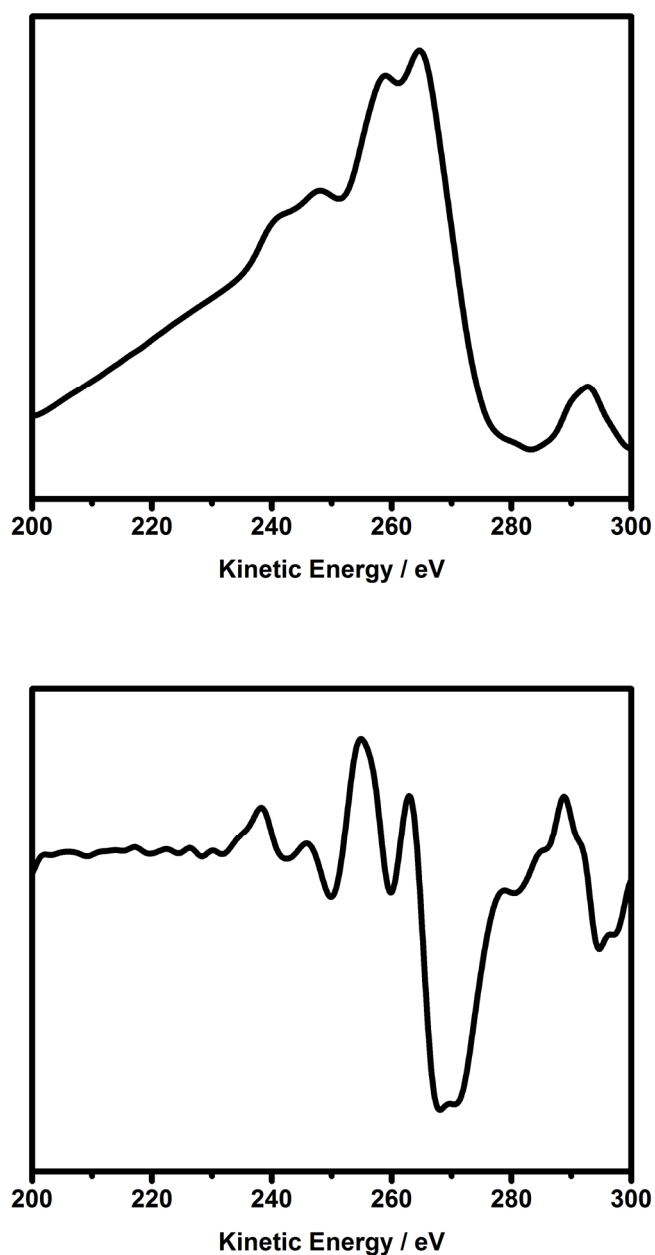


**Figure F25.** Representative Auger (top) and the first derivative Auger spectra (bottom) of a three to one blend of poly(styrene) and poly(ethylene). The  $D$ -parameter was calculated from the distance between the maximum and minimum point on the derivative spectra.

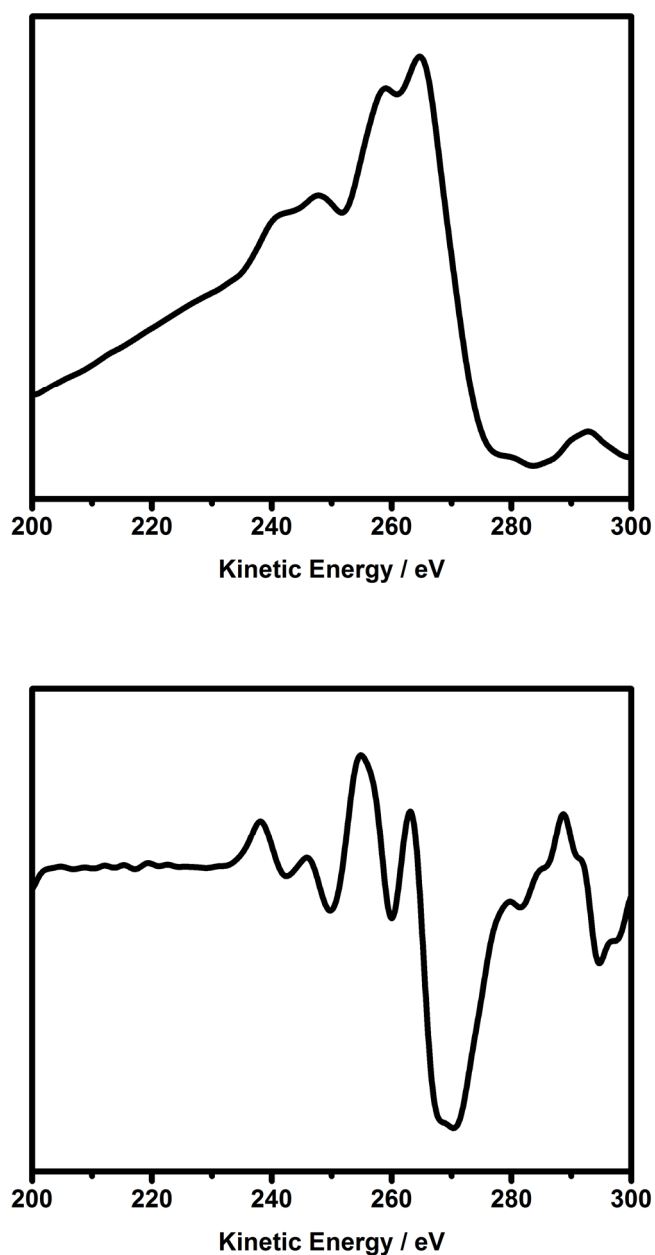


**Figure F26.** Representative Auger (top) and the first derivative Auger spectra (bottom) of a one to three blend of poly(styrene) and poly(ethylene). The  $D$ -parameter was calculated from the distance between the maximum and minimum point on the derivative spectra.



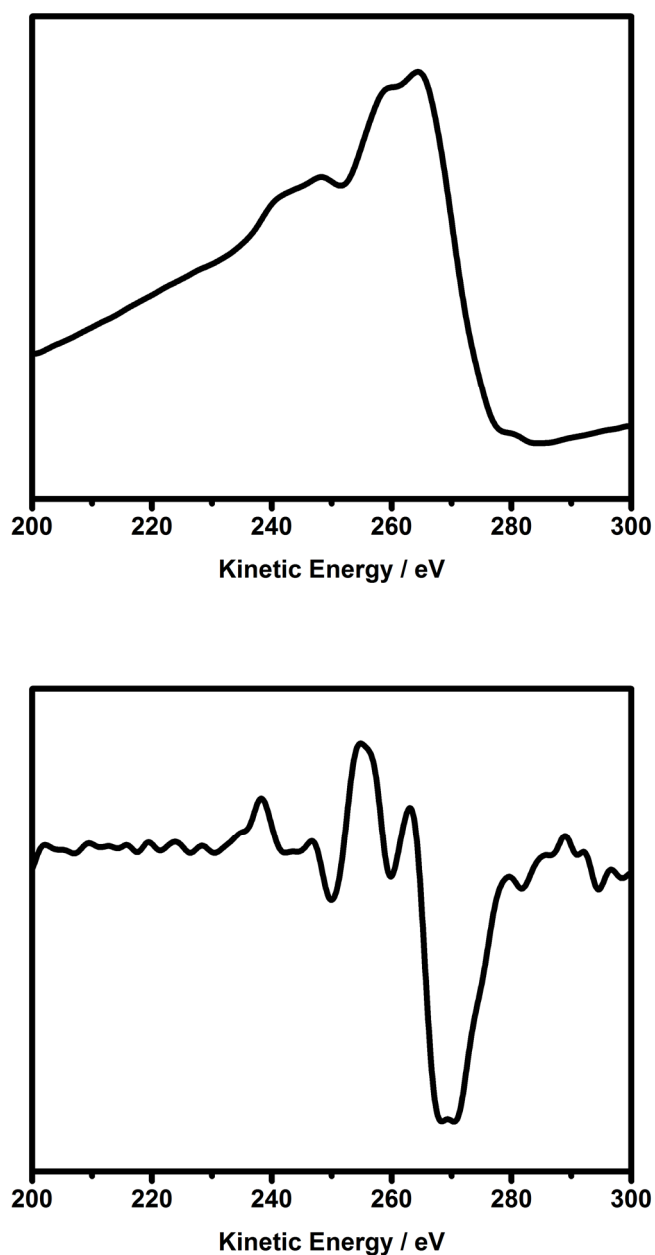


**Figure F27.** Representative Auger (top) and the first derivative Auger spectra (bottom) of a poly(styrene)-*block*-poly(ethylene)-*block*-poly(styrene). The  $D$ -parameter was calculated from the distance between the maximum and minimum point on the derivative spectra.